The Generation of Antibodies as Tools to Characterise Triggering Receptor Expressed on Myeloid Cells 2 (TREM2) and Explore its Role in Alzheimer's Disease

Dina Fathalla

Thesis presentation for the degree of Doctor of Philosophy

(Medicine)

2021

Acknowledgements

I would like to express my deep gratitude to Professor Paul Morgan for giving me the opportunity to undertake my PhD in his lab and for his guidance throughout the project. I would like to thank my co-supervisor Professor Nick Allen, and thanks to Professor Phil Taylor for all his advice and for the cell lines he provided. Thanks also to Dr Tim Hughes for his help with immunisations, and to Wiola, Angharad and Claire for their contributions to this work and for their continued support and afternoon tea catch-ups.

From my time with the Taylor group, thanks to Rob for his infinite patience whenever I asked for help during his own thesis writing, and to Ruth for her constant encouragement and delicious baked treats.

From the DRI BPM group, thank you to Rob for the scientific brainstorming and amusing conversations on our Heath-to-HEB treks, to Sarah and Beth for their wonderful support and endless encouragement and to Nikoleta for making me feel right at home. Thank you to Roanne and Johny for keeping me smiling through the difficult times and to Geneviève for the enjoyable Friday morning chats on the way to lab meetings. Thanks also to Georgina, Ryan, Alison, Charlotte and Steph for their help and advice during thesis writing.

Thank you to my wonderfully supportive parents and to Amira, Jack and little Sophie, my shining star, I could not have done it without you. Thanks to Megan for keeping me sane and for taking me under her wing and teaching me some crucial last minute lab techniques! Thank you to Andrew for his incredible support, from that very first emergency chocolate bar to the final full stop in the thesis, and to Natacha and Anthony, my extended family here in Cardiff, for their wonderful support - both scientific and food-related - and their encouragement throughout the entire experience.

Summary

Alzheimer's disease (AD) is the most common form of dementia, accounting for 60-70% of cases. Genome-wide association and genetic meta-analysis studies have identified several risk genes linked with late onset AD, a major one being triggering receptor expressed on myeloid cells 2 (TREM2). Variants of TREM2 have been associated with partial loss of function, such as impaired ligand binding and reduced microglial inflammatory responses, and recent studies have demonstrated a key role for TREM2 in microglial modulation in the healthy brain and in AD. However, conflicting results in the literature indicate that the role of TREM2 is more complex than once thought, and a better understanding of the functions and relevance of TREM2, and its soluble counterpart, is necessary to further the knowledge of AD pathogenesis and identify potential therapeutic targets.

There is currently a lack of reliable commercial anti-TREM2 antibodies that can detect and modulate TREM2 in human and animal systems. This thesis describes the production and characterisation of a panel of monoclonal and polyclonal antibodies raised against human and mouse TREM2. Of these antibodies, a complementary pair was selected and optimised for the establishment of an in-house ELISA for the detection of soluble TREM2 in human samples. This assay was used to analyse a cohort of AD and mild cognitive impairment (MCI) patients alongside age-matched controls, where sTREM2 levels were found to positively correlate with age, but not clinical status. Novel antibodies were also generated against peptides representing the two most common TREM2 variants associated with increased susceptibility to AD; R47H and R62H.

Overall, this thesis discusses the characterisation and application of the generated anti-TREM2 antibodies and demonstrates their future potential for use in functional assays.

Contents

List of Figures

List of Tables

Abbreviations

AD	Alzheimer's disease
ADAM	A disintegrin and metalloproteinase domain-containing protein
AID	activation-induced cytidine deaminase
ALS	Amyotrophic lateral sclerosis
Amp	Ampicillin
A-MuLV	Abelson leukaemia virus
ANOVA	Analysis of variance
Apo	Apolipoprotein
APP	Amyloid precursor protein
APS	Ammonium persulfate
ATP	Adenosine triphosphate
BBB	Blood-brain barrier
BCA	Bicinchoninic acid
BLAST	Basic Local Alignment Search Tool
bp	Base pair
BSA	Bovine serum albumin
cDNA	Complementary deoxyribonucleic acid
CDR	Complementarity-determining region
CFA	Complete Freund's adjuvant
CLU	Clusterin
CMV	Cytomegalovirus
CNS	Central nervous system
CO_2	Carbon dioxide
CR1	Complement receptor 1
CRP	C-reactive protein
CSF	Cerebrospinal fluid
CSR	Class switch recombination
Ct	Cycle threshold
CTF	C-terminal fragment
CV	Coefficient of variation
DAM	Disease-associated microglia
DAP12	DNAX-activation protein 12
DMEM	Dulbecco's Modified Eagle medium
DMSO	Dimethyl Sulfoxide

ECL	Enhanced chemiluminescence
EDTA	Ethylenediaminetetraacetic acid
ELISA	Enzyme-linked immunosorbent assay
EMEM	Eagle's minimum essential medium
ERK	Extracellular signal-regulated kinase
Fab	Fragment antigen-binding
FBS	Fetal bovine serum
Fc	Fragment crystallisable
FcγR	Fcγ receptor
FPLC	Fast protein liquid chromatography
FSC	Forward scatter
FTD	Frontotemporal dementia
GAPDH	Glyceraldehyde-3-phosphate dehydrogenase
GFAP	Glial fibrillary acidic protein
GWAS	Genome-wide association study
HAT	Hypoxanthine-aminopterin-thymidine
HBSS	Hank's Balanced Salt Solution
HGPRT	Hypoxanthine-guanine-phosphoribosyltransferase
His	Histidine
HLA	Human leukocyte antigen
HRP	Horseradish peroxidase
HT	Hypoxanthine-thymidine
IBA1	Ionized calcium binding adaptor molecule 1
ICD	Intracellular domain
IFA	Incomplete Freund's adjuvant
Ig(V)	Immunoglobulin (variable)
IHC	Immunohistochemistry
IL	Interleukin
IP	Intraperitoneal
ITAM	Immunoreceptor tyrosine-based activation motif
J	Joining
kDa	Kilodalton
KLH	Keyhole limpet hemocyanin
KO	Knockout
LB	Luria Broth
Log_{10}	Logarithm base 10
LPS	Lipopolysaccharide

mAb	Monoclonal antibody
MCI	Mild cognitive impairment
MCS	Multiple cloning site
MCSF	Macrophage colony-stimulating factor
MGnD	Microglial neurodegenerative
MHC	Major Histocompatibility Class
MOE	Molecular Operating Environment
MOM	Mouse-on-mouse
MRI	Magnetic resonance imaging
mRNA	Messenger RNA
mTOR	Mammalian target of rapamycin
MW	Molecular weight
NCBI	National Center for Biotechnology Information
NEAA	Non-essential amino acids
Neo	Neomycin
NfL	Neurofilament light chain
NFT	Neurofibrillary tangle
NHD	Nasu-Hakola disease
NHS	N-hydroxysuccinimide
NIHR	National Institute for Health Research
NK	Natural killer
NR	Non-reducing
NTDK	Neural Tissue Dissociation Kit
NY-ESO-1	New York esophageal squamous cell carcinoma 1
OPD	Orthophenylenediamine
Ori	Origin of replication
P	Calculated probability
PBS	Phosphate buffered saline
PBS-T	PBS-Tween-20
PD	Parkinson’s disease
PEG	Polyethylene glycol
PET	Positron emission tomography
PFA	Paraformaldehyde
pH	Potential of hydrogen
PI3K	Phosphoinositide 3-kinase
PKC	Protein kinase C
PLCγ	Phospholipase Cγ

PLOSL	Polycystic lipomembranous osteodysplasia with sclerosing leukoencephalopathy
PSC	Pluripotent stem cell
PSEN	Presenilin
p-tau	Protein tau
qPCR	Quantitative polymerase chain reaction
R	Reducing
r	Rho
RIPA	Radioimmunoprecipitation assay
Rn	Normalised reporter
RNA	Ribonucleic acid
RPMI	Roswell Park Memorial Institute medium
rRNA	Ribosomal RNA
RT	Reverse transcriptase
SD	Standard deviation
SDS-PAGE	Sodium dodecyl sulphate polyacrylamide gel electrophoresis
SEM	Standard error of mean
SOC	Super Optimal broth with Catabolite repression
SSC	Side scatter
sTREM2	Soluble TREM2
Sulfo-SMCC	Sulfosuccinimidyl 4-[*N*-maleimidomethyl]cyclohexane-1-carboxylate
Syk	Spleen tyrosine kinase
TBE	Tris-borate-EDTA
TCEP	Tris(2-carboxyethyl)phosphine hydrochloride
TEMED	Tetramethylethylenediamine
TGF-β1	Transforming growth factor-β1
TLT	TREM-like transcript
TNF	Tumor necrosis factor
TREM	Triggering receptor expressed on myeloid cells
TREML	TREM-like
t-tau	Total tau
TYROBP	Tyrosine kinase binding protein
UK	United Kingdom
WT	Wild type

Chapter 1

Introduction

1 Introduction

Recent genomic studies have identified several genes associated with an increased risk of Alzheimer's disease. This project aims to investigate one such gene, which encodes triggering receptor expressed on myeloid cells 2 (TREM2), by generating antibodies against the encoded protein in order to explore its binding and distribution properties. This chapter will introduce the main aspects of the disease, the characteristics and proposed functions of TREM2 and the production of monoclonal antibodies.

1.1 Alzheimer's Disease

1.1.1 Pathology of Alzheimer's Disease

Dementia affects ~850,000 people in the United Kingdom (UK) and almost 50 million worldwide and numbers are increasing year-on-year (Prince *et al.*, 2014; World Health Organisation Dementia Fact Sheet, 2017). Dementia care costs around £34 billion a year in the UK, posing a challenge both on an economic and public health level (Wittenberg *et al.*, 2019). Alzheimer's disease (AD) is the most common form of dementia, responsible for almost two-thirds of dementia cases in the UK (Holtzman *et al.*, 2011; Prince *et al.*, 2014). The disease that became known as AD was first described in 1906 by the German physician, Alois Alzheimer; he documented a 5-year study of his patient, Auguste D, who suffered from disorientation, worsening memory loss and delusions. After her death, he studied her brain and described brain shrinkage and the presence of the plaques and tangles now considered the pathological signatures of AD (Alzheimer, 1907; Stelzmann *et al.*, 1995). As this index case showed, AD is characterised by a gradually progressive cognitive decline and has devastating personal and socioeconomic implications. There is currently no cure for AD, and while current treatment options aim to make symptoms more manageable, they do not stop disease progression (Hermann *et al.*, 2011).

The main neuropathological hallmarks of AD are the extracellular aggregations of amyloid-β (Aβ) peptides, which can result in plaque formation over time, and the intracellular formation of neurofibrillary tangles (NFTs) of hyperphosphorylated microtubule-associated protein tau (p-tau). These highly insoluble structures can cause neuronal damage and disrupt synaptic signalling, resulting in impaired memory

and cognition (Terry *et al.*, 1991; Mandelkow and Mandelkow, 1998). This accumulation of Aβ and tau proteins can precede clinical symptoms by several years, emphasising the importance of early therapeutic intervention in AD (Bateman *et al.*, 2012; Beason-Held *et al.*, 2013).

The exact mechanism and sequence of how amyloid and tau interact has not been fully elucidated, but several animal studies support an initiating effect by Aβ plaque deposition of damaging proximal synapses (Koffie *et al.*, 2009; Zempel *et al.*, 2010; Spires-Jones and Hyman, 2014). This may evoke the activation of brain cells, such as astrocytes and microglia, to aid in the clearance of damaged synapses (Paresce *et al.*, 1996; Wyss-Coray *et al.*, 2003). But as Aβ continues to accumulate and as synaptic damage increases, the overactivation of these glial cells can lead to abnormally increased levels of inflammatory mediators (Ranaivo *et al.*, 2006; Fleisher-Berkovich *et al.*, 2010), provoking hyperphosphorylation of tau protein and thus triggering axonal loss and neurodegeneration (Howlett *et al.*, 2008). A recent study on human subjects supported the findings in animal studies by demonstrating an association of Aβ with synaptic damage and memory impairment at early stages of disease, and an association of tau with axonal damage and cognitive decline at later stages (Pereira *et al.*, 2021). Further work is required to confirm these findings in humans and to better define the interaction between the two proteins and to investigate the relative role of their soluble versus aggregated forms.

1.1.2 Brain Homeostasis and Neuroinflammation

Brain homeostasis involves the intake of nutrients from the periphery to meet the energy demands of the brain and the clearance of waste products back into the circulation (Cheng and Haorah, 2019). As in other organs and systems, acute inflammation plays a protective role in the brain, defending against infection and disposing of waste products; immune homeostasis in the brain is maintained through the function of neurovascular barriers and a host of neuronal and glial cells, such as microglia, which play a central role in neuroinflammation as described further below.

1.1.2.1 The Blood-Brain Barrier

The blood-brain barrier (BBB) comprises an endothelial membrane with tight junctions, supported by astrocytes and vascular pericytes (Ueno *et al.*, 2016). This acts as a selectively permeable barrier that separates the central nervous system (CNS) from the peripheral environment and plays a key role in CNS homeostasis by

controlling the transfer of cells, nutrients and waste products into and out of the brain (Abbott *et al.*, 2006).

Vascular dysfunction and BBB disruption have been linked to AD and other neurodegenerative diseases (Toledo *et al.*, 2013; Arvanitakis *et al.*, 2016), and changes in vascular biomarkers have been reported, suggesting an early disruption of the vascular system during LOAD progression (Iturria-Medina *et al.*, 2016). Breakdown of the BBB leads to increased permeability, allowing the passage of immune cells and inflammatory components from the periphery into the brain. The accumulation of albumin and other serum proteins can also contribute to brain oedema and increased levels of thrombin can mediate neurotoxicity (Mhatre *et al.*, 2004; Zlokovic, 2011). Together, these events can provoke astrocytic and microglial responses, increasing the inflammatory state in the brain and contributing to Aβ accumulation and neuronal damage, including the formation of toxic tau tangles (Abbott *et al.*, 2006; Shlosberg *et al.*, 2010; Sweeney *et al.*, 2015; Sweeney *et al.*, 2018). Several factors can affect BBB integrity, including inflammation and trauma, which can lead to an influx of immune cells that generate reactive oxygen species and pro-inflammatory cytokines (Tomkins *et al.*, 2008; Shlosberg *et al.*, 2010); in the context of AD, both tau tangles and Aβ deposits have been suggested to contribute to further loss of BBB integrity (Hartz *et al.*, 2012; Blair *et al.*, 2015).

1.1.2.2 Microglia in the Healthy and AD Brain

Microglia are the resident macrophages in the brain, they constitute between 5 and 15% of the cells in the CNS (Lawson *et al.*, 1990; Mittelbronn *et al.*, 2001; Pelvig *et al.*, 2008) and are important regulators of brain development and homeostasis. Microglia derive from the yolk sac during embryonic development (Ginhoux *et al.*, 2010) and have a unique phenotypic signature that differentiates them from other myeloid cells in the CNS in both humans and mice (Butovsky *et al.*, 2014). In the adult brain under physiological conditions, microglia have a homeostatic and immune-surveillant role, dynamically presenting highly branched processes to patrol the microenvironment over a restricted region and aid in the recognition and clearance of cellular debris (Nimmerjahn *et al.*, 2005). If brain homeostasis is disrupted, microglia adopt an activated phenotype characterised by a more amoeboid morphology (Figure 1.1) and increased phagocytic activity to respond to foreign matter or injury (Paolicelli *et al.*, 2011; Kettenmann *et al.*, 2013). Microglial morphology is not limited to these two states and includes a range of changes, which give a limited insight into their actual functional change (Stence *et al.*, 2001; Heindl *et al.*, 2018).

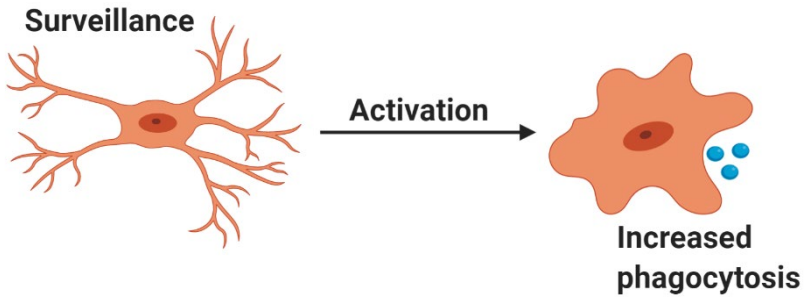

Figure 1.1 – Resting and activated microglial morphologies.
Microglia maintain a ramified morphology for immune surveillance under physiological conditions in the brain. Microglia adopt an amoeboid shape if homeostasis is disrupted and are recruited to the site of injury or inflammation and display increased phagocytic activity. Created by BioRender.com.

The activation of microglia and astrocytes, known as microgliosis and astrogliosis respectively, were initially noted in plaque-containing brain tissue by Alois Alzheimer and were thought to be consequences of the disease (Alzheimer, 1907). However, later studies suggested that cytokines released by activated glial cells could contribute to cell damage, amyloid deposition and neuroinflammation (Griffin *et al.*, 1989; Heneka *et al.*, 2005), raising the question of whether gliosis is a cause or consequence of AD.

Astrocytes are involved in brain homeostasis, they also provide trophic support to neurons and maintain synapses (Pfrieger and Barres, 1997). The nature of cross-talk between astrocytes and microglia can affect neuronal survival in brain injury and neuroinflammation (Matejuk and Ransohoff, 2020). Recent studies demonstrated that microglia activated using lipopolysaccharide (LPS) or adenosine triphosphate (ATP), led to the activation of recipient astrocytes (Drago *et al.*, 2017; Liddelow *et al.*, 2017). Further investigation implicated the role of cytokines, interleukin (IL)-1α, tumor necrosis factor (TNF)-α, and complement component C1q, in inducing astrocyte reactivity. The reported neurotoxic effect of these activated astrocytes in addition to their detection in human neurodegenerative tissue (Liddelow *et al.*, 2017) demonstrate the relevance of microglial-astrocytic interaction in AD.

Both amyloid precursor protein (APP) and its derivative amyloid peptides can activate microglia (Meda *et al.*, 1995; Barger and Harmon, 1997), and clustering of activated microglia around amyloid plaques has been observed in the human AD brain (Dickson *et al.*, 1988; Mattiace *et al.*, 1990). In transgenic AD mouse models overexpressing

APP, activated microglia were shown to surround plaques and take up Aβ peptides, suggesting that Aβ plaque formation drives the activation and recruitment of microglia to the plaque site where they clear or limit amyloid deposition (Paresce *et al.*, 1996; Herber *et al.*, 2007; Bolmont *et al.*, 2008; Meyer-Luehmann *et al.*, 2008; Zhao *et al.*, 2017). While this initially lends activated microglia a neuroprotective role, chronic activation can have detrimental effects due to excessive secretion of inflammatory mediators and decreased phagocytic capacity, resulting in the accumulation of Aβ and neuronal injury (Meda *et al.*, 1995; Sheng *et al.*, 1998; Hickman *et al.*, 2008).

1.1.2.3 Synaptic Pruning

During the early years of brain development in humans, and early weeks in mice, neurons develop an excess of synapses, which are brain structures that allow signal transmission between neurons. A subset of these synapses is matured and maintained to establish optimal brain circuitry, while the rest are removed; this process is known as synaptic pruning (Hua and Smith, 2004). Microglia and astrocytes play a key role in this elimination of unwanted synapses (Nimmerjahn *et al.*, 2005; Paolicelli *et al.*, 2011) and studies have suggested that interactions with the classical complement system proteins, C1q and C3, (Stevens *et al.*, 2007; Schafer *et al.*, 2012) and other immunologically relevant candidates, such as the microglial chemokine receptor CX3CR1 (Paolicelli *et al.*, 2011) and Major Histocompatibility Class (MHC) molecules (Lee *et al.*, 2014), can contribute to this mechanism.

Synapse loss during development is a physiological process necessary for proper brain function; however, synaptic loss in later life can contribute to disease. In AD, synapse loss correlates strongly with cognitive decline in the early stages of the disease process (DeKosky and Scheff, 1990; Scheff *et al.*, 2006; Goetzl *et al.*, 2016). Mucke *et al.* (2000) demonstrated that Aβ peptides are synaptotoxic, independent of amyloid plaque presence. A role for complement in this process was suggested by studies investigating complement (C1q and C3)-deficient AD mouse models; these showed reduced synapse loss compared to complement-sufficient AD models (Fonseca *et al.*, 2004; Wu *et al.*, 2019). The focus of this project, TREM2, has also been implicated in synapse loss, as will be discussed later in this chapter; microglial expression of TREM2 in animal models was shown to regulate synaptic refinement by astrocytes (Filipello *et al.*, 2018; Jay *et al.*, 2019). This inappropriate synaptic elimination, complement activation and chronic activation of microglia around amyloid plaques could account for the neurodegeneration and cognitive dysfunction that are characteristic of AD.

1.1.3 Genetics of Alzheimer's Disease

The rare familial forms of AD affect middle-aged individuals and are caused by single genetic mutations either in the *APP* gene, the precursor to Aβ, or in presenilin 1 and 2 (*PSEN1*, *PSEN2*), both components of the γ-secretase complex that is involved in generating Aβ from APP (Kang *et al.*, 1987; Levy-Lahad *et al.*, 1995; Rogaev *et al.*, 1995; Sherrington *et al.*, 1995). APP can be processed via amyloidogenic and non-amyloidogenic pathways that normally co-exist in equilibrium (Martorana *et al.*, 2015). Aβ are 38-42 amino acid peptides that are produced as a result of sequential cleavage of APP and its carboxyl-terminal fragment β (CTFβ) by-product (Figure 1.2).

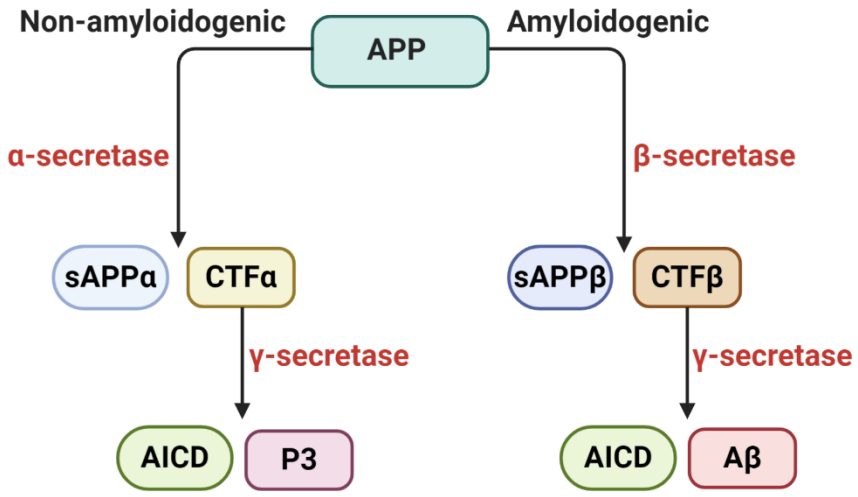

Figure 1.2 – Amyloidogenic and non-amyloidogenic APP processing pathways. APP processed by α-secretase in the non-amyloidogenic pathway results in the generation of soluble APPα (sAPPα) and carboxyl-terminal fragment α (CTFα), the latter is cleaved by γ-secretase to P3 peptide and APP intracellular domain (AICD). The amyloidogenic pathway involves β-secretase processing of APP into sAPPβ and CTFβ, which in turn undergoes sequential γ-secretase cleavage into AICD and Aβ. Modified from Sun *et al.* (2015), Silva *et al.* (2019), created by BioRender.com.

Aβ monomers can exist in physiological conditions, but oligomeric aggregation into plaques can lead to neuronal degeneration (Martorana *et al.*, 2015). The mutations associated with familial AD impact the way APP is cleaved and processed, resulting in increased levels of the Aβ42 peptide relative to the normally predominant Aβ40 peptide, the former is longer and more prone to aggregation (Iwatsubo *et al.*, 1994; Scheuner *et al.*, 1996).

Late onset AD (LOAD) is the most common form of AD; it occurs sporadically in older individuals, rarely before 65 years and usually much older (Hebert *et al.*, 1995). Age

is the strongest risk factor in this multifactorial disease (Jorm *et al.*, 1987; Ritchie and Kildea, 1995), and the role of genetics is highly complex. The strongest known genetic risk factor for LOAD is apolipoprotein E (*APOE*), which is involved in lipid transport and cholesterol homeostasis (Corder *et al.*, 1993; Karch and Goate, 2015). It has three polymorphic alleles: ε2, ε3 and ε4. While the ε2 allele appears to be protective, studies have shown that carriers of one ε4 allele have a 3-4-fold increased risk of AD and carriers of two ε4 alleles have a 12-fold increased risk of AD compared to ε3 homozygotes (Corder *et al.*, 1993; Strittmatter *et al.*, 1993).

To date, approximately 30 genetic risk loci have been associated with AD through genome-wide association studies (GWAS) and subsequent genetic meta-analysis studies (Bertram *et al.*, 2008; Harold *et al.*, 2009; Hollingworth *et al.*, 2011; Naj *et al.*, 2011; Lambert *et al.*, 2013; Mäkelä *et al.*, 2018; Marioni *et al.*, 2018; Jansen *et al.*, 2019; Kunkle *et al.*, 2019). Several of the key risk variants identified are involved in neuroinflammation and regulation of the innate immune response (Gagliano *et al.*, 2016; Sims *et al.*, 2017). Among these is the triggering receptor expressed on myeloid cells 2 (*TREM2*); several polymorphisms in *TREM2* have been linked to AD, these will be described in more detail later in this chapter.

Complement components clusterin, also known as apolipoprotein J (ApoJ) and complement receptor 1 (CR1) were also identified in these studies, adding to the evidence of a key role for immune dysregulation in AD (Harold *et al.*, 2009; Lambert *et al.*, 2009). Similarly to ApoE, clusterin is known for its involvement in lipid transport and metabolism (de Silva *et al.*, 1990; Jenne *et al.*, 1991), and its recent association with AD risk further highlights the importance of lipid metabolism in AD pathology, as will be discussed further in this chapter.

1.1.4 Non-Genetic Risk Factors for Alzheimer's Disease

Apart from age, other non-genetic risk factors can play a role in AD development. The incidence of AD is higher in women than in men, likely due to differences in longevity and mitochondrial biology (Viña *et al.*, 2010). Lifestyle factors, such as smoking and physical activity, are also associated with a higher risk of developing AD (Alzheimer's Association, 2014).

The occurrence of comorbidities before or during AD can affect the status and progression of disease. Vascular dysfunction, as previously mentioned, in addition to cardiovascular risk factors, such as hypertension and dyslipidaemia, have all been

associated with AD (Petrovich *et al.*, 2000; Toledo *et al.*, 2013). Biessels *et al.* (2006) reviewed a range of longitudinal studies and reported a high risk of AD in type 2 diabetes patients, proposing that alterations in the metabolism of amyloid, insulin and glucose may be involved. The consideration of these risk factors is a necessary step during the interpretation of results from human AD studies.

1.1.5 Biomarkers of Alzheimer's Disease

While diagnostic criteria for AD are mainly based on cognitive examination and identification of relevant clinical symptoms, the detection of biomarkers that reflect the neuropathological changes in AD increase the likelihood of diagnosing the disease at an earlier stage and differentiating it from other types of dementia (Biagioni and Galvin, 2011). Biomarkers can be used for risk prediction and the identification of individuals susceptible to disease, as well as for diagnostic screening and monitoring of disease progression (Mayeux, 2004). A good biomarker should demonstrate high sensitivity and specificity for AD compared to other dementia forms. It should also reflect the brain pathophysiology in AD and show reproducibility across different laboratories (Mayeux, 2004; Humpel, 2011).

1.1.5.1 Imaging Biomarkers

The use of imaging biomarkers to measure amyloid pathology and neurodegeneration is an important part of diagnosing and understanding the mechanisms behind AD. Aβ measurement via positron emission tomography (PET) imaging can generate information about the pattern of Aβ deposition in the brain, and volumetric magnetic resonance imaging (MRI) can measure and monitor the progression of neurodegeneration (Zetterberg and Bendlin, 2021). Fluid-based biomarkers are also commonly used to identify amyloidosis and detect the presence of proteins indicative of neurodegeneration and neuroinflammation.

1.1.5.2 CSF Biomarkers

CSF levels of Aβ, total tau (t-tau) and p-tau are widely used as established core biomarkers of AD. Reduced CSF levels of the Aβ42 peptide are associated with AD and indicate the formation of amyloid plaques, but are not a direct measure of amyloid plaque load (Jack Jr *et al.*, 2018). Some studies have demonstrated that measurement of the Aβ42:40 ratio resulted in improved diagnostic performance compared to Aβ42 alone (Janelidze *et al.*, 2016b; Lehmann *et al.*, 2018).

Increased levels of CSF tau reflect axonal damage and neurodegeneration, and higher t-tau levels have been consistently documented in the CSF of AD patients compared to controls (Arai *et al.*, 1995; Blennow *et al.*, 1995). However, as increased t-tau levels have also been reported in other neurodegenerative diseases, this limits the ability of t-tau to differentiate between AD and other forms of dementia (Otto *et al.*, 1997; Green *et al,* 1999). On the other hand, increased CSF hyperphosphorylated tau, p-tau, which is also associated with AD has been shown to differentiate it from other types of dementia (Sjögren *et al.*, 2001a; Buerger *et al.*, 2002). P-tau is a main component of the filaments that make up neurofibrillary tangles and occurs early in AD (Vincent *et al.*, 1998), giving it clinical value as a biomarker to predict the conversion of pre-AD cases, such as mild cognitive impairment (MCI) to AD (Buerger *et al.*, 2002; Parnetti *et al.*, 2012).

Other biomarkers more recently used in AD studies are neurofilament light chain (NfL) and neurogranin. NfL is a neuronal protein that is mainly abundant in axons (Yuan *et al.*, 2012), and while increased CSF NfL levels are associated with neurodegenerative diseases and are not specific to AD, NfL is a promising biomarker that is indicative of axonal damage or neuronal degeneration (Gaiottino *et al.*, 2013; Dhiman *et al.*, 2020). Neurogranin is a postsynaptic protein used as a biomarker of dendritic and synaptic degeneration (Gerendasy and Sutcliffe, 1997; Tarawneh *et al.*, 2016). Increased CSF neurogranin levels have been associated with both AD and MCI patients, indicating its usefulness as a biomarker of synaptic pathology in AD (Portelius *et al.*, 2015; Wellington *et al.*, 2016).

1.1.5.3 Blood-based Biomarkers

Due to the invasive and impractical nature of CSF sampling, particularly for longitudinal research, several studies have investigated the potential for biomarker measurement in blood samples. However, while this can provide a faster, more accessible and low-cost method for sample collection, it does pose challenges to data analysis and interpretation. Relevant biomarkers may exist at very low levels in the blood, unless BBB integrity is compromised. Non-cerebral sources of biomarkers or the degradation of biomarkers by blood proteases can both affect the measured concentrations providing inaccurate findings, therefore replication and validation are important to ensure these contributing factors are considered during analysis (Hampel *et al.*, 2018; Zetterberg and Burnham, 2019).

In reference to the biomarkers described above, reduced plasma Aβ42 and Aβ42:40 ratio were observed in AD patients showing positive correlations with levels in CSF (Janelidze *et al.*, 2016a, Nakamura *et al.*, 2018). Plasma t-tau levels were reportedly higher in AD cases compared to healthy controls, but showed weak or no correlation with CSF t-tau (Fossati *et al.*, 2019; Pase *et al.*, 2019, Barthélemy *et al.*, 2020). Increased plasma p-tau levels were also observed in AD patients and differentiated AD from other neurodegenerative disorders (Karikari *et al.*, 2020), and correlation with CSF p-tau levels was demonstrated (Barthélemy *et al.*, 2020; Palmqvist *et al.*, 2020). Studies also reported increased plasma NfL levels in AD patients compared to healthy controls (Gaiottino *et al.*, 2013; Mattsson *et al.*, 2017; Lewczuk *et al.*, 2018) and moderate correlation was observed between plasma and CSF levels of NfL in MCI and AD patients (Gaiottino *et al.*, 2013; Mattsson *et al.*, 2017; Osborn *et al.*, 2019). Studies on plasma neurogranin have not been as successful; no correlation was observed between CSF and plasma neurogranin (De Vos *et al.*, 2015; Kvartsberg *et al.*, 2015), implying its potential as an AD biomarker is limited to CSF.

1.1.5.4 Biomarker Panels

Utilising a combination of the core biomarkers, described above, can improve the diagnostic accuracy in comparison to using individual markers (Mattsson *et al.*, 2016; Hampel *et al.*, 2018). Several studies have also investigated the use of large biomarker panels, in CSF and blood, to diagnose AD or predict AD conversion from MCI. The panels included proteins associated with inflammation, dyslipidaemia or neurodegeneration, such as apolipoproteins, cytokines and chemokines, complement components and regulators, resulting in models that showed high levels of sensitivity and specificity (Ray *et al.*, 2007; O'Bryant *et al.*, 2010; Doecke *et al.*, 2012; Hye *et al.*, 2014; Morgan *et al.*, 2019). However, this remains an ongoing area of research to replicate and validate biomarkers for AD characterisation and prediction of AD progression.

The next section will introduce the protein that this project is focused on, TREM2, which, in its soluble form, has also been proposed as a potential biomarker for AD. These studies will be discussed further, as well as the reported effects of TREM2 on microglial modulation and the relevance of its AD-associated risk variants.

1.2 TREM2

1.2.1 TREM2 Expression and Location

The TREM family comprises a set of cell surface receptors of the immunoglobulin variable (IgV) superfamily expressed on a variety of cell types (Bouchon *et al.*, 2000). The TREM gene cluster is located on human chromosome 6p21.1 and mouse chromosome 17 (Klesney-Tait *et al.*, 2006) and the TREM family receptors share homology with each other and with a group of related receptors known as TREM-like transcripts (TLTs), listed in Table 1.1, that map to the same area of the genome (Washington *et al.*, 2002; Roe *et al.*, 2014). Region 6p21.1 is in close proximity to the human leukocyte antigen (HLA) locus, which harbours genes involved in immune response modulation and which was previously associated with AD risk via GWAS (Lambert *et al.*, 2013). One study recently reported specific haplotypes of the HLA classes I and II that may be involved in AD risk (Steele *et al.*, 2017) but the proximity of the TREM2 gene may also be a contributing factor to this association.

Gene	Species	Homology with TREM2
TREM1	Human	32%
Trem1	Mouse	26%
TREM2	Human	Not applicable
Trem2	Mouse	Not applicable
Trem3	Mouse	29%
Trem4	Mouse	No protein identified
Trem5	Mouse	No protein identified
NKp44	Human	28%
TREML1	Human	26%
Treml1	Mouse	28%
TREML2	Human	27%
Treml2	Mouse	27%
TREML3P	Human (pseudogene)	No protein identified
TREML4	Human	25%
Treml4	Mouse	30%
TREML5P	Human (pseudogene)	No protein identified
Treml6	Mouse	25%

Table 1.1 – Genes located in the human and mouse TREM clusters.
Genes encoding TREM, TREM-like (TREML) and natural killer p44 (NKp44) located in the TREM cluster are listed here, including the species they occur in (Vitale *et al.*, 1998; Chung *et al.*, 2002; Allcock *et al.*, 2003; Klesney-Tait *et al.*, 2006; Watarai *et al.*, 2008; Genua *et al.*, 2014; Roe *et al.*, 2014). Percentage homology relative to TREM2 protein (isoform 1) was compiled from the National Center for Biotechnology Information (NCBI): https://www.ncbi.nlm.nih.gov.

The gene encoding TREM2 is made up of five exons that express a 230-amino acid protein (Bouchon *et al.*, 2000; Li and Zhang, 2018). This is expressed on a subset of myeloid cells, including osteoclasts, macrophages, granulocytes, dendritic cells and microglia, and on tissue outside the CNS, such as the heart, kidney, liver and lungs (Schmid *et al.*, 2002; Turnbull *et al.*, 2006; Hickman and El Khoury, 2014; Sharif *et al.*, 2014; Jay *et al.*, 2015). The human and mouse proteins are 66% identical and 76% homologous to each other (Lessard *et al.*, 2018).

Homozygous loss-of-function mutations in the *TREM2* gene were first associated with Nasu-Hakola disease (NHD), also known as polycystic lipomembranous osteodysplasia with sclerosing leukoencephalopathy (PLOSL); a rare disease characterised by bone cysts, neurodegeneration and early onset dementia (Paloneva *et al.*, 2002). More recently, heterozygous variants of TREM2 were associated with increased risk of late onset AD, as will be discussed later in this chapter.

1.2.2 TREM2 Signalling

1.2.2.1 Structure and Ligand Binding

The full-length TREM2 protein comprises the N-terminus of an immunoglobulin-like domain, a transmembrane domain and a cytoplasmic tail lacking a signalling motif; there are two N-glycosylation sites in the immunoglobulin domain (Wunderlich *et al.*, 2013; Thornton *et al.*, 2017). A representation of the domains is depicted in Figure 1.3; the signal domain (residues 1-18) is removed during protein synthesis and maturation, the full length protein begins at residue 19; the enzyme involved during processing is not specified in the current TREM2 literature. Crystallography studies (Kober *et al.*, 2016) revealed that the structure of the TREM2 extracellular domain comprises nine β strands and two α-helix passages (Figure 1.4).

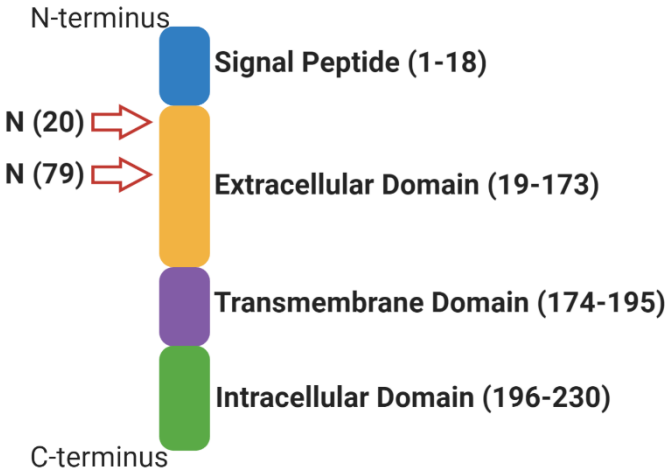

Figure 1.3 – Representation of TREM2 domains
TREM2 comprises an extracellular immunoglobulin-like domain, a transmembrane domain and an intracellular domain. The signal peptide represented here is removed during processing and the mature protein starts at residue 19. Two N-glycosylation sites (N) are present in the extracellular domain, indicated by arrows. Regions are marked by amino acid position. Figure modified from Thornton *et al.* (2017), Li and Zhang (2018); created with BioRender.com.

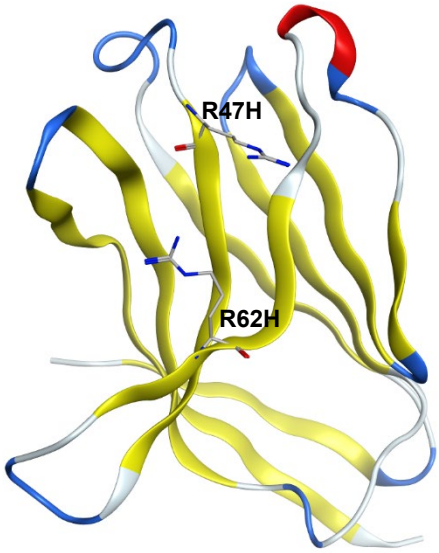

Figure 1.4 – Structure of TREM2 extracellular domain.
Structure of the TREM2 extracellular domain produced using Molecular Operating Environment (MOE) software (Chemical Computing Group) from the crystal structure (eLife, 2016). Secondary structure colours were used to display the nine β-strands in yellow and one of the α-helices in red. Positions of the two most common AD-associated risk variants, R47H and R62H, are indicated using the stick display style and can be seen along two of the central β-strands. Contributed by Georgina Menzies.

Although the endogenous ligands of TREM2 are not yet identified, *in vitro* studies have shown that TREM2 binds various ligands, including lipids (Cannon *et al.*, 2012), microbial products (Daws *et al.*, 2003) and lipoproteins, such as ApoE and clusterin (Atagi *et al.*, 2015; Bailey *et al.*, 2015; Yeh *et al.*, 2016). Jendresen *et al.* (2017) reported a TREM2-binding domain in human ApoE, and this interaction is thought to facilitate the microglial uptake of Aβ-lipoprotein complexes (Yeh *et al.*, 2016). More recently, two studies provided evidence that human and mouse TREM2 can interact directly with Aβ oligomers and suggested that this may mediate microglial migration and Aβ internalisation and degradation (Lessard *et al.*, 2018; Zhao *et al.*, 2018).

Interestingly, two of the suggested TREM2 ligands, ApoE and clusterin, are also among the strongest genetic risk factors for AD. As previously mentioned, ApoE is a carrier protein that plays a role in lipid and cholesterol transport and is the strongest known genetic risk factor for AD (Corder *et al.*, 1993; Karch and Goate, 2015). Clusterin is a chaperone molecule that is also involved in the regulation of brain cholesterol and lipid metabolism and in the regulation of the complement system (de Silva *et al.*, 1990; Jenne *et al.*, 1991; Tschopp *et al.,* 1993). The non-coding polymorphism rs11136000 in the clusterin (*CLU*) gene has recently been associated with AD (Harold *et al.*, 2009) but its exact functional effect remains unknown. Jackson *et al.* (2019) observed increased clusterin in AD brain homogenates and in synapses of AD brain compared to control samples. In synapses, this increase was greater in ε4 carriers compared to ε3 carriers and was also associated with increased synaptic Aβ. Clusterin can bind Aβ (Ghiso *et al.*, 1993; Zlokovic *et al.*, 1996) and, like ApoE, it is thought to be involved in the regulation of Aβ deposition (Matsubara *et al.*, 1996; DeMattos *et al.*, 2004).

The association of TREM2 with these two ligands indicates it may share a similar involvement in lipid metabolism. Ulland *et al.* (2017) demonstrated that TREM2 deficiency in an AD mouse model resulted in impaired signalling of mammalian target of rapamycin (mTOR), an important regulator of growth and metabolism. This was accompanied by a compensatory increase in autophagy, indicative of a defective metabolism. Together these results implicate a role for TREM2 in maintaining microglial metabolic fitness and suggest that lipid metabolism can account for AD risk, perhaps via modulating the response to Aβ deposition.

1.2.2.2 Signalling and Function

Following ligand binding, TREM2 can associate with tyrosine kinase binding protein (TYROBP), also known as DNAX-activation protein 12 (DAP12). This is a 12kDa protein that forms a disulphide-linked homodimer and associates with TREM2 via oppositely charged residues in their transmembrane domains (Bouchon *et al.*, 2000; Daws *et al.*, 2003). The cytoplasmic domain of DAP12 contains immunoreceptor tyrosine-based activation motifs (ITAMS) that are phosphorylated upon TREM2 ligand binding to recruit spleen tyrosine kinase (Syk) which in turn initiates phosphorylation and the activation of downstream signalling molecules (Takahashi *et al.*, 2005), including extracellular signal-regulated kinase (ERK), phosphoinositide 3-kinase (PI3K) and phospholipase Cγ (PLCγ)-dependent signalling pathways (Figure 1.5), (Takahashi *et al.*, 2005; Ford and McVicar, 2009; Mócsai *et al.*, 2010).

Functionally, TREM2 on microglia is involved in phagocytosis, proliferation, pro-inflammatory cytokine secretion and lipid sensing and metabolism (Takahashi *et al.*, 2005; Hickman and El Khoury, 2014; Wang *et al.*, 2015; Ulland *et al.*, 2017), and more recently has been shown to regulate microglial activity, suggesting that TREM2 expression reduces microglial inflammatory response and thus may have a protective role in the brain (Yeh *et al.*, 2016; Jendresen *et al.*, 2017; Zhong *et al.*, 2017; Lessard *et al.*, 2018; Zhao *et al.*, 2018).

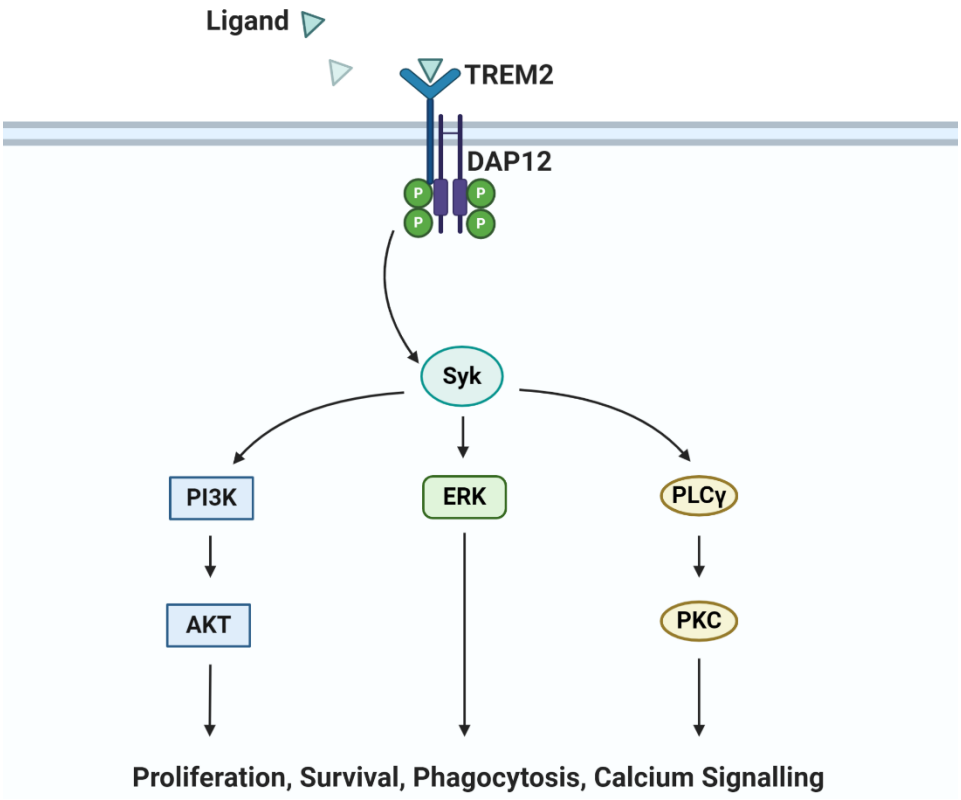

Figure 1.5 – Simplified TREM2 Signalling Pathway.
Ligand binding causes TREM2 to bind signalling adaptor DAP12, resulting in ITAM phosphorylation (P) to recruit Syk. This activates downstream signalling pathways, such as ERK, PI3K-AKT and PLCγ-protein kinase C (PKC). Figure modified from Konishi and Kiyama (2018), Yao *et al.* (2019); created with BioRender.com.

1.2.3 Soluble TREM2

1.2.3.1 Shedding of TREM2 ectodomain

TREM2 is predominantly localised in the Golgi complex and shuttles to and from the cell surface (Prada *et al.*, 2006; Wunderlich *et al.*, 2013). In addition to its role as a receptor, membrane-associated TREM2 can undergo proteolytic cleavage resulting in the release of a soluble form of TREM2 (sTREM2), which can be detected in plasma and cerebrospinal fluid (CSF) (Piccio *et al.*, 2008; Kleinberger *et al.*, 2014). A disintegrin and metalloproteinase domain-containing protein (ADAM) 10 and 17 have both been shown to cleave TREM2 at His157 (Kleinberger *et al.*, 2014; Feuerbach *et al.*, 2017; Schlepckow *et al.*, 2017; Thornton *et al.*, 2017). After shedding of the extracellular domain, there is a second cleavage step of the remaining C-terminal fragment (CTF) by γ-secretase (Wunderlich *et al.*, 2013; Glebov *et al.*, 2016), (Figure 1.6).

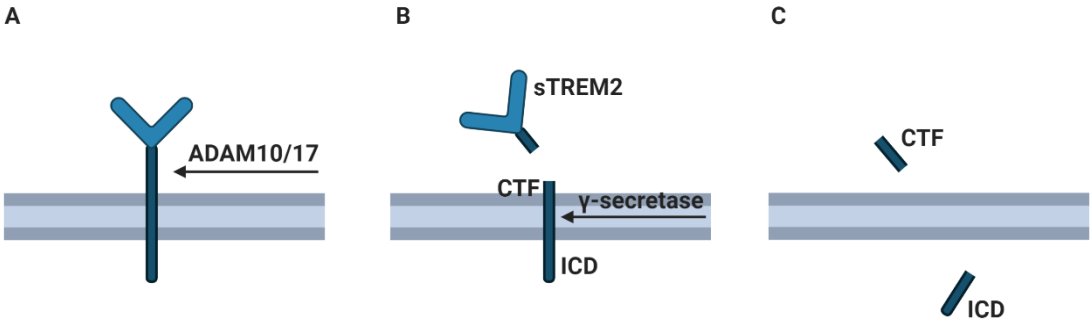

Figure 1.6 – Proteolytic cleavage of TREM2.
Shedding of the TREM2 ectodomain occurs by (A) proteolytic cleavage at amino acid position 157 to release the extracellular domain, followed by (B) sequential γ-secretase cleavage of the transmembrane region resulting in (C) the release of the C-terminal fragment (CTF) and intracellular domain (ICD). Figure modified from Schlepckow *et al.* (2017); created with BioRender.com.

The α-secretases ADAM10 and 17 are not limited to TREM2 and are associated with several substrates, one of which is APP. ADAM10/17 are key players in APP processing and are involved in the release of sAPPα as part of the non-amyloidogenic pathway (Endres and Deller, 2017). They have been implicated in AD risk and mutations in the ADAM10 prodomain have been reported to shift APP processing to favour the amyloidogenic pathway in an AD mouse model (Suh *et al.*, 2013).

Stimulating TREM2 ectodomain shedding was shown to result in increased levels of both sTREM2 and sAPPα in HEK293 cells (Schlepckow *et al.*, 2017). How ADAM10/17 activity in one protein relates to the other may hint at important implications for both processes. Importantly, the H157Y cleavage site of TREM2 coincides with an AD-associated polymorphism, which has been shown to accelerate the ADAM10/17-mediated shedding of sTREM2 resulting in less full length membrane-bound TREM2 (Schlepckow *et al.*, 2017; Thornton *et al.*, 2017). This could, for example affect the balance between amyloidogenic and non-amyloidogenic processing of APP, so investigating polymorphisms in TREM2, APP and ADAM10/17 relative to their processing outcome could be important in shedding more light on the mechanisms involved. The importance of γ-secretase in the signalling function of TREM2 was demonstrated in a study by Glebov *et al.* (2016); they showed that impaired γ-secretase activity led to the accumulation of CTFs in the membrane; this resulted in trapping of DAP12 at the membrane and hence less was available to bind full length TREM2 leading to reduced signalling. The same group also showed that

inhibiting γ-secretase led to a reduced level of TREM2-dependent phagocytosis in the murine microglial cell line BV2.

As previously described, γ-secretase is also involved in APP processing. The implications of γ-secretase inhibition in reducing TREM2 signalling may reflect the functional effect of TREM2 variants, resulting in the same partial loss of function. So while γ-secretase inhibition may be a potential strategy to reduce Aβ formation, it may have a detrimental effect on TREM2 function in AD. The use of γ-secretase inhibitors for the treatment of AD has already shown limitations as, similarly to ADAM10, γ-secretase is associated with several substrates and this multifunctionality makes it difficult to predict the impact of therapeutics targeting these enzymes, unless they can be used in a substrate-specific manner (Wolfe, 2014; Endres and Deller, 2017).

The generation of sTREM2 is also associated with alternative splicing of the gene resulting in an isoform lacking exon 4, which encodes the transmembrane domain (Schmid *et al.*, 2002; Jin *et al.*, 2014). A transcriptional study by Del-Aguila *et al.* (2019) predicted that 20-25% of sTREM2 could be due to the expression of this isoform but was unable to confirm this at the protein level as antibody-based tests cannot distinguish between proteolytic processing and alternative splicing.

The physiological function of sTREM2 is still unknown. Injection of sTREM2 into mouse brain resulted in inflammation and microglial activation (Zhong *et al.*, 2017). This could either be due to sTREM2 directly initiating an inflammatory response or perhaps more likely acting as a decoy receptor, where it competitively binds TREM2 ligands and inhibits TREM2 receptor anti-inflammatory function (Piccio *et al.*, 2008, Zhong *et al.*, 2017).

1.2.3.2 Soluble TREM2 levels in AD

Due to its presence in plasma and CSF, sTREM2 may have potential for use as a candidate biomarker for AD to indicate microglial dysfunction or neuroinflammation. However, more information is required regarding sTREM2 generation and function, both in the CNS and the periphery, to better understand the significance of the changes in sTREM2 levels observed in biological fluids.

Some studies reported increased sTREM2 in the CSF of AD patients (Heslegrave *et al.*, 2016; Piccio *et al.*, 2016), while others have shown decreased or unchanged levels (Kleinberger *et al.*, 2014; Henjum *et al.*, 2016). These contradictory results may

be linked to technical differences between the studies or differences in the stage of disease or types of assays and reagents used. One group that previously reported lower sTREM2 levels in AD samples (Kleinberger *et al.*, 2014) carried out a follow up study to investigate levels in the AD disease continuum, looking at healthy controls, preclinical AD, AD-associated MCI and dementia (Suárez-Calvet *et al.*, 2016). By comparing different stages of the disease, they observed significantly higher sTREM2 levels in MCI compared to the other stages, with the later stage of dementia showing levels that were not significantly higher than control groups. A meta-analysis followed this study and confirmed that sTREM2 levels pre-AD were consistently higher than in AD and control samples, further suggesting that sTREM2 levels may reflect microglial activation and disease progression in the early stages of the disease process (Liu *et al.*, 2018).

1.2.3.3 Correlations of Soluble TREM2

Levels of sTREM2 in CSF have been shown to positively correlate with age both in healthy controls and in AD patient groups (Piccio *et al.*, 2016; Brosseron *et al.*, 2018). Brendel *et al.* (2017) also observed a similar age dependent increase in sTREM2 levels in brain homogenates of wild type (C57BL/6) mice with more elevated levels in the amyloid mouse model PS2APP.

Associations between sTREM2 levels and core AD biomarkers, tau and Aβ42, were also investigated. Studies reported a positive correlation of sTREM2 levels with t-tau and p-tau in CSF (Henjum *et al.*, 2016; Heslegrave *et al.*, 2016; Suárez-Calvet *et al.*, 2016; Brosseron *et al.*, 2018; Suárez-Calvet *et al.*, 2019); however, this could be due to the age-dependent increase in both sTREM2 and total tau (Sjögren *et al.*, 2001b; Paternico *et al.*, 2012). Conflicting findings were reported for the link between sTREM2 and amyloid; some studies reported a positive correlation between CSF levels of sTREM2 and Aβ42 in controls but not in MCI and AD patients (Henjum *et al.*, 2016; Suárez-Calvet *et al.*, 2016), while other groups found no correlation (Heslegrave *et al.*, 2016; Brosseron *et al.*, 2018).

One study recently reported a positive association between plasma sTREM2 and NfL in AD and MCI patients (Ashton *et al.*, 2019), and another study in AD patients demonstrated that CSF sTREM2 positively correlated with neurogranin (Brosseron *et al.*, 2020). Plasma sTREM2 levels were also shown to positively correlate with the peripheral inflammation biomarker C-reactive protein (CRP) in AD and MCI patients, but CSF sTREM2 levels did not show this association (Bekris *et al.*, 2018). More

studies are required to assess the reproducibility of these individual studies, and caution must be exercised as differences between CSF and plasma sTREM2 may affect the interpretation of experimental findings. Elevated sTREM2 levels in CSF are not always reflected in plasma (Bekris *et al.*, 2018; Liu *et al.*, 2018; Ashton *et al.*, 2019), and since TREM2 expression is not limited to the CNS, BBB integrity may result in the diffusion of small quantities of TREM2 from the periphery into the CSF (Raha-Chowdhury *et al.*, 2019).

1.2.4 TREM2 and Microglial Function

The recent genetic association of TREM2 with AD, coupled with its expression on microglia, initiated several studies investigating the effects of TREM2 on microglial function. A phenotypic signature of disease-associated microglia (DAM) was recently described by Keren-Shaul *et al.* (2017), showing increased expression of genes related to phagocytosis and lipid metabolism. They reported the localisation of these microglia near AD plaques and proposed a two-step process for microglial activation; the first involving upregulation of a set of genes including *APOE* and *DAP12*, followed by a TREM2-dependent step involving upregulation of phagocytic and lipid metabolism genes. This was soon followed by a study looking into the mechanisms behind this activated form of microglia, which was also termed the microglial neurodegenerative (MGnD) phenotype (Krasemann *et al.*, 2017). This group suggested a role for the TREM2-ApoE pathway in regulating the switch in microglial phenotype from homeostatic to disease-associated and demonstrated that targeting the TREM2-ApoE pathway restored the microglial homeostatic state in AD mouse models. A recent transcriptomics study, investigating TREM2-sufficient and -deficient genotypes in an AD mouse model, showed upregulated DAM-associated genes in the wild type compared with the TREM2-deficient model, confirming that this phenotypic signature is indeed TREM2-dependent in mice (Zhou *et al.*, 2020). Importantly, this group also showed that microglia from the human AD brain, and from aged control brain, also display a disease-associated signature, but this is different from the DAM signature observed in mouse models.

1.2.4.1 Microglia in TREM2-deficient Mouse Models

Mouse models are important research tools to understand disease pathogenesis and to study the effects of disease-associated mutations. Transgenic and knockin/knockout AD models develop pathological characteristics, such as amyloid plaques or neurofibrillary tangles, and can display neurodegeneration and cognitive

defects, but no one model recapitulates all the features of AD (Hall and Roberson, 2012; Jankowsky and Zheng, 2017). Different models may develop varying levels of disease phenotypes at different rates, depending on factors such as the mutations expressed and the genetic variation between background strains (Li *et al.*, 2011; Jackson *et al.*, 2015; Neuner *et al.*, 2019). Findings derived from mouse models may not always be directly translated to human late onset AD, as this is a polygenic and multifactorial disease, but mouse models remain key tools for investigating the effects of AD risk genes and providing further information about the mechanisms of AD pathogenesis and potential therapeutic interventions (Hall and Roberson, 2012; Neuner *et al.*, 2019).

The use of TREM2-deficient mouse models, alone or crossed with AD models expressing APP, PSEN1 or MAPT transgenes, provides valuable insight into the potential effects of TREM2 on AD pathology. The types of AD mouse models mentioned throughout this chapter are detailed in Table 1.2 below, and the observations reported in the TREM2-deficient model and TREM2 overexpression studies discussed here are summarised in Table 1.3.

Mouse Model	Transgenes: Mutations	References
5XFAD	**APP**: Swedish (K670N/M671L), Florida (I716V), London (V717I) **PSEN1**: M146L, L286V	Oakley *et al.*, 2006
APP/PS1	**APP**: Swedish (K670N/M671L) **PSEN1*:*** L166P	Radde *et al.*, 2006
PS19	**MAPT:** P301S	Yoshiyama *et al.*, 2007
PS2APP	**APP**: Swedish (K670N/M671L) **PSEN2*:*** Volga German (N141I)	Ozmen *et al.*, 2009
APPswe/PS1dE9	**APP**: Swedish (K670N/M671L) **PSEN1**: deltaE9	Jankowsky *et al.*, 2001

Table 1.2 – *APP*, *PSEN* and *MAPT* mutations in AD mouse models.
Details of the mutations and transgenes expressed in mouse models commonly used to investigate AD pathology. *APP* and *PSEN* affect amyloid, while *MAPT* encodes tau proteins.

In TREM2-deficient mice (P18-20), a significantly lower number of morphologically ramified microglia was observed in the hippocampal region CA1 compared to wild type mice, indicating a lower level of microglial activation in the absence of TREM2 (Filipello *et al.*, 2018). In the same study, an increased spine density was also observed in hippocampal neurons *in situ* in TREM2-deficient mice, and *in vitro* in wild type neurons co-cultured with microglia from TREM2-deficient mice compared to wild type; these findings suggest that a role for TREM2 expression is implicated in the process of synapse elimination.

A second study investigated the effect of TREM2 on synapses using TREM2-deficient mice crossed with the APP/PS1 mouse model at the early-middle (2-6 months) and middle-late (6-10 months) disease stages. Interestingly, the study confirmed a role for TREM2 in increasing synaptic elimination, but only at the early-middle time point (Sheng *et al.*, 2019). The middle-late time point showed opposing results, which was replicated by Meilandt *et al.* (2020) on a different AD model (PS2APP) crossed with TREM2-deficient mice. This group reported that spine density loss was higher in the TREM2-deficient AD model at 6 months, suggesting that TREM2-dependent microglial activity has a neuroprotective role, if only at the middle-late disease stage in this model. Another study reported similar findings in 9-month-old transgenic APPswe/PS1dE9 mice, where overexpression of TREM2 was associated with increased levels of synaptophysin, a protein that is found in neuronal presynaptic vesicles, indicating reduced synaptic loss at this middle-late time point (Jiang *et al.*, 2014).

Regarding behaviour, Filipello *et al.* (2018) reported that 3-month-old TREM2-deficient mice showed altered social behaviour, excessive self-grooming and reduced performance in burying tasks compared to wild type mice but showed no difference in recognition and locomotor tasks. Another study (Kang *et al.*, 2018) also confirmed that TREM2 deficiency did not alter performance in recognition tasks, but no differences were observed in social behaviour between wild type and TREM2-deficient mice at six months. Spatial learning was significantly impaired in 5XFAD mice compared to wild types at 7 months old, but administration of sTREM2 to the 5XFAD mice significantly improved their performance (Zhong *et al.*, 2019). Overexpressing TREM2 in APPswe/PS1dE9 mice was reported to rescue spatial learning and memory at 7 months (Jiang *et al.*, 2014), but had no effect in aging mice at 18 months (Jiang *et al.*, 2017), suggesting that stage of disease in mice can affect the seemingly protective role of TREM2.

In studies involving TREM2-deficient mice crossed with the 5XFAD mouse model, the absence of TREM2 at an early age (4 months) was shown to impair the microglial response to Aβ with less microglial clustering observed at the plaque sites (Wang *et al.*, 2015; Wang *et al.*, 2016). Differences in plaque morphology (at 4 and 8 months) were also observed with diffuse, less compact plaque fibrils seen in TREM2-deficient models on the same AD background compared to wild types (Wang *et al.*, 2016; Yuan *et al.*, 2016). Another study replicated this finding in 6-month-old TREM2-deficient models using the PS2APP AD background (Meilandt *et al.*, 2020). However, one *in vivo* study reported the opposite finding where the overexpression of TREM2 resulted in less filamentous plaques (at 4 and 7 months) in the 5XFAD model (Lee *et al.*, 2018).

Several *in vitro* studies have shown that the ability to phagocytose apoptotic membranes and Aβ fibrils is significantly lower in microglia from TREM2-deficient compared to wild type mice (Takahashi *et al.*, 2005; Kleinberger *et al.*, 2014; Yuan *et al.*, 2016; Filipello *et al.*, 2018; Zhao *et al.*, 2018; Meilandt *et al.*, 2020). In the TREM2 overexpression study conducted by Lee *et al.* (2018), higher TREM2 levels in 5XFAD mice resulted in an upregulation of phagocytic markers *in vivo* and increased phagocytic capacity *in vitro*, the latter result also reported by another study investigating TREM2 overexpression in APPswe/PS1dE9 mice (Jiang *et al.*, 2014).

As previously discussed, impaired mTOR signalling and increased autophagy were reported in TREM2-deficient microglia from 5XFAD mice (Ulland *et al.*, 2017). The group suggested that while autophagy can enhance microglial clearance of Aβ, the impact of chronic defected mTOR signalling could affect the long-term ability of microglia to respond to Aβ deposition. Taken together, these results all demonstrate that TREM2 plays a key role in microglial metabolic fitness and in regulating microglial responses in the healthy brain and in AD.

A

Effect of TREM2 Deficiency	Mouse Model	Reference
Lower activated state of microglia	TREM2 KO PS2APP;TREM2 KO	Filipello *et al.*, 2018 Meilandt *et al.*, 2020
Less plaque-associated microglia	5XFAD;TREM2 KO	Wang *et al.*, 2015; 2016
Less compact plaque morphology	5XFAD;TREM2 KO and PS2APP;TREM2 KO	Wang *et al.*, 2016; Yuan *et al.*, 2016; Meilandt *et al.*, 2020
Decreased phagocytic capacity	TREM2 KO and 5XFAD;TREM2 KO	Takahashi *et al.*, 2005; Kleinberger *et al.*, 2014; Yuan *et al.*, 2016; Filipello *et al.*, 2018; Zhao *et al.*, 2018
Decreased Aβ degradation	TREM2 KO	Zhao *et al.*, 2018
Decreased synaptic loss (early stage)	TREM2 KO and APP/PS1;TREM2 KO	Filipello *et al.*, 2018 Sheng *et al.*, 2019
Increased synaptic loss (middle-late stage)	APP/PS1;TREM2 KO PS2APP;TREM2 KO	Sheng *et al.*, 2019 Meilandt *et al.*, 2020
Impaired mTOR signalling	5XFAD;TREM2 KO	Ulland *et al.*, 2017
Reduced social behaviour Reduced spatial learning	TREM2 KO 5XFAD	Filipello *et al.*, 2018 Zhong *et al.*, 2019

B

Effect of Overexpressed TREM2	Mouse Model	Reference
Less filamentous plaques	5XFAD	Lee *et al.*, 2018
Increased phagocytic capacity	5XFAD	Jiang *et al.*, 2014; Lee *et al.*, 2018
Decreased synaptic loss (middle-late stage)	APPswe/PS1dE9	Jiang *et al.*, 2014
Improved spatial learning and memory (no improvement in aging mice)	APPswe/PS1dE9	Jiang *et al.*, 2014, Jiang *et al.*, 2017

Table 1.3 – Effects of TREM2 deficiency and overexpression on AD pathology in mouse models.
The findings reported by studies on (A) *TREM2* KO mice, *TREM2* KO on AD backgrounds and (B) overexpressing TREM2 in AD mouse models are summarised, demonstrating the effect of TREM2 deficiency and overexpression on microglia, synaptic loss, amyloid plaques and behaviour.

1.2.5 TREM2 Variants in AD

1.2.5.1 AD-associated Variants

GWAS have recently identified rare coding variants of the *TREM2* gene associated with risk of late onset AD in populations of European and North American descent. The two most significant ones are R47H (rs75932628) (Guerreiro *et al.*, 2013; Jonsson *et al.*, 2013) and R62H (rs143332484) (Sims *et al.*, 2017); in each case the rare H variant is risk for AD. Although the prevalence of these variants is quite low in Caucasian populations, 0.3-0.6%, (Guerreiro *et al.*, 2013; Jonsson *et al.*, 2013), the relative risk of AD is high. The increased risk for heterozygous R47H carriers is around 3-fold, which is similar to that of the ε4 allele of the *APOE* gene, the strongest genetic risk factor for AD (Finelli *et al.*, 2015; Jay *et al.*, 2017). One study reported R47H to have an odds ratio of 2.92 in 8,888 controls in Iceland, compared to an odds ratio of 3.08 for APOE ε4 in the same individuals (Jonsson *et al.*, 2013). A replication cohort tested by the same study demonstrated an odds ratio of 2.83 for R47H in 2037 controls and 9727 AD cases in other European individuals. A second study reported an odds ratio for R47H of 4.5, and a lower odds ratio of 0.8 for R62H, in 1105 controls and 1091 AD cases of European and North American descent (Guerreiro *et al.*, 2013).

Yu *et al.* (2014) reported that the R47H variant was very rare in the Han Chinese population, and Jin *et al.* (2015) found no significant association of R47H with AD in an African-American population, but reported three TREM2 variants in linkage disequilibrium (L211P, T96K, W191X) that may instead be relevant to this population. These findings suggest that TREM2 risk variants (Table 1.4) can be differentially associated with AD, depending on ethnicity and genetic background, and highlight the importance of studying TREM2 variants in different populations. No protective variants of TREM2 have been reported to date.

Variant	Common Populations	Proposed Impact of Function	References
R47H	Caucasian	Impaired ligand binding and phagocytosis	Guerreiro *et al.*, 2013; Jonsson *et al.*, 2013; Wang *et al.*, 2015; Bailey *et al.*, 2015; Yeh *et al.*, 2016
R62H	Caucasian	Impaired ligand binding and phagocytosis	Jin *et al.*, 2014; Yeh *et al.*, 2016; Sims *et al.*, 2017
H157Y	Han Chinese	Increased shedding	Jiang *et al.*, 2016; Schlepckow *et al.*, 2017; Thornton *et al.*, 2017
N68K	Caucasian	Unknown	Guerreiro *et al.*, 2013
D87N	Caucasian	Impaired ligand binding	Guerreiro *et al.*, 2013; Yeh *et al.*, 2016
L211P*	African American	Unknown	Jin *et al.*, 2015
W191X	African American	Unknown	Jin *et al.*, 2015
T96K	African American	Increased ligand binding	Jin *et al.*, 2015; Kober *et al.*, 2016

Table 1.4 – Known TREM2 variants associated with increased AD risk.
Risk variants of TREM2, the populations they are commonly prevalent in and their suggested impact of function. *L211P is in linkage disequilibrium with T96K and W191X, but is likely to be the more functional of the three (Jin *et al.*, 2015).

TREM2 variants have also been implicated in other neurodegenerative diseases, including amyotrophic lateral sclerosis (ALS) (Cady *et al.,* 2014), frontotemporal dementia (FTD) and Parkinson's disease (PD) (Rayaprolu *et al.*, 2013; Borroni *et al.*, 2014); however other studies were unable to confirm a link between TREM2 variants and these diseases, particularly in relation to the R47H TREM2 variant (Lill *et al.*, 2015; Ayer *et al.*, 2019), making the risk association still unclear.

1.2.5.2 Variants R47H and R62H

Most of the TREM2 risk variants are found in the immunoglobulin-like domain, encoded by exon 2, and are therefore thought to affect ligand binding (Guerreiro *et al.*, 2013; Del-Aguila *et al.*, 2019). Only variants H157Y and L211P are located in exons 3 and 4 respectively, so likely exert a different impact on function, such as impaired protein maturation or shedding (Jin *et al.*, 2015; Del-Aguila *et al.*, 2019).

Kober *et al*. (2016) demonstrated structural differences between the TREM2 variants linked to NHD and those associated with AD. The side chains of the NHD risk variants are buried in the immunoglobulin fold and are likely to affect protein folding, leading to complete loss of function; whereas side chains of most of the AD risk variants (including R47H and R62H) are on the protein surface and are more likely to affect ligand binding, resulting in partial/selective loss of function. Evidence of impaired

ApoE and clusterin binding *in vitro* was indeed reported for the R47H and R62H variants (Wang *et al.*, 2015; Bailey *et al.*, 2015; Yeh *et al.*, 2016), including a reduction in clusterin internalisation and phagocytosis of Aβ complexes (Yeh *et al.*, 2016; Lessard *et al.*, 2018). The effect of these variants on ligand binding is important, particularly in relation to the reported role of TREM2 and ApoE in microglial activation as previously described (Keren-Shaul *et al.*, 2017; Krasemann *et al.*, 2017) and the potential interaction of TREM2 with ApoE and clusterin in lipid metabolic pathways.

Using transcriptomic analysis, Zhou *et al.* (2020) showed a lower expression of microglial genes in human brain tissue of R47H and R62H carriers, with the former showing a bigger impact on microglial response. A reduced ability to trigger microglial inflammatory responses was observed in R47H and R62H carriers (Zhong *et al.*, 2017), and a study investigating post mortem human AD brain samples reported decreased microglial numbers around compact plaques in R47H carriers (Yuan *et al.*, 2016).

Carriers of R47H, but not R62H, polymorphisms showed higher levels of CSF sTREM2 compared to non-carriers (Piccio *et al.*, 2016; Suárez-Calvet *et al.*, 2019) indicating increased shedding of the ectodomain in this variant, however the direct effect of the variant on proteolytic processing of membrane-bound TREM2 remains unclear.

Song *et al.* (2018) generated *TREM2* transgenic mice that expressed human TREM2 containing the R47H polymorphism. They reported that surface expression of TREM2 was similar in R47H-carriers and wild type mice, indicating no change in the shedding of the ectodomain between the two genotypes. They also showed lower microglial numbers and activation state in the R47H-carriers compared to wild type mice.

In order to detect and quantify the wild type and R47H/R62H variant proteins in human and mouse samples, specific monoclonal antibodies raised against these proteins would be valuable tools. Antibodies have long been in production for diagnostic and therapeutic applications and are a core part of the work in this thesis. The section below discusses antibody structure and function, and monoclonal antibody production in more detail.

1.3 Monoclonal Antibody Production

1.3.1 History of Antibodies

The earliest known reference to the activity we now ascribe to antibodies was in 1890 by Emil von Behring and Shibasabura Kitasato who published a study showing that serum from animals immunised against diphtheria contained a heat-stable factor that could be transferred to infected animals to treat the disease (von Behring and Kitasato, 1890). Around a decade later, the first model for an antibody (then referred to as anti-toxin) was proposed by Paul Ehrlich; he predicted a branched structure that could bind foreign bodies and activate the heat-labile serum bactericidal activity discovered and named “alexin” by Jules Bordet that Ehrlich re-named “complement” (Davies and Chacko, 1993; Kaufmann, 2008).

The recognition that antibodies generated by immunisation or infection with a pathogen in one animal could transfer specific immunity to another, termed passive immunisation, led to a lot of interest in its potential to treat human infectious diseases and is a re-emerging topic in the current pandemic. A serious disadvantage of using foreign serum as a treatment however was its toxicity, known as serum sickness, which occurred due to the generation of immune complexes against the foreign serum proteins in the circulation (Llewelyn *et al.*, 1992). This limitation was later overcome with the introduction of immunoglobulin preparations separated from normal immune human blood to treat early stage measles (Stokes *et al.*, 1944).

Shortly after the discovery of this passive immunisation, plasma cells were identified as the source of antibodies by Astrid Fagraeus in 1948 and the molecular structure of an antibody was published in landmark studies by Gerald Edelman and Rodney Porter independently in the 1960s (Fagraeus A, 1948; Edelman GM, 1959; Porter RR, 1959).

1.3.2 Structure and Function of Antibodies

Antibodies, or immunoglobulins (Igs), are heterodimeric glycoproteins consisting of two heavy and two light chains linked by disulphide bonds (Llewelyn *et al.*, 1992). The heavy chains contain one variable and three constant domains, while the shorter light chains contain one of each domain as illustrated in Figure 1.7. The variable domains provide two identical binding sites in the fragment antigen-binding (Fab) region, lending antibodies their variability and specificity, and this region connects via a

flexible hinge to the fragment crystallisable (Fc) region that recruits and activates the host's defence systems (Llewelyn *et al.*, 1992; Davies and Chacko, 1993).

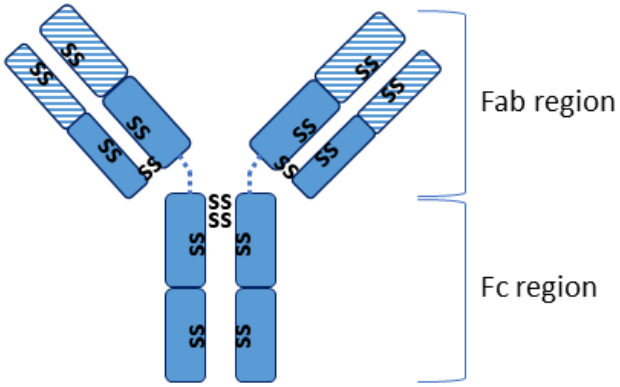

Figure 1.7 – Antibody monomeric structure
Antibody structure illustrating variable (striped) and constant (solid) domains linked by disulphide (SS) bonds. Dotted line represents hinge. Modified from Hoffman *et al*. (2016).

Plasma cells produce antibodies that are both expressed on the cell surface and secreted extracellularly to bind specific antigens (Hoffman *et al.*, 2016). Antibodies directly bind and neutralise target cells and opsonise them to initiate their removal by effector cells expressing Fcγ receptor (FcγR). The antibody-antigen complex can also activate the classical complement pathway leading to complement deposition on target cells, enhancing opsonisation and facilitating both phagocytic clearance and lysis (Llewelyn *et al.*, 1992; Hoffman *et al.*, 2016).

1.3.2.1 Antibody Isotypes

There are five classes, or isotypes, of antibodies; IgA, IgD, IgE, IgG, IgM, each consisting of distinct heavy chains differing in the Fc regions (Table 1.5) and κ or λ light chains.

IgA

IgA can be divided into two subclasses, where A1 contains a longer hinge region than A2. IgA is the major subclass found in mucosal secretions and its main role is protecting mucosal surfaces from pathogen invasion (Woof and Kerr, 2004). In plasma, IgA circulates in its monomeric form where it binds and neutralises antigens, but it can also exist as a dimer, trimer or tetramer in its secreted form; its polymers

linked by a polypeptide joining (J) chain (Johansen *et al.*, 2000; Schroeder and Cavacini, 2010).

IgD

Membrane-bound IgD is found on B cell surfaces while secreted IgD in serum has a short half-life and circulates at low levels (0.0001-0.2g/l), its role however is poorly understood (Llewelyn *et al.*, 1992; Levan-Petit *et al.*, 2000; Schroeder and Cavacini, 2010).

IgE

IgE is present in serum at a very low concentration ($5x10^{-5}$g/l) compared to the other subclasses and can bind FcγRI on cells, such as basophils, to induce a hypersensitivity response to allergens (Schroeder and Cavacini, 2010; Murphy, 2012).

IgG

IgG is the predominant immunoglobulin in human serum, ranging from 7-16g/l (Dati *et al.*, 2001), and which connects the adaptive and innate immune systems. It can be further divided into four subclasses, IgG1-IgG4, which differ in their effector functions and in their ability to bind both FcγR and C1q, the first component of the complement system (Llewelyn *et al.*, 1992; Hoffman *et al.*, 2016). IgG3 shows the highest affinity for C1q followed by IgG1 then IgG2, while IgG4 fails to bind C1q (Schroeder and Cavacini, 2010). IgG antibodies are responsible for secondary immune reactions and their effector functions depend on the types of antigen they bind, which in turn determines the subclass of antibody involved (Vidarsson *et al.*, 2014).

IgM

IgM is the first class of antibodies that is produced in a primary antibody response and can activate complement upon binding pathogens. It can be displayed on B cell surfaces as a B cell receptor (in monomeric form) but mainly exists as a pentamer in plasma, a structure which lends it a higher antigen-binding efficiency (Llewelyn *et al.*, 1992; Schroeder and Cavacini, 2010).

Isotypes	Subclasses	Heavy Chain	Mass (kDa)	Serum Concentration (g/l)
IgA	IgA1,2	$\alpha_{1,2}$	160, 160	0.5-3
IgD	-	δ	185	0.0001-0.2
IgE	-	ε	188	$5x10^{-5}$
IgG	IgG1,2,3,4	$\gamma_{1,2,3,4}$	146,146,165,146	7-16
IgM	-	μ	970	0.4-2.3

Table 1.5 – Isotypes of human antibodies.
The isotypes and characteristics of human antibodies (Llewelyn *et al*., 1992; Vladutiu, 2000; Schroeder and Cavacini, 2010; Murphy, 2012; Vidarsson *et al.*, 2014; Hoffman *et al*., 2016).

1.3.2.2 Class Switching

Plasma cells undergo antibody class switching after an activation event, such as infection or immunisation (Stavnezer *et al.*, 2008). Except for IgD expression, which is generated via alternative splicing of the IgM transcript, isotype switching of immunoglobulins occurs via class switch recombination (CSR) (Xu *et al.*, 2012). Repetitive DNA switch regions located upstream of the heavy chain constant genes guide activation-induced cytidine deaminase (AID) to the site. This leads to DNA breaks in the switch regions that remove the existing isotype gene, followed by end-joining recombination onto a new constant gene to allow for the expression of a new isotype (Li *et al.*, 2004; Xu *et al.*, 2012). The resulting isotype depends on the environment that the plasma cells are in during activation, and surrounding cells, such as T cells, produce cytokines to direct the class switch, resulting in a honed, effective immune response (Stavnezer *et al.*, 2008).

1.3.3 Monoclonal and Polyclonal Antibodies

1.3.3.1 Production of Polyclonal Antibodies

Polyclonal antibodies comprise a mix of antibodies that bind to different epitopes of the same target antigen (Busby *et al.*, 2016). This clonal diversity is an important feature of polyclonal antibodies as it makes them more sensitive in certain immunoassays and more likely to bind the target antigen even if some of the epitopes are compromised, such as in immunohistochemistry techniques (Ascoli and Aggeler, 2018).

Polyclonal antibodies are produced by immunising animals with the target antigen and retrieving their antiserum for purification (Delahaut, 2017). While this is a quick and low-cost method for antibody generation, it results in a unique batch of antibodies, which is a finite supply specific to each animal's immune response (Busby *et al.*,

2016). To overcome this limitation, the use of monoclonal antibodies results in specific and reproducible binding across batches, but their production is more costly and time consuming compared to that of polyclonal antibodies (Ascoli and Aggeler, 2018).

1.3.3.2 Production of Monoclonal Antibodies

Monoclonal antibodies (mAb) are antibodies that are generated by a single B lymphocyte clone; so that every molecule binds the same epitope (Liu, 2014). This is dependent on the clonal selection theory, which proposes that a clone originating from a single B cell expands and all clonal cells produce identical antibodies, (Burnet, 1957). Experimental evidence of this was later provided by Nossal and Lederberg (1958) confirming that one B cell produces only one antibody (Nossal and Lederberg, 1958).

The first successful hybrid formation of human and mouse cells was established in 1965 by Harris and Watkins, who used inactivated Sendai virus to fuse cells from the two species (Harris and Watkins, 1965). This significant observation later led to the development of the hybridoma technique to produce monoclonal antibodies in 1975 by Köhler and Milstein (Köhler and Milstein, 1975). The traditional production method involves immunising an animal with a specific antigen and retrieving antibody-producing plasma cells from the spleen. To enable these cells to grow in culture, they are fused in polyethylene glycol (PEG) with a myeloma cell line lacking the hypoxanthine-guanine-phosphoribosyltransferase (HGPRT) gene. The hybrid cells are immortal because of the myeloma component and continue to produce the plasma cell mAb. HGPRT deficiency allows for the use of a selective reagent in the culture medium, hypoxanthine-aminopterin-thymidine (HAT), which blocks *de novo* DNA synthesis and prevents the growth of myeloma cells that have not fused with (HGPRT-positive) plasma cells. Unfused plasma cells die spontaneously after a few days in culture and only the fused cells, or hybridomas, survive. Hybridomas are seeded to multi-well plates and grown; at this stage each well contains multiple clones so secreted antibodies are polyclonal in nature. Several limiting dilution cloning steps are necessary to acquire single clone derived cultures secreting mAb (Liu, 2014). At each cloning step, culture supernatants are retrieved for screening to identify clones of interest; monoclonal wells are then expanded to produce large quantities of antibodies.

Another method of mAb production is the phage display technique. This *in vitro* method involves the amplification of specific Ig variable domain gene sequences from

the cDNA of B lymphocytes and cloning them into a phage vector. This is then inserted into *E. coli* along with a helper phage to allow packaging of the phage DNA. Selection for mAb of interest involves panning of these phage libraries on the target antigen. Variable regions in specific phages identified in this way are cloned, sequenced and inserted into appropriate vectors for recombinant mAb production (Bazan *et al.*, 2012; Liu, 2014).

1.3.3.3 Monoclonal Antibody Uses

The development of mAb technology means that large amounts of reagents can be specifically generated against a wide range of antigens, lending mAb an important role in diagnostic and therapeutic applications.

In diagnostic settings, mAb can be used to test for the presence of specific pathogens or disease-associated antigens in human tissues and biological fluids (Payne *et al.*, 1988). The development of humanised mAb, where human antibody domains are fused with murine domains, began in the 1980s to improve the clinical efficacy of antibody therapies and to overcome unwanted immune reactions of the human body to unaltered murine antibodies (Morrison and Oi, 1989). The use of mAb as therapeutics relies on the ability of antibodies to bind specific antigens to either block or activate signalling pathways and effector mechanisms; they can also be used as drug delivery systems for treatment of specific cells and tissues (Berger *et al.*, 2002; Suzuki *et al.*, 2015).

1.3.4 Commercial TREM2 Antibodies

This section describes findings reported before or during the start of this project but does not include antibodies produced over the past year, the latter will be covered in the final chapter of this thesis. There are currently several commercial antibodies, raised against both human and mouse TREM2, that show varying degrees of success.

One of these, a human TREM2 antibody from R&D Systems (AF1828), was used in this project as a comparison for the performance of the in-house generated antibodies. The supplier documentation demonstrated the successful use of this antibody in western blots, ELISA and immunohistochemistry (IHC). However, a more in-depth look revealed that some studies have shown discrepancies in the apparent molecular weight of TREM2 in western blots using HEK293 cell lysates and human

brain tissue; each study showing different binding ranges for TREM2 (Kleinberger *et al.*, 2014; Lue *et al.*, 2015; Thornton *et al.*, 2017).

A comparative study by Satoh *et al.* (2013) investigated the binding of seven commercial anti-TREM2 antibodies to recombinant human TREM2 protein in western blots and reported TREM2 reactivity for only three of the antibodies: HPA010917 (Sigma-Aldrich), 2B5 (Novus Biologicals Inc.) and the AF1828 antibody (R&D Systems) used in this project. When these three antibodies were used to stain paraffin-embedded human brain, bone marrow and spleen tissue, only HPA010917 successfully labelled TREM2-expressing cells in these tissues. Taken together, these observations highlight the different reactivities of commercial antibodies and how this may, in part, result in some of the discrepancies seen between TREM2 findings across studies.

1.3.5 In-House Generated TREM2 Antibodies

The in-house antibodies described in this project were generated using the classical hybridoma technique, selected to bind human and mouse TREM2, then used to detect the native proteins in various settings as described in the chapters that follow.

The generation of mAb against TREM2 in this project included antibodies raised against human and mouse protein, in addition to mAb raised against peptides representing the risk-associated variants of TREM2, R47H and R62H. Although these variants display only one amino acid modification, the production of antibodies specific to these regions was attempted based on the success of previous studies (De Vito *et al.*, 1993; Mani and Cucurou, 1994; Yu *et al.*, 2007; Roblek *et al.*, 2010). Examples include the production of mAb that could differentiate between haemoglobins A and S (Stanker *et al.*, 1986) and between placental and germ-like alkaline phosphatases (Hoylaerts and Millán, 1991), with one study from the host lab that generated antibodies against the Y402H polymorphism in the complement regulator factor H (Hakobyan *et al*., 2008). These studies were likely able to achieve this specificity as single residue substitutions are often associated with conformational changes, resulting in a detectable difference between the two proteins (De Vito *et al.*, 1993; Mani and Cucurou, 1994).

The benefits of having antibodies against TREM2 variants are that they can be used to set up variant-specific ELISAs for the simple and rapid screening of biological fluids in AD cohort studies. This could provide additional demographic information for

existing AD patients and could also function as a risk predictor in longitudinal studies to identify whether healthy controls and MCI patients carrying the variants convert to an AD diagnosis. The antibodies could also be used to investigate functional aspects of TREM2, such as testing the effects of the antibodies on the reduced ligand binding reported in variant TREM2 studies. While the prevalence of TREM2 variants is relatively low, its associated high risk of AD makes it important to learn more about TREM2 function overall and about the mechanistic differences between wild type and variant TREM2 proteins.

1.4 Aims and Objectives

The overarching hypothesis underpinning this thesis is that AD-associated variants in TREM2 impact function by altering expression or ligand binding. The specific aims are:

1. To develop a panel of monoclonal antibodies (mAb) against human and mouse TREM2;
2. To characterise the mAb for binding to native TREM2 using western blotting, flow cytometry and microscopy;
3. To identify complementary pairs of antibodies and use them to develop enzyme-linked immunosorbent assays (ELISAs) for quantification of soluble human and mouse TREM2;
4. To measure soluble TREM2 levels in biological fluids from relevant patient cohorts and from animal models;
5. To develop novel mAb specific for the R47H and R62H TREM2 variants

There is currently a lack of good quality reagents that can detect and quantify TREM2 on cells and tissues and in biological fluids in both human and animal systems as described in this chapter; this project will address this gap by developing in-house monoclonal and polyclonal antibodies against TREM2 and a sensitive ELISA to measure soluble TREM2 in mouse and human plasma. The development of mAb against TREM2 variants will enable the specific detection and quantification of the mutant proteins in biological fluids, on cells and in tissues.

Chapter 2

Materials and Methods

2 Materials and Methods

Details and sources of all the reagents used in this project are listed in Appendix I.

2.1 Cell Culture

2.1.1 General Culture Conditions

All cell culture was carried out under aseptic conditions and cells were regularly tested throughout the duration of the project to ensure they remained mycoplasma negative. Cell lines were maintained in 75cm^2 flasks in a humidified incubator at 37°C with 5% CO_2. Fetal bovine serum (FBS, Gibco, ThermoFisher Scientific) was heat inactivated at 56°C for 30 minutes and 0.22µm-filtered before use. Roswell Park Memorial Institute (RPMI) 1640 medium, Dulbecco's Modified Eagle medium (DMEM)-F12, Hank's Balanced Salt Solution (HBSS), Phosphate Buffered Saline (PBS) and non-essential amino acids (NEAA) were obtained from Gibco, ThermoFisher Scientific. Eagle's Minimum Essential Medium (EMEM), dimethyl sulfoxide (DMSO), L-glutamine, penicillin-streptomycin and sodium pyruvate were all obtained from Sigma-Aldrich, Merck. All centrifugal spin steps were carried out at 1500rpm for 5 minutes unless otherwise specified.

2.1.2 Cell Cryopreservation and Recovery

To maintain cell stocks in liquid nitrogen, cells that reached a 70% confluency were spun down and the supernatant was aspirated. Cell pellets were resuspended in freezing medium (FBS + 10% DMSO) and aliquoted into cryovials as 10^6 cells in 1ml volumes. The vials were then placed in a specialised cell-freezing container at -80°C overnight before being transferred into liquid nitrogen tanks for long term storage.

When required, cells were quickly defrosted by immersion in a 37°C water bath until thawed, diluted in the appropriate medium and spun down. The cell pellet was resuspended in fresh medium then seeded into a 25cm^2 flask.

2.1.3 Cell Counting and Viability

Cell viability and quantification were carried out using a Neubauer Bright-Line haemocytometer. Trypan blue differentiates between live and dead cells by dye exclusion as it stains dead cells blue, while live cells with intact membranes remain clear in appearance. Only samples with a cell viability of 95% or higher were used for lysate preparations and flow cytometry experiments.

To quantify the number of cells/ml, cells were diluted 1 in 10 using 0.4% trypan blue solution (Hyclone, Fisher Scientific), pipetted onto the counting chamber and viewed using a Zeiss Primovert light microscope (Carl Zeiss, Fisher Scientific). Cells were counted in each of the four main corner squares of the haemocytometer grid and the calculation below was applied:

$$\text{Cells/ml} = \frac{\text{Total number of cells counted x dilution factor}}{\text{Number of squares}} \times 10{,}000$$

2.2 Cell Lines

Human Embryonic Kidney (HEK) 293 cells (CRL-1573) were obtained from ATCC. RAW264.7 and THP1 cell lines were kindly provided by Professor Philip Taylor, Cardiff University, UK. Passage numbers were monitored for all lines and cells used for antibody characterisation did not exceed a maximum of 20 passages to ensure reproducibility between experiments (Park *et al.*, 2004; Aldo *et al.*, 2013; Taciak *et al.*, 2018).

2.2.1 RAW264.7

RAW264.7 is an adherent murine macrophage-like cell line, produced by tumour induction in male BALB/c mice using Abelson Leukaemia Virus (A-MuLV), (Raschke *et al.*, 1978). RAW264.7 cells express CD11b, CD11c, CD86 and CXCR4 (Taciak *et al.*, 2018; Tian *et al.*, 2019) and were selected for antibody characterisation in this project due to their expression of TREM2 (Humphrey *et al.*, 2006; Kober *et al.*, 2016). The cells were cultured in RPMI supplemented with 10% FBS, 50 Units penicillin, 50µg/ml streptomycin, 1mM sodium pyruvate and 2mM L-glutamine. They were sub-cultured every 2-3 days by using a cell scraper to detach them from the flask surface and spun down before being seeded at 1:10 into fresh flasks.

2.2.2 HEK293

HEK293 is an adherent human epithelial cell line transformed using adenovirus type 5 DNA (Graham *et al.*, 1977). Due to their high transfection efficiency and reliable protein translation and processing, HEK293 cells are a popular choice for use as a protein expression host (Thomas and Smart, 2005; Ooi *et al.*, 2016). They were used in this project for the expression of wild type and variant TREM2 to further

characterise the binding of the in-house generated antibodies. The cells were grown in EMEM containing 1% non-essential amino acids (NEAA) and supplemented as above. They were sub-cultured every 4 days by discarding the media, washing once with PBS and incubating in Trypsin-EDTA (0.05%) at 37°C for 3-5 minutes. Once cells became detached, an equal volume of 10% FBS-RPMI was added to neutralise the trypsin and the cells were spun down and seeded at 1:10 in fresh complete EMEM medium.

2.2.3 THP1

THP1 is a non-adherent human cell line cultured from a patient with acute monocytic leukaemia (Tsuchiya *et al.*, 1980) and is used as a model to study monocyte and macrophage activities. THP1 cells express CD11b and CD14, although the latter varies in expression levels even in unstimulated cells (Aldo *et al.*, 2013; Bosshart and Heinzelmann, 2016). These cells were selected for antibody characterisation as they also endogenously express TREM2 (Allcock *et al.*, 2003; Turnbull *et al.*, 2006). THP1 cells were cultured in RPMI containing 50μM β-mercaptoethanol (ThermoFisher Scientific) and supplemented as above. Cells were sub-cultured every 4 days by spinning down and resuspending in fresh medium at a ratio of 1:20, cells were always maintained below 10^6 cells/ml.

2.3 Animals

All animal procedures in this project were performed under the United Kingdom Home Office licences 3003120 and PF4167C0A in accordance with the 1986 Animals (Scientific Procedures) Act guidelines. Animals were housed at Cardiff University's JBIOS facility in conventional cages grouped according to genotype, under standard pathogen-free conditions, with a 12-hour light/dark cycle and access to chow and water *ad libitum*. TREM2 knockout (KO) mice were kindly provided by the St. George-Hyslop laboratory, Cambridge Institute for Medical Research, UK. Their strategy for generating TREM2 KO mice involved targeted homologous recombination to delete exons 1 and 2, thus removing the start codon and most of the extracellular IgG domain. Mice were matched by age and gender where possible using the C57BL/6J strain to represent wild type (WT) mice in experiments. One young adult New Zealand White rabbit was used for anti-TREM2 polyclonal antibody production, immunisation details are described in Section 2.7. Animals were culled by asphyxiation with a slow

rising concentration of CO_2 followed by dislocation of the neck unless otherwise specified.

2.4 Isolation and Immunostaining of Primary Monocytes

2.4.1 Monocyte Preparation

The method used for isolating primary monocytes from mouse brain was modified from Grabert and McColl (2018). Unless otherwise specified, all spin steps were conducted in a 4°C centrifuge at 1500rpm for 5 minutes, without a brake during deceleration. HBSS without calcium or magnesium was used for the washes and all manual steps were carried out on ice.

2.4.1.1 Brain Homogenisation

Prior to isolation, a 96-well micro-clear bottom plate (CELLSTAR, Greiner) was coated with 0.1mg/ml poly-L-lysine (Sigma Aldrich, Merck) and incubated at 37°C overnight. WT and TREM2 KO 11-week old mice were terminally anaesthetised, exsanguinated then perfused with cold PBS. Whole brains were then extracted and finely minced in ice-cold HBSS. These were spun down before removing the supernatant and replacing with enzyme mix 1 of the Neural Tissue Dissociation Kit (P) (NTDK, Miltenyi Biotec). The brains were transferred to gentleMACS C tubes (Miltenyi Biotec) and mixed with enzyme mix 2 of the same kit. The tubes were then loaded onto the gentleMACS Octo Dissociator with heaters (Miltenyi Biotec) and rotated at 37°C for 15 minutes to allow for enzymatic dissociation and homogenisation.

2.4.1.2 Myelin Removal and Bead Separation

After homogenisation, the brains were transferred into centrifuge tubes and spun down. The supernatant was removed and pellets were resuspended in 35% isotonic Percoll (GE Healthcare). HBSS was overlaid onto the Percoll and the tubes were spun at 2050rpm (4°C) for 30 minutes. The myelin-containing supernatant was removed before resuspending the pellet in HBSS and spinning down as initially described. After aspirating the supernatant, cell pellets were resuspended in MACS Separation Buffer (Miltenyi Biotec) and loaded onto the auto MACS pro (Miltenyi Biotec). This is an automated cell sorting system that separates cells using magnetic beads, in this case CD11b microbeads (Miltenyi Biotec). CD11b-sorted fractions were

spun down and cells were resuspended in plain DMEM-F12 and counted as described in Section 2.1.3.

Before plating out the cells, the poly-L-lysine coated plate (Section 2.4.1.1) was washed twice in HBSS and once in plain DMEM-F12 then allowed to dry. Cells were plated out at a density of 5 x 10^5/ml in DMEM-F12 containing 50 Units Penicillin-50µg/ml Streptomycin, 10% FBS, 10ng/ml macrophage colony-stimulating factor (MCSF) and 50ng/ml transforming growth factor-β1 (TGF-β1), then incubated for 7 days with a 50% medium change at day 3.

Isolation techniques are fraught with consequences affecting microglial activation status; a limitation of this technique is the use of serum, which has been shown to strongly alter microglial morphology and function (Bohlen *et al.*, 2017). This must be taken into consideration as activating the isolated microglia in this way may affect their surface expression of TREM2 and other receptors. The use of serum-free medium can circumvent this issue, but the inclusion of astrocyte-conditioned medium would be required to provide the necessary survival and growth factors (Bohlen *et al.*, 2017).

2.4.2 Immunofluorescent Staining of Monocyte Preparation

Cells were fixed in the culture plate in 4% paraformaldehyde (PFA; Sigma-Aldrich, Merck) for 15 minutes then washed twice in 1X PBS. The cells were blocked using 5% goat (Vector Laboratories), corresponding to host species of secondary antibodies used, in PBS containing 0.5% Triton X-100 (Sigma-Aldrich, Merck) for 1 hour. They were probed with 5µg/ml α-TREM2 mAb 9D10 and co-stained with a polyclonal antibody (1:1000) against the macrophage/microglial marker ionized calcium binding adaptor molecule 1 (IBA1, Wako, Alpha Laboratories) for 1 hour. The cells were washed twice before the addition of fluorescently-labelled secondary antibodies (ThermoFisher Scientific) for 1 hour in the dark: 2µg/ml Alexa Fluor 568 goat anti-mouse IgG for mAb 9D10, 4µg/ml Alexa Fluor 488 goat anti-rabbit IgG for anti-IBA1. Two more washes were carried out before the addition of the Hoechst (ThermoFisher Scientific) nuclear counterstain (1µg/ml) for 10 minutes. After a final wash, cells were imaged using a Leica DMi8 microscope (Leica Microsystems, UK).

2.5 Immunostaining of Cell Lines and Mouse Brain Sections

Cryopreserved mouse brain tissue (20µm sagittal sections) from WT and TREM2 KO mice, provided by Megan Torvell, were fluorescently stained using mAb 9D10 and 8G10, and THP1 and RAW264.7 cell lines were stained alongside for comparison using the in-house polyclonal antibody and mAb 9D10.

Human THP1 cells were prepared, on the day of staining, by spinning down 50,000 cells onto Superfrost Plus glass slides (ThermoFisher Scientific) for 5 minutes at 1000rpm using cytofunnel chambers (Shandon Double Cytofunnel, ThermoFisher Scientific) in a Cytospin 4 Cytocentrifuge (ThermoFisher Scientific). The desired staining area was marked using a hydrophobic pen (VWR) and cells were washed in 1X PBS before fixing in 4% PFA for 10 minutes at room temperature. One day prior to staining, mouse RAW264.7 cells were seeded onto 15mm thick coverslips (VWR) at 10^5 cells/coverslip and incubated overnight.

For polyclonal antibody staining, THP1 and RAW264.7 cells were washed twice in 1X PBS and blocked for 1 hour using 10% goat serum (Vector Laboratories). Cells were then probed with 20µg/ml α-TREM2 polyclonal antibody in block solution overnight, then washed three times and incubated with 2µg/ml Alexa Fluor 488 goat anti-rabbit IgG (ThermoFisher Scientific) for 1 hour in the dark. After three washes, cells were stained with the Hoechst (ThermoFisher Scientific) nuclear counterstain (1µg/ml) for 10 minutes. The cells were washed three times and coverslips were placed over the glass slides using FluorSave mounting medium (Sigma Aldrich, Merck). Z stack images were created and maximum projected using a Zeiss Cell Observer spinning disc confocal (Carl Zeiss Ltd., UK) and Zen 2 (blue edition) software (Carl Zeiss Microscopy).

For mAb 9D10 and 8G10 staining, all cells were washed twice in 1X PBS and brain tissue sections, from WT and TREM2 KO mice, were hydrated in 1X PBS. THP1 cells were blocked using 10% goat serum (Vector Laboratories) for 1 hour. To block endogenous mouse IgG in mouse brain tissue and RAW264.7 cells, a mouse-on-mouse (MOM) peroxidase immunodetection kit (Vector Laboratories) was used; samples were blocked in MOM mouse IgG blocking reagent for 1 hour followed by two washes and a 5 minute incubation in MOM diluent (protein concentrate) as per manufacturer's instructions. Samples were incubated in 10µg/ml α-TREM2 mAb diluted in block solution overnight, then washed three times before secondary

antibody incubations for 1 hour in the dark. THP1 cells were incubated in Alexa Fluor 488 goat anti-mouse antibody (ThermoFisher Scientific). Mouse tissue and RAW264.7 cells were incubated in MOM biotinylated anti-mouse IgG for 1 hour as per manufacturer's instructions, followed by three washes and incubating in 2µg/ml Alexa Fluor 488 streptavidin (ThermoFisher Scientific) for 1 hour. Samples were then washed three times, Hoechst-counterstained and imaged as described above.

Biotinylated mAb 9D10 staining was trialled on mouse brain tissue for comparison with staining using unlabelled mAb 9D10. Tissue stained with biotinylated mAb underwent an additional step to block endogenous biotin, before using the MOM immunodetection kit. This involved incubation in avidin for 15 minutes, followed by two 1X PBS washes then incubation in biotin for 15 minutes, as per manufacturer's instructions for the avidin/biotin blocking kit (Vector Laboratories).

2.6 Generation of TREM2-expressing Cell Lines

2.6.1 Plasmid Preparation

Four plasmids (pcDNA3.1(+), Genscript) were designed containing ampicillin and neomycin resistance genes and the DNA sequences of either human (wild type or variants 47H, 62H) or mouse TREM2 (Figure 2.1).

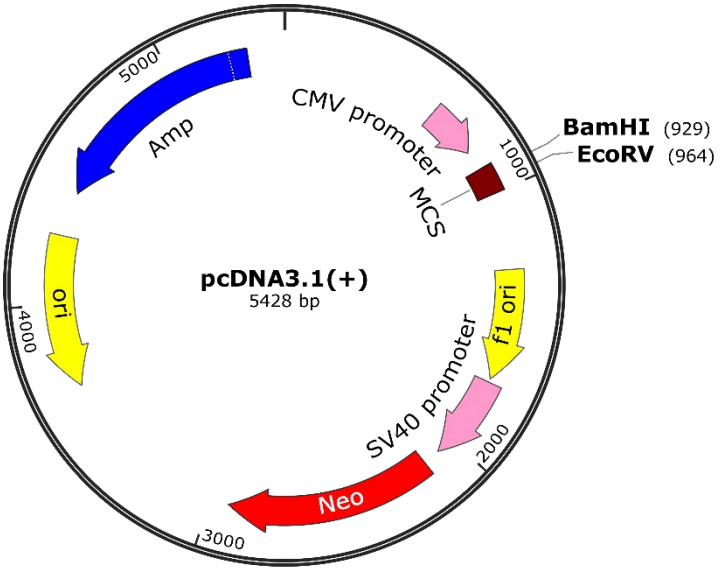

Figure 2.1 – Plasmid design for generation of TREM2-expressing cell lines.
TREM2 sequences were inserted in the pcDNA3.1(+) plasmid; containing restriction enzymes BamHI and EcoRV in the multiple cloning site (MCS), origins of replication (ori), cytomegalovirus (CMV) and simian virus 40 (SV40) promoters and resistance genes against ampicillin (Amp) and neomycin (Neo). Figure created with SnapGene Viewer 4.3.4.

Each plasmid (10ng) was added to a vial of 50ul Subcloning Efficiency™ DH5α™ Competent Cells (ThermoFisher Scientific). The cells were incubated on ice for 30 minutes and were heat-shocked at 42°C for 20 seconds before incubating on ice for a further 2 minutes. Pre-warmed Super Optimal broth with Catabolite repression (SOC) medium (ThermoFisher Scientific) was added to the cells and incubated with shaking at 37°C, 225rpm, for 1 hour. Cells were spread at neat concentrations and at 1 in 10 dilutions on LB plates containing 100µg/ml ampicillin (Sigma-Aldrich, Merck) then incubated at 37°C overnight.

Colonies were selected and incubated with shaking in ampicillin-containing LB broth at 37°C, 225rpm, overnight and glycerol stocks of the bacterial cultures were prepared and stored at -80°C. Plasmid purification of the remaining cultures was carried out using a Maxiprep kit (Qiagen) as per the manufacturer's instructions. DNA concentrations were measured (DeNovix DS-11 FX+ spectrophotometer, Cambridge Bioscience) and purified plasmids were stored at -20°C.

2.6.2 Antibiotic Killing Assay

Before transfection, a killing assay was performed to select the appropriate antibiotic concentration. HEK293 cells were plated at 0.25 x 10^6 cells/well in a 6-well plate and incubated to reach 80% confluence prior to the addition of the neomycin analogue G418 sulfate (Geneticin, Gibco, ThermoFisher Scientific) at a range of concentrations (0, 200, 400, 600, 800, 1000µg/ml) in plain RPMI medium containing 10% FBS. Medium (containing G418 sulfate) was replaced every two days and cells were monitored daily to determine the lowest antibiotic concentration that would kill non-transfected cells.

2.6.3 Stable Vector Transfection

For each plasmid, cells were seeded at 0.25 x 10^6 cells/well in a 6-well plate and incubated to reach 70% confluence. Lipofectamine 3000 (Invitrogen, ThermoFisher Scientific) was diluted in Opti-MEM medium (Gibco, ThermoFisher Scientific) and, in separate tubes, plasmid DNA was combined with the accompanying P3000 transfection reagent in Opti-MEM medium as seen in Table 2.1. The two mixes for each well were combined in a 1:1 ratio and incubated at room temperature for 15 minutes then added dropwise to the cells and incubated at 37°C for 24 hours. The

transfection medium was then replaced with fresh complete medium for another 24 hours.

G-418 sulfate was added to the cells at the previously determined concentration in 10% FBS-RPMI. Cells were maintained under antibiotic selection until non-transfected cells were eliminated. Colonies of cells containing the plasmid were transferred to fresh plates and expanded for use in flow and western blot experiments.

Well	Lipofectamine mix	DNA/P3000 mix
No plasmid, no lipofectamine	0	0
No plasmid, lipofectamine	3.75µl lipofectamine	0
Plasmid, no lipofectamine	0	2.5µg DNA + 2µg P3000/µl of DNA
Plasmid, 3.75µl lipofectamine	3.75µl lipofectamine	2.5µg DNA + 2µg P3000/µl of DNA
Plasmid, 7.5µl lipofectamine	7.5µl lipofectamine	2.5µg DNA + 2µg P3000/µl of DNA

Table 2.1 – Transfection reagents used for generation of TREM2-expressing cell lines. Lipofectamine and plasmid DNA mixes diluted in equal volumes of Opti-MEM medium for transfection.

2.7 Nucleic Acid Amplification

2.7.1 Quantitative Polymerase Chain Reaction

The quantitative polymerase chain reaction (qPCR) method was used to investigate gene expression levels in cell lysates. Lysis of cell pellets and ribonucleic acid (RNA) extraction were carried out using RNeasy Mini Kit (Qiagen) as per manufacturer's instructions. RNA absorbance levels were measured at 260nm and concentrations were calculated using a DeNovix DS-11 FX+ spectrophotometer (Cambridge Bioscience). Absorbances at 230nm and 280nm were also measured to check RNA purity using 260/280 and 260/230 ratios; 260/280 ratios indicated whether the extracted RNA was free from proteins that absorb close to 280nm, 260/230 ratios were used as a secondary measure to test for the presence of other contaminants that absorb at 230nm (Gallagher, 2001; Desjardins and Conklin, 2010). Extracted RNA was stored at -80°C until required.

Reverse transcription was performed using the high capacity RNA to complementary deoxyribonucleic acid (cDNA) kit (Applied Biosystems, ThermoFisher Scientific). Master mixes were prepared as per manufacturer's instructions and incubated with 2µg RNA at 37°C for 1 hour, then 95°C for 5 minutes, on a Mastercycler Nexus GSX1 system (Eppendorf, Merck). The National Center for Biotechnology Information (NCBI) tool Primer-Basic Local Alignment Search Tool (Primer-BLAST, Ye *et al.*, 2012) was used for qPCR primer design. Primers were designed to contain a 40-60% GC content and with no more than a 3° difference in melting temperatures between each primer pair. Importantly, primers were ensured to span an exon-exon junction to avoid the amplification of contaminating genomic DNA in the samples. Primers were screened to check that they were specific to the desired target to avoid amplification of pseudogenes. Sequences of all primers (Sigma-Aldrich, Merck) used are detailed in Table 2.2.

Primer	Sequence (5'-3')
Human TREM2 – Forward	TCTCCGGCTGCTCATCTTAC
Human TREM2 – Reverse	TCATAGGGGCAAGACACCTG
Mouse TREM2 – Forward	CAGTGTCAGAGTCTCCGAGG
Mouse TREM2 – Reverse	CACAGGATGAAACCTGCCTGG
Mouse 18S – Forward	CCCAGTAAGTGCGGGTCAT
Mouse 18S – Reverse	CCGAGGGCCTCACTAAACC
Human GAPDH – Forward	TGCACCACCAACTGCTTAGC
Human GAPDH – Reverse	GGCATGGACTGTGGTCATGAG

Table 2.2 – Primers used in real-time PCR amplification.
Sequences of the primers used for the cDNA amplification of cell lysates, including housekeeping genes 18S and Glyceraldehyde-3-Phosphate Dehydrogenase (GAPDH).

Reaction qPCR mixes were prepared on ice using 1X PowerUp SYBR Green master mix (Applied Biosystems, ThermoFisher Scientific) and 0.5µM primers targeted against human or mouse TREM2 (Sigma-Aldrich, Merck). Mixes were distributed in triplicates into MicroAmp Fast Optical 96-well plates (Applied Biosystems, ThermoFisher Scientific) and cDNA was added. Additional mixes were prepared by substituting TREM2 primers with primers against the housekeeping genes, 18S and Glyceraldehyde-3-Phosphate Dehydrogenase (GAPDH). Positive controls containing TREM2-expressing cell lines (THP1, RAW264.7) and negative controls lacking cDNA were included. The samples were amplified using a QuantStudio7 Real-Time PCR System (Applied Biosystems, ThermoFisher Scientific) under the following thermal

protocol: (1) 50°C for 2 minutes, 95°C for 10 minutes; (2) 40 cycles of 95°C for 15 seconds, 60°C for 1 minute; (3) 95°C for 15 seconds, 60°C for 1 minute, 95°C for 15 seconds.

Analysis was conducted using QuantStudio Real-Time PCR Software v1.3. To compare cycle threshold (Ct) values between samples relative to the housekeeping gene, amplification curves were analysed using the following double delta (2^ΔΔCt) formula (Pfaffl, 2001):
Expression fold change = 2^ - [(Experimental TREM2 Ct-housekeeping Ct) - (Control TREM2 Ct-housekeeping Ct)]
where 'experimental' represents the tested samples and 'control' represents the sample used as a reference, for example a wild type or untreated sample.

2.7.2 Genotyping PCR

The TREM2 KO and matched WT mice were genotyped using mouse TREM2 primers (Sigma-Aldrich, Merck) yielding a 2357 base pair (bp) product in the presence of TREM2. Samples were also genotyped for CX3CR1, a chemokine receptor expressed on the surface of monocytes, to demonstrate the successful extraction of DNA; primers for CX3CR1 (Sigma-Aldrich, Merck) yield a 410bp product. As previously described, PCR primer design was performed using the NCBI tool Primer-BLAST (Ye *et al.*, 2012). Primers were designed to contain a 40-60% GC content and with no more than a 3° difference in melting temperatures between forward and reverse primers. Primers were screened to check that they only aligned with the desired target to avoid non-specific amplification. Primer sequences are detailed in Table 2.3.

Primer	Sequence (5'-3')
TREM2 – Forward	AAGTACTGGTGGAGGTGCT
TREM2 – Reverse	GGGACCCAGAGATCTCCAG
CX3CR1 – Forward	GTCTTCACGTTCGGTCTGGT
CX3CR1 – Reverse	CCCAGACACTCGTTGTCCTT

Table 2.3 – Mouse primers used for genotyping.
Sequences of the primers used to genotype wild type and TREM2 knockout mouse models.

Mice were ear-notched and DNA was extracted from the ear notches by incubating them in mammalian lysis buffer (100mM Tris, 5mM EDTA, 200mM sodium chloride, 0.2% SDS, pH8.5) containing 100µg/ml Proteinase K solution (Invitrogen, ThermoFisher Scientific) on a shaking heat block at 52°C for 1 hour, followed by 72°C for 30 minutes to deactivate the enzyme. Samples were diluted (1:8) in nuclease-free water (Promega) prior to PCR amplification. DNA concentrations were measured at 260nm using a DeNovix DS-11 FX+ spectrophotometer (Cambridge Bioscience). Diluted DNA (50ng) and 0.4µM mouse TREM2 primers were added to 1X GoTaq Green master mix (Promega). Negative controls involved the substitution of DNA with nuclease-free water. Samples were run on a Mastercycler Nexus GSX1 system (Eppendorf, Merck); for the TREM2 PCR, the following conditions were used: (1) 95°C for 2 minutes; (2) 30 cycles of 95°C for 30 seconds, 62°C for 30 seconds, 72°C for 2.5 minutes; (3) 72°C for 5 minutes. For the CX3CR1 PCR, a touchdown protocol was used as follows: (1) 94°C for 2 minutes; (2) 10 cycles of 94°C for 20 seconds, 65°C for 15 seconds, 68°C for 10 seconds; (3) 28 cycles of 94°C for 15 seconds, 60°C for 15 seconds, 72°C for 10 seconds; (4) 72°C for 5 minutes.

Amplified products were loaded on a 1.5% agarose (Fisher Scientific) gel containing 1X SYBR Safe (Invitrogen, ThermoFisher Scientific) alongside a 1kb molecular weight ladder (GeneRuler, ThermoFisher Scientific) for TREM2 PCR products and 100bp DNA ladder (Promega) for CX3CR1 PCR products. Electrophoresis was conducted in Tris-borate-EDTA (TBE) buffer (0.9M Tris, 0.9M boric acid, 0.02M EDTA) at 100V for 45 minutes. Gels were imaged using a G:BOX Chemi XX9 imager (Syngene).

2.8 Antibody Generation

2.8.1 Protein Immunisation

For mAb production, TREM2 KO mice (3 mice per protein) were injected subcutaneously with 40µg/mouse of commercial recombinant human or mouse TREM2 protein (Sino Biological Inc., Stratech Scientific Ltd.); the former comprised 174 residues and the latter 168 residues of the ectodomain portion, both fused to a poly-histidine (6-His) tag. Proteins were emulsified in complete Freund's adjuvant (CFA) for mAb production. After 4 weeks, all mice received a subcutaneous boost of the appropriate TREM2 protein emulsified in incomplete Freund's adjuvant (IFA), and another boost on week 5, accompanied by a test bleed to screen for antibody

production as described in Section 2.8.4.1. An intraperitoneal (IP) boost containing 30µg protein/mouse in 1X PBS was administered to mice showing high antibody titres in the screening assay and the spleen was harvested for fusion 48 hours later.

For polyclonal antibody production, a young adult New Zealand White rabbit was immunised with 50µg of the human TREM2 protein in CFA and boosted with protein in IFA at 4 and 5 weeks. A 10ml test bleed was carried out at 6 weeks to check for successful antibody production, then the rabbit was exsanguinated, antiserum acquired and 0.22µm filtered for purification.

2.8.2 Peptide Immunisation

An additional immunisation approach utilised peptides to produce antibodies against the specific TREM2 variants. Peptides (Severn Biotech Ltd.) were designed for the wild type and mutant TREM2 variants at amino acid positions 47 and 62 (Table 2.4). A terminal cysteine was added to each peptide to enable conjugation via a crosslinker to keyhole limpet hemocyanin (KLH), which is a large and highly immunogenic carrier protein, or to bovine serum albumin (BSA). Prior to immunisation, peptides were first reduced using Tris(2-carboxyethyl)phosphine hydrochloride (TCEP) then coupled to KLH or BSA as described below.

Site of Interest	Status	Amino Acid Sequence
Position 47	Wild type	PYDS MKHWGRRKAW C
Position 47	Mutant	PYDS MKHWGR<u>H</u>KAW C
Position 62	Wild type	QRVVSTHNLWLLS C
Position 62	Mutant	Q<u>H</u>VVSTHNLWLLS C

Table 2.4 – Peptide designs for variant-targeted mAb generation.
Wild type and mutant peptides used to generate variant-specific antibodies. Substitutions were designed at amino acid positions 47 and 62 (underlined).

2.8.2.1 TCEP Reduction

TCEP Disulfide Reducing Gel (Pierce, ThermoFisher Scientific) was washed in PBS 3 times by vortexing and centrifuging at 1000g for 1 minute, resuspended back to the original volume in PBS then aliquoted for individual reactions. An equal volume of each peptide, at 1mg/ml concentration, was added to each aliquot. The tubes were vortexed and incubated on a rotating wheel at room temperature for 1 hour, then

centrifuged at 1000g for 1 minute and the supernatant containing the reduced peptide was recovered.

2.8.2.2 Peptide Conjugation

Immediately after reduction, peptides were conjugated to the carrier proteins, KLH and BSA, which are commonly used in generating antibodies against peptides (Harlow and Lane, 1988). KLH-conjugated peptides were used for immunisation and BSA-conjugated peptides were reserved for use in screening assays during the production process to ensure that only peptide-specific antibodies, and not antibodies against the KLH conjugate, were positively screened for. The heterobifunctional crosslinker sulfosuccinimidyl 4-[*N*-maleimidomethyl]cyclohexane-1-carboxylate (sulfo-SMCC, ThermoFisher Scientific) was used for conjugation to prevent the aggregation of carrier or peptides. This crosslinker comprises N-hydroxysuccinimide (NHS) ester groups that covalently conjugate amine-carrying proteins, such as KLH and BSA, and contains maleimide groups that bind free sulfhydryl groups on reduced peptides.

Sulfo-SMCC was mixed with KLH and BSA at a molar excess of 20:1 (crosslinker:carrier protein) in conjugation buffer (100mM sodium phosphate, 150mM sodium chloride, pH 7.9). This mixture was incubated on a rotating wheel at room temperature for 1 hour. Excess crosslinker was removed using a Zeba Spin desalting column (ThermoFisher Scientific) equilibrated in conjugation buffer. The reduced peptides were then added at a 100X molar excess (for KLH) or 30X molar excess (for BSA) to the crosslinker-carrier mixture and incubated on a rotating wheel at 4°C for 2 hours. All peptide-carrier conjugates were aliquoted and stored at -80°C. Immunisation using KLH-conjugated peptides was carried out following the same protocol as described for protein immunisation.

2.8.3 Fusion

Prior to the fusion, mouse macrophages were obtained by peritoneal lavage using 5ml of plain RPMI, pelleted and resuspended in 50ml complete medium, then plated in 50µl/well volumes over 10 plates (per fusion) and incubated at 37°C overnight.

The following day, immunised mice were culled as described in Section 2.3 and the spleen was aseptically harvested and immediately transferred to a tissue culture hood. Splenocytes were obtained by spleen perfusion with RPMI and spun down at 1500rpm for 5 minutes then washed in cold plain RPMI medium twice. They were

then resuspended in warm RPMI and combined in a ratio of 1:1 with mouse SP2 myeloma cells freshly harvested from culture that had undergone the same wash steps. The pooled mixture was pelleted then gently resuspended in 1.5ml of tissue culture grade polyethylene glycol (PEG 1500, Sigma-Aldrich, Merck) warmed to 37°C, added drop-by-drop over a 2-minute period to mediate fusion. The mixture was then left to stand for 1 minute, then slowly diluted in RPMI to 50ml over 2 minutes before being spun down and resuspended in 50ml 1X HAT (Gibco, ThermoFisher Scientific) in 15% FBS-RPMI, supplemented with 50 Units penicillin, 50µg/ml streptomycin, 1mM sodium pyruvate, 2mM L-glutamine. The HAT additive acts as a selective medium to propagate only the fused hybridoma cells. As described in the Introduction, aminopterin in the HAT supplement inhibits *de novo* DNA synthesis. Unfused myeloma cells lack the necessary HGPRT enzyme that is required to utilise the DNA synthesis salvage pathway and are thus eliminated. Unfused plasma cells do not replicate in culture and die spontaneously, meaning only hybridomas (myeloma cells fused with HGPRT-positive plasma cells) survive in culture.

Following resuspension, cells were then distributed (50µl/well) into ten 96-well flat-bottomed plates that had been pre-seeded with mouse peritoneal macrophages (50µl/well) as feeder cells. Fusions were incubated at 37°C and observed daily from day 10 for hybridoma growth.

2.8.4 Screening

2.8.4.1 Test serum screening

Blood samples (10µl) from the tail veins of immune mice were spun down at 13,000rpm for 20 minutes at 4°C, and the serum was recovered for screening. For samples from protein-immunised mice, high binding 96-well plates were coated with 0.5µg/ml TREM2 protein in carbonate buffer (15mM Na_2CO_3, 35mM $NaHCO_3$, pH9.6) for 1 hour at 37°C. For serum samples from peptide immunisations, protein coating was substituted with 0.5µg/ml unconjugated peptides for 1 hour at 37°C, followed by a second coating of 0.5µg/ml BSA-conjugated peptides for another hour at 37°C. This double-coating step allows unconjugated peptide to first bind to the plate surface, after which the BSA component of the second coating step fills in remaining gaps thus increasing the peptide surfaces available for binding (Figure 2.2). Plates were blocked in 2% BSA blocking buffer for 1 hour at room temperature and washed 3 times in PBS-0.05%Tween-20 (PBST). Serum samples were added at a starting dilution of 1:100 and serially diluted (1 in 2) down the plate. A non-immune serum sample was

run alongside as a negative control. Samples were incubated for 1.5 hours at 37°C. The plates were washed 3 times in PBST and antibody binding was detected using HRP-conjugated donkey anti-mouse IgG (1:1000, Jackson Immunoresearch, Stratech Scientific Ltd.) for 1 hour at room temperature. After washing, colour development was achieved using orthophenylenediamine (OPD, Sigma-Aldrich, Merck) and measured at 492nm absorbance using a spectrophotometric plate reader (Tecan Infinite F50, Labtech International Ltd., UK).

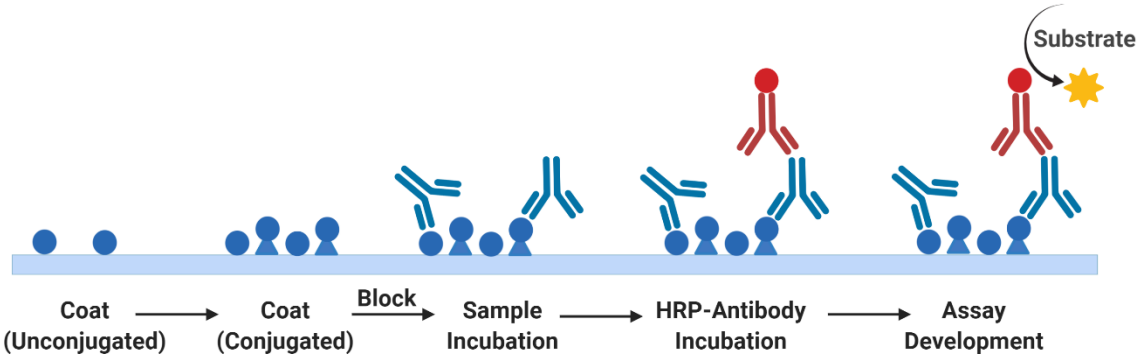

Figure 2.2 – Modified ELISA technique for screening peptide immunisations.
ELISA screening method used to detect TREM2 antibodies in test sera and fusion supernatant. A double-coating step was used to maximise the amount of peptide available for binding. Figure created with BioRender.com.

Samples showing the strongest positive results were identified and the corresponding mice selected for a follow-up IP boost and fusion while the remaining mice were given another sub-cutaneous boost and screened again 1 week later.

2.8.4.2 Fusion screening

For fusions from protein immunisations, plates were coated with 0.5µg/ml TREM2 protein. For peptide immunisations, plates were coated with the relevant unconjugated and BSA-conjugated peptides as described above. Plates were blocked and washed then undiluted fusion supernatant (50µl/well) was added and incubated for 1 hour at 37°C. The plates were washed, incubated with detection antibody and developed as described above. Wells showing good absorbance readings (>0.6) were harvested and limiting dilution cloned into fresh 96-well plates of pre-seeded peritoneal macrophages in 1X HT supplement in 15% FBS-RPMI containing 50 Units penicillin, 50µg/ml streptomycin, 1mM sodium pyruvate, 2mM L-glutamine. For limiting dilution cloning, 10µl aliquots of harvested cells from the original screened well were distributed into the first row of wells in the macrophage-

containing plate then titrated down at a 1 in 6 serial dilution (10µl into 50µl; Figure 2.3). Plates were incubated at 37°C for 10-12 days prior to screening of hybridoma-containing wells from the lowest dilution rows as above.

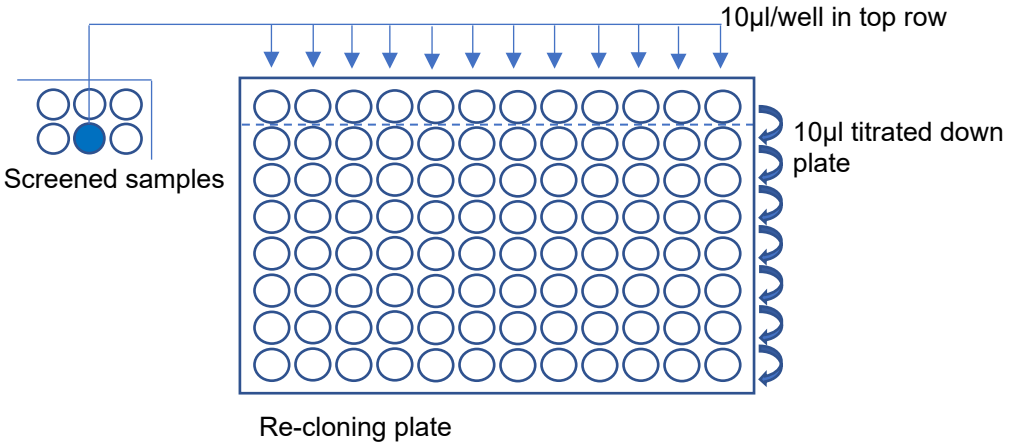

Figure 2.3 – Re-cloning strategy for positively screened clones.
A volume of 120µl of cells from each selected well was equally distributed across the first row of a 96-well plate containing pre-plated macrophages (50µl), then 10µl aliquots titrated down the plate.

Re-cloning and screening procedures were performed two more times before selecting optimal single clones to identify antibody class and confirm monoclonality. Selected clones were gradually expanded by transferring cells sequentially from 96-well plates to 24-well then to 6-well plates and the amount of FBS in the media was reduced to 10%. When semi-confluent in 24-well or 6-well plates, the cells were then further expanded into 25cm^2 flasks then 75cm^2 flasks while gradually introducing ultra-low IgG FBS (Gibco, ThermoFisher Scientific) to replace the regular FBS in the media. For high yield production, cells from four 75cm^2 flasks at 70% confluency were seeded into CELLine 1000 Wheaton bioreactor flasks (Fisher Scientific) containing RPMI supplemented with 50 Units penicillin, 50µg/ml streptomycin. Supernatant harvests were collected every 7 days; 20ml aliquots were removed from the cell compartment of the flask, which was replaced with fresh medium. Aliquots were then spun down at 2000rpm for 20 minutes to pellet cells and the supernatant containing the antibody stored prior to purification.

2.8.5 Antibody Purification

All buffers and samples were 0.22µm filtered before loading onto the ÄKTA Pure 25 fast protein liquid chromatography (FPLC) system (GE Healthcare). A 5ml HiTrap protein G column (GE Healthcare) was used for the purification of polyclonal antibody from antiserum and monoclonal IgG antibodies from tissue culture or CELLine supernatants. A 10mM tris-buffer (10mM tris, 150mM sodium chloride, 0.1% sodium azide, pH 7.4) was used as binding/washing buffer and antibodies were eluted off the column using 0.1M glycine (pH 2.5). Antibody-containing aliquots were identified by absorbance, immediately neutralised by the addition of 10% volume of 1M tris (pH8) and dialysed into PBS. Concentrations were estimated by measuring absorbance at 280nm (DeNovix DS-11 FX+ spectrophotometer) and dividing absorbance by 1.36, the molar extinction coefficient of IgG.

For IgM antibodies, purification over a 1ml HiTrap protein L column (GE Healthcare) was carried out using the same buffers as above. Absorbance was measured at 280nm and values were divided by 1.18, the molar extinction coefficient of IgM, to obtain protein concentration.

To accurately measure antibody concentrations, aliquots of final pools were tested in a bicinchoninic acid (BCA) assay (Micro BCA kit, Pierce, ThermoFisher Scientific) against protein standards as per the manufacturer's instructions. Purity of final pools was confirmed by sodium dodecyl sulphate polyacrylamide gel electrophoresis (SDS-PAGE). Antibodies were aliquoted and stored at -20°C.

2.8.6 Biotin Conjugation of Antibodies

To avoid cross reactivity between anti-mouse secondary antibodies with mouse samples in assays, antibodies were conjugated with biotin using the EZ-Link Sulfo NHS-LC-Biotin kit (ThermoFisher Scientific) as per the manufacturer's instructions. The antibodies were incubated with the biotin reagent for 30 minutes at room temperature, then spun down in Zeba spin desalting columns (40k MWCO, ThermoFisher Scientific) to remove excess biotin. The antibody was then aliquoted and stored at -20°C until required.

2.9 Antibody Characterisation

Monoclonal antibody classes, subclasses and light chain composition were determined using the IsoStrip™ Mouse Monoclonal Antibody Isotyping Kit (Roche, Merck) prior to purification and specificity was confirmed using plate binding assays, flow cytometry and western blotting as described below.

2.9.1 Plate Binding Assay

Plates were coated with 0.5µg/ml commercial human TREM2 protein (or double coated with coupled and uncoupled peptide as demonstrated in Figure ***2.2***) for 1 hour at 37°C and blocked in 2% BSA blocking buffer for 1 hour at room temperature. Serial dilutions of the purified antibodies were added and plates were incubated for 1.5 hours at 37°C. The plates were washed and antibody binding was detected using HRP-conjugated donkey anti-mouse IgG for the mAb, or donkey anti-rabbit IgG for the polyclonal antibody, for 1 hour at room temperature. After washing, colour development was obtained using OPD and measured as above. As the commercial protein used for immunisation included a polyhistidine tag, purified antibodies raised against the full protein were also screened against 0.5µg/ml of an irrelevant histidine-tagged protein (His-Tag-NY-ESO-1 protein, kindly provided by the Moser group, Cardiff University, UK) to ensure that the antibodies were not generated against His-Tag rather than TREM2.

The polyclonal antibody was additionally compared to a commercial goat polyclonal antibody (AF1828, Human TREM2 Antibody, R&D Systems Inc.) on a plate binding assay to determine relative binding activities against human and mouse TREM2.

2.9.2 Coomassie and Western Blot Gels

2.9.2.1 Cell Lysate Preparation

Cells were cultured and prepared in aliquots of 10^6 cells/100µl. Cells were spun down and the pellets resuspended in radioimmunoprecipitation assay (RIPA) buffer (Pierce, ThermoFisher Scientific) containing 1X cOmplete™ protease inhibitor mix (Roche, Merck) and incubated on ice for 10 minutes. They were then sonicated with two bursts of 10 seconds each before centrifuging at 10,000rpm for 1 minute. Supernatants were stored at -80°C.

2.9.2.2 Gel Preparation

For SDS-PAGE, gels were prepared by casting a 10% or 12.5% resolving gel followed by a 4% stacking gel (Table 2.5) into Bolt mini-cassettes (Novex, ThermoFisher Scientific).

Component	10% Resolving Gel (ml)	12.5% Resolving Gel (ml)	4% Stacking Gel (ml)
Resolving buffer *(1.5M Tris, 0.4% SDS, pH 8.8)*	1.875	1.875	0
Stacking buffer *(0.5M Tris, 0.4% SDS, pH 6.8)*	0	0	0.600
Acrylamide, 40%	1.875	2.250	0.253
Distilled water	3.625	3.250	1.597
APS, 10%	0.075	0.075	0.025
TEMED	0.0075	0.0075	0.0025

Table 2.5 – Components of gels used in SDS-PAGE.
Reagents and volumes used to prepare 10% or 12.5% resolving gels, and 4% stacking gels, required for SDS-PAGE.

2.9.2.3 Gel Electrophoresis

For Coomassie staining, samples were prepared at 2.5µg/well in non-reducing (23mM Tris, 117mM sucrose, 0.8% SDS, 1:300 bromophenol blue, pH 6.8) and reducing (as non-reducing buffer, supplemented with 5% β-mercaptoethanol) conditions. They were denatured at 90°C for 10 minutes and loaded onto a polyacrylamide gel alongside a 10-250 kilodalton (kDa) protein ladder (PageRuler Plus, ThermoFisher Scientific) in a Bolt Mini Gel tank (ThermoFisher Scientific). After electrophoresis using 1X running buffer (25mM tris, 192mM glycine, 1% SDS), the gels were removed from their cassettes and incubated in a Coomassie stain (0.25% Coomassie R-250, 10% acetic acid, 40% methanol) on a rocker at room temperature for 1 hour. The stain was discarded and the gel was incubated with a destain buffer (10% acetic acid, 40% methanol) at room temperature for 30 minutes. The solution was replaced with fresh destain buffer every 30 minutes until the gel background was clear and bands became visible. Gels were imaged in white light using a G:BOX Chemi XX9 imager (Syngene).

For western blots, commercial TREM2 protein (1µg) and cell lysates (20µg) were denatured in non-reducing and reducing conditions and run alongside a protein ladder as described above. After electrophoresis, the gel was placed in a transfer cassette containing a blotting pad and filter paper pre-soaked in 1X transfer buffer (25mM tris,

192mM glycine, 20% methanol). A sheet of nitrocellulose membrane was placed over the gel, followed by another layer of filter paper that was rolled out to remove any air bubbles on the gel. A final blotting pad was added on top before closing the cassette and immersing it into the gel tank containing 1X transfer buffer.

The transfer was carried out at 10V for 1 hour and the membrane was retrieved and blocked using 5% BSA-PBST for 1 hour at room temperature. The membrane was incubated overnight at 4°C with 2µg/ml of mAb, or 5µg/ml polyclonal, then washed 3 times in PBST. It was incubated for 1 hour at room temperature with 1:10,000 HRP-conjugated donkey anti-mouse or anti-rabbit antibodies for mAb and polyclonal primary antibodies respectively. The membrane was then washed 3 times in PBST before development using enhanced chemiluminescence (ECL, Amersham ECL Detection Reagents, GE Healthcare) and imaged using G:BOX Chemi XX9 (Syngene).

2.9.3 Flow Cytometry

Cells were washed in plain RPMI and plated at 100µl volumes in a 96-well U-bottomed plate at 2 x 10^5 cells/well. The cells were spun down at 1500rpm for 5 minutes and washed in assay buffer (2% FBS-PBS). This was followed by a 15 minute incubation on ice in either 1:100 anti-mouse CD16/32 Fc-blocking antibody (Biolegend) for mouse cell lines or 1:8 TruStain FcX™ antibody (Biolegend) for human cell lines, supplemented with 5% goat serum (Vector Laboratories) for mAb or donkey serum (Sigma-Aldrich, Merck) for the polyclonal antibody. Cells were then incubated with the α-TREM2 antibodies for 30 minutes on ice. After washing, the cells were stained with Alexa Fluor 647-conjugated anti-mouse (for mAb) or anti-rabbit (for polyclonal) antibodies (Biolegend) on ice for 30 minutes in the dark. Staining using the commercial AF1828 anti-TREM2 antibody (R&D Systems Inc.) was detected with Alexa Fluor 647-conjugated anti-goat antibody (Abcam). Negative controls included cells stained with the fluorophore-conjugated antibody only and cells stained with an isotype control corresponding to the tested antibodies (Table 2.6). The cells were then washed twice and fixed using 4% paraformaldehyde for 15 minutes on ice. Cells were washed twice again, resuspended in assay buffer and measured using the Attune NxT flow cytometer (ThermoFisher Scientific). Data was analysed using FlowJo v.10 (FlowJo, LLC) software.

Antibody	Clone	Use	Source
Alexa Fluor 647 Anti-Mouse IgM	RMM-1	Detection	Biolegend
Alexa Fluor 647 Donkey α-Goat IgG	n/a	Detection	Abcam
Alexa Fluor 647 Donkey α-Rabbit IgG	Poly4064	Detection	Biolegend
Alexa Fluor 647 Goat α-Mouse IgG	Poly4053	Detection	Biolegend
Anti-human TruStain FcX™ antibody	n/a	Fc block	Biolegend
Anti-mouse CD16/32 antibody	n/a	Fc block	Biolegend
Anti-GFAP antibody	n/a	Isotype control	Abcam
Monoclonal (anti-FH) IgM antibody	n/a	Isotype control	In-house
Polyclonal (anti-C4) antibody	n/a	Isotype control	In-house
Purified Mouse IgG2a, κ	MG2a53	Isotype control	Biolegend

Table 2.6 – Antibodies used for flow cytometry.
The polyclonal and IgM isotype control antibodies were generated in-house, while the other antibodies were obtained commercially (Abcam and Biolegend, UK).

2.10 Development of Human sTREM2 ELISA

A sandwich ELISA for the detection of sTREM2 in human plasma using mAb 9D10 as a capture antibody paired with the polyclonal antibody was set up by Angharad Morgan.

A 96-well flat-bottomed high binding plate was coated with mAb 9D10 at 5µg/ml in carbonate buffer and incubated at 4°C overnight. After 3 washes with PBST, the plate was blocked with 2% BSA-PBST at 37°C for 1 hour. Commercial TREM2 protein was added in duplicates at a starting concentration of 6ng/ml and titrated down the plate in a 1 in 2 serial dilution. Plasma samples were prepared (neat and at 1 in 2 dilution) and the plate was incubated overnight at 4°C. After 3 PBST washes, the polyclonal anti-TREM2 was added at 10µg/ml and the plate was incubated at 37°C for 1 hour. The plate was then washed 3 times before the addition of HRP-labelled donkey anti-rabbit IgG antibody diluted 1:1000. The plate was incubated at 37°C for 1 hour, washed and developed using OPD, absorbance was measured at 492nm. Samples, protein standard and detection antibodies were all diluted using 0.1% BSA-PBST. Standard curves including standard error of mean (SEM) and data interpolation were plotted using Prism 5 (GraphPad) software.

Plasma samples of 663 individuals from the European cohort AddNeuroMed (Lovestone *et al.*, 2009) were tested using this assay. Samples comprised 241 AD, 184 mild cognitive impairment (MCI) and 238 age-matched controls, and were kindly

provided by the National Institute for Health Research (NIHR) Biomedical Research Centre and NIHR Dementia Biomedical Research Unit hosted at Kings College London and South London and the Maudsley NHS Foundation Trust. Informed consent was obtained according to the Declaration of Helsinki (1991), and protocols were approved by Institutional Review Boards at each collection site. Demographic information included diagnosis, age, gender, ApoE status and age of onset but my work was limited to age and gender as variables in my analysis, as demonstrated in Chapter 5.

Chapter 3

Results: Production and Characterisation of Antibodies against TREM2

3 Results: Production and Characterisation of Antibodies against TREM2

3.1 Introduction

The development of monoclonal antibody (mAb) technology, based on the seminal work of Caesar Milstein and colleagues in the mid-1970s (Köhler and Milstein,1975), means that large amounts of homogenous antibody reagents can be specifically generated against a wide range of antigens. Over the last 30 years, this field has significantly progressed through humanisation of mAb and engineering improvements in their efficacy. This has led to their increased use in diagnostic settings, where they can detect the presence of antigens in patient samples, and in therapeutic applications where they can kill cancer cells and alter the immune response to disease (Li and Zhu, 2010; Liu, 2014; Singh *et al.*, 2018).

As discussed in Chapter 1, there is currently a lack of reliable commercial anti-TREM2 mAb that can identify and quantify TREM2 in human and animal systems. Given the evidence implicating TREM2 in AD, the lack of reliable reagents to identify and quantify TREM2 is an important unmet need. TREM2 has been reported to have multiple roles in AD depending on factors such as stage of disease and the type of disease model under investigation; the lack of good detection reagents in part explains the inconsistencies seen in the literature and poses challenges for diagnosis and potential therapeutic strategies. A more in-depth understanding of the distribution and functions of TREM2 is important to clarify its roles in AD; to achieve this there is a need to develop good quality reagents.

3.1.1 Aims and Objectives

The first aim of this chapter is to produce and characterise a panel of in-house mAb that bind to human and mouse TREM2 proteins. The second aim is to generate mAb specific for the AD-associated TREM2 variants, R47H and R62H.

3.2 Results

3.2.1 TREM2 Genotyping Results

DNA extraction and PCR amplification using mouse TREM2 primers was carried out on the C57BL/6J (WT) and TREM2 KO mice (six mice per genotype) to confirm their respective genotypes. Amplified TREM2 DNA, with an expected band size of 2357bp, was only observed in the wild type samples as expected (Figure 3.1A).

To confirm the presence of DNA in the TREM2 KO samples, an additional PCR was carried out for three of the TREM2 KO samples using primers against the chemokine receptor CX3CR1. Bands were observed at 410bp as expected, confirming that DNA extraction for these samples was successful and that the absence of bands in the TREM2 PCR was a true result (Figure 3.1B). A better method to confirm this result would be the use of primers designed to target the region of TREM2 unaffected by the knockout strategy, exon 3 for example, in KO samples 1-6. Demonstrating absence of bands using primers targeting exon 2, together with presence of bands using primers targeting exon 3, would better represent the KO genotype.

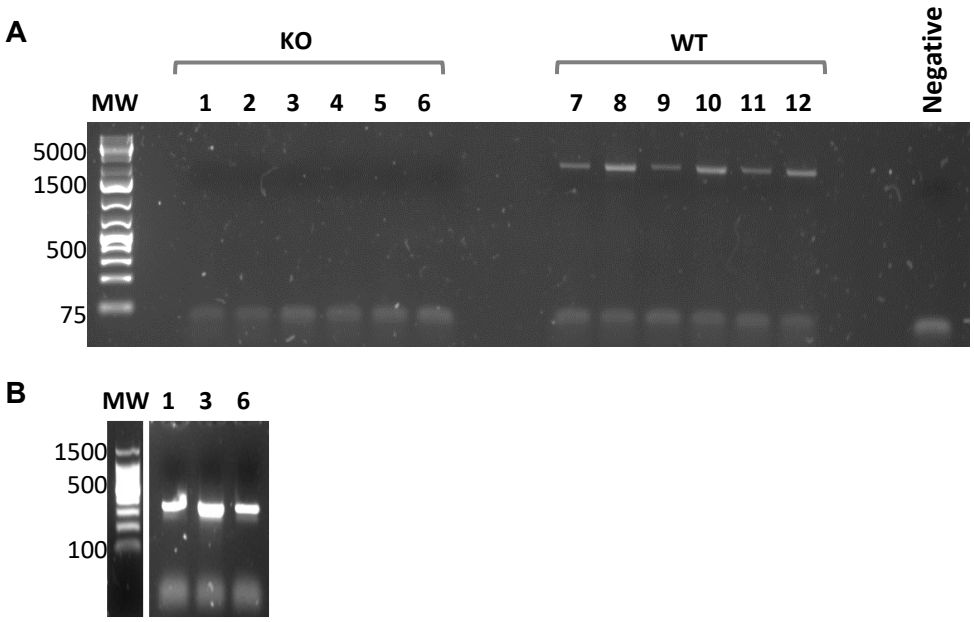

Figure 3.1 – TREM2 and CX3CR1 genotyping PCR.
(A) PCR amplification using mouse TREM2 primers on DNA from TREM2 KO (samples 1-6) and WT mice (7-12). A 1kb molecular weight (MW) ladder was loaded in the leftmost lane, only main bands are labelled for clarity. A negative control was included, where DNA was replaced with nuclease free water. TREM2 DNA was only observed in the WT at the expected band size: 2357bp. (B) Three of the six TREM2 KO samples (1,3,6) were also genotyped using CX3CR1 primers to confirm the presence of DNA in the samples, yielding 410bp products as expected, run alongside a 100bp ladder in the leftmost lane.

3.2.2 Anti-Human TREM2 Antibodies

3.2.2.1 Isotyping and Plate Binding Assays

Immunisations (in rabbits for polyclonal and in TREM2 KO mice for mAb) and fusions for mAb were conducted as described in Materials and Methods (Chapter 2). Initial fusions were carried out by Wioleta Zelek, resulting in two of the mAb raised against human TREM2 (9D10 and 9A9-3). All subsequent fusions and characterisation of these and all other mAb were conducted entirely by me as part of this project. One polyclonal antibody was purified from the rabbit anti-serum using a protein G column.

Serum samples from injected mice were screened throughout the immunisation procedure to monitor antibody levels and select the mice with the highest titres for subsequent hybridoma production (Figure 3.2).

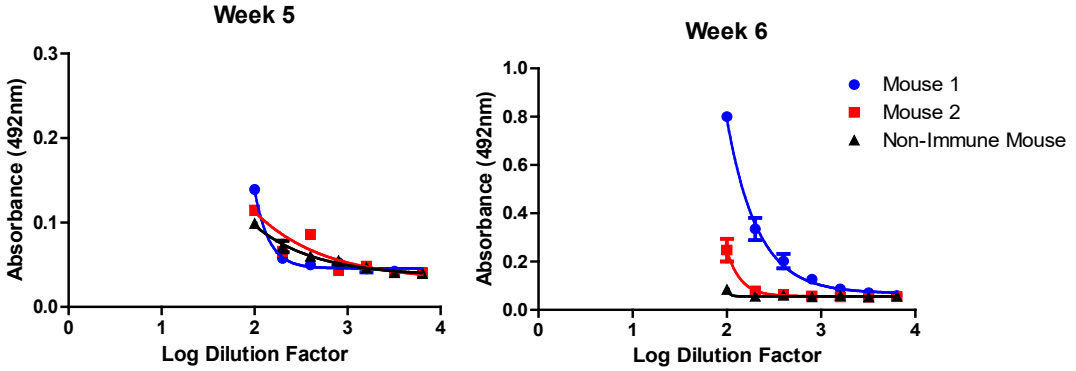

Figure 3.2 – Serum screening to monitor antibody levels in immunised mice.
Example of screening serum samples (serial dilutions starting from 1:100) after injection boosts on weeks 5 and 6 after the initial immunisation. Mouse 1 was selected for a final boost followed by fusion and hybridoma production, mouse 2 was given another boost before re-testing serum on week 7. A non-immune serum sample was tested in parallel as a negative control.

Antibodies from selected hybridoma lines were purified and screened against commercial recombinant TREM2 proteins to investigate their binding capacity. They were also screened against His-Tagged irrelevant protein to rule out false positive results arising from antibodies raised against the His-Tagged portion of the immunisation proteins. Any antibodies showing positive His-Tag results were eliminated from the study. Another test that could have been used as a negative control, following His-Tag screening, is the use of scrambled proteins; where TREM2 protein sequences are randomised to test the specificity of the generated antibodies.

All mAb strongly bound human TREM2 in a plate binding assay and all, except 5D11, bound mouse TREM2 (Figure 3.3). Binding to the human protein did not demonstrate a clear titrated effect for three of the mAb (Figure 3.3A-C), indicating that the assay reached its saturation limit and should be repeated with lower antibody concentrations to generate a titration curve.

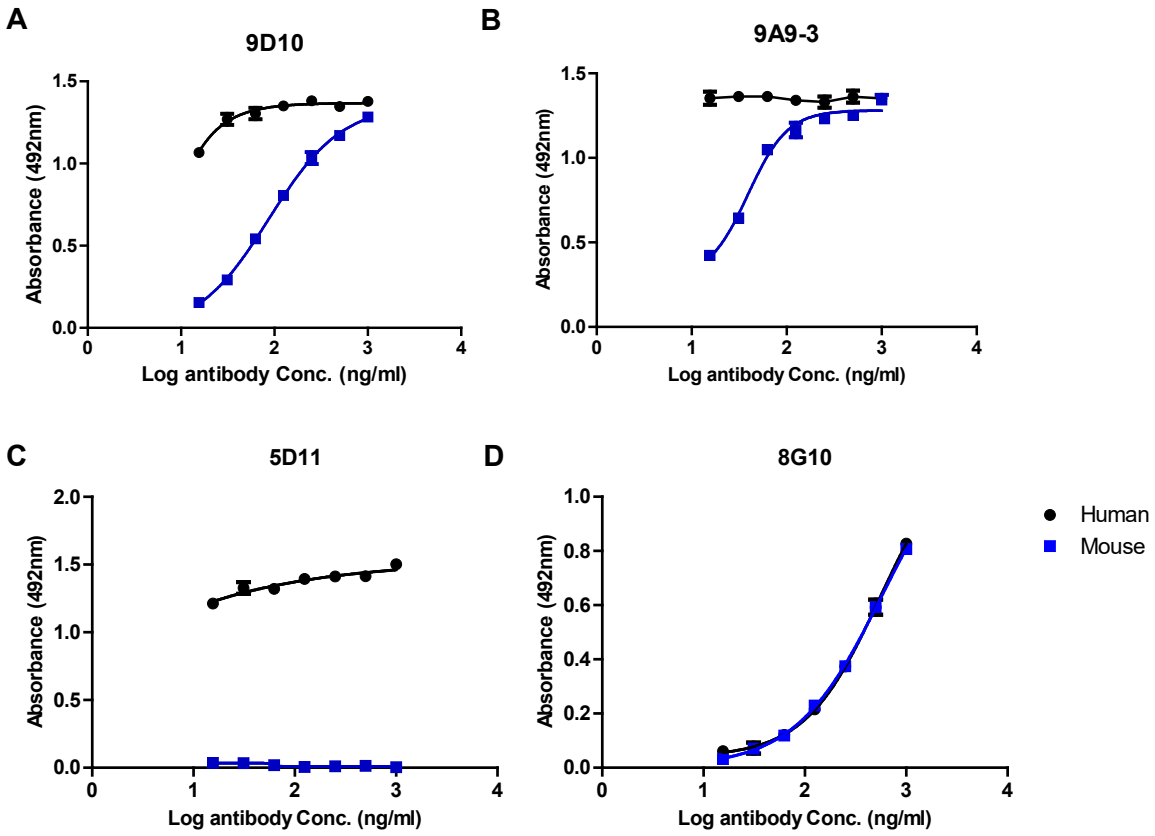

Figure 3.3 – ELISA reactivity of mAb against recombinant human and mouse TREM2. ELISA comparing binding of mAb (A) 9D10, (B) 9A9-3, (C) 5D11 and (D) 8G10 to immobilised human (black) and mouse (blue) TREM2 protein. Bound antibody (Ab) was detected by incubation with HRP-labelled anti-mouse IgG followed by OPD substrate to develop the assay. Error bars represent mean +/- SEM of duplicates in the assay.

Comparing the in-house polyclonal antibody to a commercial α-TREM2 antibody (AF1828, R&D Systems Inc.) by ELISA showed that both antibodies strongly bound human TREM2, but that the commercial antibody had a higher capacity to bind mouse protein (Figure 3.4).

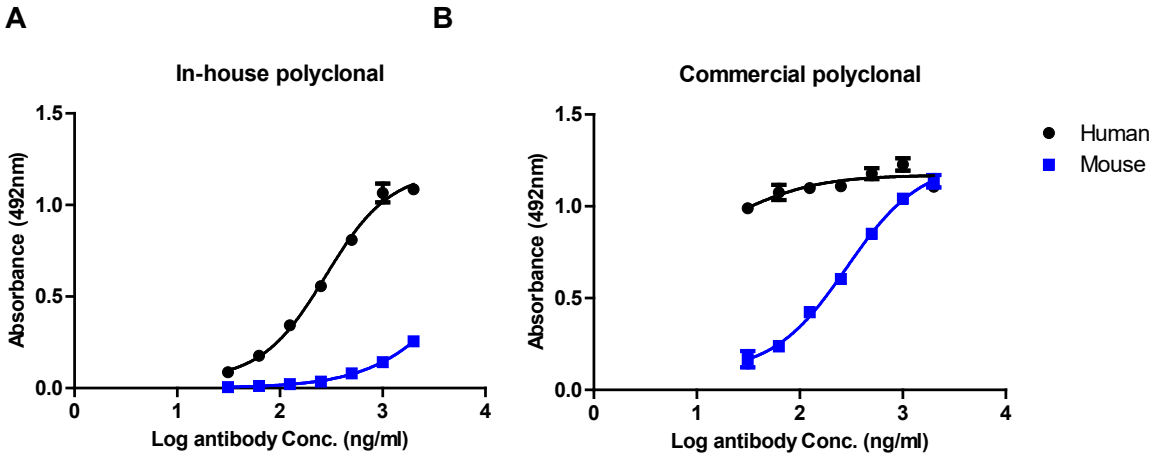

Figure 3.4 – ELISA reactivity of in-house and commercial polyclonal antibodies.
ELISA comparing binding of (A) in-house and (B) commercial polyclonal antibodies to immobilised human (black) and mouse (blue) TREM2 protein. Error bars represent mean +/- SEM of duplicates in the assay.

An unusual result was obtained with mAb 5D11 and 8G10 using isotyping strips as bands for both IgG1 and IgG3 were detected. These antibodies were re-cloned under the assumption that they may not be monoclonal as initially concluded; however, re-testing resulted in the detection of the same two isotypes. To specifically determine the true isotype of these mAb, anti-IgG1 and -IgG3 antibodies (Biolegend) were used to detect them in an ELISA setting and provided conclusive evidence of the isotype IgG1 (Figure 3.5).

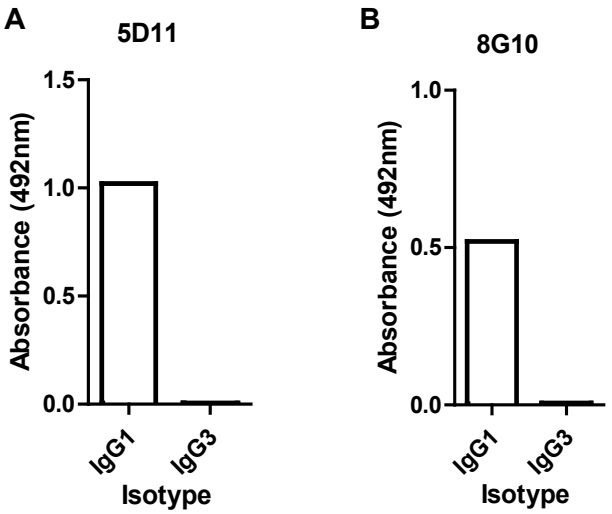

Figure 3.5 – ELISA isotype confirmation of mAb 5D11 and 8G10.
Specific anti-IgG1 and -IgG3 antibodies were used to identify the isotypes of the two mAb (A) 5D11 and (B) 8G10 after obtaining unclear results using isotyping strips. Both mAb were clearly confirmed as IgG1.

Table 3.1 summarises the isotypes and reactivity of the polyclonal and mAb raised against human TREM2, against both human and mouse TREM2 protein, and with His-Tagged irrelevant protein.

Name	Host	Isotype	Human TREM2 binding	Mouse TREM2 binding	His-tag binding
AF1828	Goat	n/a	yes	yes	n/a
Polyclonal	Rabbit	n/a	yes	weak	no
9D10	Mouse	IgG2a (κ)	yes	yes	no
9A9-3	Mouse	IgG2a (κ)	yes	yes	no
8G10	Mouse	IgG1	yes	yes	no
5D11	Mouse	IgG1	yes	no	no

Table 3.1 – Summary of isotypes and ELISA reactivity of human antibodies.
Host species and isotypes of the mAb, in-house polyclonal and commercial polyclonal (AF1828, R&D Systems) antibodies. Antibody reactivity to recombinant human TREM2, mouse TREM2 and irrelevant His-Tag protein was tested in a plate-binding assay. Only human TREM2 binding was observed with mAb 5D11 while all other antibodies showed binding to both TREM2 proteins. All antibodies were His-tag negative, testing binding for AF1828 was not applicable (n/a) as it was not raised against a His-Tagged protein.

3.2.2.2 Antibody Binding of TREM2 Proteins and Cell Lysates

Western blotting was used to demonstrate specific binding of the generated antibodies to TREM2 protein. The antibodies were used to detect recombinant TREM2 protein and native TREM2 in human monocytic (THP1) and mouse macrophage (RAW264.7) cell lysates, chosen because these lines are reported to express TREM2 (Allcock *et al.*, 2003; Humphrey *et al.*, 2006; Turnbull *et al.*, 2006; Kober *et al.*, 2016). Negative controls, where only HRP-labelled secondary antibody was used, were included. The predicted molecular weight of recombinant TREM2 is ~20-25kDa but the protein migrates at a higher apparent molecular weight of ~35-40kDa on SDS-PAGE due to glycosylation, as described by the supplier's documentation. In my hands, the recombinant proteins also ran as a broad smear between 35 and 40kDa under reduced and non-reduced conditions (Figure 3.6C). To validate this observation, these human and mouse TREM2 proteins should have been deglycosylated and run alongside original aliquots for comparison to demonstrate the correct molecular weight of the deglycosylated protein, but this was not done in this project.

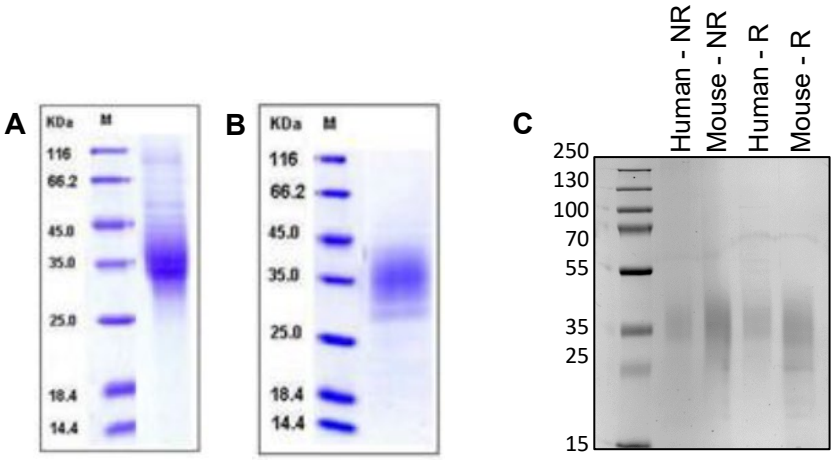

Figure 3.6 – Molecular weight of recombinant TREM2 on SDS-PAGE.
(A) Human and (B) mouse recombinant TREM2 protein on a Coomassie gel, provided by the supplier's website (Sino Biological Inc.), (C) the recombinant TREM2 proteins (2.5µg/well) run in-house on a 12.5% gel and Coomassie-stained, under reducing (R) and non-reducing (NR) conditions.

In western blots, mAb 9D10 strongly bound both the human and mouse recombinant TREM2 protein under reducing (R) and non-reducing (NR) conditions (Figure 3.7A), while mAb 9A9-3 and 8G10 showed strong binding to human TREM2 protein at the expected molecular weight, but only a faint smear was observed with the mouse protein (Figure 3.7B,D). mAb 5D11 and the in-house polyclonal antibody strongly bound human TREM2 but showed no cross-reactivity with mouse protein (Figure 3.7C,E) confirming ELISA results. Unexpectedly, the commercial polyclonal antibody only bound human TREM2 protein on western blot (Figure 3.7F).

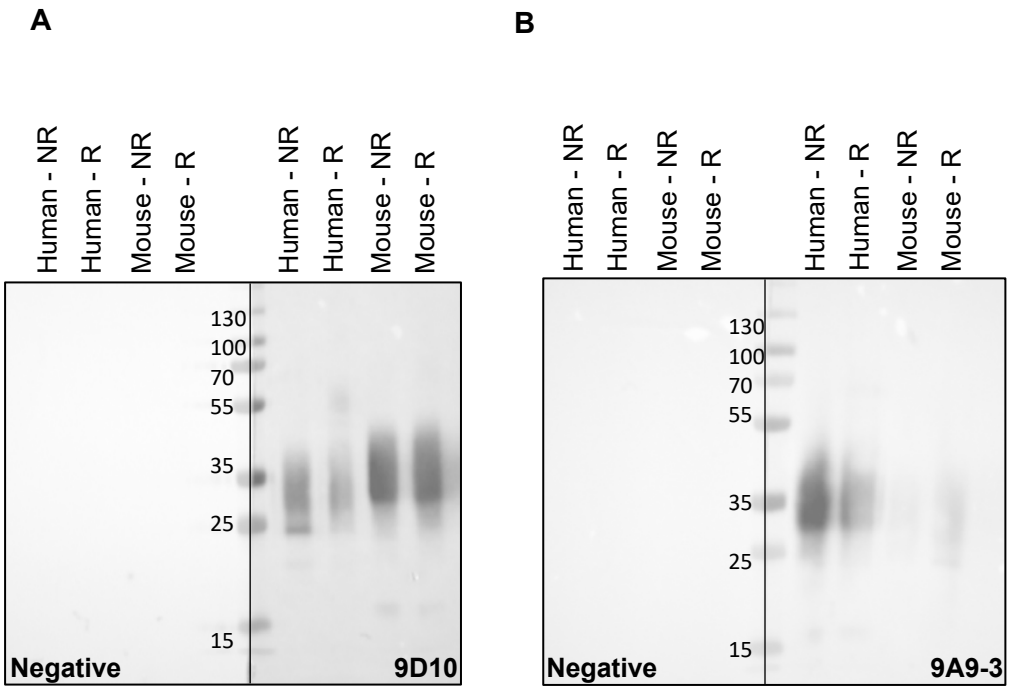

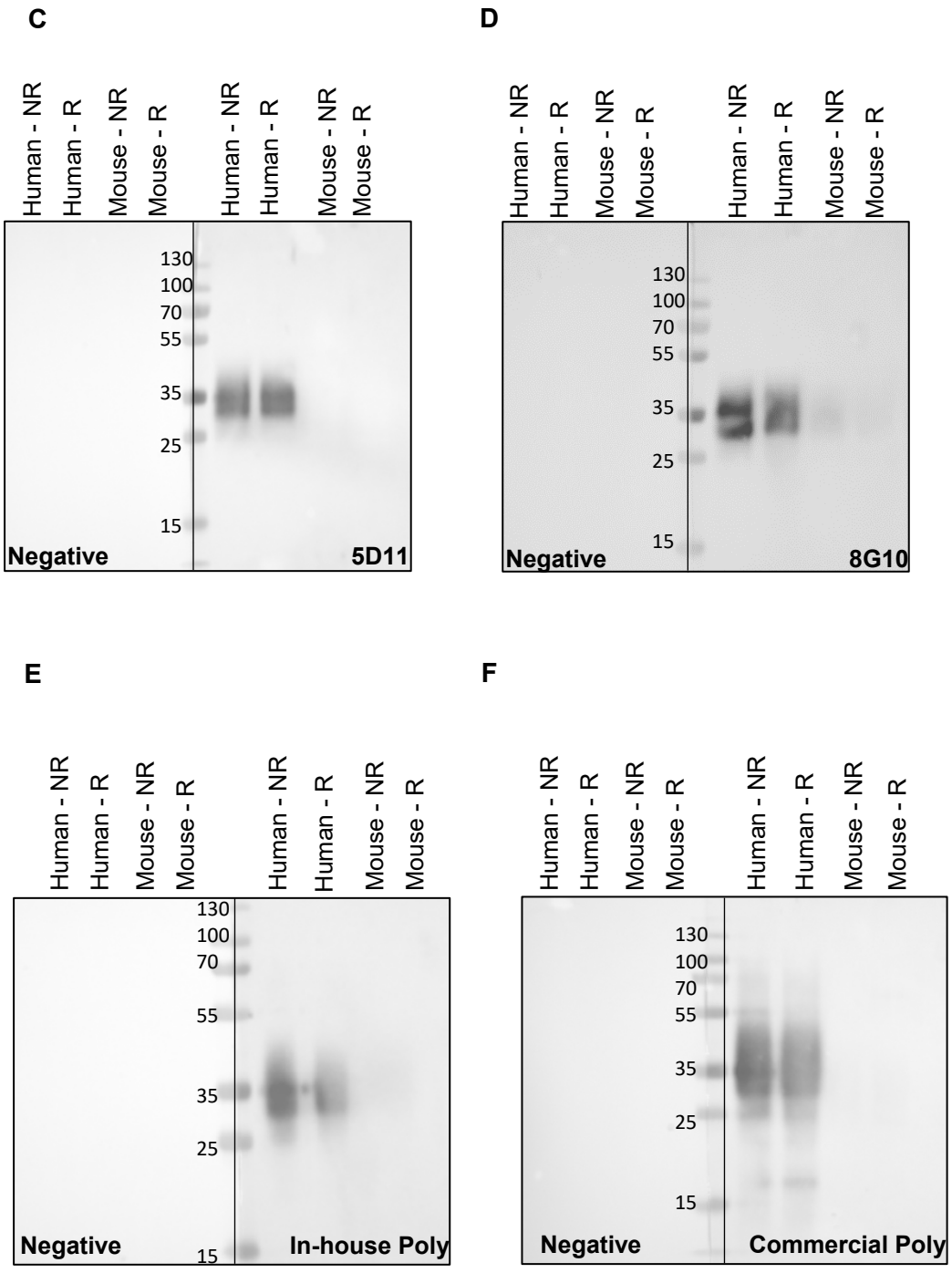

Figure 3.7 – Binding of antibodies to recombinant human and mouse TREM2 protein. Western blots showing binding of: (A) mAb 9D10, (B) mAb 9A9-3, (C) mAb 5D11, (D) mAb 8G10, (E) in-house polyclonal and (F) commercial polyclonal anti-TREM2 antibody to human and mouse TREM2 under reducing (R) and non-reducing (NR) conditions. Negative controls comprised the same proteins probed with HRP-secondary antibody only. After transfer, the membrane was divided at the molecular weight ladder, and each half probed separately.

Probing of SDS-PAGE separated lysates from the human THP1 and mouse RAW264.7 cell lines with mAb 9D10 detected bands only in the reduced lysate; the major band in lysates from both sources was at ~65kDa (Figure 3.8A). A major band of the same size was detected when lysates were probed with mAb 9A9-3 under reducing conditions while a slightly lower molecular weight band (~60kDa) was detected in the non-reduced lysates (Figure 3.8B), and mAb 5D11 bound only the human cell line in both non-reduced and reduced lysates (Figure 3.8C). Secondary-only controls were negative under all conditions. mAb 8G10 was not tested against these cell lysates in western blot due to time constraints.

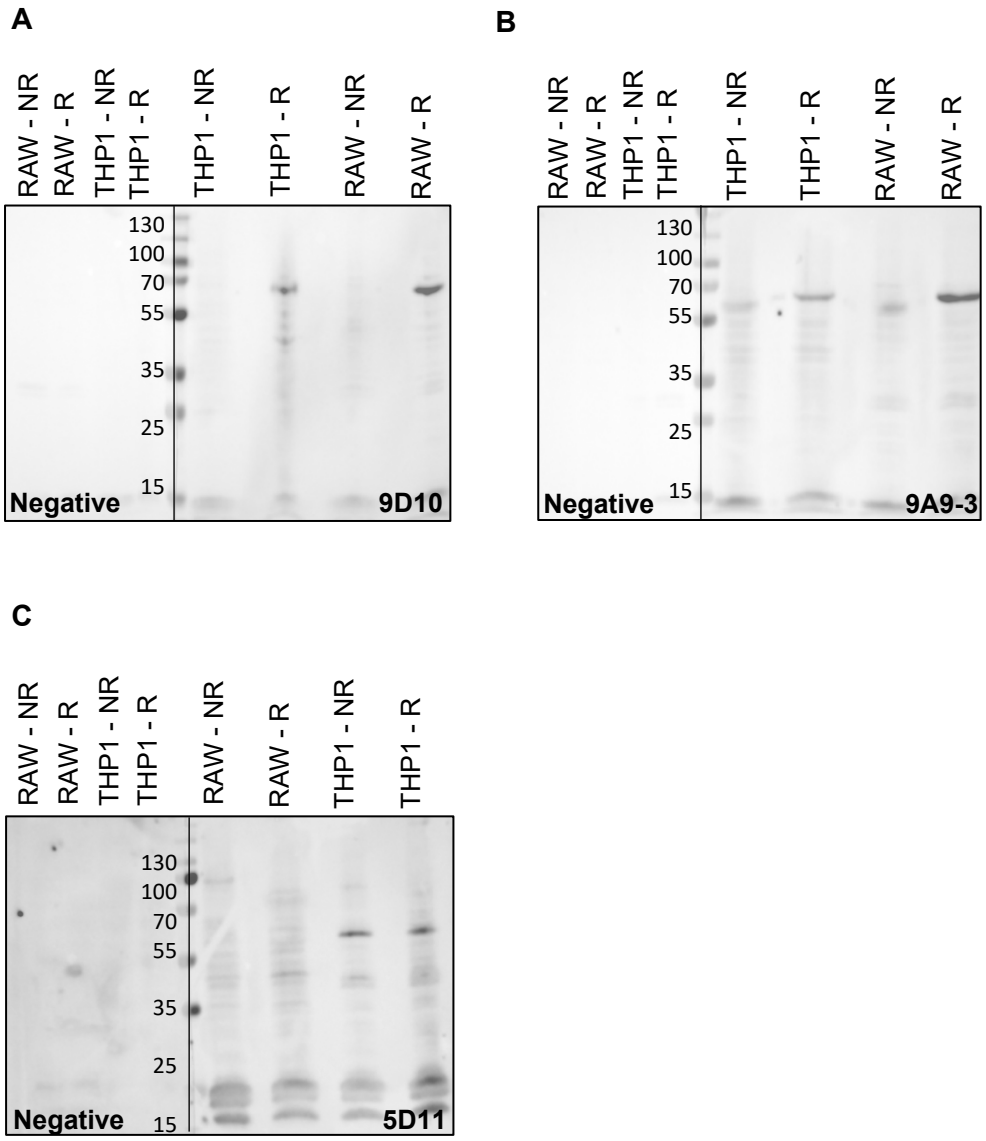

Figure 3.8 – Binding of mAb to THP1 and RAW264.7 lysates.
Western blots showing binding of anti-TREM2 mAb (A) 9D10, (B) 9A9-3 and (C) 5D11 to THP1 and RAW264.7 lysates under reducing (R) and non-reducing (NR) conditions. Negative controls were loaded to the left of the molecular weight ladder, and the membrane was divided post-transfer and each half probed separately.

The reactivity of in-house and commercial polyclonal antibodies against human and mouse TREM2 in cell lysates was compared as above using Western blotting. Probing of blots with the commercial anti-TREM2 polyclonal antibody detected a single major band at ~45kDa and several higher and lower molecular weight minor bands in both lysates and under R and NR conditions (Figure 3.9A); in contrast, the in-house polyclonal antibody detected major bands at ~55kDa in human cell lysates, but not in mouse cell lysates (Figure 3.9B). The binding patterns of the human antibodies to cell lysates are summarised in Table 3.2.

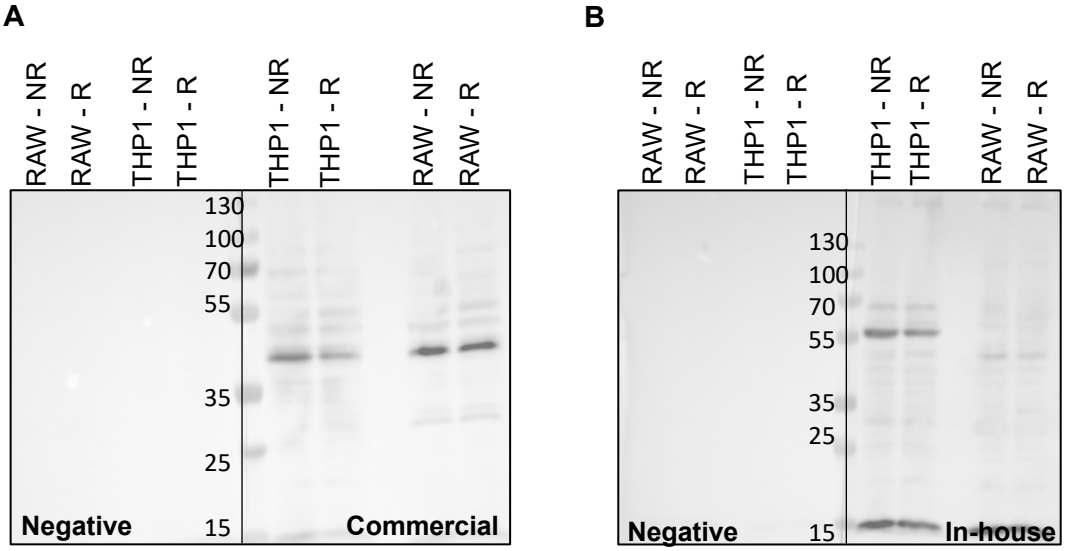

Figure 3.9 – Binding of polyclonal antibodies to human and mouse cell lysates.
Western blots showing (A) commercial AF1828 polyclonal anti-TREM2 antibody and (B) in-house anti-TREM2 antibody probing of THP1 and RAW264.7 lysates under reducing (R) and non-reducing (NR) conditions. Negative controls were loaded on the left of each molecular weight ladder, and the membrane was divided post-transfer and each half probed separately.

Name	THP1 binding	RAW264.7 binding
9D10	65kDa (R)	65kDa (R)
9A9-3	65kDa (R), 60kDa (NR)	65kDa (R), 60kDa (NR)
8G10	*Not tested*	*Not tested*
5D11	65kDa	None
Polyclonal (in-house)	55kDa	None
Polyclonal (commercial)	45kDa	45kDa

Table 3.2 – THP1 and RAW264.7 binding patterns with human antibodies.
Summary table showing TREM2 binding of the human antibodies to THP1 and RAW264.7 cell lysates, under reducing (R) and non-reducing (NR) conditions. mAb 8G10 was not tested due to time constraints and limited laboratory access during pandemic restrictions.

3.2.2.3 Antibody Binding of Membrane-Bound TREM2

The antibodies generated against the recombinant human TREM2 protein were tested against THP1 and RAW264.7 cells using flow cytometry to explore binding of membrane-bound TREM2. None of the antibodies showed binding above the isotype controls to the THP-1 cell line (Figure 3.10C,E). Only mAb 9D10 and 9A9-3 showed a large shift in binding to RAW264.7 cells in comparison with controls (Figure 3.10D) and the commercial AF1828 polyclonal antibody did not bind either cell line (negative results not shown).

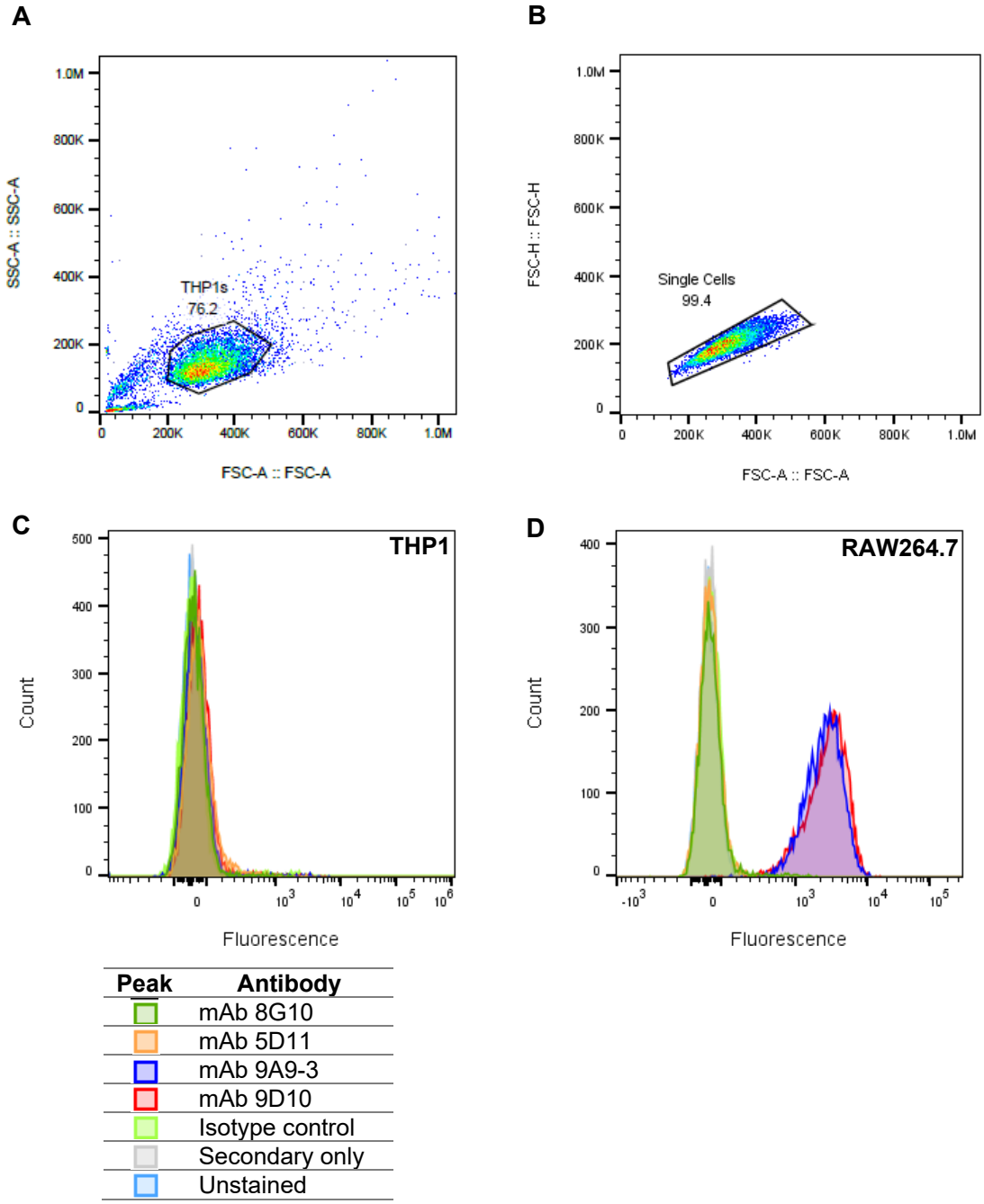

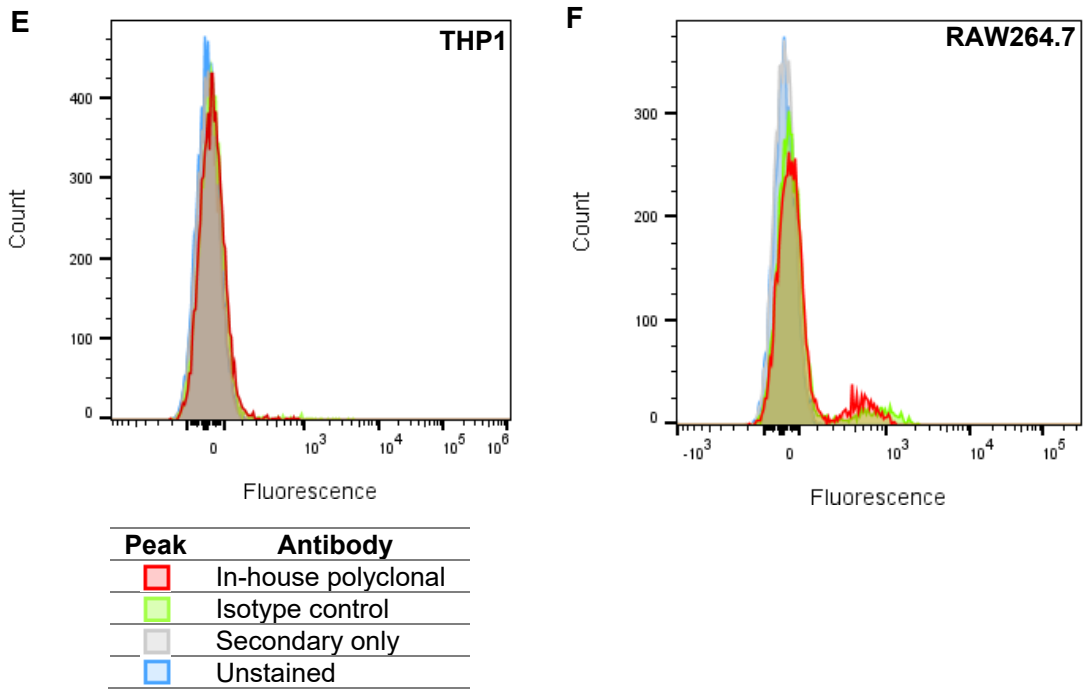

Figure 3.10 – Binding of antibodies to human and mouse cell lines by flow cytometry. Example of the flow cytometry gating strategy: (A) dead cells were first excluded by gating forward scatter area (FSC-A) against side scatter area (SSC-A), (B) then only single cells were analysed by gating FSC-A against forward scatter height (FSC-H). Flow cytometry histograms depicting cell count versus fluorescence to show binding of human anti-TREM2 mAb to (C) THP1 and (D) RAW264.7 cells, and binding of the in-house generated polyclonal antibody to (E) THP1 and (F) RAW264.7 cells. Controls included cells stained with secondary antibody only and cells stained with isotype controls for both the mAb (mouse) and the polyclonal (rabbit).

3.2.3 Anti-Mouse TREM2 Antibodies

3.2.3.1 Antibody Isotyping

Three fusions were carried out for the generation of mouse antibodies against TREM2; all immunisations were in TREM2-deficient mice. From these fusions, twenty mAb clones from seven primary clones were selected for initial characterisation; isotyping using a commercial isotyping kit indicated that all of the selected clones were of the IgM class. This result was surprising given that the screening ELISA utilised a commercial HRP-labelled anti-IgG (Jackson Immunoresearch) to detect antigen-bound mAb; positive clones were therefore expected to be of the IgG class, but instead this finding demonstrated that this commercial antibody is not IgG-specific. The result was therefore further investigated using western blotting and plate binding assays as described below.

Neat supernatant from the selected clones was run on SDS-PAGE under reducing conditions, western blotted and then probed with the same secondary HRP-labelled anti-IgG antibody used in the screening ELISA. Results showed the characteristic μ heavy chain of IgMs (~70kDa) for the tested supernatants whereas a control IgG run as a positive control on the blots showed strong staining of ~55kDa IgG γ chain (Figure 3.11).

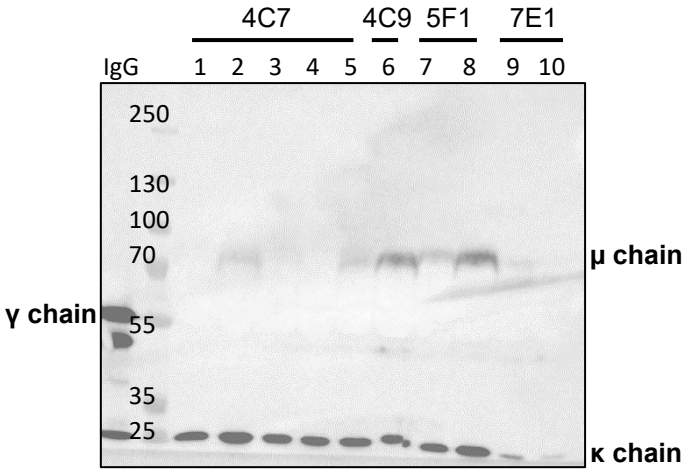

Figure 3.11 – Western blot of mouse mAb clone supernatant
Western blot showing the detection of the IgM μ heavy chain at ~70kDa in several of the mAb clone supernatants and the ~55kDa IgG γ chain of the leftmost IgG sample. Both Ig classes contain the ~25kDa κ light chain. Lane numbers represent: (1-5) 4C7 subclones -F12, -G11, -E3, -E5, -G6; (6) 4C9-F11; (7-8) 5F1-C9, -D9; (9-10) 7E1-D7, -E8.

Evidence from the isotyping kit and western blotting demonstrated that the anti-mouse IgG secondary antibody used for screening assays was binding both IgG and IgM antibodies; the plate binding assay was therefore repeated using γ-chain and μ-chain specific HRP-labelled antibodies (Sigma-Aldrich, Merck, UK). Clone supernatants all showed binding to different degrees with the μ-chain specific antibody but no binding was seen with the γ-chain specific antibody for any of the clone supernatants, confirming that they are all of the IgM class (Figure 3.12). The three strongest binding mAb from three different original clones (clones 4C7:E5, 5F1:D9, 7E1:E8) were taken forward for purification and further characterisation.

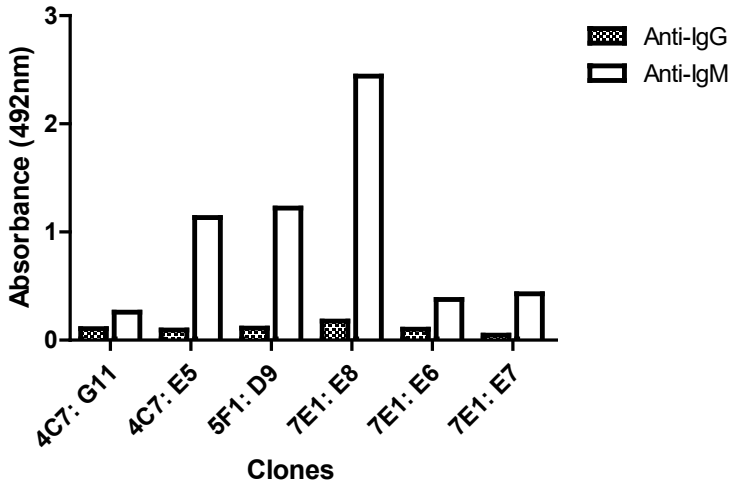

Figure 3.12 – Determination of mAb isotype using class-specific antibodies in ELISA.
Example of six mAb clone supernatants showing strong reactivity with the μ-chain-specific secondary antibody but no reactivity with the γ-chain-specific secondary antibody, confirming that they are all of the IgM class.

3.2.3.2 Purification and Plate Binding Assays

Selected sub-clones were purified on the ÄKTA Pure 25 FPLC system (Figure 3.13) by passage over a protein L column, which binds the κ light chains of antibodies irrespective of heavy chain type, and Coomassie stained after SDS-PAGE to check purification quality.

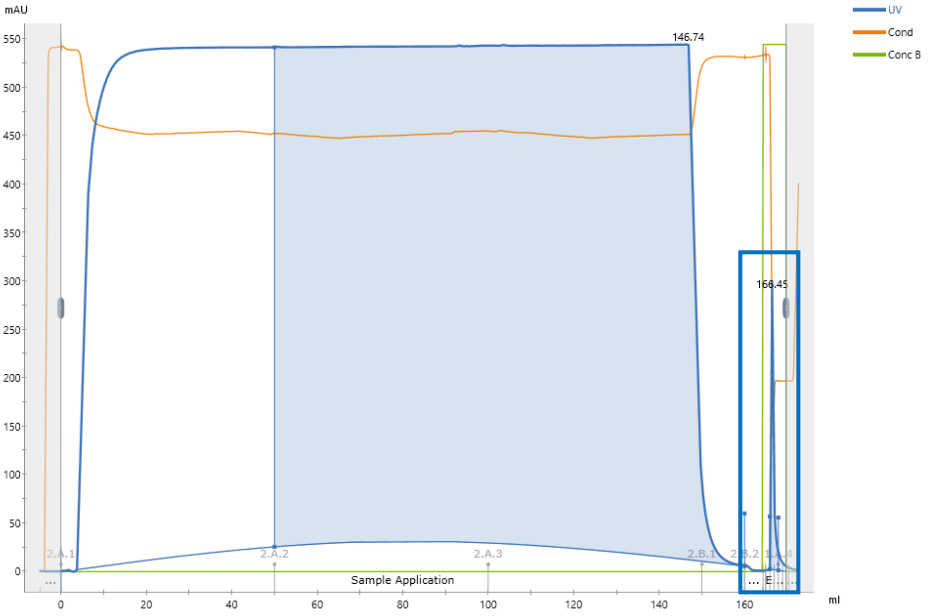

Figure 3.13 – FPLC purification of mAb 7E1-D4
Example of a purification trace showing the elution peak (rectangle) of anti-mouse TREM2 mAb 7E1-D4.

Purification was not successful for the selected mAb as no protein was eluted from the supernatant, so different sub-clones previously derived and frozen away from the three original clones were regrown and trialled. Clones 7E1-D4 and -E10 showed promising SDS-PAGE results post-purification (Figure 3.14) but after re-testing in a plate binding assay, only 7E1-E10 appeared to weakly bind human and mouse TREM2 protein (Figure 3.15).

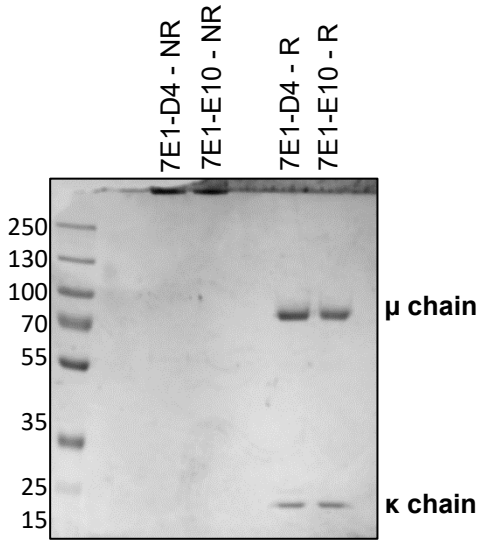

Figure 3.14 – SDS-PAGE of anti-mouse mAb 7E1-D4 and -E10.
Coomassie staining of purified mAb raised against mouse TREM2. Reducing (R) conditions show the μ heavy chain of IgM at ~70kDa and the κ light chain at ~25kDa. NR: non-reducing.

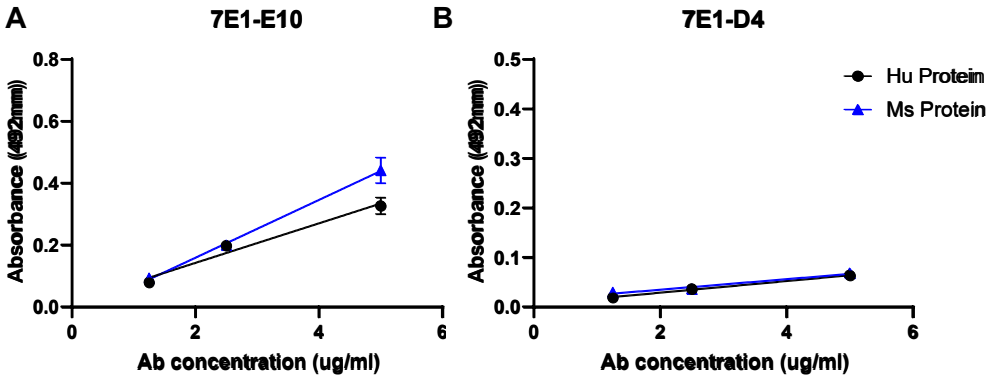

Figure 3.15 – ELISA reactivity of mAb against recombinant human and mouse TREM2.
ELISA comparing binding of mAb (A) 7E1-E10 and (B) 7E1-D4 to immobilised human (hu) and mouse (ms) TREM2 protein. Bound mAb were detected using a μ-chain specific HRP-labelled secondary. Error bars represent mean +/- SEM of duplicates in the assay.

Only mAb 7E1-E10 was taken forward for further testing, despite the low level of binding demonstrated in Figure 3.15. No bands were detected by this mAb in western blots of recombinant human and mouse TREM2 protein and no TREM2 staining was observed in flow cytometry of RAW264.7 cells (negative data not shown). Due to time constraints, no further characterisation of the anti-mouse IgM antibodies was performed.

3.2.4 TREM2 Variant-Specific Antibodies

3.2.4.1 Isotyping and Plate Binding Assays

For production of antibodies against the AD-associated TREM2 variants (R47H and R62H), TREM2-deficient mice were immunised with commercially sourced peptides designed in-house to include the wild-type and variant sequences at these positions. These peptides were conjugated to KLH, a large immunogenic carrier protein, to elicit a sufficient antibody response during immunisation. Generating antibodies against short peptides in general was expected to yield successful results. It was appreciated, however, that the production of antibodies specific to a single amino acid change would prove challenging, yet possible as was reported in previous studies (Stanker *et al.*, 1986; Hoylaerts and Millán, 1991; Yu *et al.*, 2007; Hakobyan *et al.*, 2008).

From the first round of immunisations, two fusions were performed (p.47 and p.62 wild types). Following the re-cloning and screening stages, only three clones were strongly positive from the p47 fusion against the immunised peptide and none of these showed specificity for p.47 wild type over p.47 mutant peptide (Figure 3.16). The p.62 wild type initially showed promising results but after the necessary multiple re-cloning steps, no peptide-specific antibody-producing clones were detected (negative data not shown).

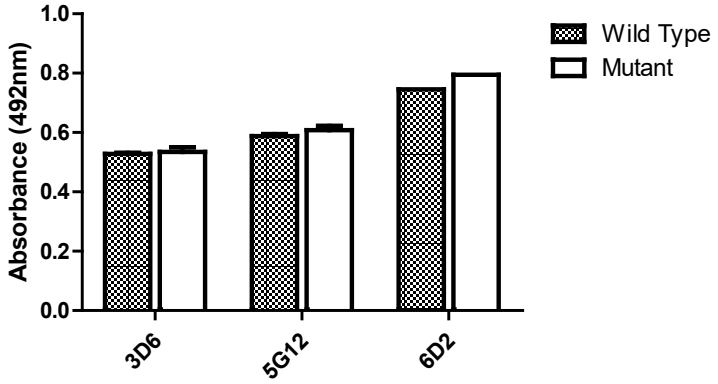

Figure 3.16 – Reactivity of first round of generated p.47 mAb against peptides.
Reactivity of clone supernatant from the first p.47 wild type fusion against wild type (R47) and mutant (H47) peptides. Error bars represent mean +/- SEM of duplicates in the assay.

A second batch of mice was immunised (3 mice per peptide) but this time the screening method was modified using the double-coating technique described in Chapter 2. Instead of coating with unconjugated peptide alone, a second coating step using BSA-conjugated peptide was introduced to increase the amount of peptide on the surface available for test serum or fusion supernatant to bind. Supernatant from clones generated using peptide immunisations was screened in duplicate against wild type and mutant (R47H, R62H) peptides to test their specificity; they were additionally screened against full-length recombinant wild type protein.

3.2.4.1.1 Immunisations using p.47 Peptide

Positive clones from the new p.47 wild type fusion were screed as above (Figure 3.17A); all clone supernatants showed similar reactivity to wild type and mutant peptides. All but one (5G10) of the clones screened were generated from the same primary clone (2A11) and showed similar affinity to both peptides. The 5G10 clone showed a higher binding to mutant versus wild type peptide and, along with 2A11 F1, showed stronger binding to the full protein compared to the other clones from this fusion (Figure 3.17B).

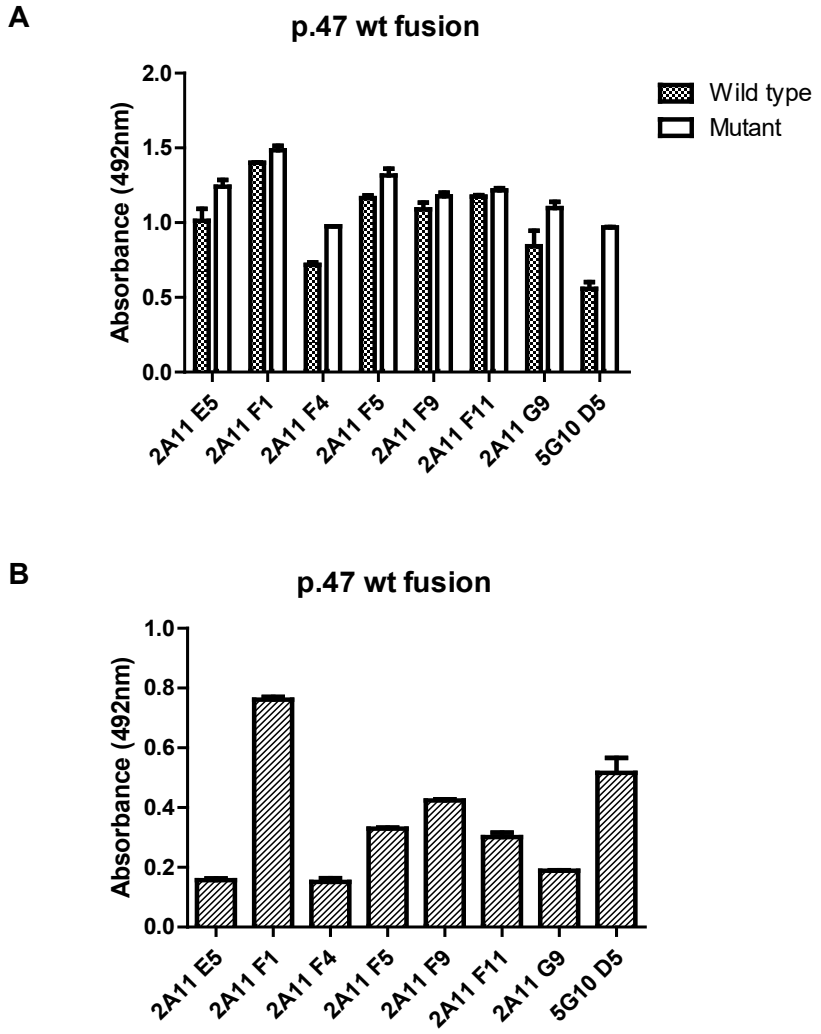

Figure 3.17 – Binding of p.47 wild type mAb to peptides and recombinant TREM2. Reactivity of clone supernatant from one p.47 wild type (wt) fusion against (A) wild type and mutant peptides and (B) TREM2 wild type protein. Seven out of the eight subclones originated from the same primary clone (2A11), the eighth was from a different clone (5G10). Error bars represent mean +/- SEM of duplicates in the assay.

From the two p.47 mutant fusions, the positive sub-clones were from seven different primary clones. None of these showed any significant differences in binding between the two peptides (Figure 3.18A); they all bound the full-length recombinant protein with varying strength of signal in the assay (Figure 3.18B).

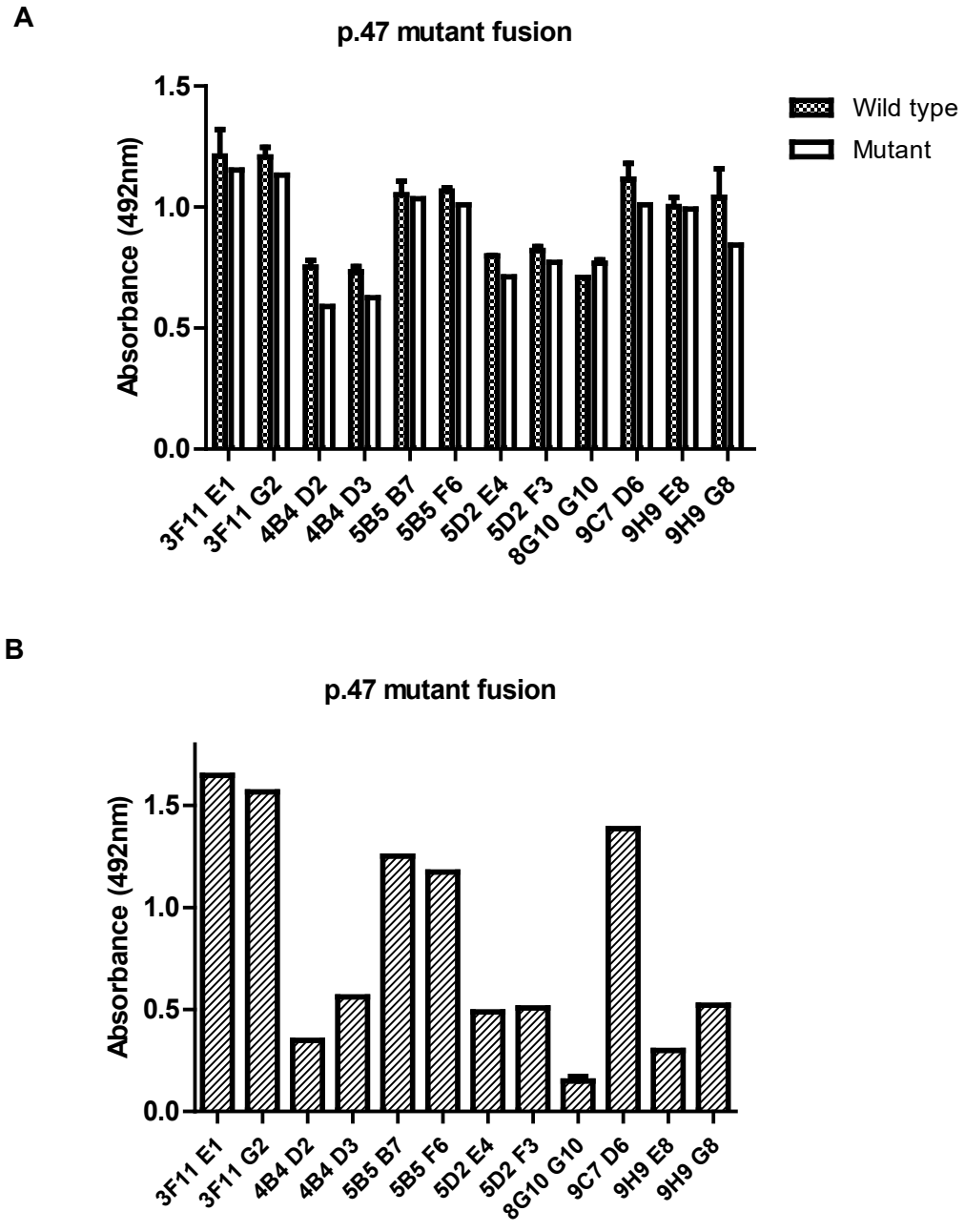

Figure 3.18 – Binding of p.47 mutant mAb to peptides and recombinant TREM2.
Reactivity of clones from two p.47 mutant fusions against (A) wild type and mutant peptides and (B) full length recombinant TREM2 wild type protein. Error bars represent mean +/- SEM of duplicates in the assay.

3.2.4.1.2 Immunisations using p.62 Peptide

From the p.62 wild type immunisation, selected sub-clones originated from seven primary clones (2A2, 3B12, 7H11, 8E11, 9B9, 9G2, 10G12). While most of the clones bound the wild type and mutant peptides to a similar degree, three showed clear preferential binding of one peptide over the other in the plate binding assay (Figure

3.19A). Clones 2A2-E3 and 7H11-C12 showed stronger binding to the wild type peptide over the mutant, and clone 9B9-C11 showed stronger binding to the mutant peptide over the wild type. Interestingly, the latter clone also showed very low binding to the full-length wild type TREM2 protein (Figure 3.19B).

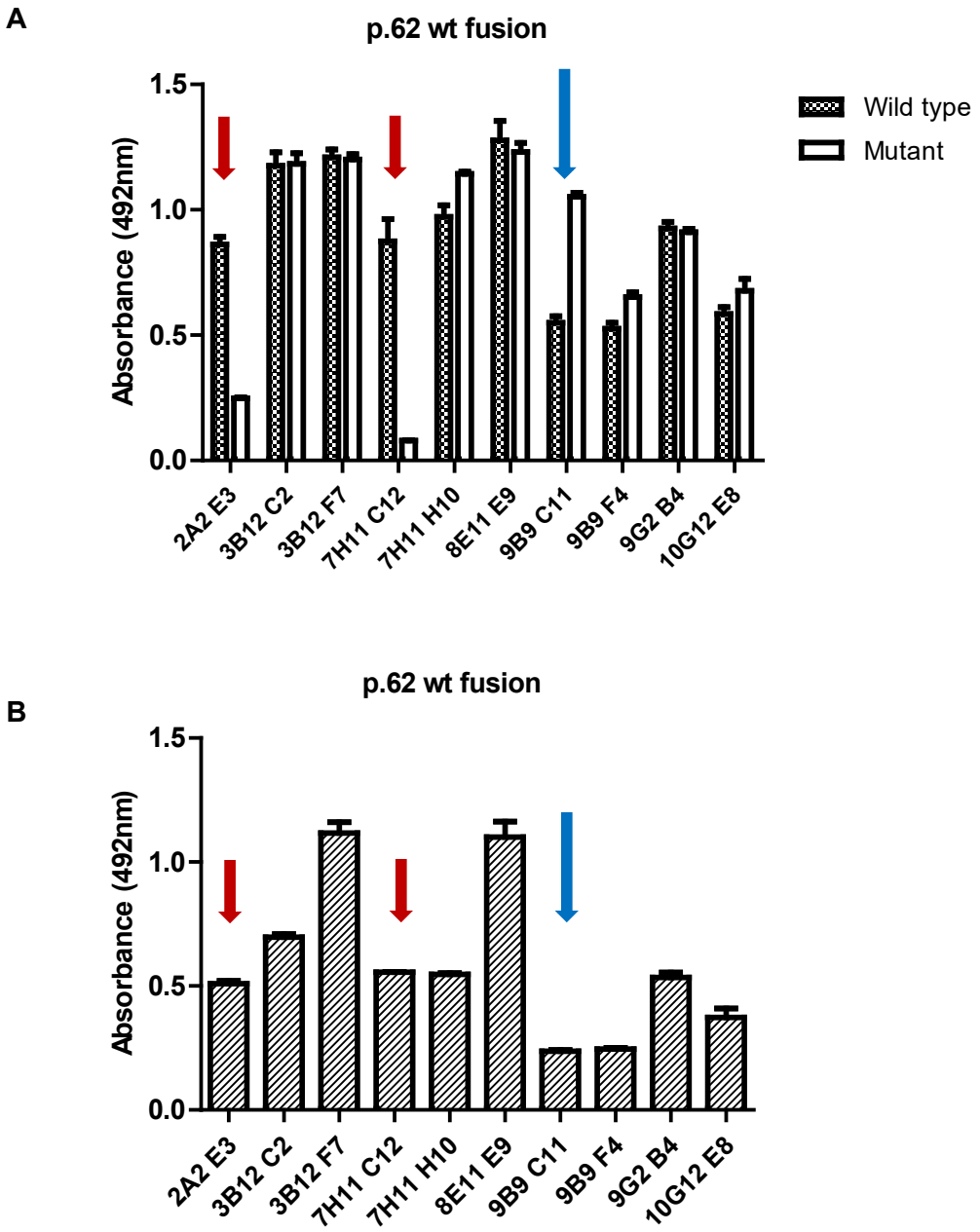

Figure 3.19 – Binding of p.62 wild type mAb to peptides and recombinant TREM2. Reactivity of clones from two fusions of p.62 wild type against (A) wild type and mutant peptides and (B) TREM2 wild type protein. Short red arrows indicate two sub-clones that bound wild type peptide stronger than mutant, while the long blue arrow indicates a single sub-clone that bound mutant peptide stronger than wild type. Error bars represent mean +/- SEM of duplicates in the assay.

From the p.62 mutant fusions, three primary clones were selected; Figure 3.20A shows the reactivity of sub-clones selected from each of these against p.62 mutant and wild type peptides; there was no clear selectivity between peptides for any of the subclones. Binding of most of the supernatants to the wild type protein was low (Figure 3.20B).

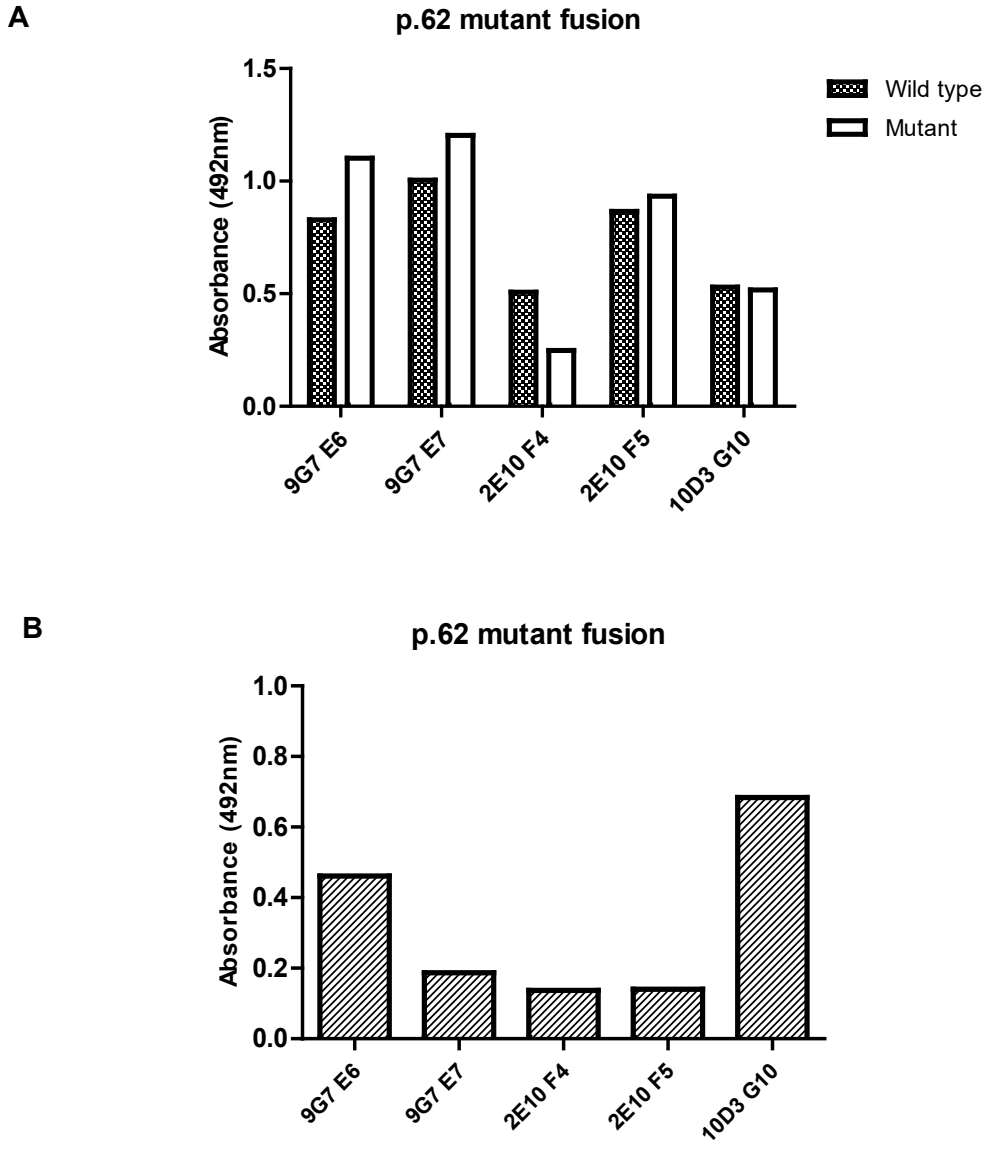

Figure 3.20 – Binding of p.62 mutant mAb to peptides and recombinant TREM2.
Reactivity of clones from two fusions of p.62 mutant against (A) wild type and mutant peptides and (B) TREM2 wild type protein. The selected sub-clones originated from 3 primary clones (9G7, 2E10 and 10D3).

All generated variant antibodies were tested and confirmed to be of the IgM class, as observed with the anti-mouse TREM2 antibodies described in the previous section. Supernatants from selected sub-clones were purified over a protein L column and Coomassie-stained to check quality. Successfully purified variant antibodies are shown in Table 3.3 and Figure 3.21.

p.47 antibodies	p.62 antibodies
3F11-G2 *(mut)*	2A2-E3 *(wt)*
8G10-G10 *(mut)*	7H11-C12 *(wt)*
	9B9-C11 *(wt)*
	10D3-G10 *(mut)*

Table 3.3 – Summary of generated p.47 and p.62 variant-targeted antibodies.
Selected antibodies from p.47 and p.62 fusions, brackets indicate whether the peptide used for immunisation was wild type (wt) or mutant (mut).

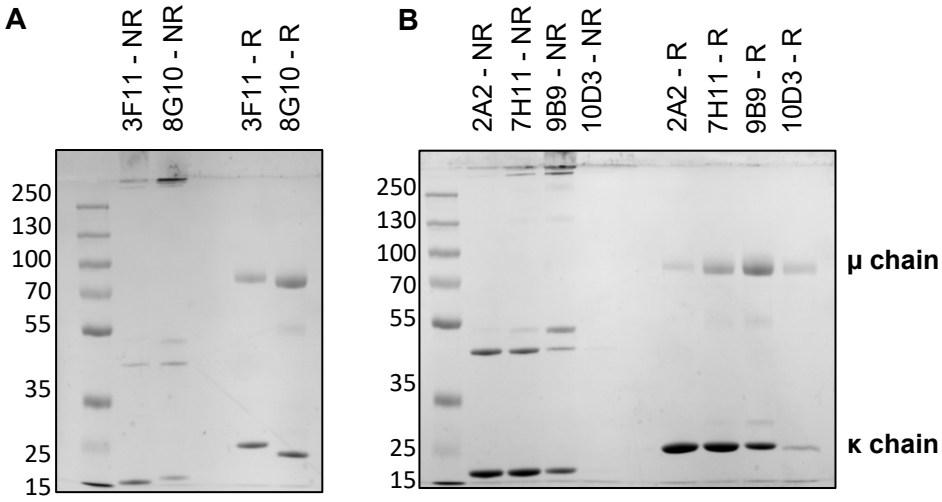

Figure 3.21 – SDS-PAGE of generated p.47 and p.62 variant-targeted antibodies.
Coomassie staining of purified mAb raised against (A) p.47 peptide and (B) p.62 peptide. Reducing (R) conditions show the μ heavy chain of IgM at ~70kDa and the κ light chain at ~25kDa. NR: non-reducing.

3.2.4.2 Variant Antibody Specificity

Purified mAb were tested by ELISA on wild type and mutant peptides, and on recombinant wild type TREM2 protein, to investigate overall binding efficiency and to confirm the specificity previously observed in supernatants from the clones (Figure 3.19A) for the mAb 2A2-E3, 7H11-C12 and 9B9-C11. The observed difference in specificity was not replicated with the purified mAb (Figure 3.22). However, two of the other purified antibodies (3F11-G2 and 10D3-G10) did show preferential binding to mutant versus wild type peptides, and did not bind wild type TREM2 protein (Figure 3.23).

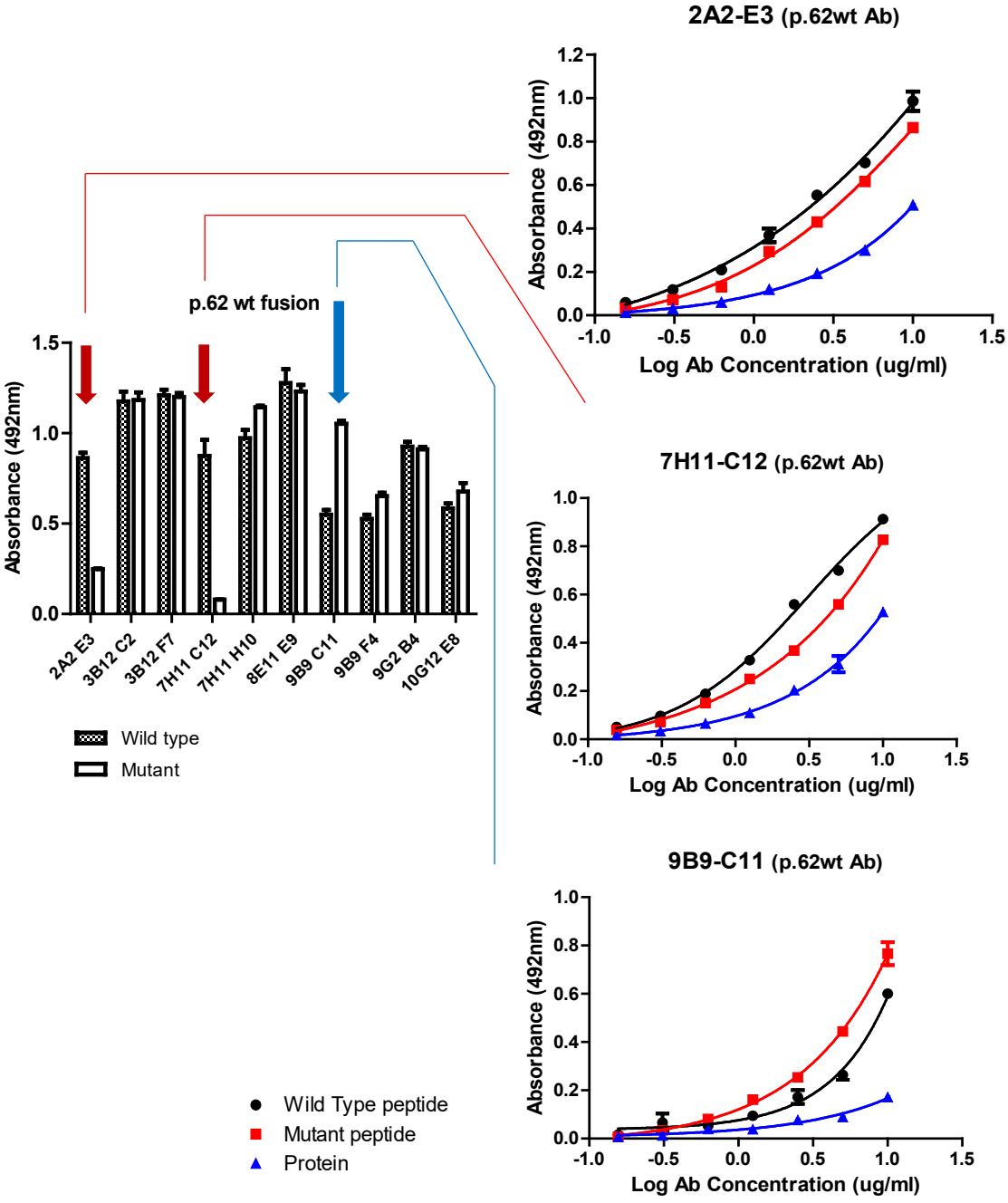

Figure 3.22 – Reactivity of variant antibodies pre- and post-purification.
Specificity previously observed for the supernatant of variant antibodies 2A2-E3, 7H11-C12 and 9B9-C11 was lost after the antibodies were purified and re-tested on wild type and mutant peptides. Supernatants 2A2-E3 and 7H11-C12 initially showed higher binding to wild type over mutant peptide but after purification, the mAb strongly bound both peptides similarly. Supernatant 9B9-C11 showed higher binding for the mutant versus the wild type peptide but after purification, binding for both peptides were similar with almost no binding to wild type protein. Error bars represent mean +/- SEM of duplicates in the assay.

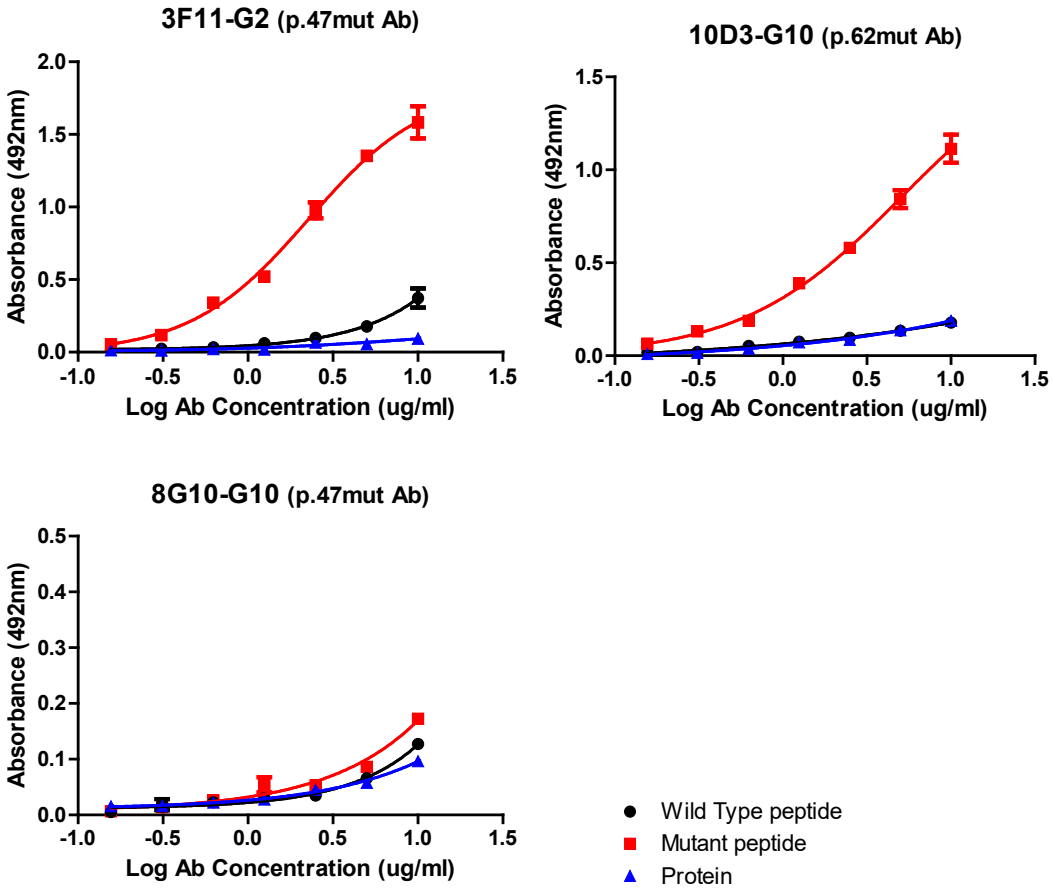

Figure 3.23 – Reactivity of variant-targeted mAb against peptides and TREM2 protein. Binding of variant-targeted mAb against wild type peptide (black), mutant peptide (red) and recombinant wild typeTREM2 protein (blue). Antibodies 3F11-G2 and 10D3-G10 showed stronger binding to the mutant over the wild type peptides and weak or negative binding to TREM2 recombinant protein. Antibody 8G10-G10 showed poor binding to both peptides post-purification. Error bars represent mean +/- SEM of duplicates in the assay.

The specificity of these two antibodies was also tested by western blotting, using peptides conjugated to a different carrier protein (BSA) rather than the KLH protein that was used for immunisation. An equal concentration of BSA alone was run alongside the samples as a negative control. The mAb 3F11-G2 gave strong bands at molecular weights of ~68kDa and ~100kDa for the p.47 mutant, but not p.47 wild type, peptide conjugate and only under reducing conditions; no bands were seen in the BSA control lanes (Figure 3.24A). The multiple bands at different sizes observed are a consequence of the formation of conjugates containing different BSA-peptide ratios; unconjugated BSA has a molecular weight of 65kDa and each peptide adds ~1.6kDa to the apparent mass. The mAb 10D3 gave strong bands at molecular weights of ~68kDa and ~100kDa for the p.62mut only under reducing conditions, but

not p.62wt peptide conjugate; a trace of staining was seen in the BSA control lane (Figure 3.24B). All other controls were negative (Figure 3.24C).

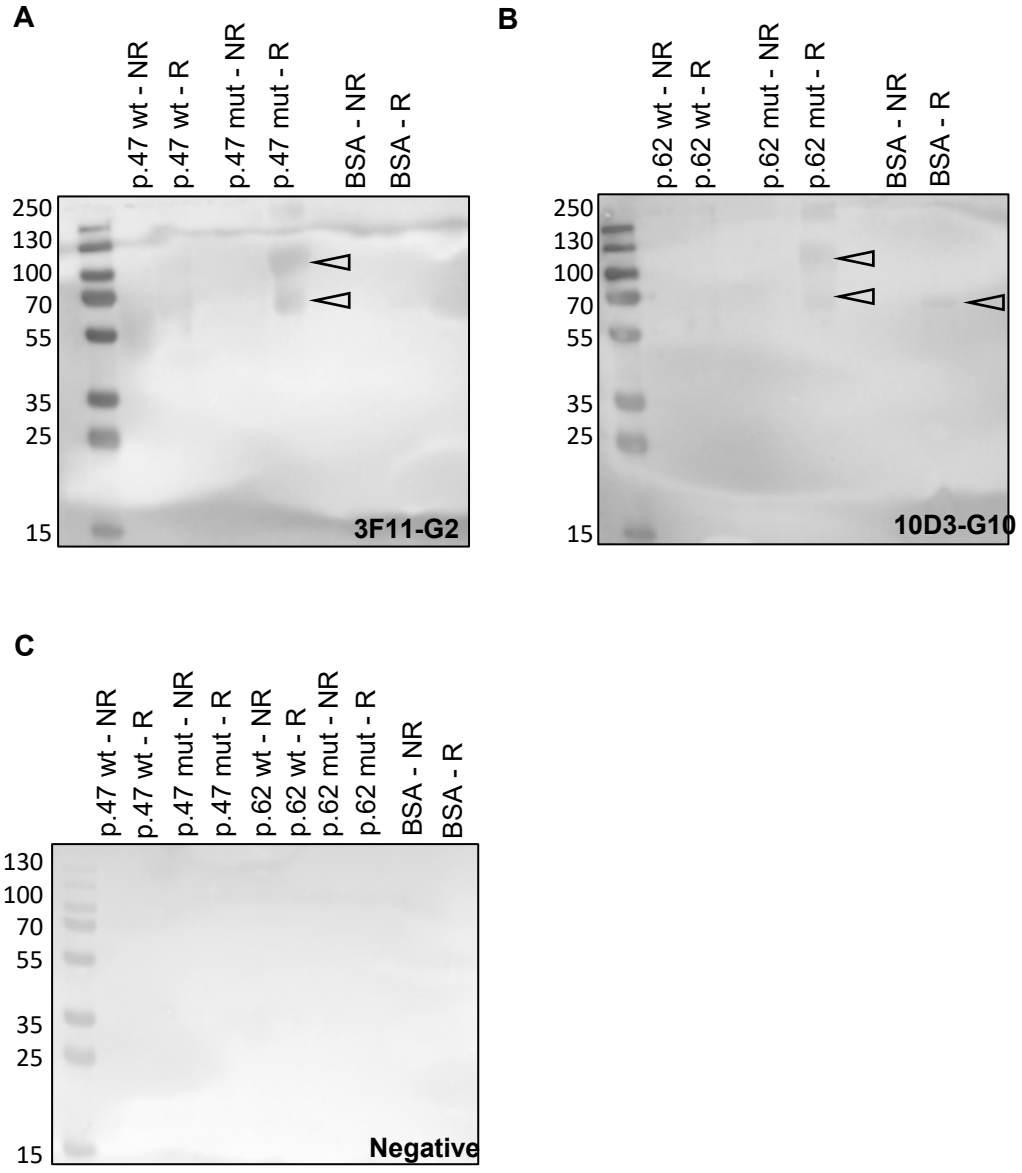

Figure 3.24 – Western blot of variant-targeted mAb 3F11 and 10D3.
Western blots showing specific binding of each of (A) 3F11-G2 and (B) 10D3-G10 to the mutant (mut) peptide in reducing (R) conditions. Faint binding of BSA alone was observed with mAb 10D3. (C) Negative controls were loaded on a separate gel. BSA alone was loaded on each gel as an additional negative control. Arrows indicate band positions.

As further proof of specificity, the two mAb were tested on irrelevant BSA-conjugated peptides and BSA alone in a plate binding assay: p.47-targeted mAb 3F11 was tested on p.62 peptides, and p.62-targeted mAb 10D3 was tested on p.47 peptides. Surprisingly, the 3F11 mAb raised against mutant p.47 peptide bound the mutant, but not the wild type, p.62 peptide, while the 10D3 mAb raised against mutant p.62 peptide also bound the mutant and (more weakly) the wild type forms of the p.47 peptide; binding to BSA alone was absent for 3F11 and weak for 10D3 (Figure 3.25). To investigate whether this finding was due to non-specific binding to BSA, the assay was repeated using milk as blocking agent but this change resulted in no binding of the antibodies to any of the peptides, including the ones they were raised against.

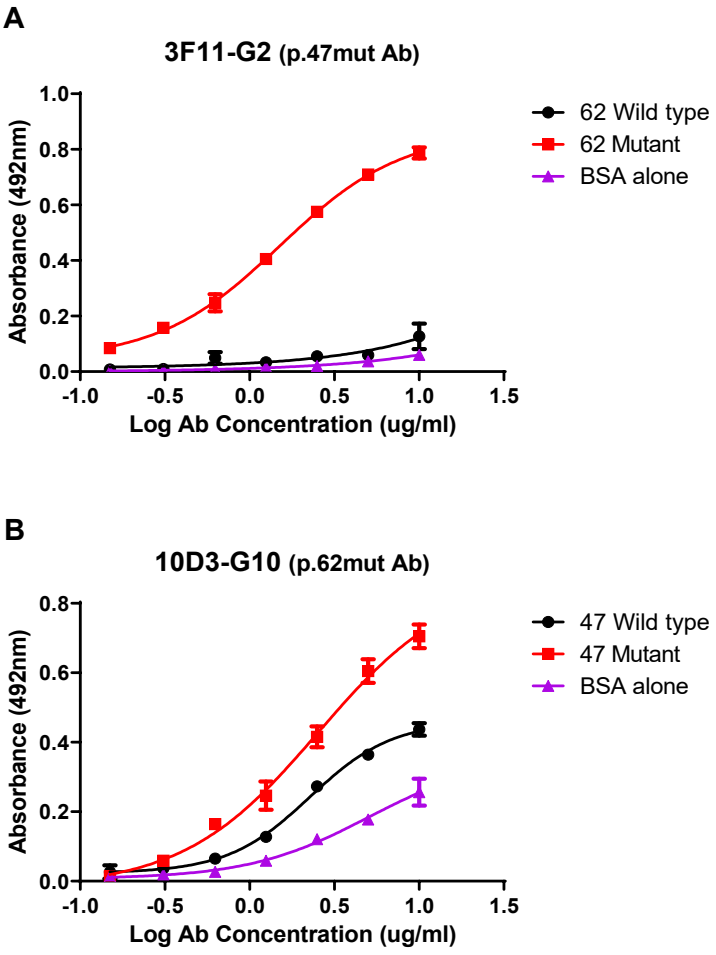

Figure 3.25 – Binding of variant mAb to irrelevant peptides.
Binding was observed for the (A) p.47-targeted mAb 3F11 with the mutant form of the p.62 peptide. (B) The p.62-targeted mAb 10D3 bound the mutant form of the p.47 peptide, with lower binding observed for the wild type and for BSA alone. Error bars represent mean +/- SEM of duplicates in the assay.

The peptides used for immunisation were designed without an overlap as demonstrated in Figure 3.26, so antibodies raised against one peptide should not bind to the other. Further investigation is required to confirm specificity of these antibodies, such as the use of variant TREM2-expressing cell lines as positive controls.

```
                    p.47 peptide              p.62 peptide
Design:       PYDSMKHWGRHKAW----------QHVVSTHNLWLLS
Protein: 37   PYDSMKHWGRRKAWCRQLGEKGPCQRVVSTHNLWLLS  73
```

Figure 3.26 – Alignment of peptide sequences with TREM2 protein sequence.
Sequence design for peptides covering p.47 and p.62 were aligned with the TREM2 protein sequence to demonstrate the lack of overlap between peptides. Numbers indicate the position of the first and last amino acid relative to the protein. Protein sequence available from Protein [Internet], NCBI: https://www.ncbi.nlm.nih.gov/protein/NP_061838.1 (Allcock *et al.*, 2003).

3.3 Discussion

3.3.1 Human TREM2 Antibodies

This chapter describes the production and characterisation of mAb against human and mouse TREM2, including mAb designed to be selective for the AD-associated variants in the human protein. The anti-human TREM2 mAb were raised against a commercially sourced protein comprising the extracellular portion of TREM2 (174 amino acids) fused to a poly-His tag (Sino Biological Inc., Stratech Scientific Ltd).

3.3.1.1 Reactivity of Human Antibodies to Recombinant TREM2 Protein

As a first check for antibody specificity, plate binding assays comparing the test protein with an irrelevant His-tagged protein confirmed that the selected anti-human TREM2 mAb were not reactive with the His-tag. Strong binding to recombinant human TREM2 protein was observed on western blots and in plate binding assays for mAb 9D10, 9A9-3, 5D11, 8G10 and for the polyclonal antibodies; all western blots gave major bands at the expected size (~35kDa for the glycosylated protein made in HEK293 cells according to supplier data). With the exception of 5D11 and the in-house polyclonal antibody, all mAb showed binding to recombinant mouse TREM2 in plate binding assays, but only mAb 9D10 showed clear binding to mouse TREM2 on a western blot (Figure 3.7). This difference between assays may be explained by the higher level of sensitivity of plate binding assays compared to western blot (Bass *et al.*, 2017).

3.3.1.2 Characterisation Comparison of Commercial and In-House Antibodies

A commercial anti-TREM2 polyclonal (AF1828; R&D Systems) was added to the characterisation process for comparison. Both the in-house and commercial polyclonal antibodies strongly bound human TREM2 in ELISA and western blots. The commercial antibody bound mouse TREM2 in ELISA, but not western blot. Both antibodies also detected bands in the human THP1 cell lysate on western blots, but only the R&D antibody detected bands in the mouse RAW264.7 cell lysate. The sizes of the bands detected in lysates were different for the two polyclonal antibodies; the in-house polyclonal antibody detected a major band at ~55kDa, while the commercial detected a major band at ~45kDa (Figure 3.9). The commercial supplier's website (R&D Systems, Inc.; https://www.rndsystems.com/products/human-trem2-antibody_af1828) shows probing of THP1 lysates with the AF1828 polyclonal detecting a major band at 28kDa and a second strong band at ~45kDa, the latter similar to that described above.

Similarly to the antibodies generated in this project, the R&D polyclonal antibody was raised against recombinant human protein produced in a eukaryotic cell line. This means that the protein was glycosylated during processing making it similar to protein expressed in human or mouse cells, a feature that makes antibodies designed in this way more likely to bind epitopes on native proteins, unlike antibodies created using short synthetic peptides (Walker and Lue, 2018). As described in Chapter 1, TREM2 has two known N-glycosylation sites in its extracellular immunoglobulin domain and while the predicted molecular weight based on protein sequence is ~20-25kDa, the recombinant protein migrates at 35-40kDa due to its glycosylated state (Figure 3.6).

Discrepancies in the apparent molecular weights of TREM2 in western blots of cell or tissue lysates have been observed in other studies using the same R&D polyclonal antibody tested here. A study by Thornton *et al.* (2017), probing lysates of primary human macrophages and TREM2-expressing HEK293 cells identified major bands at 35kDa and 50kDa in lysates, with the second species also found in cell supernatants. Lue *et al.* (2015) reported TREM2 at 35-40kDa in western blots of human brain, and Kleinberger *et al.* (2014) observed multiple bands between 36-60kDa in lysates and supernatants of TREM2-expressing HEK cells; each study attributed these differing weights to variations in glycosylation. Thus, the higher apparent molecular weights of TREM2 in cell lysates detected by the in-house polyclonal antibody (~55kDa) and by

the mAb (~65kDa) may be due to the antibodies preferentially binding different glycosylation states of TREM2.

3.3.1.3 Reactivity of Human Antibodies to Native TREM2

All mAb, except the human-specific 5D11, detected bands in mouse and human cell lysates at ~65kDa, but differed in whether they detected bands in reduced lysate only or both non-reduced and reduced lysates (Figure 3.8). Binding of mAb 8G10 to the cell lysates was not tested and is required in future work. One interesting observation in this project was the similar molecular weights observed under reducing and non-reducing conditions for the recombinant proteins used for immunisation and antibody production (Figure 3.6C). This may indicate that the supplied protein was already in a denatured state; if the antibodies were raised against a specific structural orientation, this could result in the differences seen in binding native protein in cell lysates. This data is conflicting, however, because the in-house polyclonal, mAb 9D10 and 9A9-3 can detect TREM2 in serum as later demonstrated in Chapter 4, so the protein they were raised against must have a native (non-denatured) component, if only in part. Future work to shed more light on this question could involve mapping the mAb epitopes to investigate which TREM2 regions the antibodies bind to. Other work could include deglycosylation of the recombinant protein and cell lysates, for example using PNGase, to test effects on apparent molecular weight and impact on antibody binding.

The anti-human TREM2 mAb and polyclonal were next tested for capacity to bind surface expressed TREM2 using flow cytometry on THP1 and RAW264.7 cells, both known to express TREM2 (Allcock *et al.*, 2003; Humphrey *et al.*, 2006; Turnbull *et al.*, 2006; Kober *et al.*, 2016). For the THP1 cell line, none of the antibodies gave positive staining over background, including the commercial anti-TREM2 antibody (Figure 3.10C). Increasing concentrations of primary and secondary antibodies and pre-fixing the cells were attempted, but only slight increased staining above background was observed; these findings may indicate that the THP1 cells may display a low TREM2 surface expression and may require cell activation prior to flow cytometry. While inflammatory conditions are known to increase TREM2 expression *in vivo*, they appear to decrease it *in vitro* (Jay *et al.*, 2017), and the use of anti-inflammatory cytokines, such as IL-4, has been documented to increase TREM2 expression peritoneal macrophages (Turnbull *et al.*, 2006); THP1 stimulation in this way would be an interesting follow-up experiment to investigate whether increasing TREM2 surface expression displays stronger antibody staining.

In contrast to the human cell line, mAb 9D10 and 9A9-3 both showed strong staining of the mouse RAW264.7 cells (Figure 3.10D). mAb 8G10, which was expected to bind this cell line, did not show positive staining, however the specific batch used for this experiment was purified out at too low a concentration to be used accurately so this result may be unreliable and was not repeated due to time constraints. As expected, mAb 5D11 and both polyclonal antibodies did not stain RAW264.7 cells. Overall these results strongly suggested that mAb 9D10 and 9A9-3 detected native mouse TREM2, and failure of the polyclonal antibodies to stain these cells is unsurprising given that they did not bind recombinant mouse TREM2 protein on a western blot (Figure 3.7E-F); however, they did bind mouse TREM2 in a direct ELISA, suggesting that the polyclonal antibodies do cross-react with mouse TREM2, but weakly in comparison with mAb 9D10. Additional controls that should have been included in the above experiments include the use of an irrelevant primary antibody for the western blot work, such as an antibody against the neuronal marker NeuN which would not be expected to bind THP1 and RAW264.7 cell lysates. While the flow cytometry experiments included the use of isotype-matched antibodies as negative controls, it would have been useful to also include a positive control, such as an antibody against the chemokine receptor CX3CR1.

Table 3.4 summarises the characterisation results for the tested in-house and commercial (AF1828) antibodies.

Name	Plate Binding		Western Blot (Protein)		Western Blot (Cell Lines)		Flow Cytometry	
	Human	Mouse	Human	Mouse	Human	Mouse	Human	Mouse
AF1828	+	+	+	-	+	+	-	-
Polyclonal	+	/	+	-	+	-	-	-
9D10	+	+	+	+	+	+	-	+
9A9-3	+	+	+	/	+	+	-	+
5D11	+	-	+	-	+	-	-	-
8G10	+	+	+	/	*Not tested*		-	-

Table 3.4 – Characterisation of anti-human TREM2 antibodies
Summary table showing the binding of the human antibodies to human and mouse TREM2 recombinant protein using plate binding assays and western blots, and to human THP1 and mouse RAW264.7 cell lines using western blots and flow cytometry. + strong binding, / weak binding, - no binding.

3.3.2 Mouse TREM2 Antibodies

TREM2-deficient mice were immunised with the recombinant extracellular portion of mouse TREM2 (168 amino acids) including a poly-His tag (Sino Biological Inc.). Immune mice were identified, and three independent fusions were performed over the course of three months. Seven primary clones were selected based on ELISA screening for binding mouse TREM2 and numerous subclones of these were obtained at monoclonality.

3.3.2.1 Isotype Characterisation of Mouse Antibodies

A surprising finding was that when supernatants from these clones were isotyped using a commercial kit, all were IgM. This finding was investigated first by western blotting of the supernatants using the HRP-labelled anti-IgG antibody used in the screening assay, then further confirmed by purifying the different mAb on an IgM-compatible matrix and using class-specific antibodies in an ELISA, to demonstrate the presence of the μ-chain (Figure 3.12).

This finding was unexpected as long experience of making monoclonal antibodies against protein antigens in the host lab has taught that, with the protocol used, the large majority of resultant mAb are expected to be of IgG class. IgM antibodies are the earliest isotype secreted in an immune response and generating a large amount of IgM mAb can indicate that insufficient immunisation boosts were administered before the fusions were conducted. However, as mice in these immunisations received several boosts over 6-8 weeks in line with the regularly used protocol, other ideas were explored among the host lab group, including the suggestion that because the immunised mice were TREM2-deficient, they may have an affected immune response, as was reported by Hikida *et al.* (2009). This study explored whether PLCγ2, a protein downstream of TREM2, was required for the maintenance of memory B cells and reported an impaired secondary IgG response in a PLCγ2-deficient mouse model. Similar processes may be in effect in the TREM2 KO mice, deficits in the same pathway resulting in a higher ratio of IgM production over IgG, but unfortunately due to the time constraints of this PhD, further investigation of this finding was not possible. If an impaired immunoglobulin response is indeed linked to the absence of TREM2, it could implicate immunodeficiency in diseases such as Nasu-Hakola disease, where TREM2 mutations are associated with complete loss of function, as opposed to the partial loss of TREM2 function associated with AD.

3.3.2.2 Further Work for Characterisation of Mouse Antibodies

Several of the anti-mouse TREM2 clones did not grow as well as expected in culture, and surviving hybridoma supernatants, initially positive, showed reduced or entirely absent binding of mouse TREM2 protein after antibody purification; for example, mAb 7E1-D4 (Figure 3.15). As a consequence, only clone 7E1-E10 was taken forward for further characterisation and after purification demonstrated low binding to mouse and human TREM2 proteins in a plate binding assay. No TREM2 binding was observed for recombinant protein on western blots or membrane-bound protein in flow cytometry. Further testing is required to investigate whether these results indicate a true loss of reactivity or whether problematic secondary anti-IgM antibodies are responsible for the negative results, but continuation of this work was suspended due to time constraints.

3.3.3 Variant Antibodies

Although variants of TREM2 have been reported with low prevalence rates in Caucasian populations (Guerreiro *et al.*, 2013; Jonsson *et al.*, 2013), their associated high AD risk initiated several studies focusing on the role of TREM2 in AD. These investigations have been important in identifying TREM2 structure and function and in providing clues as to how the variants may affect ligand binding and microglial activity. Generating variant-specific antibodies could be useful in screening assays of both disease (AD, MCI) and control individuals to look at variant prevalence and as a potential risk predictor. The activating/blocking potential of these antibodies could also be investigated to test their effect in TREM2 ligand binding studies.

To obtain mAb specific for the AD-associated TREM2 variants, peptide immunisations of TREM2-deficient mice were performed using peptides containing the target variant epitopes. These generated numerous mAb that were reactive against the relevant peptide and the native TREM2 protein. The core aim of this part of the work was to generate mAb that differentiated the variants at R47H and R62H; however, plate binding assays testing the specificity of mAb raised against either the p.47 peptides or the p.62 mutant peptide showed, for the majority of the mAb, good peptide binding but little or no difference between binding of wild type versus mutant peptides regardless of which was immunised. Their reactivity to recombinant human TREM2 protein also varied widely between mAb (Figure 3.17-Figure 3.20).

3.3.3.1 Specificity of Variant Antibodies to p.47 and p.62 Peptides

A few clones from the p.62 variant peptide fusions showed more evidence of specificity when supernatants were tested in plate binding assays. These assays suggested that clones 2A2-E3 and 7H11-C12 bound wild type peptide (R62) more strongly than the mutant peptide (H62), while clone 9B9-C11 showed stronger binding to mutant over wild type peptide (Figure 3.19A). The reactivity of these antibodies to recombinant wild type TREM2 protein also varied with the latter clone showing very poor binding (Figure 3.19B). However, when these antibodies were purified, these findings of selectivity for variant peptides were not replicated (Figure 3.22).

Two variant-targeted mAb did show differences in specificity after purification. The 3F11-G2 mAb (raised against the p.47 mutant peptide; H47) and the 10D3-G10 mAb (raised against the p.62 mutant peptide; H62) both showed preferential binding to the mutant over the wild type peptides, and also showed poor reactivity, as anticipated, to wild type TREM2 protein (Figure 3.23). This peptide specificity was also demonstrated on a western blot using the relevant peptides bound to a different carrier protein (Figure 3.24), however this blot is not very clear and future work could involve repeating it using higher concentrations of loaded peptides for better visualisation of the blots.

3.3.3.2 Reactivity of Variant Antibodies to Irrelevant Peptides

When the mAb were tested against the opposite peptides, which was expected to yield a negative result, binding was observed. The peptide sequences for p.47 and p.62 do not overlap as demonstrated in Figure 3.26 and non-specific binding of BSA conjugate of the peptides was tested by substituting BSA for milk in the blocking step of the plate-binding assay. This inhibited binding of the mAb to all peptides, including those they were generated against, resulting in no further clues to the aberrant binding pattern previously observed. A follow up experiment could involve the use of PBS alone as a blocking agent to overcome the inhibitory effects seen with the milk block. An important step that should have been taken, prior to the start of these experiments, is sequencing the commercially-sourced peptides to ensure they are the correct sequences and accurately represent wild type and variant forms of TREM2. This would have demonstrated early on whether the identity of the peptides was connected in any way to the discrepancies observed throughout the antibody characterisation process.

Additional evidence is needed to support the specificity of these two mAb for their respective mutant TREM2 proteins. This is explored in the next chapter using wild type and mutant TREM2-expressing cell lines to test the binding specificity of the mAb. The next chapter will also describe further characterisation of the generated human antibodies, including mouse cross reactivity and expression profiles in TREM2-deficient and -sufficient mouse models.

Chapter 4

Results: Generation of Controls for Antibody Characterisation

4 Results: Generation of Controls for Antibody Characterisation

4.1 Introduction

The expression of TREM2 was first discovered on dendritic cells (Bouchon *et al.*, 2001) and was later reported on osteoclasts, macrophages and microglia (Daws *et al.*, 2001; Allcock *et al.*, 2003; Humphrey *et al.*, 2006; Turnbull *et al.*, 2006; Kober *et al.*, 2016). In the previous chapter, THP1 and RAW264.7, respectively human and mouse cell lines that express TREM2 (Allcock *et al.*, 2003; Humphrey *et al.*, 2006; Turnbull *et al.*, 2006; Kober *et al.*, 2016), were used to characterise the anti-human TREM2 antibodies. To test the specificity of the variant antibodies produced in this project, positive controls that expressed the R47H and R62H variants were required. Transfection of cells was performed using vectors containing sequences that represented either the wild type (R47; R62) or the variant forms of TREM2. Messenger RNA (mRNA) expression of the cell lines was assessed using qPCR and protein expression was investigated using western blotting and ELISA.

As described in Chapter 1, mouse models are important research tools to further understand AD pathogenesis, risk-associated mutations and clinical implications of therapeutics. TREM2 KO mice were used for monoclonal antibody production and additionally for characterisation by comparing antibody binding in monocytic isolates, brain tissue and serum samples between KO and matched wild type mice. This comparison aimed to confirm cross-reactivity of the antibodies with mouse TREM2 and examine their suitability for use with mouse models and the development of functional assays.

4.1.1 Aims and Objectives

The aims of this chapter are to produce TREM2-expressing cell lines for characterisation of the variant antibodies, and to investigate immunostaining of cells and tissue from WT and KO mice as a means of further confirming the specificity of human antibodies that cross-react with mouse TREM2.

4.2 Results

4.2.1 Antibody Characterisation using TREM2-Expressing Cell Lines

4.2.1.1 Antibiotic Selection

The vector used for transfection was designed to contain antibiotic resistance genes for ampicillin and neomycin. Ampicillin was used for the positive selection of colonies during the cloning and transformation of the vector into bacterial cells. Neomycin was intended for the positive selection of cells after vector transfection, but initial trials using neomycin at recommended doses on non-transfected cells showed no cell death. G418 sulfate (Geneticin), a neomycin analogue that inhibits protein synthesis by binding 80S ribosomes (Bar-Nun *et al.*, 1983), has been documented as an efficient selective agent in mammalian cells (Davies and Jimenez, 1980; Chen and Okayama, 1987) and proved more successful than neomycin in the following experiment.

HEK293 cells, which do not express TREM2 (Uhlén et al., 2015; Thul et al., 2017), were selected for lipofectamine transfection with separate vectors containing human wild type, human variant (R47H or R62H) or mouse TREM2. G418 sulfate was added to the non-transfected cells at increasing concentrations to evaluate what concentration of the selective antibiotic would kill cells. Percentage confluence of cells was monitored daily and medium was replaced with fresh antibiotic-containing medium every 2 days. The lowest antibiotic concentration that killed 100% of non-transfected cells after 8 days was determined to be 600µg/ml (Figure 4.1).

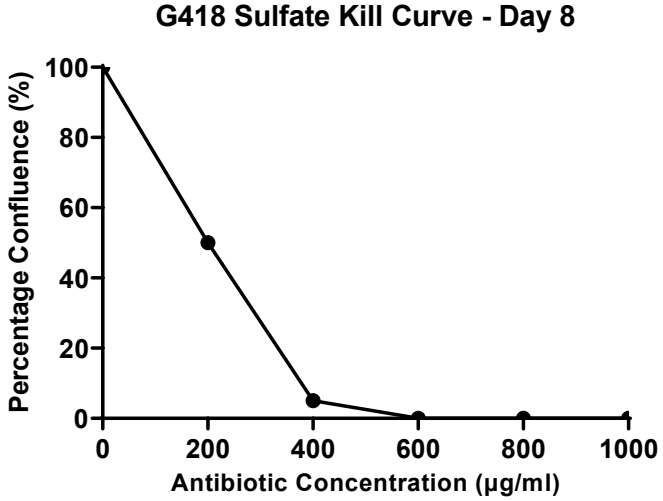

Figure 4.1 – G418 sulfate kill curve on day 8 of antibiotic selection.
A kill curve was generated by adding increasing concentrations of G418 sulfate to non-transfected cells, a 600µg/ml concentration was selected for cell treatment post-transfection.

4.2.1.2 Expression of Protein in Transfected Cell Lines

As this project is mainly protein-focussed, protein expression from cell lysates generated in the transfection experiments was investigated. Lysates from non-transfected and transfected HEK293 cells were separated by SDS-PAGE to investigate binding of the polyclonal antibody to expressed TREM2. As previously demonstrated in Chapter 3, the in-house polyclonal was expected to bind native TREM2 in lysates at ~55kDa – a band size that was unexpectedly detected in both the non-transfected and transfected cells (Figure 4.2A).

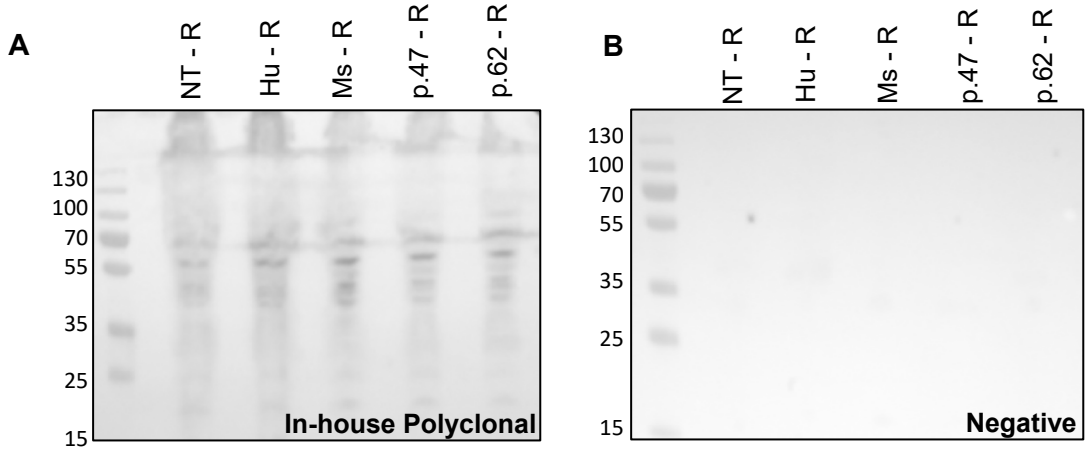

Figure 4.2 – Western blots showing TREM2 binding in transfected HEK293 lysates. TREM2 was detected in non-transfected (NT) and transfected cell lines for human (Hu), mouse (Ms), TREM2 variants p.47 and p.62, using (A) the in-house polyclonal antibody under reducing (R) conditions. (B) A negative control blot comprising the same lysates was probed with the HRP-labelled anti-rabbit secondary antibody alone.

Protein expression of human and variant TREM2-expressing cell lysates was also investigated using the human TREM2 ELISA, which will be described in more detail in Chapter 5. Lysates from THP1 cells and non-transfected HEK293 cells were included as positive and negative controls, respectively. The lower limit of detection for this assay (as described in Chapter 5) was calculated to be 0.4ng/ml; this was similar to the TREM2 concentration detected for non-transfected cells so this is likely a negative result as expected. The assay detected TREM2 in the THP1 positive control and in the variant TREM2-expressing cell lines, with a low level detected in the human wild type-expressing line (Figure 4.3).

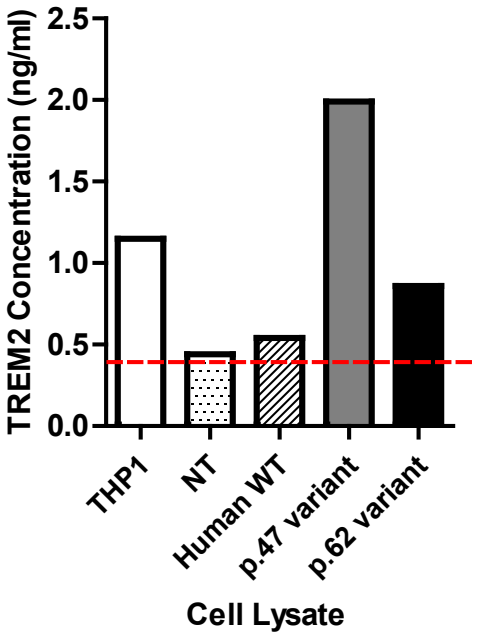

Figure 4.3 – TREM2 expression in transfected and non-transfected cell lysates.
Graphical representation of TREM2 concentrations observed in transfected and non-transfected cell lysates. The TREM2 level in non-transfected (NT) cells was considered negative, red dashed line denotes assay detection limit (0.4ng/ml). TREM2 was detected in the positive control (THP1) and the two variant-expressing lines, with a much lower level observed in the human wild type (WT)-expressing line.

While the ELISA suggested that the non-transfected cell line did not express TREM2, since the level detected was similar to the assay's background levels, it is unclear why the polyclonal antibody detected bands in all samples, including the non-transfected line, in the western blot. To investigate these conflicting findings, and to assess the mouse TREM2-transfected line that could not be analysed by the human ELISA, focus turned to measuring TREM2 expression at the mRNA level.

4.2.1.3 Expression of mRNA in Transfected Cell Lines

To measure TREM2 mRNA expression, qPCR was performed on both the non-transfected and transfected cell lines. RNA was extracted from the lysates and concentrations were measured by spectrophotometry prior to cDNA generation. To assess the purity of extracted RNA, the ratios of absorbance at 260nm and 280nm (260/280) and at 260nm and 230nm (260/230) were calculated. A 260/280 ratio of 1.9-2.0 and a 260/230 ratio of 1.8-2.2 normally indicate high RNA purity; a low 260/280 ratio indicates the presence of protein or phenols with an absorbance range close to 280nm, while a low 260/230 ratio indicates the presence of other

contaminants that absorb at 230nm (Gallagher, 2001; Desjardins and Conklin, 2010). The extracted RNA concentrations, 260/280 and 260/230 ratios are displayed in Table 4.1.

The 260/280 ratios for all samples were within the expected range indicating the sample were free from protein contaminants, while the 260/230 ratios varied between samples but were considerably lower than expected. This indicated the presence of contaminants in the sample that absorb at 230nm, likely the guanine thiocyanate component in the Qiagen kit lysis buffer used during the first extraction step. There is generally no acceptable lower limit of this ratio to determine sample suitability for downstream processes, such as qPCR, and studies have shown that low 260/230 ratios do not compromise qPCR amplification efficiency (Cicinnati *et al.*, 2008; von Ahlfen and Schlumpberger, 2010; Kuang *et al.*, 2018). However, future work should include an additional wash step to desalt and further purify the samples during RNA extraction.

HEK293 Lysate	RNA Concentration (ng/µl)	260/280 Ratio	260/230 Ratio
Non-transfected	345.7	2.0	0.3
Human wild type	132.6	2.1	0.2
Mouse wild type	361.1	2.1	0.9
p.47 variant	448.7	2.1	1.0
p.62 variant	195.9	2.0	0.6

Table 4.1 – RNA concentrations of HEK293 cell lysates.
RNA concentrations (ng/µl) of non-transfected and transfected HEK293 lysates. Nucleic acid purity is represented as the ratio of absorbance at 260nm and 280nm (260/280) and at 260nm and 230nm (260/230).

Human TREM2 primers were used for the non-transfected HEK293 cells and for cells expressing human wild type and variant forms of the protein. Mouse TREM2 primers were used for the transfected cells expressing mouse TREM2. qPCR was run on cDNA that was generated from the HEK293 RNA samples, alongside THP1 cDNA as a positive control and GAPDH as a housekeeping gene. Negative controls included no-template controls, where cDNA was substituted for nuclease-free water, and no-reverse transcriptase (no-RT) controls, where RNA samples had not undergone reverse transcription, therefore lacked cDNA.

Amplification results were plotted as delta normalised reporter (ΔRn) value against number of cycles, with Rn being the fluorescent signal normalised to the reference dye, and ΔRn representing the strength of the amplification signal by subtracting the equipment's baseline Rn value from the experimental Rn value. The positive control THP1 cell line showed a strong TREM2 amplification as expected, but the non-transfected and transfected cell lines showed amplification 10-12 cycles later, (Figure 4.4). No amplification curve was observed for the mouse TREM2-expressing cell line (negative data not shown).

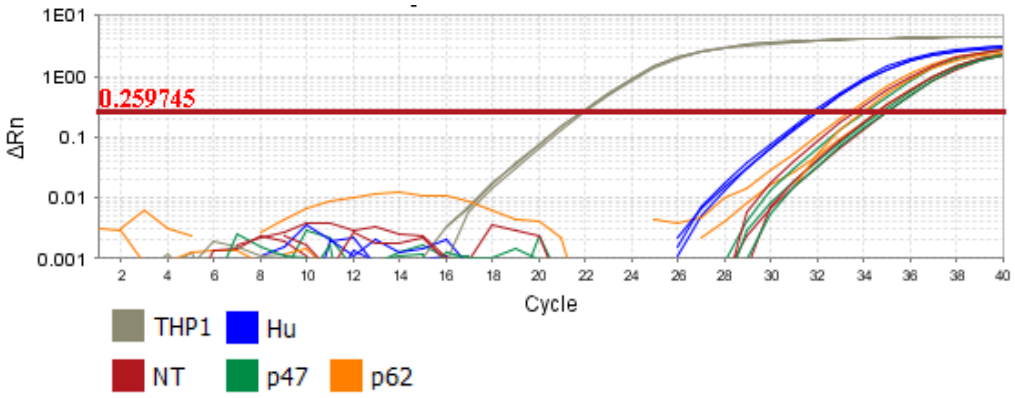

Figure 4.4 – Real-time PCR amplification of generated HEK293 cell lines.
Graphical representation of TREM2 amplification curves of non-transfected (NT) and transfected HEK293 cell lines, for human (Hu) and variant (p47, p62) TREM2, compared to the THP1 positive control. Magnitude of amplification is represented by ΔRn and threshold is indicated by the horizontal line.

To quantify TREM2 mRNA expression of the tested samples, Ct values were analysed relative to the housekeeping gene using the ΔΔCt method described in Section 2.7.1. Ct values represent the number of cycles required to increase the fluorescent signal above the threshold, or background level. Non-transfected HEK293 cells were not expected to express TREM2, observing amplification curves for this sample was not ideal and Ct values were analysed to reassure that these curves were not significant and to demonstrate the difference in TREM2 expression between theHEK293 transfections and the positive control, THP1 cells (Figure 4.5). To further investigate the unexpected finding of amplification curves in non-transfected samples, the qPCR reaction products should have been run on an agarose gel and additionally sequenced to identify the amplicons, but time constraints prevented this step from being carried out.

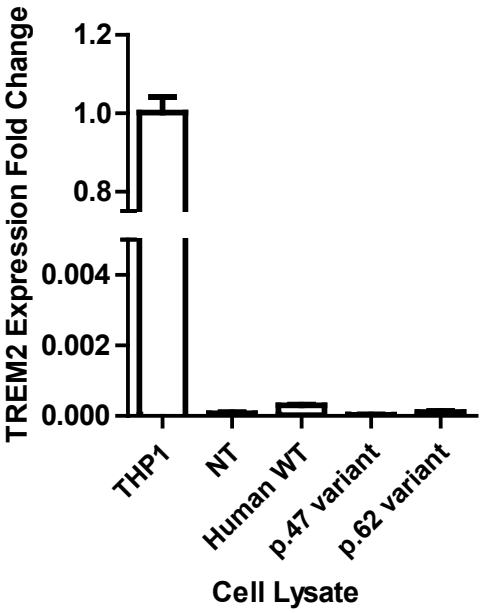

Figure 4.5 – Comparison of TREM2 expression between THP1 and HEK293 cells. Although amplification curves were observed for non-transfected cells, using THP1 as a reference (mean=1.0002) for comparison indicated that non-transfected HEK293 cells did not express TREM2 mRNA (mean=0.00008) as expected. Transfected cells also failed to express TREM2 (means=0.00005-0.003). Error bars represent mean +/- SEM of triplicates in the assay. NT: non-transfected, WT: wild type.

NCBI-BLAST software was used to check for discrepancies that may explain the qPCR results. The vector provided by Genscript was created based on the optimal codon sequence to generate the amino acid sequences requested. While the DNA sequences were predicted to correctly translate to the human or mouse TREM2 proteins, they did not align to the human or mouse DNA sequences using NCBI-BLAST (Altschul *et al.*, 1990). The closest resemblance (77% alignment) was with TREM2 mRNA sequences for another species (Equus genus), explaining the failure of the amplification using human or mouse TREM2-specific primers and the lack of TREM2 mRNA expression seen in the transfected cell lines. Requesting DNA, instead of protein, sequences would have avoided this problem. Confirming that the peptides received were correct would also be necessary, both by checking accompanying documents and by sequencing the peptides. Vector design therefore required correction prior to repeating the transfection experiment, but this was not possible due to time constraints and limited laboratory access during pandemic restrictions.

4.2.2 Investigation of Antibody Cross-Reactivity to Mouse TREM2

To further validate the antibodies that showed binding to mouse TREM2 in Chapter 3, primary monocytes were isolated from WT and TREM2 KO mice to act as positive and negative controls respectively. Monocytic isolates were first analysed using qPCR to demonstrate their suitability as controls before antibody binding in flow cytometry and immunofluorescence was tested.

4.2.2.1 Quantitative PCR of WT and TREM2 KO Primary Monocytic Isolates

Primary monocytes were isolated from two mice per genotype using CD11b-microbead separation. CD11b selects for a cell population that is highly enriched in, but not specific to, microglia, so brains were perfused with saline prior to isolation to minimise the presence of other myeloid cells. While CD11b sorting is commonly used during microglial isolation techniques (Garcia *et al.*, 2014; Grabert and McColl, 2018; Bohlen *et al.*, 2019), additional selective markers should have been used in downstream processes, as will be discussed later in this chapter.

Isolated cells were lysed and RNA extracted and quantified (Table 4.2), RNA purity assessment showed expected values for the 260/280 ratio and low values for the 260/230 ratio, as previously observed and discussed.

Monocytic Sample	RNA Concentration (ng/µl)	260/280 Ratio	260/230 Ratio
WT 1	44.9	2.0	0.5
WT 2	36.0	1.9	0.7
KO 1	54.4	1.9	0.1
KO 2	33.3	2.0	0.1

Table 4.2– RNA concentrations of monocytic isolates.
RNA concentrations (ng/µl) of primary monocytes from WT and TREM2 KO mice (2 mice per genotype). Nucleic acid purity is represented as the ratio of absorbance at 260nm and 280nm (260/280) and at 260nm and 230nm (260/230).

Clear TREM2 amplification was observed for the WT samples as expected. Although the KO samples did show weak amplification in the system, these appeared 12-16 cycles later in the reaction and are likely not significant (Figure 4.6).

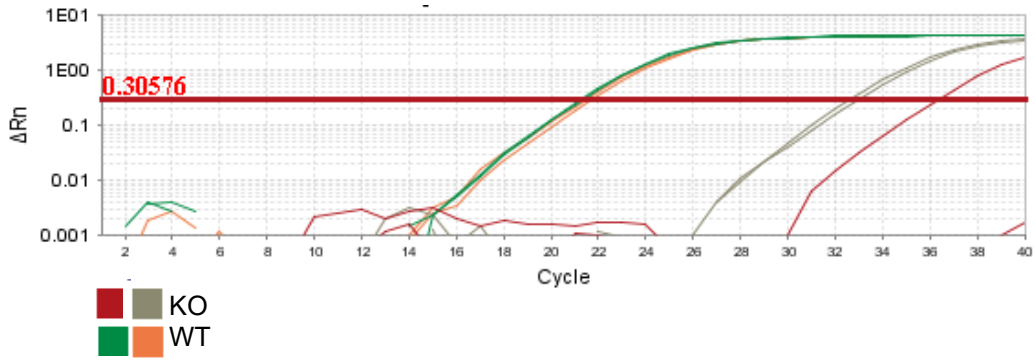

Figure 4.6– Real-time PCR amplification of WT and TREM2 KO monocytic isolates. Graphical representation of TREM2 amplification curves of WT and TREM2 KO monocytic isolates. Strong amplification is observed for the WT samples, amplification in the TREM2 KO samples is detected 12-16 cycles later. Magnitude of amplification is represented by ΔRn and threshold is indicated by the horizontal line.

As previously described, ΔΔCt analysis was performed to calculate the TREM2 mRNA expression fold change between wild type and KO samples. A wild type sample (WT 1) was used as the reference control and Ct values were analysed relative to the housekeeping gene. Detecting amplification curves in the KO samples was unexpected, so the final mean ΔΔCt values were combined and plotted for each genotype, to reassure that the detected KO signal did not reflect a significant difference in expression compared to the wild type results (Figure 4.7).

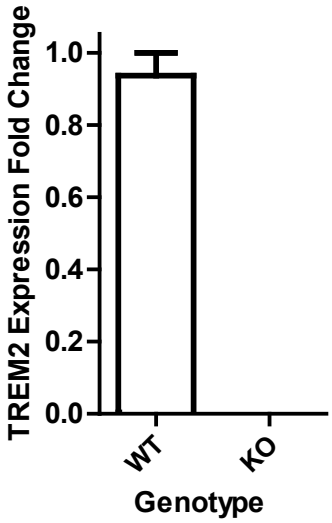

Figure 4.7 – TREM2 mRNA expression fold change between WT and KO mice. Compared to the WT (mean=0.9364), TREM2 KO (mean=0.0002) mice showed no expression of TREM2 as expected. Error bars represent mean +/- SEM of duplicates in the assay.

While all no-template and no-RT controls tested with TREM2 primers were negative as expected, amplification of the housekeeping gene was unexpectedly detected in no-RT controls containing RNA only (Figure 4.8). The melt curve plots for 18S amplification with and without cDNA were compared to investigate whether non-specific amplification or the presence of primer-dimers were responsible for the unexpected amplification seen in the above negative controls. The curves were plotted as the derivative reporter (-Rn') against temperature, with -Rn' indicating the rate of change in fluorescence during the temperature ramp. The plots demonstrated amplification of the same product in samples with and without cDNA, suggesting the presence of genomic DNA contamination in the samples (Figure 4.9). No monocytic isolates were left over after the experiment to troubleshoot this reaction and time constraints prevented further steps to resolve this observation, such as sequencing the amplified no-RT control products to identify the amplicons.

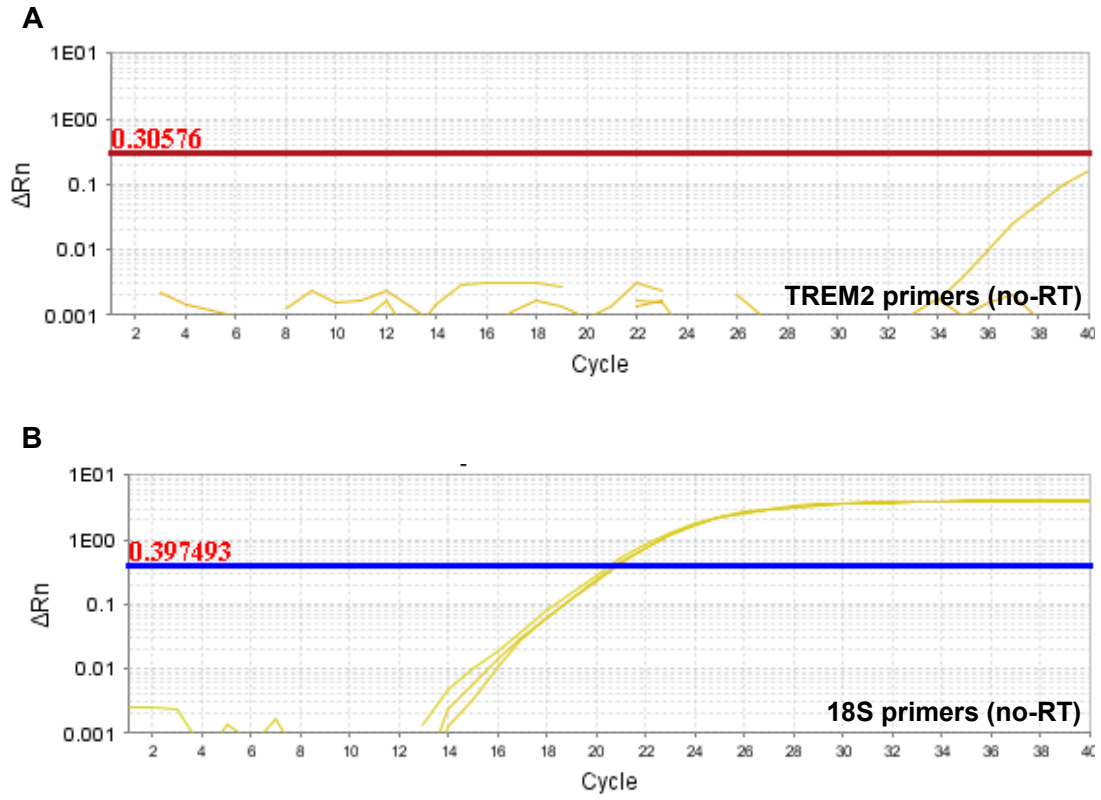

Figure 4.8 – Amplification for -RT negative controls lacking cDNA.
Probing no-RT negative controls that do not contain cDNA with (A) TREM2 primers did not result in amplification as expected. However, strong amplification was detected using (B) 18S housekeeping primers with these no-RT controls.

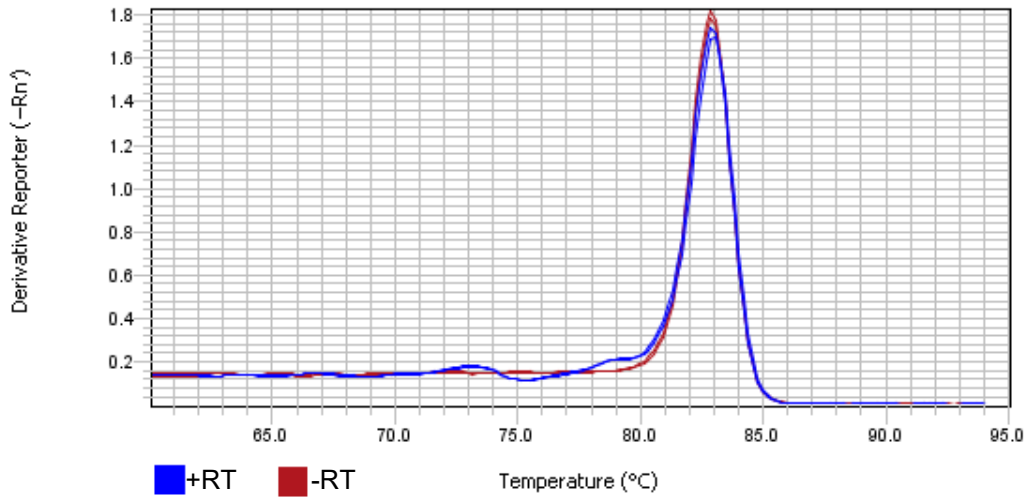

Figure 4.9 – Melt curves for 18S amplification of samples with and without cDNA. Identical melt curves (plotted as the derivative reporter (-Rn') against temperature) were observed for samples with (blue) and without (red) cDNA, indicating the possibility of genomic DNA contamination.

4.2.2.2 Flow Cytometry of WT and TREM2 KO Monocytic Isolates

Monocytic isolates from three mice per genotype were fixed post-extraction and run on flow cytometry with mAb 9D10, which previously showed strong cross-reactivity with recombinant mouse protein and the mouse cell line RAW264.7 (Chapter 3). This antibody unexpectedly showed binding of both the WT and KO isolates (Figure 4.10). This finding is not due to human error or pipetting technique as multiple aliquots were measured per condition and care was taken to keep different genotypes separate throughout preparation and culture of isolates.

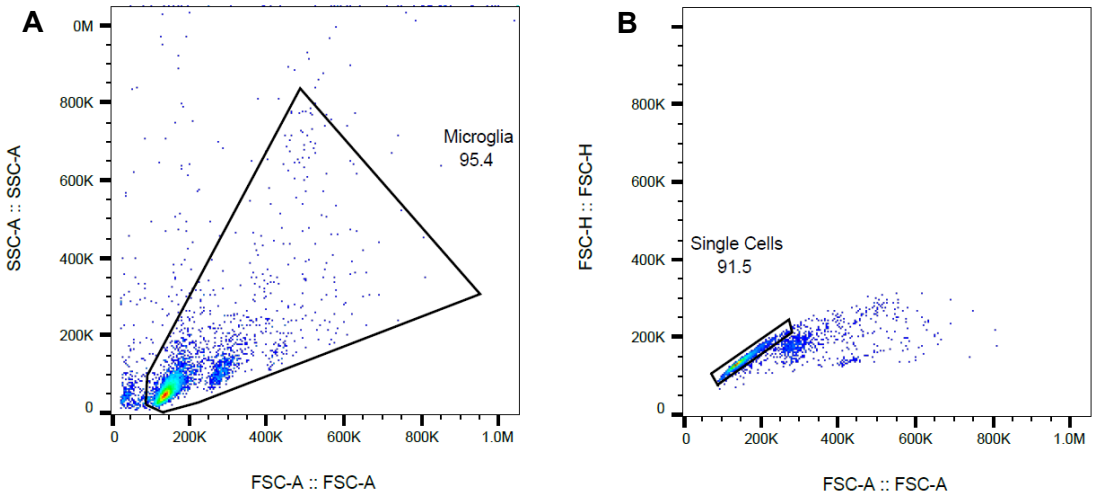

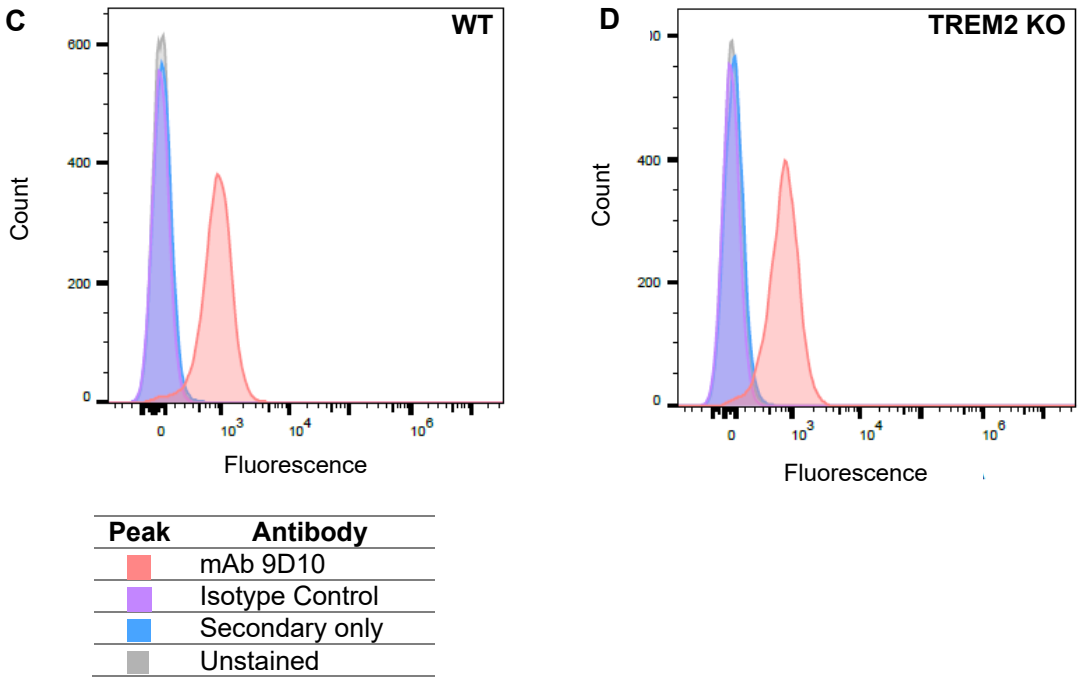

Figure 4.10 – Binding of mAb 9D10 to monocytic isolates by flow cytometry.
The gating strategy for flow cytometry involved (A) the exclusion of dead cells by plotting forward scatter area (FSC-A) against side scatter area (SSC-A) followed by (B) the selection of single cells for analysis by plotting FSC-A against forward scatter height (FSC-H). Staining of mAb 9D10 was performed for (C) wild type (WT) and (D) TREM2 knockout (KO) samples (3 mice per genotype). Controls included cells stained with secondary antibody only and cells stained with a matched isotype control.

4.2.2.3 Immunostaining of WT and TREM2 KO Monocytic Isolates

Alongside the flow cytometry experiments, monocytic isolates were fluorescently stained using mAb 9D10 as a primary antibody, and co-stained with IBA1 (ionized calcium binding adaptor molecule 1, Wako), known to be constitutively expressed by macrophages/microglia and commonly used as a marker for immunostaining (Mittelbronn *et al*., 2001). While IBA1 staining was successful, TREM2 staining appeared to be non-specific as staining was observed both in WT and KO monocytes (Figure 4.11) as seen in the above flow cytometry experiment (Figure 4.10). Samples stained with secondary antibody only were negative as expected (Figure 4.12).

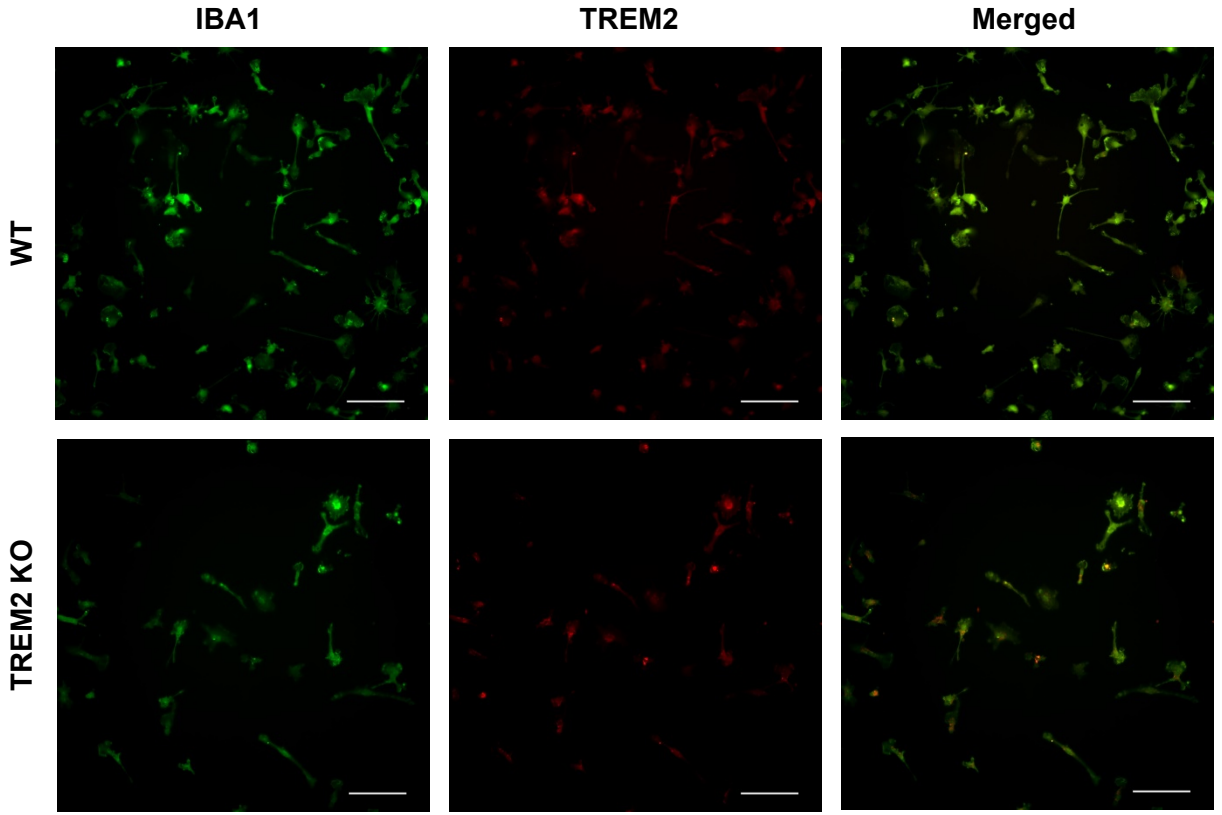

Figure 4.11 – TREM2 and IBA1 staining of primary monocytes from WT and TREM2 KO mice.
Successful IBA1 staining of primary monocytes isolated from WT and TREM2 KO mice, TREM2 staining appeared in both samples indicating non-specific binding of mAb 9D10. Scale bar, 50μm.

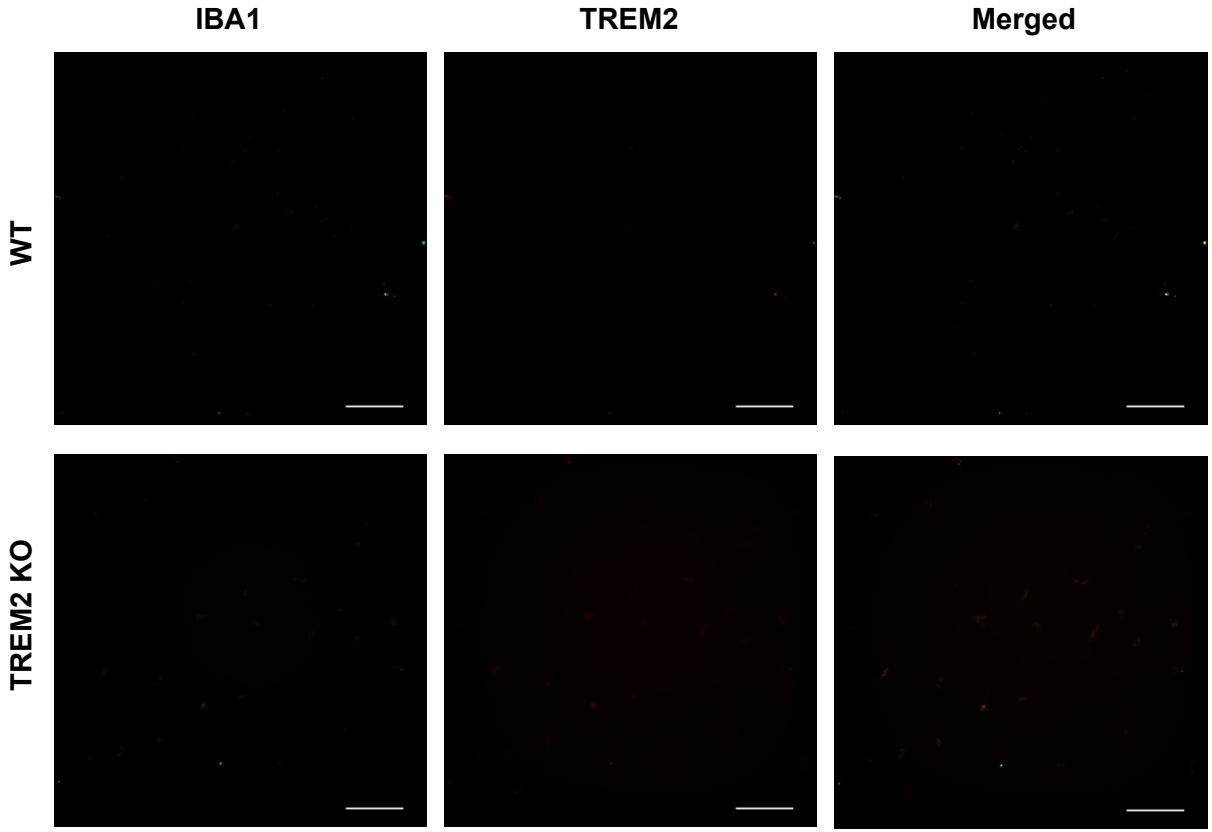

Figure 4.12 – Secondary antibody staining of primary monocytes from WT and TREM2 KO mice.
Secondary antibody staining of monocytes isolated from WT and TREM2 KO mice; fluorescently labelled anti-rabbit and anti-mouse secondary antibodies were used alone to represent the negative controls for IBA1 and TREM2 respectively. As expected, no positive staining was observed. Scale bar, 50μm.

These results were indicative of non-specific binding likely caused by using a mAb raised in a mouse host with a mouse monocytic sample. To address this issue, all subsequent staining was performed using a mouse-on-mouse (MOM) immunodetection kit to block endogenous mouse IgG and directly biotinylated mAb 9D10 was introduced to eliminate the use of anti-mouse secondary antibodies. This finding is not likely due to human error as multiple samples were tested per condition, culture wells and antibody solutions were carefully labelled to avoid cross-contamination or pipetting errors.

4.2.3 Further Antibody Validation in Brain Tissue and Cell Lines

4.2.3.1 Immunostaining of Mouse Brain Tissue

Staining of sagittal brain sections from WT and TREM2 KO mice was performed using mAb 9D10 and 8G10, after blocking with the MOM kit as previously described. Using mAb 8G10, stronger TREM2 staining of the WT, compared to the TREM2 KO, sample was observed (Figure 4.13); however staining was still seen in the negative control (Figure 4.16). Positive cells of microglial morphology in the WT tissue were also detected, but no microglial marker was used in this staining to confirm cell type (Figure 4.14). Staining using mAb 9D10 showed similar TREM2 staining in both WT and KO samples (Figure 4.15), suggesting non-specific binding as seen in primary monocytes stained with this antibody. The negative control for both mAb, staining using an anti-mouse antibody alone, demonstrated background staining in the WT sample (Figure 4.16).

Staining using biotinylated mAb 9D10, to avoid the use of an anti-mouse secondary antibody, still resulted in high background staining seen in both WT and KO brain tissue (Figure 4.17), similar images were obtained for the negative control using streptavidin substrate alone (Figure 4.18).

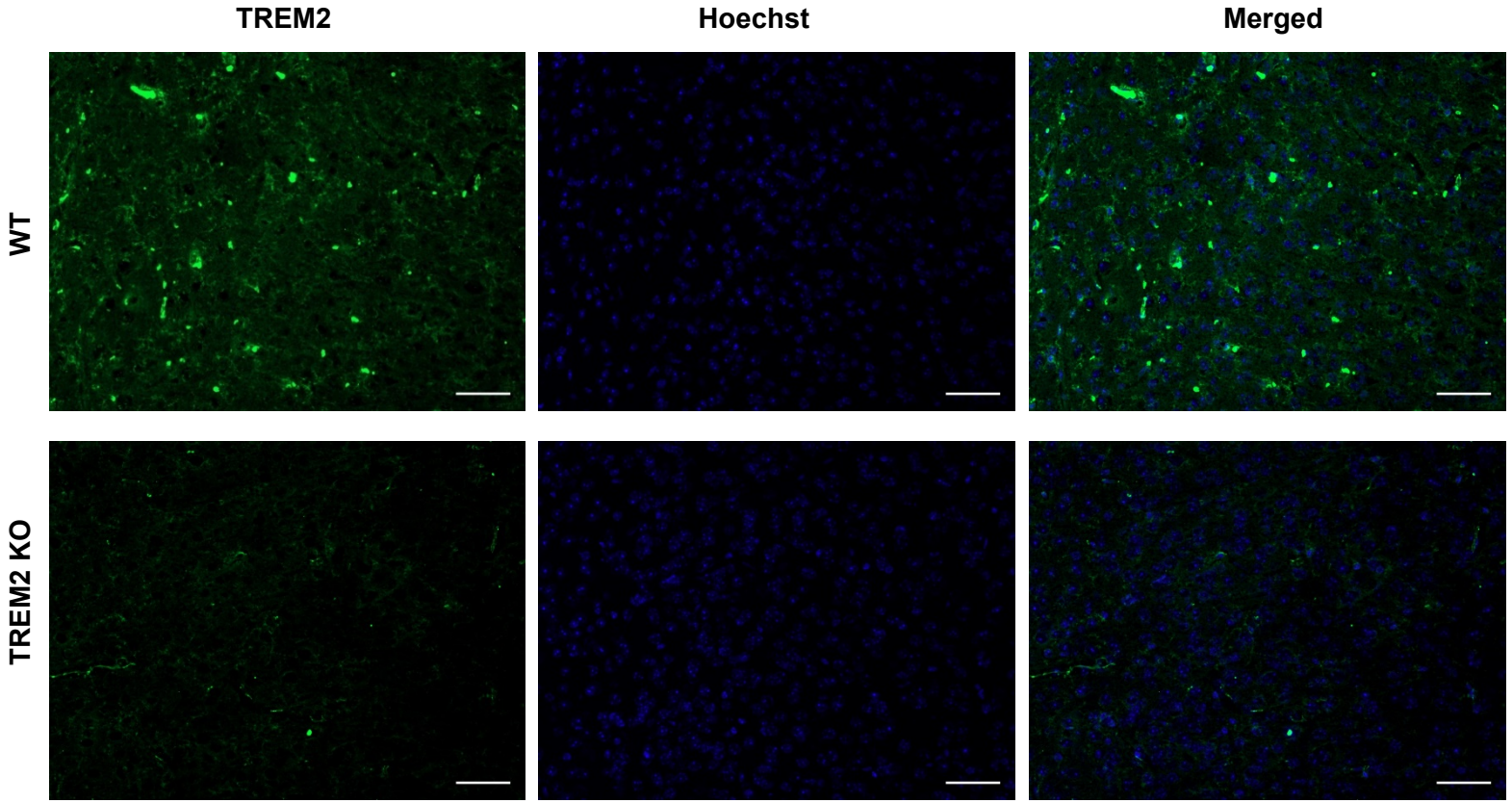

Figure 4.13 – TREM2 and Hoechst nuclear staining of WT and TREM2 KO mouse brain tissue using mAb 8G10.
Stronger TREM2 staining was observed in the WT compared to the TREM2 KO sample using mAb 8G10 followed by a fluorescently labelled anti-mouse antibody, in conjunction with a mouse on mouse (MOM) immunodetection kit. Scale bar, 50μm.

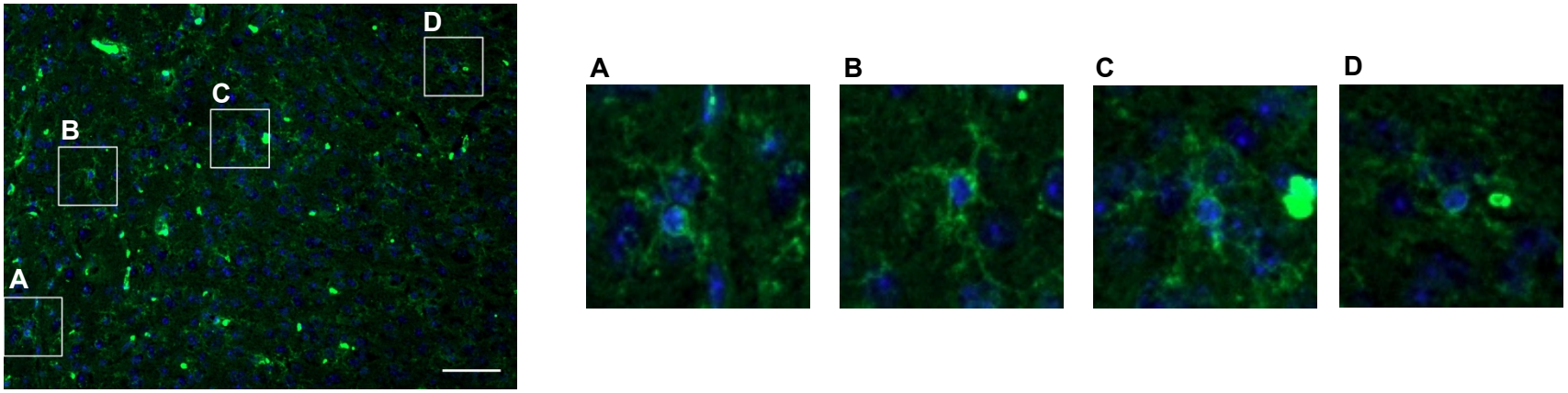

Figure 4.14 – Detection of cells of microglial morphology in WT mouse brain tissue using mAb 8G10.
TREM2 mAb 8G10 and Hoechst nuclear staining depicted cells of microglial morphology (A-D) in WT mouse brain tissue. Scale bar, 50μm.

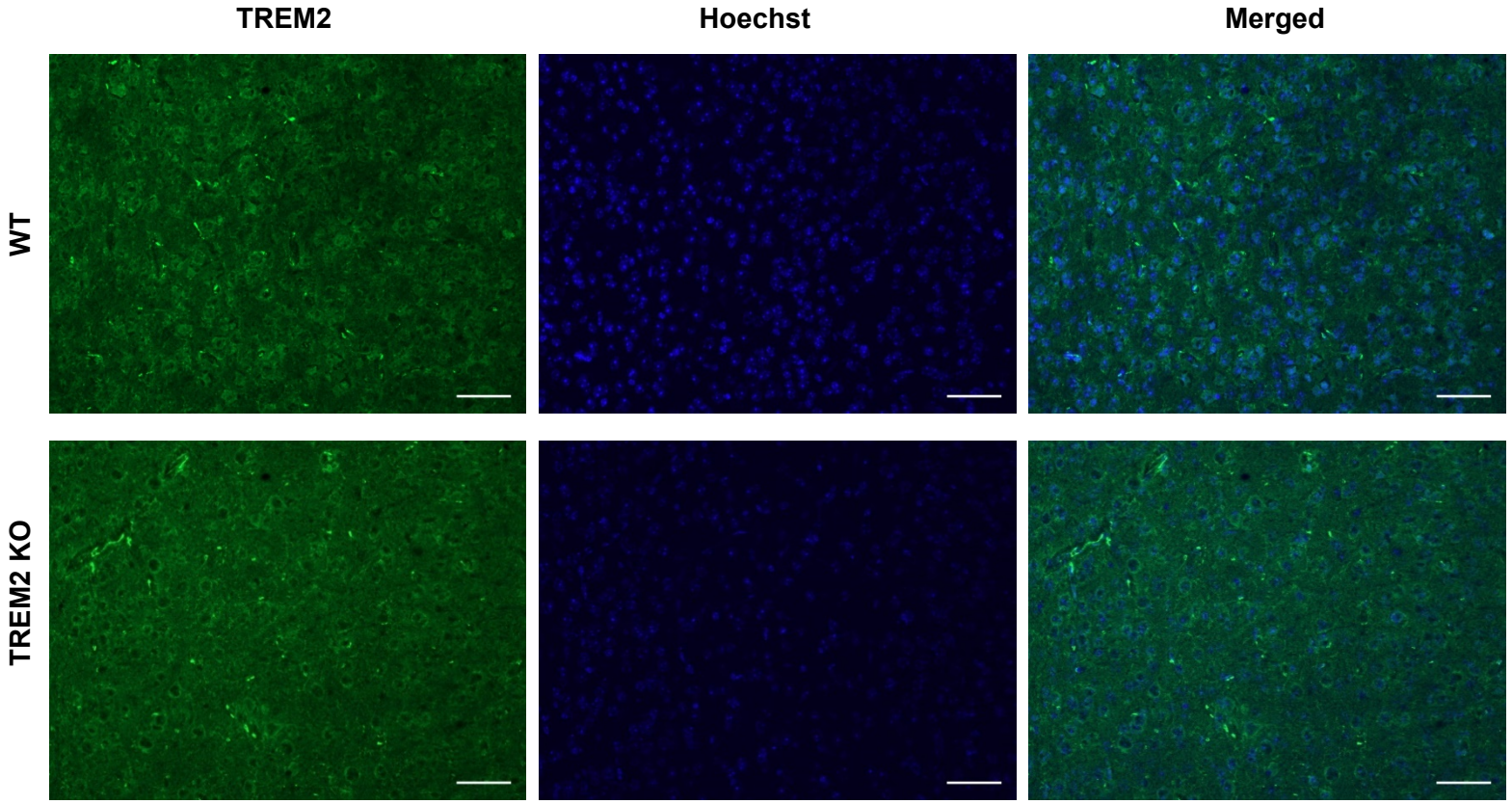

Figure 4.15 – TREM2 and Hoechst nuclear staining of WT and TREM2 KO mouse brain tissue using mAb 9D10.
Similar staining was observed in both WT and TREM2 KO mice using mAb 9D10 followed by a fluorescently labelled anti-mouse antibody, in conjunction with a mouse on mouse (MOM) immunodetection kit. Scale bar, 50µm.

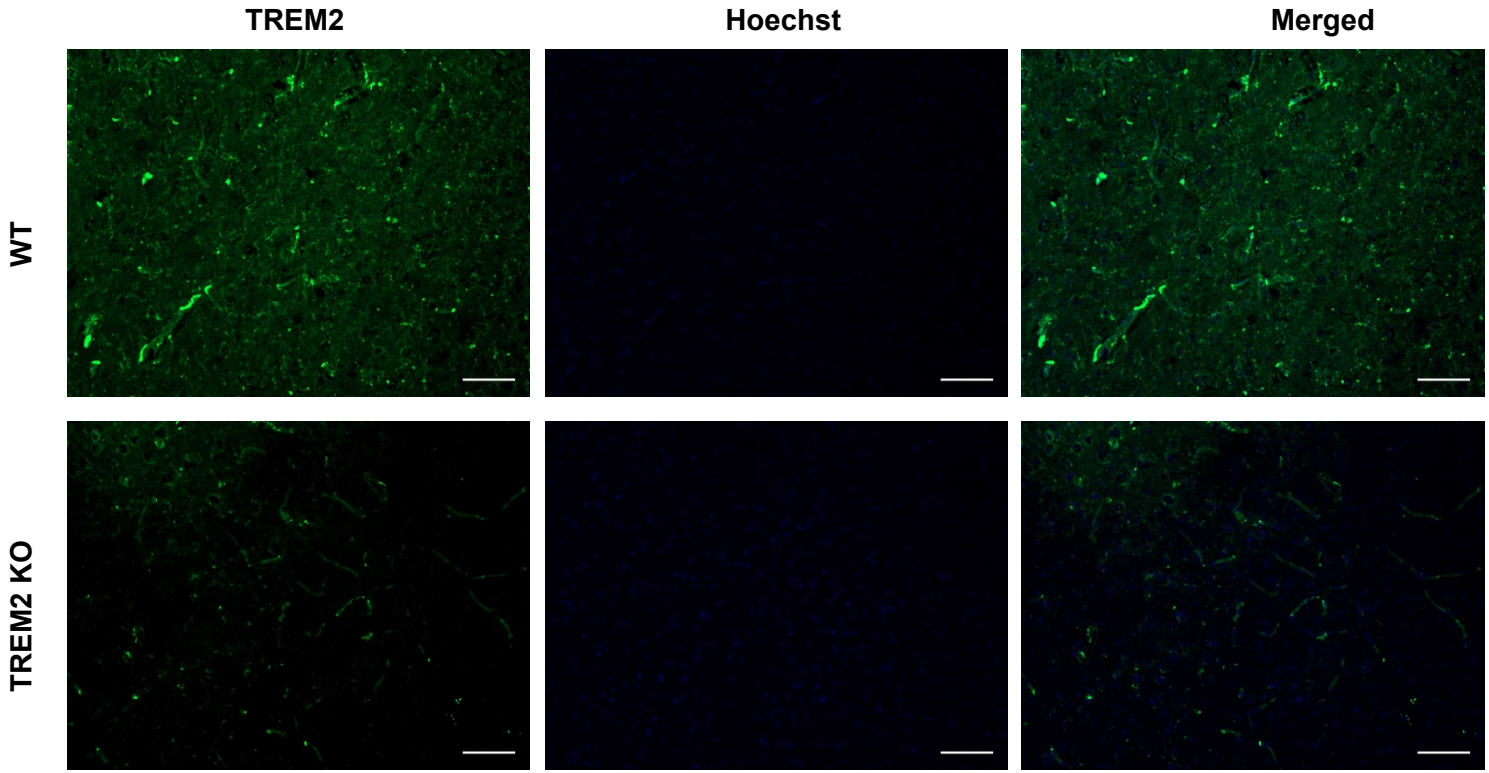

Figure 4.16 – Secondary antibody staining of WT and TREM2 KO mouse brain tissue.
Secondary antibody staining of brain tissue from WT and TREM2 KO mice; fluorescently labelled anti-mouse secondary antibody was used alone to represent the negative controls for mAb 8G10 and 9D10. Staining was observed in the WT sample indicating a high level of non-specific background staining. Scale bar, 50µm.

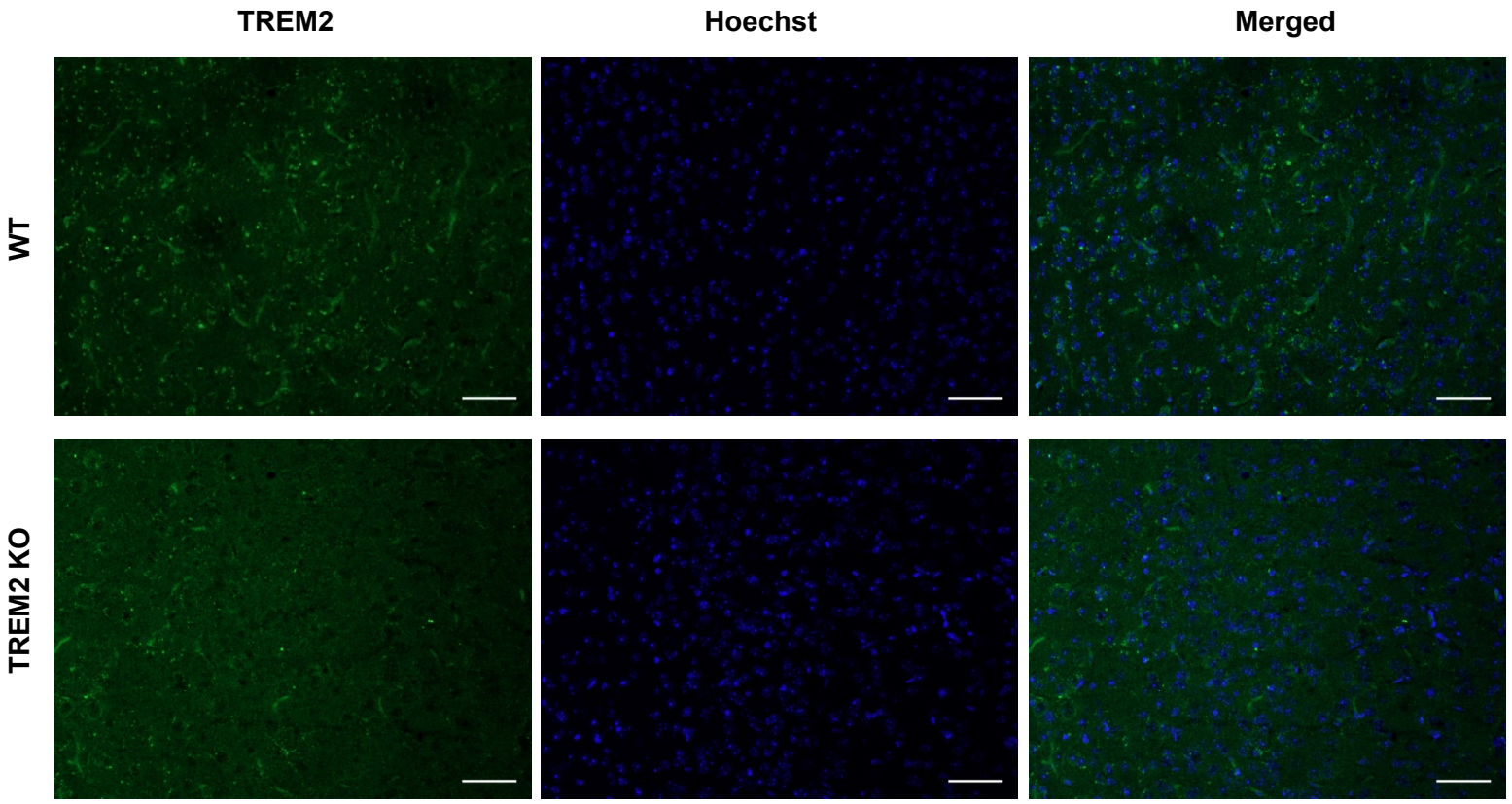

Figure 4.17 - TREM2 and Hoechst nuclear staining of WT and TREM2 KO mouse brain tissue using biotinylated mAb 9D10.
Using directly labelled mAb 9D10, with a mouse on mouse (MOM) immunodetection kit, showed high background staining in both WT and KO samples. Scale bar, 50µm.

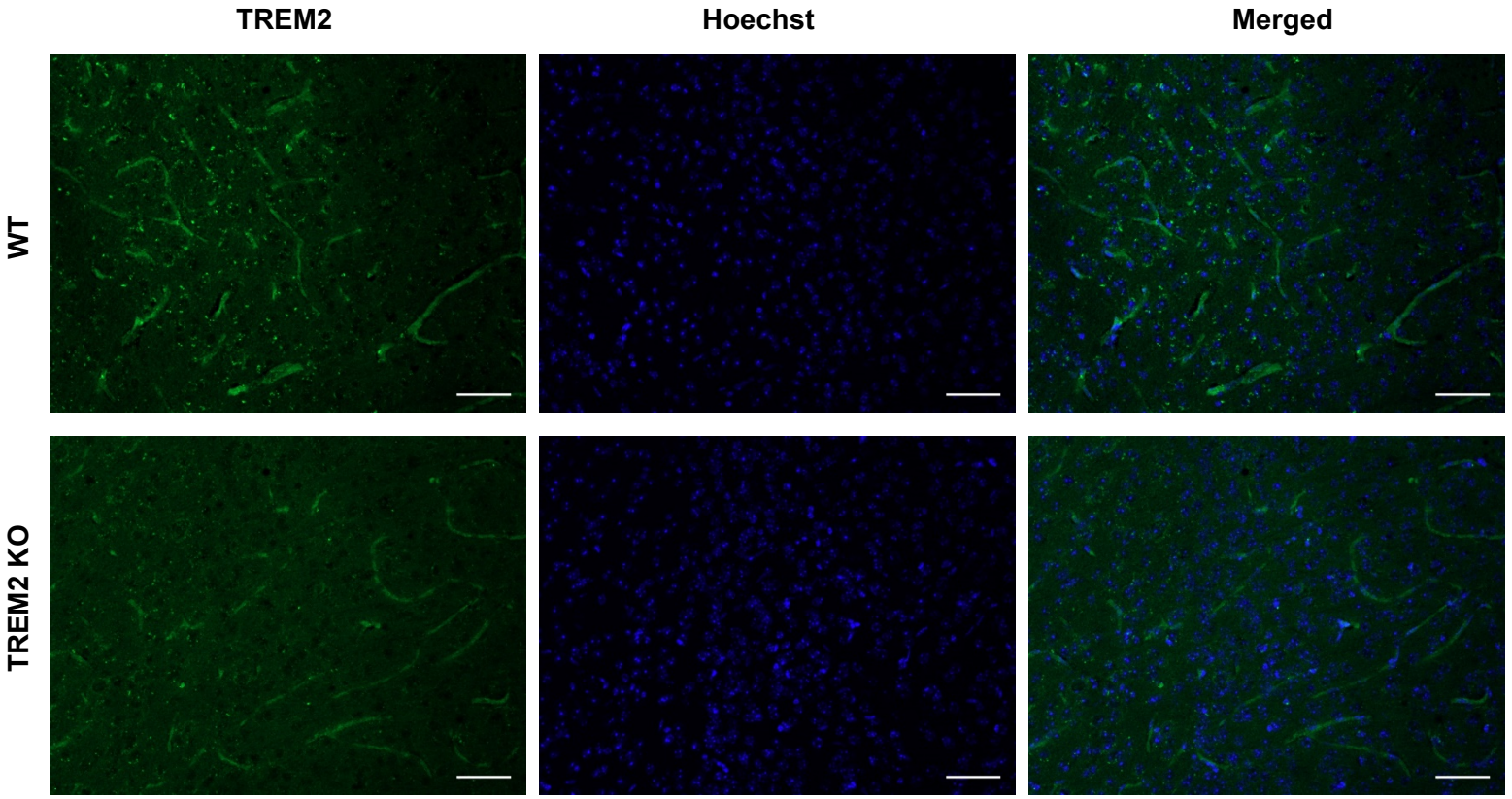

Figure 4.18 – Negative control for WT and TREM2 KO mouse brain tissue stained with biotinylated mAb.
Staining of brain tissue from WT and TREM2 KO mice using fluorescently labelled streptavidin alone was used as a negative control for tissue stained using biotinylated mAb. Non-specific staining was observed in both WT and KO tissue. Scale bar, 50µm**.**

4.2.3.2 Immunostaining of Cell Lines

Staining of the THP1 and RAW264.7 cell lines, previously used for antibody characterisation in Chapter 3, was also performed using mAb 9D10 and the in-house polyclonal antibody as a comparison alongside the tissue staining presented above.

TREM2 staining using mAb 9D10 was observed in both cell lines; weak background staining was observed in THP1 cells probed with the anti-mouse secondary antibody alone, and to a much lesser extent in RAW264.7 cells (Figure 4.19, Figure 4.20).

Strong TREM2 staining was also observed in both cell types using the in-house generated polyclonal anti-TREM2, with no staining detected in negative controls for both cell lines as expected (Figure 4.21,Figure 4.22).

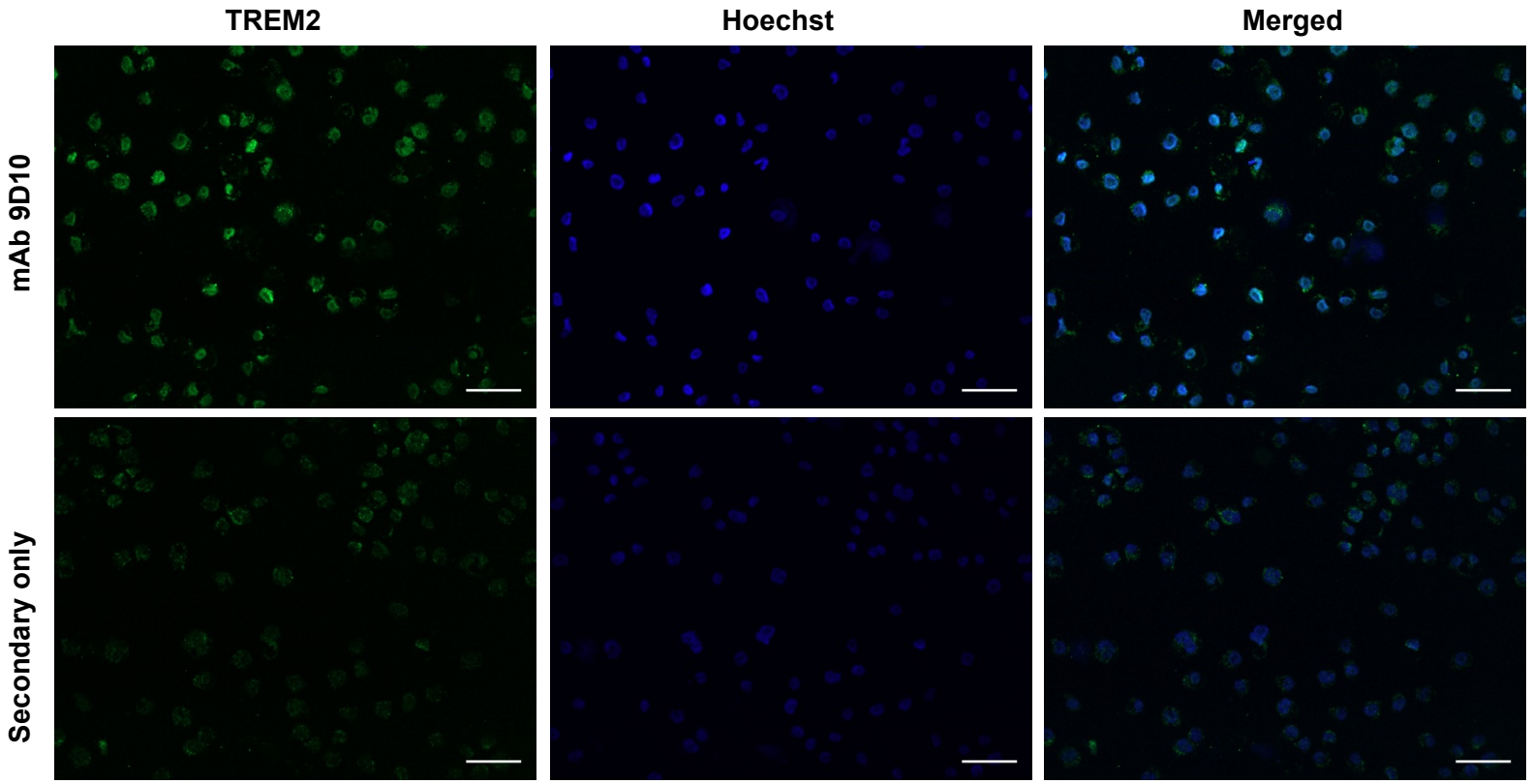

Figure 4.19 – TREM2 staining of THP1 cells using mAb 9D10.
Positive immunostaining of the human THP1 cell line using mAb 9D10, with Hoechst nuclear counterstain. Weak staining was also observed in cells incubated with anti-mouse secondary antibody only (bottom row, leftmost image). Scale bar, 50µm.

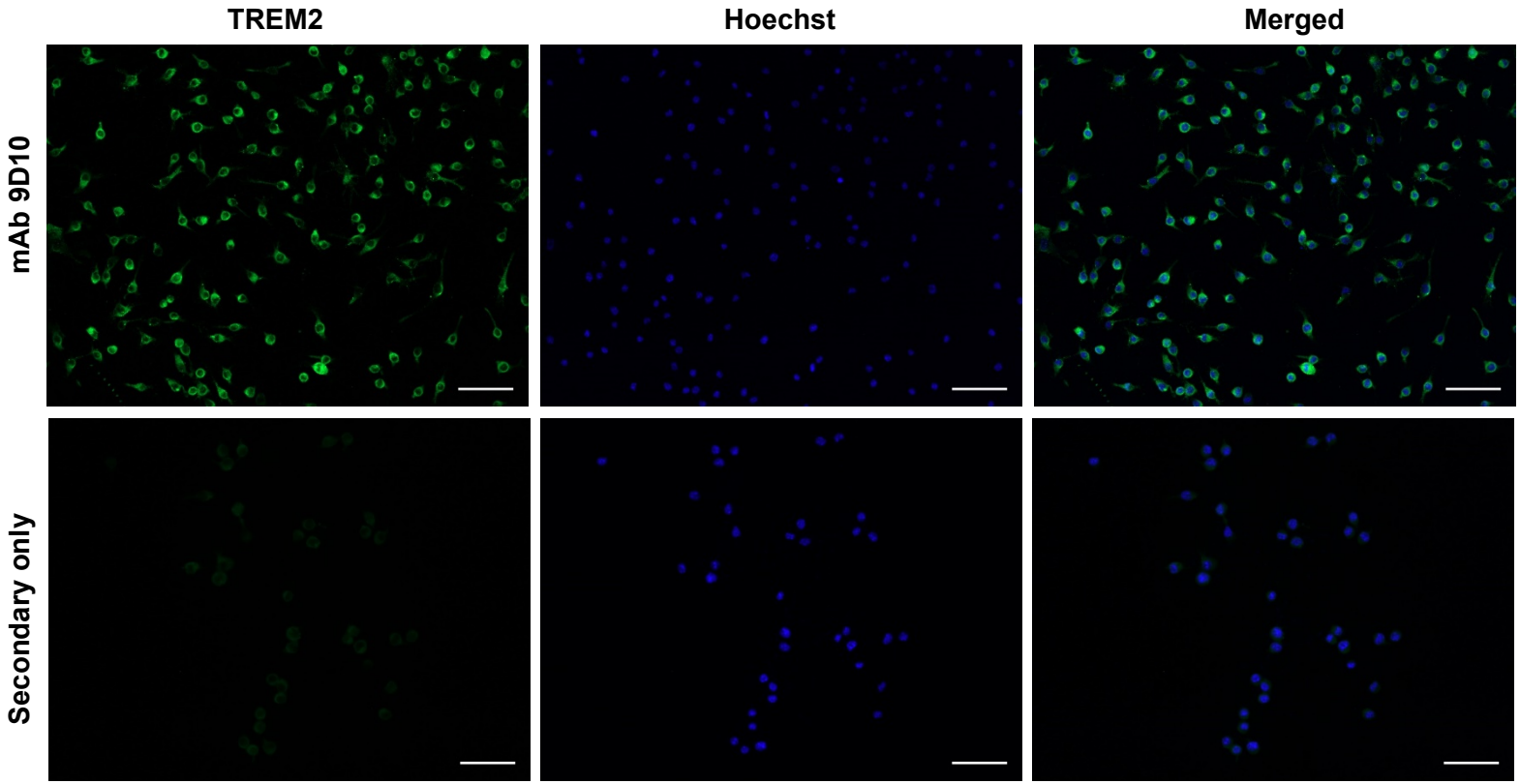

Figure 4.20 –TREM2 staining of RAW264.7 cells using mAb 9D10.
Positive immunostaining of the mouse RAW264.7 cell line using mAb 9D10, with Hoechst nuclear counterstain. Very weak staining was observed in cells incubated with anti-mouse secondary antibody only (bottom row, leftmost image). Scale bar, 50μm.

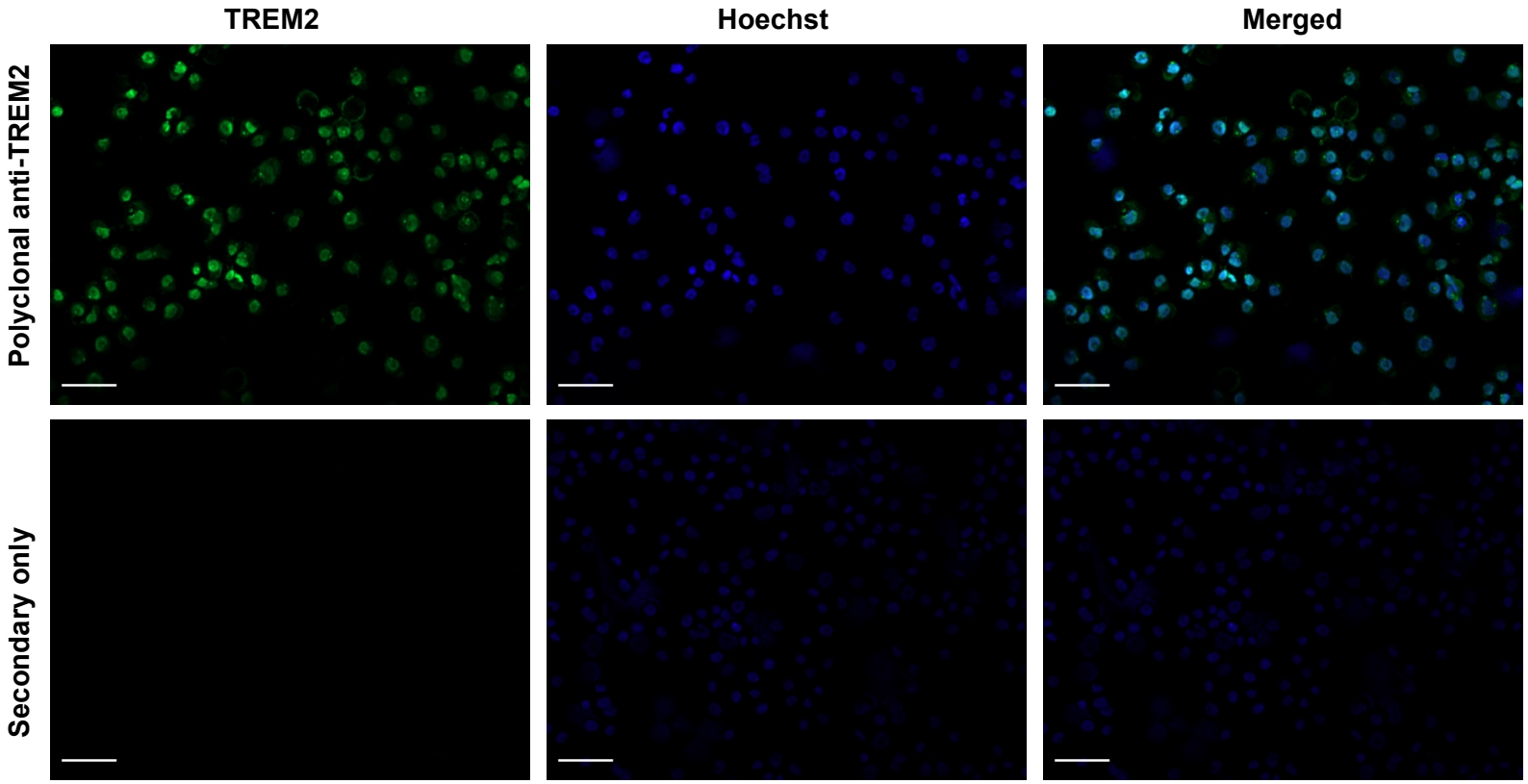

Figure 4.21 – TREM2 staining of THP1 cells using polyclonal anti-TREM2 antibody.
Positive TREM2 staining of the human THP1 cell line using the in-house polyclonal antibody, with Hoechst nuclear counterstain. No positive staining was observed in the secondary only control as expected. Scale bar, 50μm.

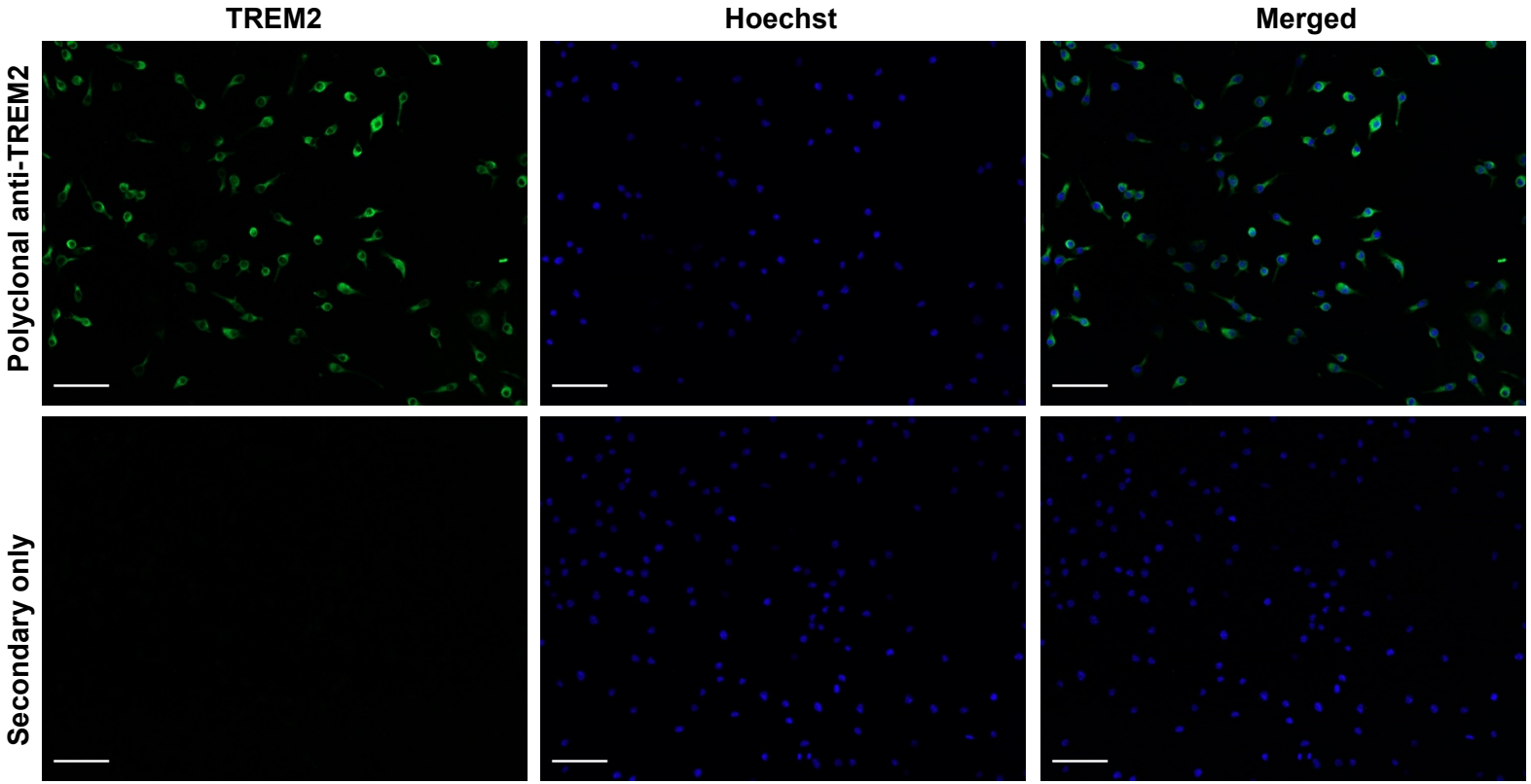

Figure 4.22 – TREM2 staining of RAW264.7 cells using polyclonal anti-TREM2 antibody.
Positive TREM2 staining of the mouse RAW264.7 cell line using the in-house polyclonal antibody, with Hoechst nuclear counterstain. No positive staining was observed in the secondary only control as expected. Scale bar, 50µm.

4.2.4 Detection of sTREM2 in Serum

Directly labelled mAb were also used to assess the presence of sTREM2 in sera by western blotting. Biotinylated antibodies were validated on TREM2 protein in western blots and ELISA before use then added to the western blots at 5µg/ml, followed by HRP-labelled streptavidin (1:200) before development. Sera from WT and TREM2 KO mice were probed using biotinylated mAb 9D10 to detect TREM2. The expected size of TREM2 is 25kDa, and bands at around this weight were observed in both sera under reducing conditions, with multiple additional bands between 50-65kDa.

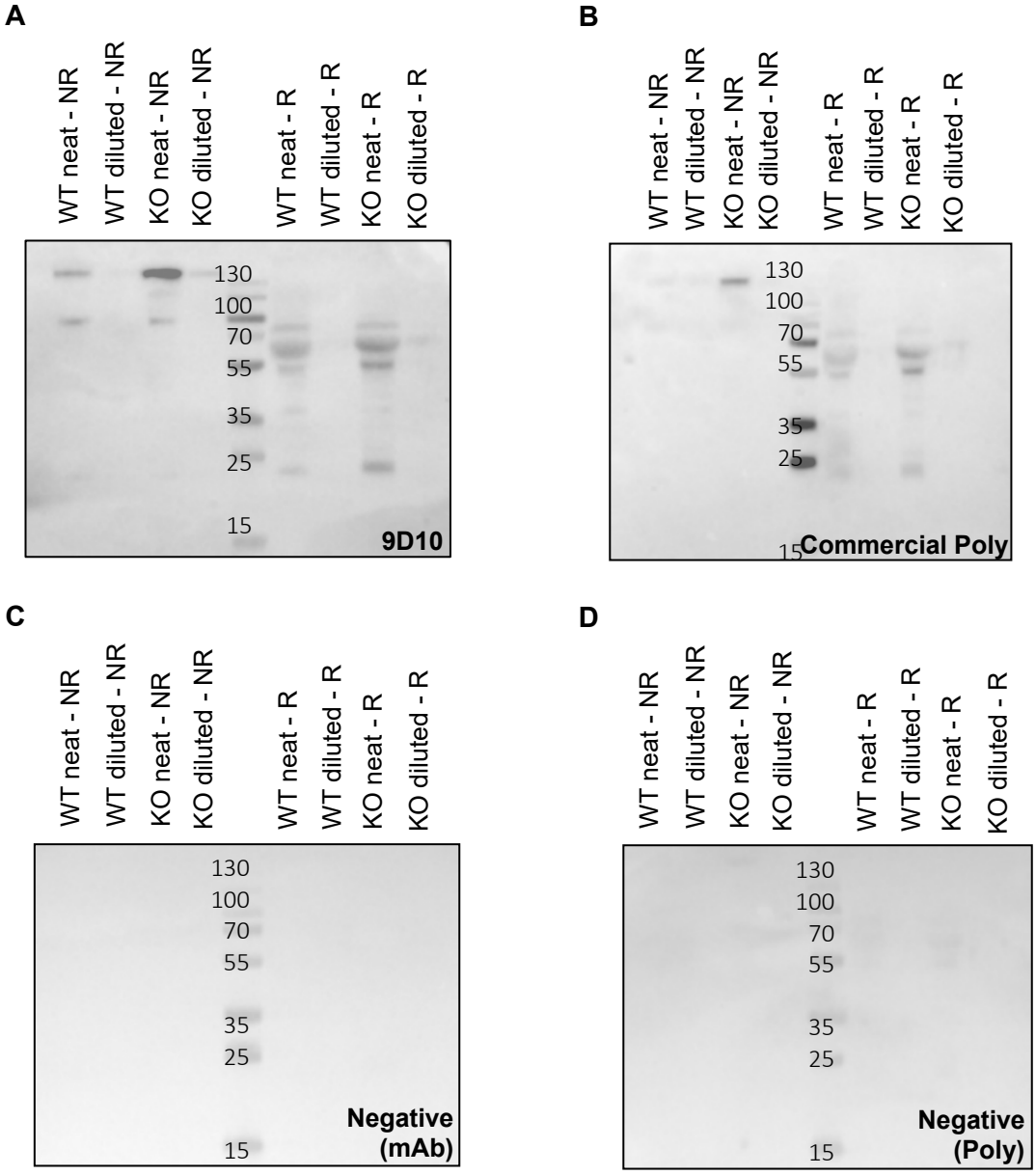

Figure 4.23 – Western blots depicting antibody binding of WT and TREM2 KO sera. TREM2 binding was observed in both WT and TREM2 KO sera using (A) mAb 9D10 and (B) the commercial polyclonal antibody (AF1828, R&D Systems) under reducing (R) conditions. Sera was tested neat and diluted (1 in 10). Negative controls (C,D) comprising the same sera were probed with secondary anti-mouse and anti-goat antibodies alone. NR: non-reducing.

The same binding pattern was detected in the WT and KO samples (Figure 4.23A), a result previously seen in immunostaining and flow cytometry experiments. Testing the commercial AF1828 antibody (R&D Systems) on these sera also generated the same results, indicating a lack of specific binding for mouse TREM2 in western blots for both the commercial and in-house antibodies (Figure 4.23B). It was not possible to test for what the antibodies were binding exactly; the observation that these bands were detected in blots of both WT and KO samples using anti-TREM2 antibodies, but not in secondary only negative controls suggests some specificity, but no clues as to what.

In order to determine whether the antibodies bound TREM2 in human serum by western blotting and how this compared to the binding patterns seen above, neat mouse sera and diluted (1 in 10) human serum were run by SDS-PAGE and probed with mAb 9D10. Strong binding to human serum was observed at ~25kDa and ~50kDa (Figure 4.24A). Increased chemiluminescent exposure of the western blot (Figure 4.24B) showed more clearly the binding pattern previously observed in both WT and TREM2 KO mouse (Figure 4.23A).

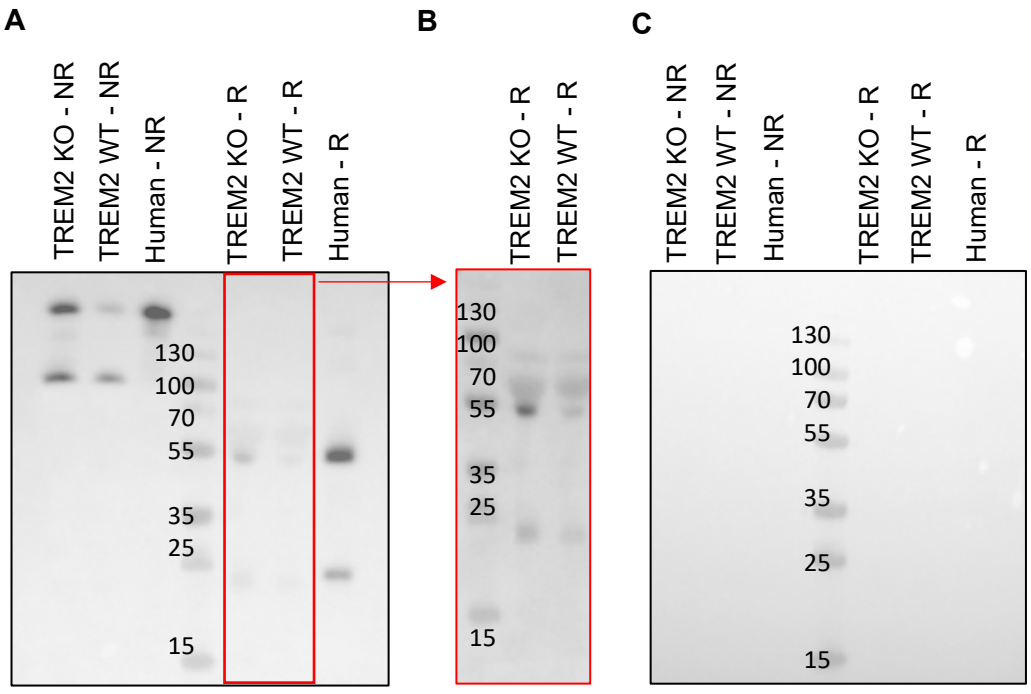

Figure 4.24 – mAb 9D10 TREM2 binding patterns in mouse and human sera.
Binding of TREM2 by biotinylated mAb 9D10 was observed in (A) human sera at ~25kDa and ~50kDa under reducing (R) conditions, similarly to the binding patterns in mouse WT and KO sera. (B) Increased exposure of blot membrane confirmed the presence of bands previously seen in both genotypes of mouse sera. (C) The negative control, comprising the same sera, was probed with HRP-labelled streptavidin only and showed no binding as expected. NR: non-reducing.

Testing mAb 9A9-3 and the polyclonal antibody, which previously showed some cross-reactivity with mouse protein in ELISA and western blots, resulted in similar binding patterns in human, WT and TREM2 KO mouse sera (Figure 4.25). Both antibodies bound bands in human serum at ~25kDa and ~50kDa as seen with mAb 9D10 (Figure 4.24), but showed the same likely non-specific bands in TREM2 KO and WT mouse sera. The negative control for the polyclonal antibody displayed comparable faint bands for WT and TREM2 KO suggesting non-specific binding of this antibody to the mouse sera (Figure 4.25C), but this is not seen in the negative control for the mAb (Figure 4.25A). It is difficult to find out what the seemingly non-specific bands are, it is possible for the antibodies to be binding TREM2 in addition to another protein of similar molecular weight, confounding the interpretation of results. As binding to the human serum is clearer and demonstrated similar results to a study in the literature (Raha-Chowdhury *et al.*, 2018), as will be discussed later, the decision was made to focus the use of these antibodies on human work in the hope that future work would continue characterisation of their interaction with mouse samples.

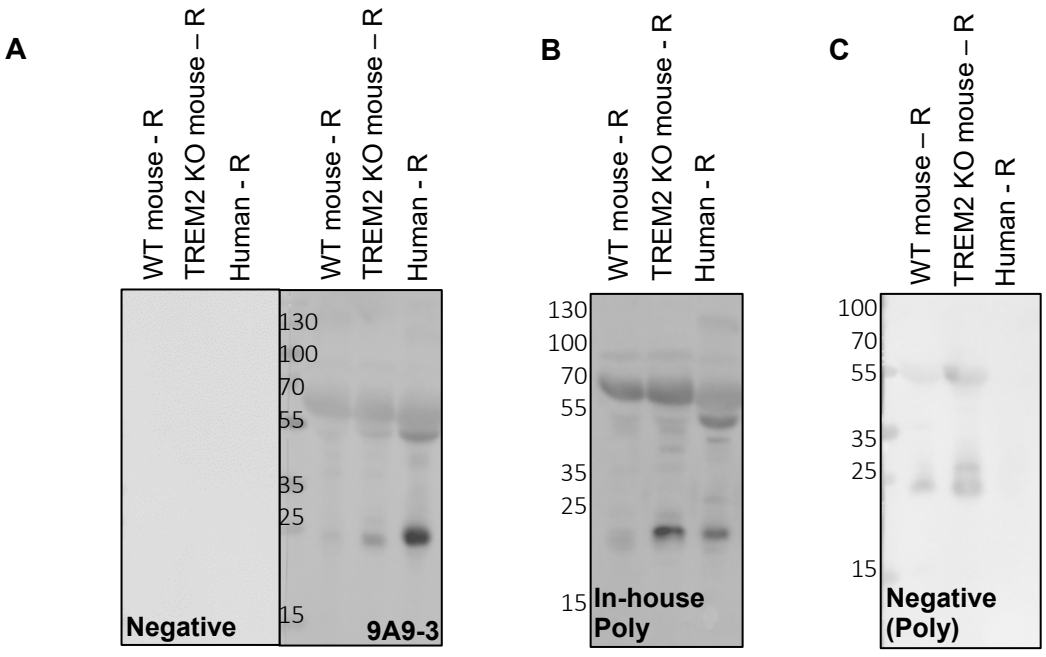

Figure 4.25 – Reactivity of mAb 9A9-3 and polyclonal with human and mouse sera. Western blots showing binding of human (A) biotinylated mAb 9A9-3 including secondary only control, (B) in-house polyclonal antibody and (C) anti-rabbit secondary only control to human and mouse WT/TREM2 KO sera under reducing (R) conditions. The membranes were divided post-transfer and each section probed separately.

These results overall suggested that the tested antibodies bound sTREM2 in human serum as expected, but while initial cross-reactivity to mouse TREM2 was clearly observed for most antibodies in Chapter 3, comparing antibody binding patterns in wild type and TREM2 knockout samples indicated that this reactivity was not specific to mouse TREM2, rendering the antibodies unsuitable for use in functional assays using mouse samples. This finding does additionally call into question the TREM2 specificity in human samples and this should also be confirmed as described in the discussion below.

4.3 Discussion

4.3.1 Generation of TREM2-expressing Cell Lines

This chapter set out to describe the use of TREM2-expressing cell lines as characterisation controls for the generated antibodies, in addition to the use of TREM2 WT and KO mouse samples to validate the cross-reactivity of human antibodies to mouse TREM2. While these experiments require further troubleshooting, they did reveal unexpected findings, such as the reactivity of antibodies to both TREM2 WT and KO samples. This is worth future work to investigate whether this is non-specific binding, or more likely the interaction of the antibodies with another protein in addition to mouse TREM2 as will be discussed later.

In order to further characterise the antibodies generated in Chapter 3, control cell lines expressing human wild type, variant and mouse TREM2 were generated. Western blotting using the in-house polyclonal antibody showed non-specific binding of both non-transfected and transfected cells (Figure 4.2). Measurement of TREM2 using an in-house ELISA demonstrated the presence of TREM2 in the transfected lines and in the positive control, THP1, but not in the non-transfected line (Figure 4.3). To further investigate the discrepancy between the two experiments, TREM2 expression at the mRNA level was measured in the cell lines.

Investigating TREM2 mRNA expression by qPCR demonstrated that the non-transfected HEK293 cell line did not express TREM2, compared to the THP1 positive control cell line, as expected. However, the transfected cells also showed no TREM2 expression (Figure 4.5). Housekeeping genes confirmed the presence of cDNA for all but the mouse TREM2-expressing line, indicating that only the human TREM2-

expressing samples were successfully reverse transcribed prior to qPCR amplification. Repeated transfection of cells with the mouse TREM2 vector is required and a suitable positive control, such as RAW264.7 cells, needs to be included in the qPCR experiment. Insufficient quality control at various stages was evident in this experiment and future work should include steps to ensure the correct sequences are in use throughout the experiment as described below.

Troubleshooting this experiment revealed that the DNA sequences used for vector expression were generated by the company as the optimal sequences to yield the requested proteins using the specified eukaryotic cells for transfection. These DNA sequences differed from human or mouse TREM2 DNA, explaining why the qPCR primers used here did not bind to cDNA of transfected cell lines. Amplification curves were still observed despite this, albeit several cycles later, and sequencing these qPCR reaction products would be necessary to identify what these amplicons were.

By sending protein sequences to the company, this created scope for drift introducing additional variables to the experiment. Next steps would require sending out the exact DNA sequences required to completely match human or mouse TREM2 DNA, and the generation of new vectors, for successful qPCR amplification and more efficient protein production. Sequencing the region of interest in the commercially-sourced vectors to confirm that the correct DNA was inserted would also be a necessary step prior to vector use. An additional aspect, omitted in the initial vector design, would be the insertion of a reporter gene, to allow for an early check of transfection success or failure and the transfection of cells with an empty vector (lacking TREM2 DNA) as an additional negative control. Time constraints did not allow for the generation of new vectors or sourcing alternative vectors to repeat the transfection.

4.3.2 Generation of Controls from WT and TREM2 KO Mice

4.3.2.1 Binding of Antibodies to TREM2 in Brain Tissue and Monocytic Isolates

Primary monocytic isolates from WT and TREM2 KO mice were generated as an additional characterisation method for antibodies showing mouse cross-reactivity. WT and KO cells were first analysed by qPCR analysis and shown to be suitable for use as positive and negative controls (Figure 4.7). Isolation involved the positive selection of CD11b-expressing cells in the brain; this is a common method used in isolation techniques that selects for a population enriched with microglia, but preparations also contain other CD11b-positive myeloid cells. To analyse microglia specifically, additional markers must be included in downstream processes, such as the flow

cytometry and immunostaining experiments conducted in this project. This was not possible due to the constraints of time and limited laboratory access; only the macrophage/microglia marker IBA1 was used in some of the immunostaining work. Ideally, the use of the microglial-specific marker TMEM119 should have been used, or the identification of a CD11b-positive, CD45low, CD11c-negative population in flow cytometry would have more accurately represented microglial cells (Garcia *et al*., 2014).

To explore the unusual results obtained with the housekeeping primers in the no-RT negative controls (containing RNA only), melt curves were analysed to investigate if non-specific binding or primer dimers were responsible for the amplification curves observed. The overlapping melt curves of samples with and without cDNA ruled out the presence of non-specific binding of another amplicon, as this would have otherwise been represented as a separate curve (Kuang *et al.*, 2018). Primer dimers were also not responsible for this finding, as they would have been represented as smaller, broader peaks since they melt at lower temperatures than the amplified product (Ruiz-Villalba *et al.*, 2017).

A next step to troubleshoot this issue should include the DNAse digestion of the RNA samples, to eliminate any potential genomic DNA contamination prior to reverse transcription. Serial dilution of the samples would also be a good method to observe the effect of diluting any contaminants and whether this would phase out the amplification curves seen in the no-RT negative controls. The use of additional housekeeping genes would also be useful to investigate whether this result is limited to the use of 18S as a housekeeping control; 18S ribosomal RNA (rRNA) expression is considerably higher than the mRNA of the target genes so template RNA would require a high dilution before amplification for a more accurate comparison between samples and controls (Paolacci *et al.*, 2009). An interesting and more general finding was that Stephens *et al.* (2011) reported higher variability in expression of 18S, compared to other housekeeping genes, in mouse osteoblasts, osteoclasts and macrophages; this suggests that the use of different housekeeping controls may be a preferable direction to take when repeating this qPCR experiment on monocytic isolates.

Primary monocytic cells from WT and KO mice were fixed and stained for flow cytometry with the anti-human TREM2 antibody mAb 9D10, which cross-reacted with

mouse TREM2 as seen in Chapter 3. Positive staining was unexpectedly observed in both the WT and KO samples (Figure 4.10) suggesting non-specific staining.

The same effect was observed in primary monocytes that were cultured from these mice and fluorescently stained using mAb 9D10. Positive IBA1 staining confirmed the presence of monocytes in the cultures, but TREM2 staining was similar in both WT and KO cells. Initially, this was thought to be a mouse-on-mouse effect as the mAb and the monocytic cultures were both derived from a mouse host, so for subsequent immunostaining of mouse brain tissue, a MOM immunodetection kit was introduced to avoid the cross-reactivity of endogenous mouse IgG. However, this did not reduce the signal to noise ratio. Directly biotinylating mAb 9D10 was trialled to eliminate the use of anti-mouse secondary antibodies thus reducing the likelihood of cross-reactivity between these antibodies and the samples. While background staining was slightly reduced in samples stained with biotinylated mAb 9D10, no clear TREM2 staining was observed (Figure 4.17), with the streptavidin negative control also showing unexpected cross-reactivity (Figure 4.18).

Troubleshooting the immunostaining experiments to give cleaner backgrounds mainly focused on using the MOM kit and directly biotinylating primary antibodies. Other modifiable factors that could be investigated are the duration and type of fixation, stage of fixation (pre-/post-fixation), time and temperature of antibody incubation, antigen retrieval methods and serum concentration in blocking solutions. Staining the brain sections with the astrocytic marker glial fibrillary acidic protein (GFAP) and the neuronal marker NeuN, in addition to IBA1, would provide a more complete picture of TREM2 distribution in brain tissue. Running positive and negative antibody controls, such as IBA1 and an isotype control matched to the primary antibody respectively, alongside these samples would also provide a better sense of the strength of background signal being detected and provide more clues as to which factors may require modification.

Staining of the THP1 and RAW264.7 cell lines was also performed using mAb 9D10 and the in-house polyclonal antibody as a side comparison. The antibodies strongly stained both cell lines, demonstrating that the mAb 9D10 did recognise human TREM2 on expressing cells; residual background staining was seen in 9D10-negative controls in both lines (Figure 4.19, Figure 4.20), albeit not strongly, further emphasising cross-reactivity issues caused by the secondary antibody, even on human cell lines.

From the preliminary results on mouse brain tissue, mAb 8G10 appeared to better differentiate between WT and KO samples than mAb 9D10. Staining was clearly stronger in WT compared to KO samples and cells of microglial morphology were observed in mouse brain tissue using this antibody. This hints to mAb 8G10 as being a more promising candidate for TREM2 detection in mouse samples. Unfortunately, these findings were generated just before the pandemic lockdown restrictions and restricted laboratory access prevented further work on this antibody. Future work requires troubleshooting, as discussed above, to generate negative controls with less background staining, then co-staining mouse brain tissue using 8G10 alongside macrophage/microglial marker IBA1 and microglial marker TMEM119 as this would provide further confirmation of antibody binding to TREM2 expressed by macrophages/microglia in relation to other cell types.

4.3.2.2 Binding of Antibodies to sTREM2 in Sera

Sera from WT and TREM2 KO mice were used to further investigate the binding capacity of the generated antibodies by western blotting. In human serum, bands of ~25kDa and ~50kDa were detected using mAb 9D10 under reducing conditions, a result which is in line with a study by Raha-Chowdhury *et al.* (2018). This group reported that the 25kDa band in human serum represented monomeric sTREM2, with additional bands noted at ~18kDa and ~50kDa, proposed to be a truncated TREM2 protein and a sTREM2 dimer respectively. These data confirm that mAb 9D10 recognises sTREM2 in human serum.

mAb 9D10, 9A9-3 and the polyclonal antibody all gave similar binding patterns in western blots of sera from both WT and TREM2 KO mice, confirming that the mAb did not specifically bind mouse sTREM2, supporting the findings seen in flow cytometry and immunostaining. The commercial AF1828 anti-TREM2 antibody also bound both WT and KO sera, suggesting an overall lack of specificity to mouse TREM2 for all tested antibodies. AF1828 was not tested on human serum in this project but is used in other studies as a capture antibody to measure human CSF TREM2 by ELISA (Henjum *et al.*, 2018; Nordengen *et al.*, 2019). The supplier website notes that AF1828 shows less than 50% cross-reactivity with mouse TREM2 via direct ELISA. This may explain the bands observed in the WT samples probed by AF1828, but not in the KO, unless cross-reactivity with other mouse TREM family members is involved. The negative control for the in-house polyclonal antibody showed faint bands at the same molecular weights as detected by the polyclonal, indicating that

part of the reactivity was due to non-specific anti-rabbit secondary antibody binding (Figure 4.25C), this non-specific staining was not seen in the negative control for the biotinylated mAb (Figure 4.24C, Figure 4.25A).

4.3.2.3 Troubleshooting Potential Antibody Cross-Reactivity

Aside from background staining by secondary antibodies, it is possible that the anti-human TREM2 antibodies were binding another TREM family protein, present in both the WT and TREM2 KO mice. Mouse TREM1 and TREM3 are of similar expected protein mass to that of the bands observed here and have 26-29% homology with TREM2, as presented in Chapter 1. Of the known mouse TREM-like (TREML) proteins, only TREML6 has a similar protein mass to TREM2, with 25% homology (Vitale et al., 1998; Chung et al., 2002; Allcock et al., 2003; Klesney-Tait et al., 2006; Watarai et al., 2008; Genua et al., 2014; Roe et al., 2014). Binding of the antibodies to commercially-sourced TREM1 and TREM3 would demonstrate whether the antibodies were indeed cross-reacting to these proteins. Mapping where the in-house antibodies bind could also indicate whether the antibodies bind different proteins of the TREM family. The in-house mAb could be used in pull down assays for WT and KO sera, where assay eluate components could subsequently be investigated in western blotting using commercially available antibodies specific to other TREM family proteins, such as anti-mouse TREM1 and TREM3, but unfortunately time did not allow for this.

This finding does also highlight the need to test these antibodies against other human TREM proteins as well, to confirm specificity of the antibodies to human TREM2 and investigate their cross-reactivity to other human proteins in the TREM family. This can be done in a similar way as described above. The in-house antibodies can be used to deplete TREM2 from human serum and the removed components tested using commercial antibodies against TREM2 and other TREM proteins. The antibodies can also be used in a direct ELISA against other TREM proteins similar to TREM2, to compare their binding capacity between proteins of the same family. Where available, TREM2 specificity of antibodies can also be tested by probing lysates from human stem cell-derived TREM2 WT and KO lines.

While the findings described in this chapter were unexpected, a lot was learned throughout the process, particularly regarding the use of sufficient quality control steps at various stages during the experiments. Correcting these issues in the generation of TREM2-expressing cell lines shows promise in generating reliable

controls for TREM2 antibody characterisation in future. These findings also highlighted an important specificity issue for the human antibodies showing cross-reactivity for mouse TREM2. Binding of the antibodies to both WT and KO samples in several different cell and tissue types demonstrated that the finding was not down to human error, and the absence of this binding in most negative controls suggested there was some specificity involved. This warrants future work to investigate the binding capacity of these antibodies to other (mouse and human) TREM proteins, with a particular focus on 8G10 as this showed more promise for true mouse TREM2 cross-reactivity over mAb 9D10. As a short term solution for this project, the antibodies were deemed unsuitable for use in mouse functional assays pending further characterisation and were taken forward for detecting TREM2 by ELISA in human samples only, as demonstrated in the following chapter.

Chapter 5

Results: Quantification of sTREM2 by ELISA

5 Results: Quantification of sTREM2 by ELISA

5.1 Introduction

As the soluble form of TREM2 (sTREM2) is present in CSF and plasma, it may be a potential candidate biomarker for diagnosis and may expand our understanding of the TREM2 mechanisms involved in AD. As discussed in Chapter 1, contradictory results from measurement of sTREM2 in biomarker studies in AD patient samples (Kleinberger *et al.*, 2014, Henjum *et al.* 2016; Heslegrave *et al.*, 2016; Piccio *et al.*, 2016) suggest differences in the types of cohorts or the stage of disease tested, but also highlight technical differences, including the anti-TREM2 reagents used in the assay.

As demonstrated in Chapter 3, discrepancies in the molecular weights of TREM2 in cell lysates and/or fluids were reported in studies with the commercial R&D polyclonal antibody used in this project (Lue *et al.*, 2015; Thornton *et al.*, 2017). Significant differences in TREM2 specificity were also reported between commercial anti-TREM2 antibodies used in western blots and immunohistochemistry (Satoh *et al.*, 2013), illustrating the lack of reproducibility in studies using anti-TREM2 antibodies.

To address the lack of good anti-TREM2 reagents, one of the main aims of this project was to utilise the generated antibodies to set up specific and sensitive assays for sTREM2 detection in both human and mouse systems. Chapters 3 and 4 covered the characterisation of the generated antibodies and their binding capacities to recombinant TREM2 protein and to native protein in human and mouse cell lines and sera, and in primary monocytic isolates and brain tissue from WT and TREM2 KO mice. The latter part of this characterisation cast doubt on the cross-reactivity of the human TREM2 antibodies with mouse TREM2 protein, so the antibodies were reserved for use in human systems only and this chapter will cover the optimisation and establishment of a quantitative assay using two of the characterised antibodies.

5.1.1 Aims and Objectives

The aim of this chapter is to develop an ELISA for the quantification of human sTREM2, which can be used to investigate the expression profile of sTREM2 in human samples.

5.2 Results

5.2.1 Human sTREM2 ELISA

5.2.1.1 Assay Establishment

The initial assay set-up, including the selection of mAb 9D10 and the polyclonal antibody as capture and detection antibodies respectively, was performed by another team member, Angharad Morgan, and the assay validation experiments were conducted by me. The assay antibodies were selected because they strongly bound recombinant and native human TREM2 in direct ELISAs and western blotting as shown in Chapter 3, and demonstrated sTREM2 binding in human serum as shown in Chapter 4. During optimisation, initial high background levels in the assay were addressed by the inclusion of two overnight steps, enabling the generation of an appropriate standard curve (Figure 5.1) using recombinant human TREM2 protein (Sino Biological Inc.).

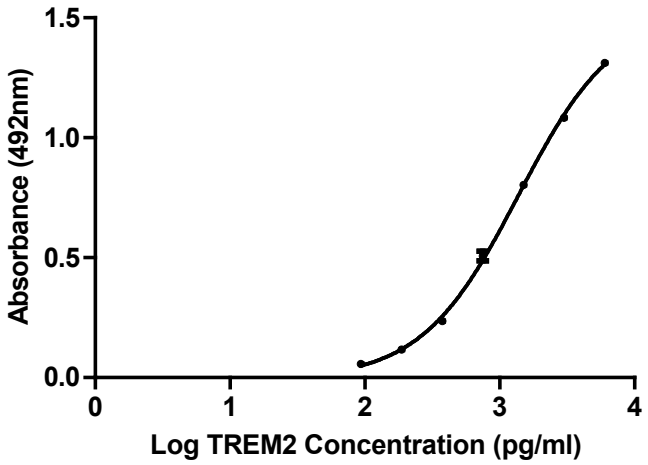

Figure 5.1 – Standard curve of human sTREM2 ELISA.
Standard curve of sTREM2 ELISA generated using recombinant human TREM2 protein (Sino Biological Inc.), starting at 6000pg/ml (6ng/ml) and titrated down in a 1 in 2 dilution series. Curve was plotted as 492nm absorbance readings against log_{10}-transformed TREM2 standard concentrations (conc.) in pg/ml. Error bars represent mean +/- SEM of duplicates in the assay.

5.2.1.2 Assay Validation

To validate the assay performance, multiple measures from diluted batches of ten in-house plasma controls were analysed. The intra-assay coefficient of variation (CV) was 5%, the lower limit of detection for this assay was 0.4ng/ml, calculated by adding the mean of ten replicates of absorbance readings from wells representing assay background levels to two standard deviations (SD) of those replicates (Armbruster and Pry, 2008). To test assay sensitivity, TREM2 protein was added into a neat plasma sample that had previously generated absorbance values below assay detection. Protein add-back concentrations started at 10ng/ml and were titrated down in a 1 in 2 dilution series. Only concentrations between 0.4ng/ml and 5ng/ml were accurately detected in the assay; the top three add-back concentrations that fell in this range (1.25, 2.50 and 5.00ng/ml) showed 83-92% spike recovery demonstrating the assay's high sensitivity (Table 5.1). A lower spike recovery (73%) was detected for the 0.63ng/ml add-back, detected at 0.46ngml, which is close to the assay's lower limit of detection.

Protein Concentration (ng/ml)	Detected Concentration (ng/ml)	Percentage Recovery (%)
10.00	Above detection	n/a
5.00	4.60	92
2.50	2.24	90
1.25	1.04	83
0.63	0.46	73
0.31	Below detection	n/a

Table 5.1 – TREM2 protein spike recovery assay.
Concentrations detected by the assay reflected concentrations of protein initially added into the plasma, percentage recovery for the assay overall ranged between 73-92%. n/a: not applicable.

This assay was also used to measure 13 CSF (non-neurological disease) samples, at a 1 in 2 dilution, from another study in the host lab. Measured sTREM2 levels ranged between 3-12ng/ml, mean: 6.7ng/ml and SD: 2.1 (Table 5.2). This preliminary data showed that the assay can sensitively detect sTREM2 in CSF.

Sample	sTREM2 (ng/ml)
CSF 1	7.0
CSF 2	6.9
CSF 3	6.7
CSF 4	7.4
CSF 5	6.3
CSF 6	7.4
CSF 7	5.5
CSF 8	5.6
CSF 9	12.3
CSF 10	3.9
CSF 11	7.9
CSF 12	3.8
CSF 13	6.4

Table 5.2 – sTREM2 concentrations in CSF samples.
Concentrations (in ng/ml) of sTREM2 in thirteen CSF samples from a non-neurological disease cohort. Mean sTREM2 concentration: 6.7ng/ml, SD: 2.1.

5.2.1.3 Quantification of sTREM2 in plasma from an AD Cohort

The human sTREM2 ELISA was used to measure sTREM2 levels in 663 individuals from a European cohort as part of the AddNeuroMed study (Lovestone *et al.*, 2009; Morgan *et al.*, 2019). These samples were measured by team members Angharad Morgan and Claire Leckey, and the subsequent statistical analysis was conducted by me. Samples were obtained from 241 AD patients, 184 mild cognitive impairment (MCI) patients and 238 age-matched healthy controls. Demographic data for this cohort is shown in Table 5.3, including statistical analysis by the Kruskal-Wallis test followed by Dunn's multiple comparison test to demonstrate that the samples between clinical groups were suitably matched for number, age and gender. Probability (P) values below 0.05 were considered significant.

Group	Individuals, number (%)	Age, mean years (SD, range)	Gender, number females (%)
Control	238 (36)	74.5 (7.0, 53-93)	137 (56)
MCI	184 (28)	76.2 (6.1, 57-94)	99 (54)
AD	241 (36)	77.2 (6.6, 58-96)	153 (64)
P-value	ns	ns	ns

Table 5.3 – Demographic data for the AddNeuroMed cohort
Number of individuals and details of age and gender for each of the three groups in the AddNeuroMed cohort, P-values represent statistical differences between each variable in the groups, these were above 0.05 for all categories indicating values were not significant (ns) and demonstrating that the three groups were well matched for these demographic factors.

Measured sTREM2 levels ranged between 2-24ng/ml (mean: 8ng/ml, SD: 3.5) in the tested cohort. To compare sTREM2 levels between the three groups, sTREM2 concentrations were first transformed using logarithm base 10 (log_{10}) to achieve a normal distribution of data (Figure 5.2) and this was confirmed using the Shapiro-Wilk normality test. Subsequent statistical analysis was performed using one way analysis of variance (ANOVA) followed by Tukey's post-hoc test, P values below 0.05 were considered significant.

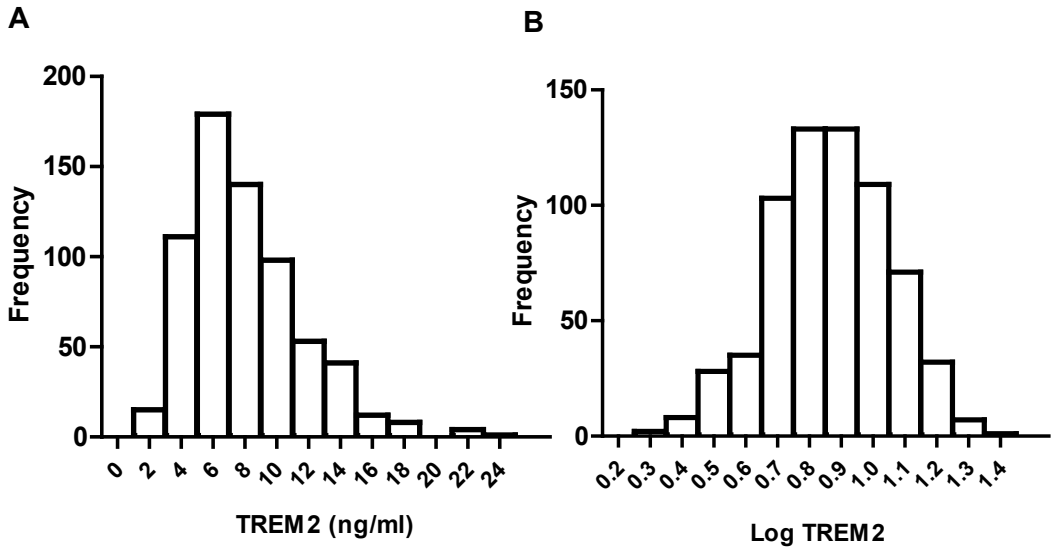

Figure 5.2 – Frequency distribution before and after logarithmic transformation.
Frequency distribution graphs illustrating that (A) initial raw data was not normally distributed but (B) after log_{10} transformation, normal distribution was achieved.

Samples were first tested for an association with gender and with age, the strongest known risk factor for AD (Rocca et al., 1991; Guerreiro and Bras, 2015). While no significant relationship was observed with gender, Spearman correlation analysis revealed that sTREM2 levels positively correlated with age in the tested cohort as a whole (Figure 5.3A), with rho (r) and calculated P values of r=0.2551, P<0.0001, and in each of the three groups separately with values of r=0.2269, P=0.0004 for healthy controls, r=0.2493, P=0.0006 for MCI patients and r=0.2692, P<0.0001 for AD patients (Figure 5.3B-D).

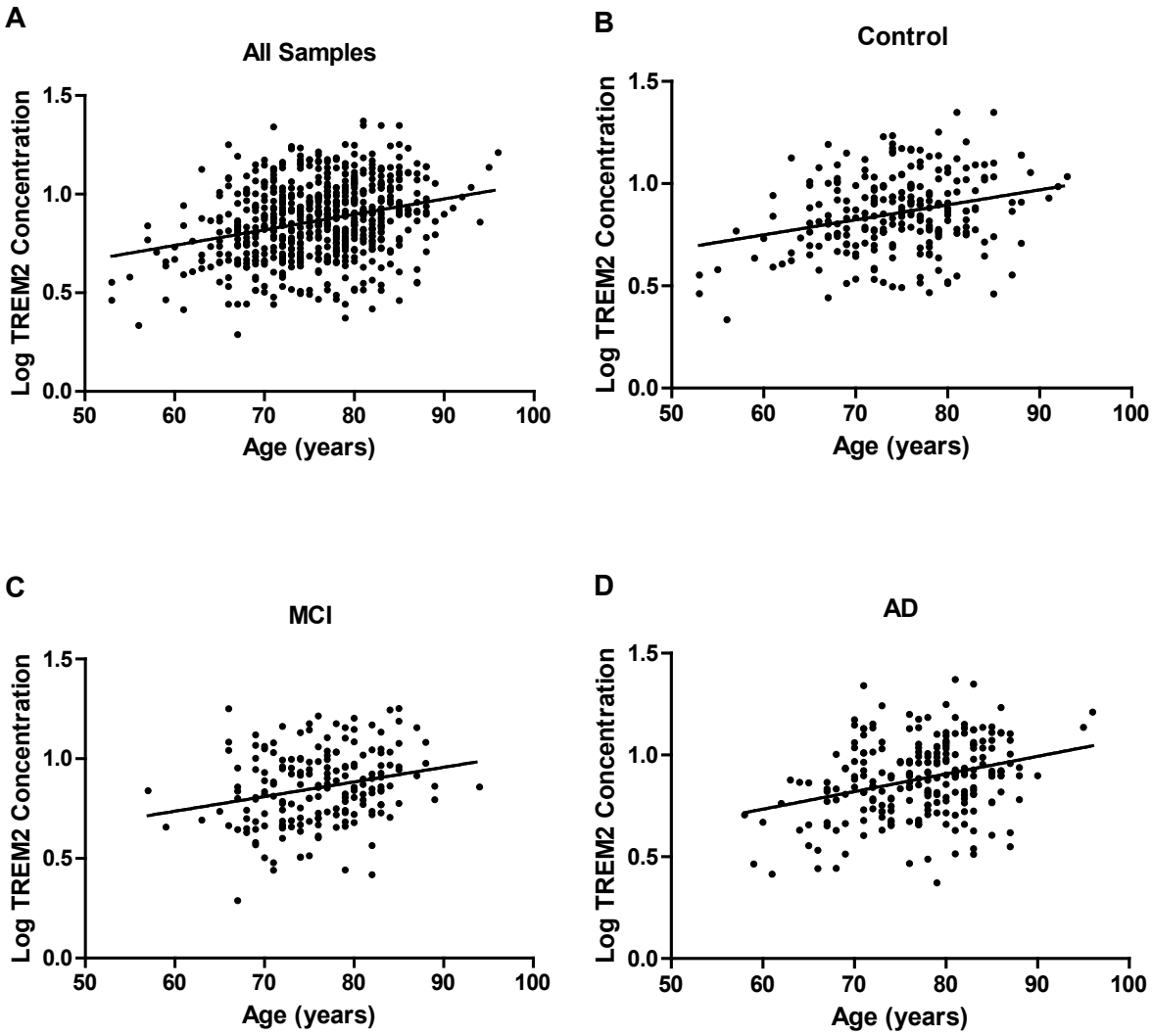

Figure 5.3 – Correlation of sTREM2 levels with age in AddNeuroMed plasma samples. Levels of sTREM positively correlated with age in (A) all tested samples (r=0.2551, P<0.0001), and in each of the groups individually; (B) healthy controls (r=0.2269, P=0.0004), (C) MCI patients (r=0.2493, P=0.0006) and (D) AD patients (r=0.2692, P<0.0001).

To further demonstrate this age effect, the above samples were divided into 10-year age blocks and levels of plasma sTREM2 compared. sTREM2 levels increased with each increasing age block for all groups, but no significant difference was observed between age blocks in the healthy controls. In the MCI group, a significant difference was observed between 60-69- and 80-89-year-old individuals (P=0.0286). In the AD group, high levels of significance were observed between 60-69 and 70-79 (P<0.0001) and between 60-69 and 80-89 age groups (P<0.0001), (Figure 5.4). The lowest levels of plasma sTREM2 were observed in the 60-69-year-old AD group, but these were not significantly different (P=0.06) from healthy controls and MCI individuals in the same age group.

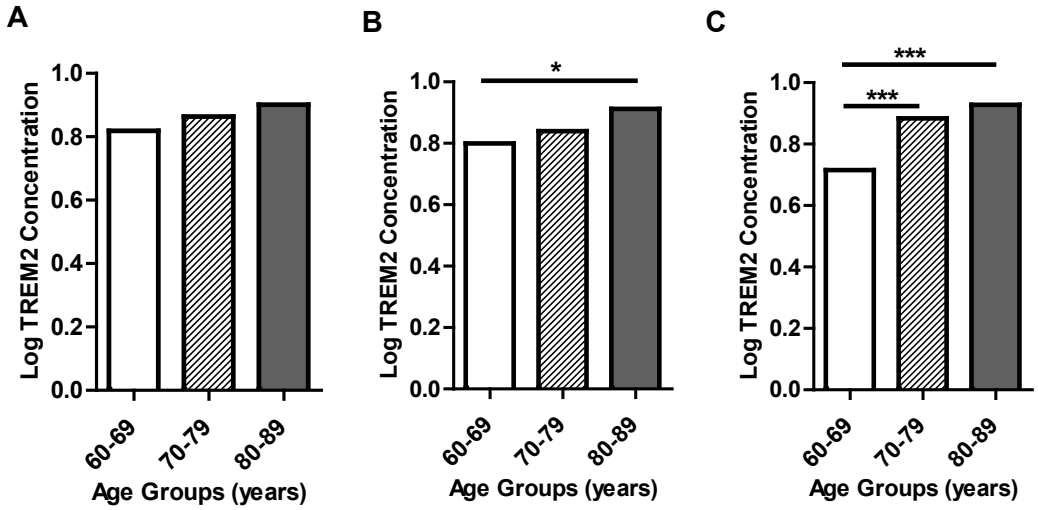

Figure 5.4 – Plasma sTREM2 levels in different age groups of AddNeuroMed cohort.
The means of log_{10}-transformed TREM2 values were compared between age groups for each clinical status. Increasing levels of sTREM2 concentration with age were observed in all three of the tested groups. (A) No significant difference was observed in the controls. (B) The MCI group demonstrated a significant difference between age groups 60-69 and 80-89 (P=0.0286). (C) Highly significant differences were observed in the AD group between 60-69 and 70-79, and between 60-69 and 80-89 age groups (P<0.0001 for both). * P<0.05, *** P<0.0001.

To investigate the age effect in younger individuals, a pilot study was conducted measuring sTREM2 in limited available samples; 5 young healthy donors, 3 older healthy controls and 13 older AD patients. Table 5.4 summarises this preliminary data which showed a potential age effect in sTREM2 levels between the young (mean: 2ng/ml, SD: 0.9) and older groups (mean: 6ng/ml, SD: 1.3), with the highest sTREM2 levels seen in the older AD patients (mean: 8.4ng/ml, SD: 3.7). Comparing where the samples fall on the standard curve of the assay visually illustrated the difference

between the younger and older samples, with the younger samples appearing between the lower and middle parts of the standard curve, and the older samples higher up on the curve, overlapping with the AD samples (Figure 5.5). Readout values for the younger group initially dropped below the detection range of the assay, so these were retested as undiluted samples to obtain a more accurate interpolation from the standard curve. Despite the low sample numbers, statistical analysis of sTREM2 levels was applied on this preliminary data and only demonstrated significance between younger healthy versus older AD individuals (P=0.004). No significance was observed between the younger and older healthy individuals, but this may be down to the very low sample numbers used.

Group	Age, Mean (years)	Age, SD	sTREM2, Mean (ng/ml)	sTREM2, SD
Young, healthy	29	4.4	2.0	0.9
Older, healthy	73	7.6	6.0	1.3
Older, AD	76	7	8.4	3.7

Table 5.4 – Quantifying sTREM2 levels in plasma samples of different age groups.
The ages and sTREM2 levels, as means and standard deviations (SD), of the three groups tested to investigate the age effect in younger individuals.

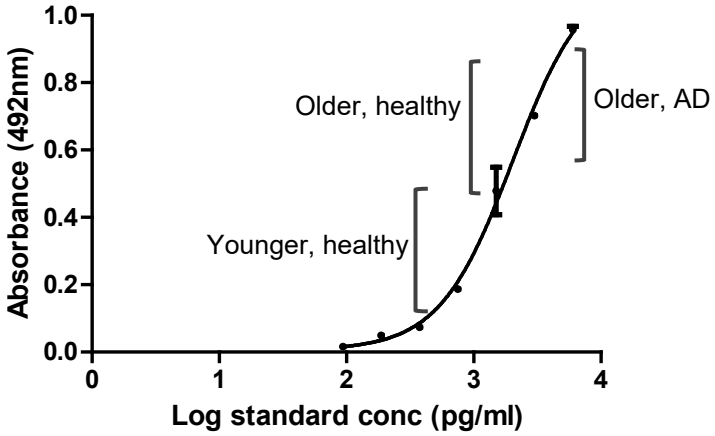

Figure 5.5 – Plasma sTREM2 levels of different age groups relative to standard curve.
Graphical representation of the sTREM2 levels in each group in relation to the assay standard curve. A clear difference was observed between younger and older age groups, with an overlap between healthy and AD samples in the two older categories. Error bars represent mean +/- SEM of duplicates in the assay.

After correcting the AddNeuroMed dataset for age using linear regression, sTREM2 levels were compared across the three clinical categories. No significant difference in sTREM2 levels was observed between the three groups; control mean: 7.9ng/ml, MCI mean: 7.8ng/ml, AD mean: 8.4ng/ml (Figure 5.6).

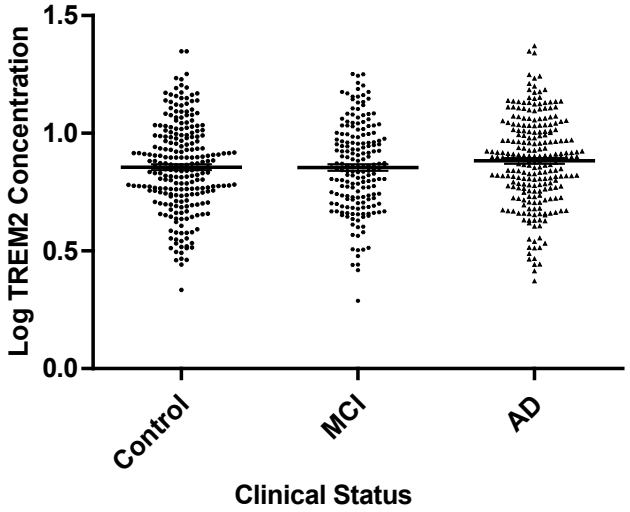

Figure 5.6 – Levels of plasma sTREM2 in the three AddNeuroMed cohort groups. Age-corrected, log_{10}-transformed TREM2 values were compared between the three tested groups, no significant difference in sTREM2 levels was observed (Control: mean=7.9ng/ml. MCI: mean=7.8ng/ml. AD: mean=8.4ng/ml). Error bars represent 95% confidence intervals.

5.2.2 Mouse sTREM2 ELISA

5.2.2.1 Assay Establishment

The following work to develop a mouse TREM2 ELISA was performed prior to the demonstration that the human antibodies did not cross-react with mouse TREM2 as was initially believed. Confirming mouse cross-reactivity should have been prioritised to avoid the unnecessary expenditure of time and reagents in the following experiments. Using mAb 9D10 as a capture antibody paired with the polyclonal as a detection antibody, as in the human ELISA, did not produce a good standard curve (Figure 5.7). A high background level was detected and extending the assay over one or two overnight steps did not resolve this.

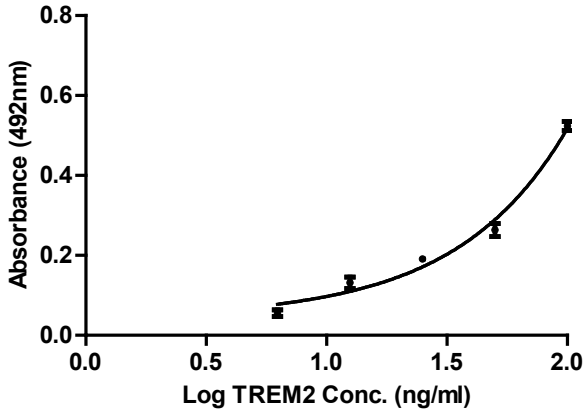

Figure 5.7 – Pairing mAb 9D10 and polyclonal antibody in a mouse TREM2 ELISA.
Using mAb 9D10 and the polyclonal with recombinant mouse TREM2 protein, top standard concentration starting at 100ng/ml, did not generate a suitable standard curve. This curve was generated after the subtraction of high background values. Error bars represent mean +/- SEM of duplicates in the assay.

The use of different blocking buffers, milk and gelatin (Sigma-Aldrich, Merck) instead of BSA, was trialled to reduce the high background signal. Gelatin lowered the background levels seen with BSA, but still did not generate a suitable curve, while milk inhibited the antibody binding that was seen using the other two blocking buffers (Figure 5.8). Swapping the positions of the capture and detection antibodies also generated a poor standard curve, and directly biotinylating antibodies to increase assay sensitivity and reduce background did not show any improvement in the assay (negative data not shown). By this stage, antibodies were demonstrated as non-specific for mouse TREM2 as discussed in Chapter 4 and they were subsequently dedicated to human work only.

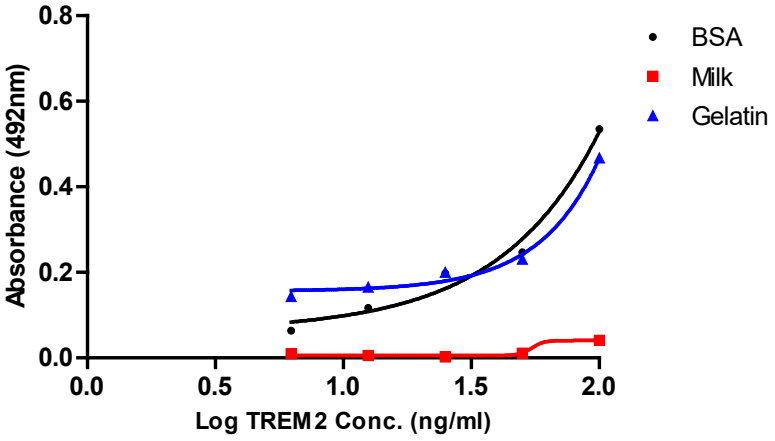

Figure 5.8 – Using different blocking buffers in the mouse sTREM2 ELISA.
Milk and gelatin blocking buffers were used as an alternative to BSA. Gelatin resulted in a similar curve to BSA with lower background levels, but milk completely inhibited the reaction.

5.3 Discussion

5.3.1 Establishment and Application of Human sTREM2 ELISA

An assay to quantify human sTREM2 was developed using the in-house generated polyclonal antibody and mAb 9D10. It was demonstrated to be highly sensitive and detected human sTREM2 in both plasma and CSF samples. The assay was used to measure sTREM2 in the AddNeuroMed cohort, as part of a larger study that quantified plasma biomarkers of inflammation and complement dysregulation in this cohort (Morgan *et al.*, 2019). After correcting the sTREM2 data for age, no significant difference in sTREM2 levels was observed between the three tested groups; AD patients, individuals with MCI and healthy controls (Figure 5.6).

In other studies investigating sTREM2 levels in AD, some groups reported higher CSF sTREM2 levels in AD and MCI compared with healthy controls (Heslegrave *et al.*, 2016; Piccio *et al.*, 2016; Bekris *et al.*, 2018), while one study reported no difference between the three groups (Henjum *et al.*, 2016). Comparing the different stages of the AD continuum, sTREM2 levels appeared to be highest at the pre-AD stage, decreasing at the later stage of dementia (Suárez-Calvet *et al.*, 2016; Liu *et al.*, 2018), this suggests that sTREM2 could be used as an important biomarker of disease progression.

Studies comparing sTREM2 levels in both CSF and plasma found that while CSF sTREM2 levels in MCI and AD patients were significantly higher than in healthy controls, these differences were not observed in plasma (Bekris *et al.*, 2018; Liu *et al.*, 2018; Ashton *et al.*, 2019). These authors concluded that their findings limit the potential use of sTREM2 as a biomarker to CSF samples, where changes during disease progression are more likely to be detected. Preliminary data in this chapter demonstrated that the human ELISA described here can sensitively quantify sTREM2 in CSF samples; further work would involve testing a higher number of CSF samples from both AD and control subjects to generate more meaningful results.

When studying a multifactorial disease such as AD, it is important to consider the impact of other factors on the observed results. It was only possible to test the effect of age and gender in this cohort for my project, and further investigation would be useful to assess the relationship of other variables with sTREM2 levels. In other studies, sTREM2 levels did not appear to depend on gender or ApoE genotype; no

differences in CSF sTREM2 levels were observed between males versus females or between APOE4 ε4 carriers versus non-carriers (Heslegrave *et al.*, 2016; Bekris *et al.*, 2018; Ma *et al.*, 2020; Knapskog *et al.*, 2020). Comorbidities, such as hypertension and type 2 diabetes, have been shown to contribute to peripheral inflammation (Newcombe *et al.*, 2018), but not all studies corrected for this factor. To focus on sTREM2 levels associated with AD pathology only, some studies excluded individuals with comorbidities that could potentially affect the levels of their tested biomarkers (Ma *et al.*, 2020; Knapskog *et al.*, 2020), so more work is required to investigate the effect of this factor on sTREM2 levels.

Changes in biomarker levels in CSF are not always reflected in plasma, and biomarker measurement in plasma as an indicator of the CNS environment is still under debate. Immune communication between the CNS and the periphery can occur, particularly if the BBB is compromised, and proteins, such as chemokines, may be involved in bidirectional communication at early disease stages (Bettcher *et al.*, 2018). In the case of sTREM2, its expression on cell types both in and outside the CNS makes it difficult to assess its contribution as a biomarker of AD pathology. However, CSF sTREM2 has been demonstrated to show better reproducibility than plasma sTREM2 across studies, thus making it a potential candidate biomarker.

5.3.2 Increase of sTREM2 Levels with Aging

An age effect was observed in the plasma samples tested using the sTREM2 ELISA; sTREM2 levels positively correlated with increasing age in the cohort as a whole and in each of the three clinical groups (Figure 5.3). This is the first study to show this association in plasma samples. Two studies in plasma so far failed to show an age effect (Bekris *et al.*, 2018; Ashton *et al.*, 2019), but in contrast to this, numerous studies in CSF showed increasing sTREM2 levels with age in healthy individuals, MCI and AD patients (Henjum *et al.*, 2016; Piccio *et al.*, 2016; Suárez-Calvet *et al.*, 2016; Bekris *et al.*, 2018; Brosseron *et al.*, 2018; Ma *et al.*, 2020).

Surprisingly, the lowest plasma sTREM2 levels in the AddNeuroMed cohort tested here were observed in the younger (60-69-year-old) AD group. As the P value (0.06) was close to statistical significance, increasing the number of samples in this group (n=26) may give a clearer indication of whether this is indeed significantly lower than sTREM2 levels in MCI (n=26) and control individuals (n=50) of the same age.

An attempt to investigate the age effect in limited available in-house samples revealed that sTREM2 is found at lower levels in plasma from young, healthy individuals. A significant difference was observed between the younger healthy and older AD individuals, but not between younger and older healthy individuals. The number of individuals per category and the difference between these numbers across the groups were not sufficient parameters to derive conclusive findings regarding age effect, yet the need to adjust dilution factors for the ELISA measurement of younger samples does hint to a difference between these and older samples, both healthy and AD. Using higher sample numbers and narrower age brackets would be an interesting follow up to further investigate this result and could be useful to determine the reference range of sTREM2 in general in the plasma of healthy individuals. Suggested sample numbers for a future study could not be accurately inferred from the pilot study due to the lack of significance between younger and older healthy samples. Power calculations for a future study could not be conducted on the AddNeuroMed cohort either as no young individuals were included in that cohort and this lowered its relevance in relation to the pilot study.

The sTREM2 ELISA described here is a highly sensitive and specific assay that can measure human sTREM2 in plasma and CSF, the latter showing promise for use in biomarker studies investigating disease progression in AD. As the polyclonal antibody and mAb 9D10 were deemed unsuitable for applications involving mouse samples, further work is required to generate antibodies specific to mouse TREM2 as will be discussed in the next chapter.

Chapter 6

Discussion

6 Discussion

6.1 Introduction

Genome-wide association studies (GWAS) have recently identified multiple genetic risk factors for late onset AD, several of which are involved in the regulation of the innate immune response (Gagliano *et al.*, 2016; Sims *et al.*, 2017). One such gene is TREM2, its most common polymorphism, R47H, conveying a 3-fold increased risk for AD making it a major genetic risk factor for AD (Jonsson *et al.*, 2013; Wunderlich *et al.*, 2013). The high relative risk conferred by this variant and the expression of TREM2 on microglia (Schmid *et al.*, 2002; Kiialainen *et al.*, 2005) generated a lot of interest in studying the effect of TREM2 on microglial function in AD. Several TREM2 functions have been demonstrated, including microglial activation and clustering around Aβ plaques (Wang et al., 2015; Filipello et al., 2018; Meilandt et al., 2020) and increased microglial phagocytic capacity (Takahashi *et al.*, 2005; Kleinberger *et al.*, 2014; Yuan *et al.*, 2016; Zhao *et al.*, 2018); however, there are many conflicting results in the literature concerning roles and relevance of TREM2. Different reports have reported contradictory effects of TREM2 on plaque morphology (Wang *et al.*, 2016; Yuan *et al.*, 2016; Lee *et al.*, 2018) and on synaptic elimination (Filipello *et al.*, 2018; Sheng *et al.*, 2019; Meilandt *et al.*, 2020). Differences were also seen between studies comparing levels of soluble TREM2 (sTREM2) in AD patients versus healthy controls (Henjum *et al.*, 2016; Heslegrave *et al.*, 2016; Piccio *et al.*, 2016; Suárez-Calvet *et al.*, 2016). These results overall indicate that the role of TREM2 is context-dependent and that the stage of disease studied and the type of anti-TREM2 reagents, and in models, the AD mouse utilised, can all contribute to the reported differences in findings.

The main objective of this project was to produce and characterise a novel panel of antibodies against human and mouse TREM2 proteins. The most suitable antibodies would then be used to develop sTREM2 quantification assays for both systems. Another objective was to produce antibodies against the two most common TREM2 variants, R47H and R62H, that have been associated with an increased risk of late onset AD in Caucasian populations (Guerreiro *et al.*, 2013; Jonsson *et al.*, 2013; Sims *et al.*, 2017).

Unfortunately, due to time constraints and lack of laboratory access imposed by the pandemic lockdown restrictions, these latter objectives were not fully completed before the project deadline. The following sections will cover the main findings of the project in relation to the current literature and discuss future work that can follow on from the results of this project.

6.2 Main Findings

6.2.1 Anti-Human TREM2 Antibodies

Monoclonal antibodies against the extracellular portion of human TREM2 were generated in TREM2 KO mice using the classical hybridoma technique, and a polyclonal antiserum was obtained from immunised rabbits and the IgG purified. Antibodies were characterised by investigating binding to recombinant human and mouse TREM2 protein and to cell lines endogenously expressing TREM2.

Differences were observed between the western blot binding patterns of the in-house polyclonal antibody compared to the commercial R&D polyclonal antibody, likely due to variations of glycosylation as reported in other studies (Lue *et al.*, 2015; Thornton *et al.*, 2018). Differences in TREM2 molecular weight in western blots were observed for the mAb, some only binding the protein in its reduced state. As previously discussed, deglycosylation of the proteins prior to assay may explain whether these differences are indeed due to this type of post-translational modification. This should have been conducted at the start of the project to ensure that the higher molecular weight observed when running the protein itself on a gel was indeed due to glycosylation as described by the supplier. Proteins should also have been sequenced to confirm protein identity prior to immunisation.

Satoh *et al*. (2013) tested seven commercial anti-TREM2 antibodies and reported western blot binding of recombinant TREM2 protein for only three of them, including the R&D polyclonal antibody tested in this project. This comparison study highlights the limitations and specificity issues of commercial antibodies against TREM2. The same group were unable to show immunohistochemical staining of human tissue using the R&D polyclonal antibody, but this is likely a result of their use of paraffin-embedded tissue sections with antigen retrieval, an issue the host lab also experienced using the in-house anti-TREM2 antibodies on paraffin-embedded samples.

Studies using cryopreserved or lightly fixed brain tissue have reported more successful TREM2 immunostaining (Piccio *et al.*, 2008; Lue *et al.*, 2015). Testing mAb 9D10 on cryopreserved mouse brain tissue in this project resulted in non-specific staining in both WT and TREM2 KO samples, a finding that was replicated with mAb 9D10 blotting of WT and KO sera and staining of monocytic isolates. The commercial R&D polyclonal antibody was also shown to bind bands in sera from WT and TREM2 KO mice similarly, indicating that this non-specific binding was not limited to the in-house antibodies. The supplier documentation reports low cross-reactivity to mouse TREM2 in ELISA for this anti-human TREM2 antibody, hinting at a possible true cross-reactivity to mouse TREM2 for both the commercial and in-house antibodies with potential cross-reactivity to other TREM proteins.

Immunostaining of cryopreserved tissue with mAb 8G10 showed more promising results than mAb 9D10; the former better differentiating between WT and TREM2 KO brain tissue. This warrants further work on mAb 8G10 as a candidate antibody against both human and mouse TREM2. Further characterisation, that was prevented by time and laboratory access restrictions, should involve investigating binding to human and mouse cell lines in western blots, flow cytometry and immunostaining. Troubleshooting mAb 8G10 immunostaining of mouse brain tissue to generate cleaner negative controls and better identify TREM2-labelled cells, by co-staining with macrophage and microglial markers, is necessary to confirm mouse TREM2 specificity of this antibody. Testing mAb 8G10 staining of cryopreserved human AD brain tissue would be another important step to determine its staining potential and future use on human tissue; a request for this tissue was indeed submitted and approved, but the tissue failed to be dispatched on time and lockdown restrictions prevented further action on this front.

6.2.2 Anti-Mouse TREM2 Antibodies

Antibodies against mouse TREM2 were generated in TREM2 KO mice immunised with the extracellular domain of recombinant mouse TREM2. All the resulting mAb from these immunisations belonged to the IgM isotype, which was surprising as the detection step carried out during screening involved the use of a commercial secondary antibody anti-IgG (Jackson Immunoresearch). This unusual result raised the question as to whether TREM2 KO mice might not class switch efficiently, but

time constraints meant that this could not be investigated further. Unfortunately, antibodies that were taken forward for characterisation were largely unsuccessful. Only one mAb, 7E1-E10, showed weak binding of recombinant mouse TREM2 in a plate binding assay, but no TREM2 binding using western blot or flow cytometry.

All clones were frozen down at different stages of the production process and re-cloning these cells from an earlier stage of mAb production would be an important next step to produce new batches of mAb to characterise. New immunisations and fusions could also be carried out, using γ-chain specific detection antibodies to select for IgG mAb during screening. Successful anti-mouse TREM2 mAb could then be used in functional assays, examples of which will be described later.

An interesting side project to follow up from this would be the investigation of the immune response of TREM2 KO mice and whether class switching in these mice is indeed impaired. The human antibodies generated in this project were of the IgG class, and IgM characterisation was limited to antibodies raised against mouse protein and variant peptides. This could indicate that the nature of antigen preparation for those specific immunisations, for example a problematic adjuvant aliquot, may have influenced antibody production. While this seems unlikely, it is worth bearing in mind alongside further immunisation of mice and measurement of the proportions of generated antibody classes.

Characterisation of TREM2 KO mice in the literature has overall shown decreased microglial activation levels and phagocytic activity, altered synaptic loss and reduced social behaviour. The absence of TREM2 in this model may be a valuable feature to study other neurodegenerative diseases; such as Nasu-Hakola disease (or PLOSL), a bone disease which presents with early onset dementia and is associated with TREM2 loss-of-function mutations (Paloneva *et al.*, 2002). Monocytes derived from DAP12- and TREM2-deficient patients with this disease were shown to exhibit delayed differentiation into osteoclasts (Paloneva *et al.*, 2003), and it would be interesting to investigate the effect of TREM2 deficiency on other immune cells and processes, namely immunoglobulin class switching, and its impact on neurodegenerative diseases.

6.2.3 Variant-Specific TREM2 Antibodies

To generate mAb against the two TREM2 risk variants, R47H and R62H, TREM2 KO mice were immunised with wild type and variant peptides conjugated to KLH, a large immunogenic protein. All antibodies produced from these fusions were also isotyped as IgM class, as described above, but hybridoma growth in culture was much more successful than that observed with cells producing anti-mouse TREM2 antibodies.

Antibodies 3F11 (raised against variant R47H) and 10D3 (raised against variant R62H) displayed specific binding to the peptide they were raised against compared to wild type peptides. However, upon testing each of them with the peptides they were not raised against, 62H for mAb 3F11 and 47H for mAb 10D3, binding was unexpectedly observed. Further characterisation is required to confirm the specificity of these two mAb and HEK293 cell lines expressing the variant forms of TREM2 were generated for this purpose. The transfected lines failed to demonstrate TREM2 mRNA expression and this was traced back to a problem with the sequences used for the vector design, making them incompatible with the human TREM2 primers used in this project. Sending DNA sequences out for vector generation is an important lesson learned to avoid introducing additional variables to the experiment, and sequencing the region of interest in the vectors is a useful future quality control check prior to transfecting cells.

After investigating protein expression of the transfected cell lines using the in-house ELISA, TREM2 was detected in both variant-expressing cell lines. It would be interesting to investigate the binding capacity and specificity of variant mAb 3F11 and 10D3 to these cell lines using western blotting and flow cytometry. Designing overlapping peptides that cover the TREM2 extracellular domain could also be used in an ELISA format to identify which region these variant antibodies bind to. This could generate useful information for investigating whether these antibodies have TREM2-activating potential, in addition to their use in screening assays to detect variants in human samples.

An important point to consider is the relevance of the TREM2 ectodomain structure to the characterisation of variant-specific antibodies. One study by Roblek *et al.* (2010) generated variant-specific antibodies to lamins using short peptides. While the majority of antibodies demonstrated successful results, one of the variant-specific antibodies failed to elicit a specific immune response. This was resolved by immunisation using an entire Ig-fold domain containing the polymorphism, rather than

a linear peptide, indicating that antigenicity, for that particular variant, depended on the conformational context of the Ig-fold as a whole. It would be interesting to investigate whether a similar situation exists for TREM2; a recent *in silico* study suggested that wild type residues at p.47 and p.62 appear outstretched from the protein domain and positive in charge. In comparison, the variant residues are more buried in the domain and neutral in charge, potentially resulting in impaired ligand binding (Menzies *et al.*, preprint). The group also reported that the R47H variant lies on binding loop complementarity-determining region 1 (CDR1), and R62H lies between the two loops CDR1 and CDR2. These structural factors could pose a challenge for the production of variant-specific antibodies using short linear peptides and are worth further consideration.

6.2.4 Establishment of Human sTREM2 ELISA

Investigating binding of sTREM2 in human serum by mAb 9D10and the in-house polyclonal using western blotting resulted in clear bands at the expected molecular weights for TREM2, indicating their suitability for use in a quantitative assay to detect TREM2 in serum or plasma. These antibodies were paired together in a sandwich ELISA to detect recombinant human TREM2 as a protein standard, and the assay was optimised using in-house plasma controls to reduce the initial high levels of background absorbance and generate a sensitive standard curve.

This assay was then used to quantify sTREM2 levels in the European AddNeuroMed cohort of 663 plasma samples from AD patients, individuals with MCI and age-matched healthy controls. A positive correlation between sTREM2 levels and age was observed across the three groups. Categorising the data into specific age groups demonstrated that younger AD patients had the lowest levels of sTREM2 when compared to age-matched MCI and control individuals. Measuring plasma samples from young healthy adults in a subsequent preliminary study showed they had low sTREM2 concentrations compared to older adults; both of these interesting findings require further investigation using higher sample numbers.

After correcting the AddNeuroMed dataset for age, there was no significant difference observed in plasma sTREM2 levels between the groups. This is in line with results from plasma studies in the literature (Berkis *et al.*, 2018; Liu *et al.*, 2018; Ashton *et al.*, 2019) and differences between clinical groups are more likely to be observed in CSF samples (Heslegrave *et al.*, 2016; Piccio *et al.*, 2016; Suárez-Calvet *et al.*, 2016; Liu *et al.*, 2018). The ELISA generated here showed promising results in measuring

sTREM2 in CSF samples and has the potential to quantify sTREM2 in CSF or plasma as a biomarker for AD progression. Using the ELISA to measure sTREM2 in paired CSF and plasma samples would be useful to investigate the correlation between the two sample types, and longitudinal studies would be valuable to determine whether the effect of variables, such as disease intensity and co-morbidities, over time is reflected in sTREM2 levels.

Recent evidence suggests that sTREM2 may have its own biological role and is perhaps not only a decoy receptor competing with membrane-bound TREM2 as initially thought (Piccio *et al.*, 2008, Zhong *et al.*, 2017). Zhong *et al.* (2019) demonstrated that sTREM2 reduced amyloid plaque deposition and stimulated microglial migration and inflammatory cytokine production when it was expressed in the 5XFAD mouse model. This suggests a neuroprotective role for sTREM2 and puts it forward as a potential therapeutic candidate for modulating immune responses in AD.

6.3 Future Work and Perspectives

6.3.1 Future Experimental Steps

The previous sections covered the steps required to troubleshoot and resolve issues that were experienced throughout this project. The immediate priority would be to obtain mAb that detect mouse TREM2 and to further characterise variant-specific mAb already generated. Future work that follows on from this project could focus on the functional aspect of the generated antibodies, but only after sufficient quality control and antibody specificity is confirmed. Ligand-binding and blockade studies could provide data on whether the antibodies activate or block TREM2 signalling. As discussed in Chapter 1, variants R47H and R62H have been associated with impaired ligand binding (Wang *et al.*, 2015; Bailey *et al.*, 2015; Yeh *et al.*, 2016) and a reduced ability for phagocytosis and triggering microglial responses (Yeh *et al.*, 2016; Zhong *et al.*, 2017; Lessard *et al.*, 2018). It would be of particular interest to test the impact of R47H and R62H variant-specific antibodies on ligand binding, phagocytosis and signalling assays. They could also be used to set up ELISAs to detect variant-specific protein in human biological samples, this would be useful as a quick screen to identify prevalence of variant carriers in existing AD cohorts and potentially as a risk predictor in control and MCI samples to investigate the conversion of carriers to AD. An additional characterisation experiment could involve the epitope mapping of the

antibodies that successfully activated or blocked signalling; this would be important to shed light on where the mAb bind and what their mechanism of action is.

As previously mentioned, investigating the immune response of TREM2 KO mice would be another crucial step to examine the ratio of IgM to other isotypes and reveal whether TREM2 KO mice have an impaired immunoglobulin response, as was reported in PLCG2 KO mice (Hikida *et al.*; 2009). The production of new antibodies specific to mouse TREM2 would fill the gap left by this project. Anti-mouse TREM2 mAb could be tested for whether they activate or block TREM2 signalling pathways by looking at their effect on calcium flux or phagocytosis. They could also be used to investigate the expression of TREM2 in various knock-in and transgenic mouse models of AD; the mAb could be used to generate an ELISA for quantification of sTREM2 in mouse plasma, and to stain primary monocytes and cryopreserved brain tissue for this purpose.

6.3.2 Limitations of Mouse Models on TREM2 Studies

While mouse models are an essential part of AD research, it is important to note the limitations of such models on the interpretation of results in relation to TREM2. The overexpression of *PSEN* and *APP* in AD mouse models may affect the activity of γ-secretase, which is a common enzyme involved in the proteolytic cleavage of both APP and TREM2, thus resulting in high sTREM2 levels as an undesirable effect (Wunderlich *et al.*, 2013). A transcriptional study of TREM2 KO models reported an upregulation in TREML1 in the Velocigene model, due to the use of a floxed neomycin cassette, compared to the Jackson and Colonna lab models (Kang *et al.*, 2018). The *TREML1* gene is immediately downstream of *TREM2* and its artificial overexpression makes it difficult to pinpoint whether experimental results can be attributed to the loss of TREM2, or the increase in TREML1, or both (Carbajosa *et al.*, 2018; Kang *et al.*, 2018). The KO strategy used for the mice in this project circumvented this issue by reversing the neomycin cassette to prevent TREML1 overexpression, but it is important to bear in mind the aforementioned limitations during interpretation of results or comparisons between TREM2 KO models.

The TREM2 R47H variant was recently reported to produce aberrant spliced transcripts leading to a reduction of TREM2 protein expression in mice, but expressing the humanised TREM2 variant gene in mice did not replicate this impaired

splicing (Xiang *et al.*, 2018), another limitation demonstrating that results derived from TREM2 knock-in models may not always be directly translated to human systems.

6.3.3 Alternative Models of AD

As human microglia cannot be readily accessed for analysis, studies are turning to the differentiation of human pluripotent stem cells (PSCs) as an AD model (Livesey, 2014). Claes *et al.* (2019) generated three microglia-like cell lines using PSC technology; two to represent the homozygous and heterozygous loss of TREM2 and one to represent the heterozygous R47H variant. The group went on to report reduced phagocytosis and amyloid plaque clearance in both knockout models, but not in the variant line. They also noted, however, that their experimental factors did not include aging and that cells derived from AD patients carrying the variant may better represent the effect of aging on these functions.

While PSC-derived microglia act as a useful model for investigating disease-associated genotypes, they pose a limitation for the study of complex processes, such as cell-to-cell interactions, cell signalling and synaptic pruning. An important factor to consider is that in the brain, microglia are exposed to environmental cues from surrounding cells, a feature that can be simulated *in vitro* by co-culturing microglia-like cells with PSC-derived neurons and/or astrocytes. This provides the anti-inflammatory cytokine response that is absent from monocultures without compromising microglial surveillant and phagocytic function (Haenseler *et al.*, 2017).

Introducing stem cell-derived cell lines would be an interesting follow up for this project; generated anti-TREM2 antibodies could be tested for binding to the supernatant or cell lysates of lines differentiated directly from fibroblasts of AD patients, particularly TREM2 variant-carriers. These cell lines could provide a more accurate context to test the generated antibodies in and may help to further understand the molecular mechanisms of TREM2 in AD and to identify potential future therapeutic targets.

6.3.4 Anti-TREM2 Antibodies in Immunotherapy

Monoclonal antibodies are commonly used therapeutically to bind target antigens or alter signalling mechanisms in disease (Berger *et al.*, 2002; Suzuki *et al.*, 2015), and the concept of using anti-TREM2 antibodies for immunotherapy has recently been of great interest as will be discussed below.

While TREM2 has been shown to regulate the microglial response and is generally thought to have an anti-inflammatory role, contradictory findings in the field make it difficult to pinpoint the exact molecular mechanisms involved and suggest that TREM2 has a more complex role than once thought. AD mouse model studies, using 5XFAD and APP/PS1 mice, reported opposing effects of TREM2 expression on amyloid accumulation and pathology depending on disease stage; beneficial at early stages of the disease (Jay *et al.*, 2015) and detrimental at later stages (Wang *et al.*, 2015; Jay *et al.*, 2017). As described in Chapter 1, spine density loss in TREM2-deficient APP/PSEN1 and PS2APP mice also differed between disease stages, with increased synaptic loss seen after 6 months (Sheng *et al.*, 2019; Meilandt *et al.*, 2020), suggesting a neuroprotective role for TREM2 in this middle-late stage of disease. Taken together, these results indicate that the role of TREM2 varies with disease progression and this seemingly dual function poses a therapeutic challenge as TREM2 may need to be activated or inhibited depending on the stage of disease.

Immunotherapeutic strategies currently under development have shown some promise involving the use of antibodies to stimulate TREM2 signalling. Schlepckow *et al.* (2020) generated an antibody (mAb 4D9) that binds the stalk region of mouse TREM2, preventing cleavage of the extracellular domain while simultaneously activating receptor signalling, and reported reduced plaque load in an APP knock-in mouse model administered 4D9. Another anti-human TREM2 antibody, AL002c, developed by Alector, Inc. recently completed a Phase 1 clinical trial. This activating antibody also binds the stalk region of TREM2 and was shown to increase microglial proliferation and reduce neurite damage during a preclinical study using 5XFAD mice expressing the human TREM2 transgene (Wang *et al.*, 2020).

Another study compared the effects of two anti-TREM2 activating antibodies, a commercial R&D Systems mAb (clone 237920) and an in-house generated mAb, on the survival of macrophages and microglia from a transgenic R47H mouse model (Cheng *et al.*, 2018). Both antibodies boosted survival of these myeloid cells in this model and in WT mice. Additionally, the commercial mAb increased microglial

migration in both genotypes while the in-house mAb did not influence migration in either. This difference in microglial modulation illustrates the complexity in the biology of TREM2 which requires further understanding, nevertheless, these studies overall have demonstrated that the therapeutic activation of TREM2 can potentially improve myeloid cell function in AD and have highlighted the importance of delivering sufficient antibody doses into the CNS.

Anti-TREM2 antibodies would also be useful to further explore the link between TREM2 and ApoE, the strongest genetic risk factor for AD (Corder *et al.*, 1993; Karch and Goate, 2015). The TREM2-ApoE interaction was shown to drive the switch of microglia from a resting to disease-associated state (Krasemann *et al.*, 2017) resulting in increased microglial phagocytosis (Atagi *et al.*, 2015; Yeh *et al.*, 2016). This ligand-receptor interaction was also shown to be significantly impaired by AD risk-associated TREM2 variants R47H and R62H (Wang *et al.*, 2015; Yeh *et al.*, 2016).

Another identified TREM2 ligand, clusterin, was also reported as a genetic risk factor for AD (Harold *et al.*, 2009). Like ApoE and TREM2, it can bind and potentially modulate the microglial clearance of Aβ (Ghiso *et al.*, 1993; Strittmatter *et al.*, 1993; Lessard *et al.*, 2018; Zhao *et al.*, 2018), and was recently demonstrated to positively correlate with APOE4 genotype in AD synapses (Jackson *et al.*, 2019), suggesting a functional link between all three risk factors. Learning more about this link is important to further current knowledge in the field and may shed light on why opposing roles have been associated with TREM2 in AD.

6.3.5 Conclusions

A vast body of literature describes the multiple functions and signalling pathways of TREM2 and the wide range of proposed ligands associated with it. Learning more about the interactions of TREM2 with these ligands can help to build a clearer picture of the complex biological role of TREM2, particularly for ligands that have themselves been associated with an increased risk of AD.

The anti-human mAb described in this project are novel reagents that have been shown to specifically bind human TREM2. The in-house established TREM2 ELISA can sensitively detect human sTREM2 in both CSF and plasma samples, making it a good biomarker assay for CSF studies of AD and other neurodegenerative diseases.

The establishment of a quantitative assay using the variant mAb could provide a quick and simple screening technique for variant TREM2 proteins in large plasma cohorts. There is strong potential for both the human wild type and variant mAb to be used in functional assays investigating the impact of the mAb on the known functions of TREM2, especially those involving interactions with the risk-associated ligands discussed above. This in turn could result in the identification of activating or blocking antibodies that could possess future therapeutic value. Further research on the complex role of TREM2 and its potential modulation, using tools such as monoclonal antibodies, could provide a more comprehensive understanding of the involvement of TREM2-related processes in the pathogenesis of AD.

References

Abbott NJ, Ronnback L, Hansson E (2006). Astrocyte-endothelial interactions at the blood-brain barrier. *Nat Rev Neurosci* 7:41-53.

Aldo PB, Craveiro V, Guller S, Mor G (2013). Effects of culture conditions on the phenotype of THP-1 monocyte cell line. *Am J Reprod Immunol* 70(1):80-6.

Allcock RJN, Barrow AD, Forbes S, Beck S, Trowsdale J (2003). The human TREM gene cluster at 6p21.1 encodes both activating and inhibitory single IgV domain receptors and includes NKp44. *Eur J Immunol* 33:567-77.

Altschul SF, Gish W, Miller W, Myers EW, Lipman DJ (1990). Basic local alignment search tool. *J Mol Biol* 215:403-410.

Alzheimer A (1907). Über eine eigenartige Erkrankung der Hirnrinde. *Allgemeine Zeitschrift für Psychiatrie und Psychisch-Gerichtliche Medizin* 64:146-8.

Alzheimer's Association (2014). 2014 Alzheimer's disease facts and figures. *Alzheimers Dement* 10(2):e47-92.

Arai H, Terajima M, Miura M, Higuchi S, Muramtsu T, Machida N *et al.* (1995). Tau in cerebrospinal fluid: a potential diagnostic marker in Alzheimer's disease. *Ann Neurol* 38(4):649-52.

Armbruster DA, Pry T (2008). Limit of Blank, Limit of Detection and Limit of Quantitation. *Clin Biochem Rev* 29(Suppl1):S49-52.

Arvanitakis Z, Capuano AW, Leurgans SE, Bennett DA, Schneider JA (2016). Relation of cerebral vessel disease to Alzheimer's disease dementia and cognitive function in elderly people: a cross-sectional study. *Lancet Neurol* 15(9):934-943.

Ascoli CA and Aggeler B (2018). Overlooked benefits of using polyclonal antibodies. *Biotechniques* 65(3):127-36.

Ashton NJ, Suárez-Calvet M, Heslegrave A, Hye A, Razquin C, Pastor P *et al.* (2019). Plasma levels of soluble TREM2 and neurofilament light chain in TREM2 rare variant carriers. *Alzheimers Res Ther* 11(1):94.

Atagi Y, Liu C-C, Painter MM, Chen X-F, Verbeeck C, Zheng H *et al.* (2015). Apolipoprotein E Is a Ligand for Triggering Receptor Expressed on Myeloid Cells 2 (TREM2). *J Biol Chem* 290(43):26043-50.

Ayer A, Wojta K, Ramos E, Dokuru D, Chen J, Karydas A *et al.* (2019). Frequency of the TREM2 R47H Variant in Various Neurodegenerative Disorders. *Alzheimer Disease & Associated Disorders* 33(4):327-30.

Bailey CC, DeVaux LB, Farzan M (2015). The Triggering Receptor Expressed on Myeloid Cells 2 Binds Apolipoprotein E. *J Biol Chem* 290(43):26033-42.

Barger SW, Harmon AD (1997). Microglial activation by Alzheimer amyloid precursor protein and modulation by apolipoprotein E. *Nature* 388:878-81.

Bar-Nun S, Shneyour Y, Beckmann JS (1983). G-418, an elongation inhibitor of 80S ribosomes. *Biochim Biophys Acta* 741(1):123-7.

Barthélemy NR, Horie K, Sato C, Bateman RJ (2020). Blood plasma phosphorylated-tau isoforms track CNS change in Alzheimer's disease. *J Exp Med* 217(11):e20200861.

Bass JJ, Wilkinson DJ, Rankin D, Phillips BE, Szewczyk NJ, Smith K *et al.* (2017). An overview of technical considerations for Western blotting applications to physiological research. *Scand J Med Sci Sports* 27(1):4-25.

Bateman RJ, Xiong C, Benzinger TL, Fagan AM, Goate A, Fox NC *et al.* (2012). Dominantly Inherited Alzheimer Network. Clinical and biomarker changes in dominantly inherited Alzheimer's disease. *N Eng J Med* 367(9):795-804.

Bazan J, Całkosiński I, Gamian A (2012). Phage display – a powerful technique for immunotherapy: 1. Introduction and potential of therapeutic applications. *Hum Vaccin Immunother* 8(12):1817-28.

Beason-Held LL, Goh JO, An Y, Kraut MA, O'Brien RJ, Ferrucci L *et al.* (2013). Changes in brain function occur years before the onset of cognitive impairment. *J Neurosci* 33(46):18008-14.

Bekris LM, Khrestian M, Dyne E, Shao Y, Pillai JA, Rao SM *et al.* (2018). Soluble TREM2 and biomarkers of central and peripheral inflammation in neurodegenerative disease. *J Neuroimmunol* 319:19-27.

Berger M, Shankar V, Vafai A (2002). Therapeutic Applications of Monoclonal Antibodies. *Am J Med Sci* 324(1):14-30.

Bertram L, Lange C, Mullin K, Parkinson M, Hsiao M, Hogan MF *et al.* (2008). Genome-wide association analysis reveals putative Alzheimer's disease susceptibility loci in addition to APOE. *Am J Hum Genet* 83:623-32.

Bettcher BM, Johnson SC, Fitch R, Casaletto KB, Heffernan KS, Asthana S *et al.* (2018). Cerebrospinal Fluid and Plasma Levels of Inflammation Differentially Relate to CNS Markers of Alzheimer's Disease Pathology and Neuronal Damage. *J Alzheimers Dis* 62(1):385-97.

Biagioni MC, Galvin JE (2011). Using biomarkers to improve detection of Alzheimer's disease. *Neurodegener Dis Manag* 1(2):127-39.

Biessels GJ, Staekenborg S, Brunner E, Brayne C, Scheltens P. (2006). Risk of dementia in diabetes mellitus: a systematic review. *Lancet Neurol* 5:64-74.

Blair LJ, Frauen HD, Zhang B, Nordhues BA, Bijan S, Lin YC *et al.* (2015). Tau depletion prevents progressive blood-brain barrier damage in a mouse model of tauopathy. *Acta Neuropathologica Communications* 3:8.

Blennow K, Wallin A, Ågren H, Spenger C, Siegfried J, Vanmechelen E (1995). Tau protein in cerebrospinal fluid: a biochemical diagnostic marker for axonal degeneration in Alzheimer's disease? *Mol Chem Neuropathol* 26:231-45.

Bohlen CJ, Bennett FC, Tucker AF, Collins HY, Mulinyawe SB, Barres BA (2017). Diverse Requirements for Microglial Survival, Specification, and Function Revealed by Defined-Medium Cultures. *Neuron* 94(4):759-773.e8.

Bohlen CJ, Bennett FC, Bennett ML (2019). Isolation and Culture of Microglia. *Curr Protocol Immunol* 125(1):e70.

Bolmont T, Haiss F, Eicke D, Radde R, Mathis CA, Klunk WE *et al.* (2008). Dynamics of the microglial/amyloid interaction indicate a role in plaque maintenance. *J Neurosci* 28(16):4283-92.

Borroni B, Ferrari F, Galimberti D, Nacmias B, Barone C, Bagnoli S *et al.* (2014). Heterozygous TREM2 mutations in frontotemporal dementia. *Neurobiology of Aging* 35(4):934.e7-e10.

Bosshart H, Heinzelmann M (2016). THP-1 cells as a model for human monocytes. *Ann Transl Med* 4(21):438.

Bouchon A, Dietrich J, Colonna M (2000). Cutting edge: inflammatory responses can be triggered by TREM-1, a novel receptor expressed on neutrophils and monocytes. *J Immunol* 164(10):4991-5.

Brendel M, Kleinberger G, Probst F, Jaworska A, Overhoff F, Blume T *et al.* (2017). Increase of TREM2 during Aging of an Alzheimer's Disease Mouse Model Is Paralleled by Microglial Activation and Amyloidosis. *Front Aging Neurosci* 9:8.

Brosseron F, Traschütz A, Widmann CN, Kummer MP, Tacik P, Santarelli F *et al.* (2018). Characterization and clinical use of inflammatory cerebrospinal fluid protein markers in Alzheimer's disease. *Alzheimers Res Ther* 10(1):25.

Brosseron F, Kleemann K, Kolbe C-C, Santarelli F, Castro-Gomez S, Tacik P *et al.* (2020). Interrelations of Alzheimer´s disease candidate biomarkers neurogranin, fatty acid-binding protein 3 and ferritin to neurodegeneration and neuroinflammation. *Journal of Neurochemistry* 00:1-15.

Buerger K, Zinkowski R, Teipel SJ, Tapiola T, Arai H, Blennow K *et al.* (2002). Differential diagnosis of Alzheimer disease with cerebrospinal fluid levels of tau protein phosphorylated at threonine 231. *Arch Neurol* 59(8):1267-72.

Burnet FM (1957). A modification of Jerne's theory of antibody production using the concept of clonal selection. *Aust J Sci* 20:67–77.

Busby M, Xue C, Li C, Farjoun Y, Gienger E, Yofe I *et al.* (2016). Systemic comparison of monoclonal versus polyclonal antibodies for mapping histone modifications by ChIP-seq. *Epigenetics & Chromatin* 9(49).

Butovsky O, Jedrychowski MP, Moore CS, Cialic R, Lanser AJ, Gabriely G *et al.* (2014). Identification of a unique TGF-β-dependent molecular and functional signature in microglia. *Nat Neurosci* 17(1):131-43.

Cady J; Koval ED, Benitez BA, Zaidman C, Jockel-Balsarotti J, Allred P *et al.* (2014). TREM2 Variant p.R47H as a Risk Factor for Sporadic Amyotrophic Lateral Sclerosis. *JAMA Neurol* 71(4):449-53.

Cannon JP, O'Driscoll M, Litman GW (2011). Specific lipid recognition is a general feature of CD300 and TREM molecules. *Immunogenetics* 64(1):39-47.

Carbajosa G, Malki K, Lawless N, Wang H, Ryder JW, Wozniak E *et al.* (2018). Loss of Trem2 in microglia leads to widespread disruption of cell coexpression networks in mouse brain. *Neurobiol Aging* 69:151-166.

Chen C, Okayama H (1987). High-efficiency transformation of mammalian cells by plasmid DNA. *Mol Cell Biol* 7(8):2745-52.

Cheng Q, Danao J, Talreja S, Wen P, Yin J, Sun N *et al.* (2018). TREM2-activating antibodies abrogate the negative pleiotropic effects of the Alzheimer's disease variant Trem2R47H on murine myeloid cell function. *J Biol Chem* 923(32):12620-33.

Cheng Y, Haorah J (2019). How does the brain remove its waste metabolites from within? *Int J Physiol Pathophysiol Pharmacol* 11(6):238-49.

Chung DH, Seaman WE, Daws MR (2002). Characterization of TREM-3, an activating receptor on mouse macrophages: definition of a family of single Ig domain receptors on mouse chromosome 17. *Eur J Immunol* 32(1):59-66.

Cicinnati VR, Shen Q, Sotiropoulos GC, Radtke A, Gerken G, Beckebaum S (2008). Validation of putative reference genes for gene expression studies in human hepatocellular carcinoma using real-time quantitative RT-PCR. *BMC Cancer* 8:350.

Claes C, Van Den Daele J, Boon R, Schouteden S, Colombo A, Monasor LS *et al.* (2019). Human stem cell-derived monocytes and microglia-like cells reveal impaired amyloid plaque clearance upon heterozygous or homozygous loss of TREM2. *Alzheimers Dement* 15(3):453-64.

Corder EH, Saunders AM, Strittmatter WJ, Schmechel DE, Gaskell PC, Small GW *et al.* (1993). Gene dose of apolipoprotein E type 4 allele and the risk of Alzheimer's disease in late onset families. *Science* 261(5123):921-3.

Dati F, Johnson AM, Whicher JT (2001). The existing interim consensus reference ranges and the future approach. *Clin Chem Lab Med* 39(11):1134-6.

Davies DR and Chacko S (1993). Antibody structure. *Acc Chem Res* 26:421-7.

Davies J and Jimenez A (1980). A New Selective Agent for Eukaryotic Cloning Vectors. *The American Journal of Tropical Medicine and Hygiene* 29(5-Pt2):1089-92.

Daws MR, Sullam PM, Niemi EC, Chen TT, Tchao NK, Seaman WE (2003). Pattern recognition by TREM-2: binding of anionic ligands. *J Immunol* 171(2):594-9.

DeKosky ST, Scheff SW (1990). Synapse loss in frontal cortex biopsies in Alzheimer's disease: correlation with cognitive severity. *Ann Neurol* 27(5):457-64.

Del-Aguila JL, Benitez BA, Li Z, Dube U, Mihindukulasuriya KA, Budde JP *et al.* (2019). TREM2 brain transcript-specific studies in AD and TREM2 mutation carriers. *Mol Neurodegener* 14(1):18.

Delahaut P (2017). Immunisation - choice of host, adjuvants and boosting schedules with emphasis on polyclonal antibody production. *Methods* 116:4-11.

DeMattos RB, Cirrito JR, Parsadanian M, May PC, O'Dell MA, Taylor JW *et al.* (2004). ApoE and clusterin cooperatively suppress Abeta levels and deposition: evidence that ApoE regulates extracellular Abeta metabolism in vivo. *Neuron* 41(2):193-202.

De Silva HV, Stuart WD, Duvic CR, Wetterau JR, Ray MJ, Ferguson DG *et al.* (1990). A 70-kDa apolipoprotein designated ApoJ is a marker for subclasses of human plasma high density lipoproteins. *J Biol Chem* 265(22):13240-7.

Desjardins P, Conklin D (2010). NanoDrop Microvolume Quantitation of Nucleic Acids. *J Vis Exp* 45:e2565.

De Vito LD, Mason BP, Jankowska-Gan E, Hogan KT, Guo JW, Lutz CT *et al.* (1993). Epitope fine specificity of human anti-HLA-A2 antibodies. Identification of four epitopes including a haptenlike epitope on HLA-A2 at lysine 127. *Hum Immunol* 37(3):165-77.

De Vos A, Jacobs D, Struyfs H, Fransen E, Andersson K, Portelius E *et al.* (2015). C-terminal neurogranin is increased in cerebrospinal fluid but unchanged in plasma in Alzheimer's disease. *Alzheimers & Dementia* 11(12):1461-9.

Dhiman K, Gupta VB, Villemagne VL, Eratne D, Graham PL, Fowler C *et al.* (2020). Cerebrospinal fluid neurofilament light concentration predicts brain atrophy and cognition in Alzheimer's disease. *Alzheimer's Dement* 12:e12005.

Dickson DW, Farlo J, Davies P, Crystal H, Fuld P, Yen SH (1988). Alzheimer's disease. A double-labeling immunohistochemical study of senile plaques. *Am J* Pathol 132(1):86-101.

Doecke JD, Laws SM, Faux NG, Wilson W, Burnham SC, Lam CP *et al.* (2012). Blood-based protein biomarkers for diagnosis of Alzheimer disease. *Arch Neurol* 69(10):1318-25.

Drago F, Lombardi M, Prada I, Gabrielli M, Joshi P, Cojoc D *et al.* (2017). ATP Modifies the Proteome of Extracellular Vesicles Released by Microglia and Influences Their Action on Astrocytes. *Front Pharmacol* 8:910.

Edelman, GM (1959). Dissociation of γ-globulin. *Am Chem Soc* 81:3155-6.

eLife. [Internet] (2016) *5:e20391.* eLife Sciences Publications, Ltd, UK. [cited 2020 Feb 20]. Available from doi: 10.7554/eLife.20391

Endres K, Deller T (2017). Regulation of Alpha-Secretase ADAM10 In vitro and In vivo: Genetic, Epigenetic, and Protein-Based Mechanisms. *Front Mol Neurosci* 10:56.

Fagraeus A (1948). The plasma cellular reaction and its relation to the formation of antibodies in vitro. *The Journal of Immunology* 58(1):1-13.

Feuerbach D, Schindler P, Barske C, Joller S, Beng-Louka E, Worringer KA *et al.* (2017). ADAM17 is the main sheddase for the generation of human triggering receptor expressed in myeloid cells (hTREM2) ectodomain and cleaves TREM2 after Histidine 157. *Neurosci Lett* 660:109-114.

Filipello F, Morini R, Corradini I, Zerbi V, Canzi A, Michalski B *et al.* (2018). The Microglial Innate Immune Receptor TREM2 Is Required for Synapse Elimination and Normal Brain Connectivity. *Immunity* 48(5):979-91.

Finelli D, Rollinson S, Harris J, Jones M, Richardson A, Gerhard A *et al.* (2015). TREM2 analysis and increased risk of Alzheimer's disease. *Neurobiology of Aging* 36:546e9-13.

Fleisher-Berkovich S, Filipovich-Rimon T, Ben-Shmuel S, Hülsmann C, Kummer MP, Heneka MT (2010). Distinct modulation of microglial amyloid β phagocytosis and migration by neuropeptides. *J Neuroinflammation* 7:61.

Fonseca MI, Zhou J, Botto M, Tenner AJ (2004). Absence of C1q Leads to Less Neuropathology in Transgenic Mouse Models of Alzheimer's Disease. *Journal of Neuroscience* 24(29):6457-65.

Ford JW, McVicar DW (2009). TREM and TREM-like receptors in inflammation and disease. *Curr Opin Immunol* 21(1):38-46.

Fossati S, Cejudo JR, Debure L, Pirraglia E, Sone JE, Li Y *et al*. (2019). Plasma tau complements CSF tau and P-tau in the diagnosis of Alzheimer's disease. *Alzheimers Dement (Amst)* 11:483-92.

Gagliano SA, Pouget JG, Hardy J, Knight J, Barnes MR, Ryten M *et al.* (2016). Genomics implicates adaptive and innate immunity in Alzheimer's and Parkinson's diseases. *Ann Clin Transl Neurol* 3(12):924-33.

Gaiottino J, Norgren N, Dobson R, Topping J, Nissim A *et al.* (2013). Increased Neurofilament Light Chain Blood Levels in Neurodegenerative Neurological Diseases. *PLoS One* 8(9):e75091.

Gallagher S (2001). Quantitation of nucleic acids with absorption spectroscopy. *Curr Protoc Protein Sci* Appendix 4:Appendix 4K.

Games D, Adams D, Alessandrini R, Barbour R, Berthelette P, Blackwell C *et al.* (1995). Alzheimer-type neuropathology in transgenic mice overexpressing V717F beta-amyloid precursor protein. *Nature* 373(6514):523-7.

Garcia JA, Cardona SM, Cardona AE (2014). Isolation and analysis of mouse microglial cells. *Curr Protoc Immunol* 104: 14.35.1-15.

Genua M, Rutella S, Correale C, Danese S (2014). The triggering receptor expressed on myeloid cells (TREM) in inflammatory bowel disease pathogenesis. *J Transl Med* 12:293.

Gerendasy DD, Sutcliffe JG (1997). RC3/neurogranin, a postsynaptic calpacitin for setting the response threshold to calcium influxes. *Mol Neurobiol* 15(2):131-63.

Ghiso J, Matsubara E, Koudinov A, Choi-Miura NH, Tomita M, Wisniewski T *et al.* (1993). The cerebrospinal-fluid soluble form of Alzheimer's amyloid beta is complexed to SP-40,40 (apolipoprotein J), an inhibitor of the complement membrane-attack complex. *Biochem J* 293(Pt1):27-30.

Ginhoux F, Greter M, Leboeuf M, Nandi S, See P, Gokhan S *et al.* (2010). Fate mapping analysis reveals that adult microglia derive from primitive macrophages. *Science* 330(6005):841-5.

Glebov K, Wunderlich P, Karaca I, Walter J (2016). Functional involvement of γ-secretase in signaling of the triggering receptor expressed on myeloid cells-2 (TREM2). *J Neuroinflammation* 13:17.

Goetzl EJ, Kapogiannis D, Schwartz JB, Lobach IV, Goetzl L, Abner EL *et al.* (2016). Decreased synaptic proteins in neuronal exosomes of frontotemporal dementia and Alzheimer's disease. *FASEB J* 30(12):4141-4148.

Grabert K, McColl BW (2018). Isolation and Phenotyping of Adult Mouse Microglial Cells. *Methods Mol Biol* 1784:77-86.

Graham FL, Smiley J, Russell WC, Nairn R (1977). Characteristics of a human cell line transformed by DNA from human adenovirus type 5. *J Gen Virol* 36(1):59-74.

Gratuze M, Leyns CEG, Holtzman DM (2018). New insights into the role of TREM2 in Alzheimer's disease. *Mol Neurodegener* 13(1):66.

Green AJE, Harvey RJ, Thompson EJ, Rossor MN (1999). Increased tau in the cerebrospinal fluid of patients with frontotemporal dementia and Alzheimer's disease. *Neuroscience Letters* 259(2):133-5.

Griffin WS, Stanley LC, Ling C, White L, MacLeod V, Perrot LJ *et al.* (1989). Brain interleukin 1 and S-100 immunoreactivity are elevated in Down syndrome and Alzheimer disease. *Proc Natl Acad Sci USA* 86(19):7611-5.

Guerreiro R, Wojtas A, Bras J, Carrasquillo M, Rogaeva E, Majounie E *et al.* (2013). TREM2 variants in Alzheimer's disease. *N Engl J Med* 368(2):117-27.

Guerreiro R, Bras J (2015). The age factor in Alzheimer's disease. *Genome Med* 7:106.

Haenseler W, Sansom SN, Buchrieser J, Newey SE, Moore CS, Nicholls FJ *et al.* (2017). A Highly Efficient Human Pluripotent Stem Cell Microglia Model Displays a Neuronal-Co-culture-Specific Expression Profile and Inflammatory Response. *Stem Cell Reports* 8(6):1727-42.

Hakobyan S, Harris CL, Tortajada A, de Jorge EG, García-Layana A, Fernández-Robredo P *et al.* (2008). Measurement of Factor H Variants in Plasma Using Variant-Specific Monoclonal Antibodies: Application to Assessing Risk of Age-Related Macular Degeneration. *Investigative Ophthalmology & Visual Science* 49(5):1983-90.

Hall AM, Roberson ED (2012). Mouse models of Alzheimer's disease. *Brain Res Bull* 88(1):3-12.

Hampel H, O'Bryant SE, Molinuevo JL, Zetterberg H, Masters CL, Lista S *et al.* (2018). Blood-based biomarkers for Alzheimer disease: mapping the road to the clinic. *Nature Reviews Neurology* 14:639-52.

Harlow E and Lane D (1988). *Antibodies: a Laboratory Manual.* Cold Spring Harbor Laboratory. New York, USA.

Harold D, Abraham R, Hollingworth P, Sims R, Gerrish A, Hamshere ML *et al.* (2009). Genome-wide association study identifies variants at CLU and PICALM associated with Alzheimer's disease. *Nat Genet* 41(10):1088-93.

Harris H, Watkins JF (1965). Hybrid Cells Derived from Mouse and Man: Artificial Heterokaryons of Mammalian Cells from Different Species. *Nature* 205:640-6.

Hartz AMS, Bauer B, Soldner ELB, Wolf A, Boy S, Backhaus R *et al.* (2012). Amyloid-β Contributes to Blood–Brain Barrier Leakage in Transgenic Human Amyloid Precursor Protein Mice and in Humans with Cerebral Amyloid Angiopathy. *Stroke* 43(2):514-23.

Hebert LE, Scherr PA, Beckett LA, Albert MS, Pilgrim DM, Chown MJ *et al.* (1995). Age-specific incidence of Alzheimer's disease in a community population. *JAMA* 273(17):1354-9.

Heindl S, Gesierich B, Benakis C, Llovera G, Duering M, Liesz A (2018). Automated Morphological Analysis of Microglia After Stroke. *Front Cell Neurosci* 12:106.

Heneka MT, Sastre M, Dumitrescu-Ozimek L, Dewachter I, Walter J, Klockgether T *et al.* (2005). Focal glial activation coincides with increased BACE1 activation and precedes amyloid plaque deposition in APP[V717I] transgenic mice. *J Neuroinflammation* 2:22.

Henjum K, Almdahl IS, Årskog V, Minthon L, Hansson O, Fladby T *et al.* (2016). Cerebrospinal fluid soluble TREM2 in aging and Alzheimer's disease. *Alzheimers Res Ther* 8(1):17.

Henjum K, Quist-Paul E, Zetterberg H, Blennow K, Nilsson LNG, Watne LO (2018). CSF sTREM2 in delirium-relation to Alzheimer's disease CSF biomarkers Aβ42, t-tau and p-tau. *J Neuroinflammation* 15(1):304.

Herber DL, Mercer M, Roth LM, Symmonds K, Maloney J, Wilson N *et al.* (2007). Microglial activation is required for Abeta clearance after intracranial injection of lipopolysaccharide in APP transgenic mice. *J Neuroimmune Pharmacol* 2(2):222-31.

Herrmann N, Chau SA, Kircanski I, Lanctôt KL (2011). Current and emerging drug treatment options for Alzheimer's disease: a systematic review. *Drugs* 71(15):2031-65.

Heslegrave A, Heywood W, Paterson R, Magdalinou N, Svensson J, Johansson P *et al.* (2016). Increased cerebrospinal fluid soluble TREM2 concentration in Alzheimer's disease. *Mol Neurodegener* 11:3.

Hickman SE, Allison EK, El Khoury J (2008). Microglial Dysfunction and Defective β-Amyloid Clearance Pathways in Aging Alzheimer's Disease Mice. *J Neurosci* 28(33): 8354–8360.

Hickman SE, El Khoury J (2014). TREM2 and the neuroimmunology of Alzheimer's disease. *Biochem Pharmacol* 88(4):495-8.

Hikida M, Casola S, Takahashi N, Kaji T, Takemori T, Rajewsky K *et al.* (2009). PLC-γ2 is essential for formation and maintenance of memory B cells. *J Exp Med* 206(3): 681–689.

Hoffman W, Lakkis FG, Chalasani G (2016). B cells, antibodies, and more. *Clin J Am Soc Nephrol* 11(1):137-54.

Hollingworth P, Harold D, Sims R, Gerrish A, Lambert JC, Carrasquillo MM *et al.* (2008). Common variants at ABCA7, MS4A6A/MS4A4E, EPHA1, CD33 and CD2AP are associated with Alzheimer's disease. *Nat Genet* 43(5):429-35.

Holtzman DM, Morris JC, Goate AM (2011). Alzheimer's disease: the challenge of the second century. *Sci Transl Med* 3(77):77sr1.

Howlett DR, Bowler K, Soden PE, Riddell D, Davis JB, Richardson JC *et al.* (2008). Aß deposition and related pathology in an APP x PS1 transgenic mouse model of Alzheimer's disease. *Histol Histopathol* 23:67-76.

Hoylaerts MF, Millán JL (1991). Site-directed mutagenesis and epitope-mapped monoclonal antibodies define a catalytically important conformational difference between human placental and germ cell alkaline phosphatase. *Eur J Biochem* 202(2):605-16.

Hua JY, Smith SJ (2004). Neural activity and the dynamics of central nervous system development. *Nat Neurosci* 7(4):327-32.

Huber CM, Yee C, May T, Dhanala A, Mitchell CS (2018). Cognitive Decline in Preclinical Alzheimer's Disease: Amyloid-Beta versus Tauopathy. *J Alzheimers Dis* 61(1):265-281.

Human Protein Atlas [Internet]. *TREM2: RNA Expression Overview*. Human Protein Atlas [2017] – [cited 2020 Mar 25]. Available from: https://www.proteinatlas.org/ENSG00000095970-TREM2/cell.

Humpel C (2011). Identifying and validating biomarkers for Alzheimer's disease. *Trends in Biotechnology* 29(1):26-32.

Humphrey MB, Daws MR, Spusta SC, Niemi EC, Torchia JA, Lanier LL *et al.* (2006). TREM2, a DAP12-associated receptor, regulates osteoclast differentiation and function. *J Bone Miner Res* 21: 237–245.

Hye A, Riddoch-Contreras J, Baird AL, Ashton NJ, Bazenet C, Leung R *et al.* (2014). Plasma proteins predict conversion to dementia from prodromal disease. *Alzheimers Dement* 10(6):799-807.e2.

Iturria-Medina Y, Sotero RC, Toussaint PJ, Mateos-Pérez JM, Evans AC, Alzheimer's Disease Neuroimaging Initiative (2016). Early role of vascular dysregulation on late-onset Alzheimer's disease based on multifactorial data-driven analysis. *Nat Commun* 7:11934.

Iwatsubo T, Odaka A, Suzuki N, Mizusawa H, Nukina N, Ihara Y (1994). Visualization of A beta 42(43) and A beta 40 in senile plaques with end-specific A beta monoclonals: evidence that an initially deposited species is A beta 42(43). *Neuron* 13(1):45-53.

Jack Jr CR, Bennett DA, Blennow K, Carrillo MC, Dunn B, Haeberlein SB *et al.* (2018). NIA-AA Research Framework: Toward a biological definition of Alzheimer's disease. *Alzheimers Dement* 14(4):535-62.

Jackson HM, Onos KD, Pepper KW, Graham LC, Akeson EC, Byers C *et al.* (2015). DBA/2J genetic background exacerbates spontaneous lethal seizures but lessens

amyloid deposition in a mouse model of Alzheimer's disease. *PLoS One* 10(5):e0125897.

Jackson RJ, Rose J, Tulloch J, Henstridge C, Smith C, Spires-Jones TL (2019). Clusterin accumulates in synapses in Alzheimer's disease and is increased in apolipoprotein E4 carriers. *Brain Commun* 1(1).

Janelidze S, Stomrud E, Palmqvist S, Zetterberg H, van Westen D, Jeromin A *et al.* (2016). Plasma β-amyloid in Alzheimer's disease and vascular disease. *Sci Rep* 26801.

Janelidze S, Zetterberg H, Mattsson N, Palmqvist S, Vanderstichele H, Lindberg O *et al.* (2016). CSF Aβ42/Aβ40 and Aβ42/Aβ38 ratios: better diagnostic markers of Alzheimer disease. *Ann Clin Transl Neurol* 3(3):154-65.

Jankowsky JL, Slunt HH, Ratovitski T, Jenkins NA, Copeland NG, Borchelt DR (2001). Co-expression of multiple transgenes in mouse CNS: a comparison of strategies. *Biomol Eng* 17(6):157-65.

Jankowsky JL, Zheng H (2017). Practical considerations for choosing a mouse model of Alzheimer's disease. *Mol Neurodegener.* 12(1):89.

Jansen IE, Savage JE, Watanabe K, Bryois J, Williams DM, Steinberg S *et al.* (2019). Genome-wide meta-analysis identifies new loci and functional pathways influencing Alzheimer's disease risk. *Nat Genet* 51(3):404-13.

Jay TR, Miller CM, Cheng PJ, Graham LC, Bemiller S, Broihier ML *et al.* (2015). TREM2 deficiency eliminates TREM2+ inflammatory macrophages and ameliorates pathology in Alzheimer's disease mouse models. *J Exp Med* 212(3):287-95.

Jay TR, Hirsch AM, Broihier ML, Miller CM, Neilson LE, Ransohoff RM *et al.* (2017). Disease Progression-Dependent Effects of TREM2 Deficiency in a Mouse Model of Alzheimer's Disease. *J Neurosci* 37(3):637-47.

Jay TR, von Saucken VE, Muñoz B, Codocedo JF, Atwood BK, Lamb BT *et al.* (2019). TREM2 is required for microglial instruction of astrocytic synaptic engulfment in neurodevelopment. *Glia* 67(10):1873-92.

Jendresen C, Årskog V, Daws MR, Nilsson LN (2017). The Alzheimer's disease risk factors apolipoprotein E and TREM2 are linked in a receptor signaling pathway. *J Neuroinflammation* 14(1):59.

Jenne DE, Lowin B, Peitsch MC, Böttcher A, Schmitz G, Tschopp J (1991). Clusterin (complement lysis inhibitor) forms a high density lipoprotein complex with apolipoprotein A-I in human plasma. *J Biol Chem* 266(17):11030-6.

Jiang T, Tan L, Zhu X-C, Zhang Q-Q, Cao L, Tan M-S (2014). Upregulation of TREM2 Ameliorates Neuropathology and Rescues Spatial Cognitive Impairment in a Transgenic Mouse Model of Alzheimer's Disease. *Neuropsychopharmacology* 39:2949-62.

Jiang T, Tan L, Chen Q, Tan MS, Zhou JS, Zhu XC *et al.* (2016). A rare coding variant in TREM2 increases risk for Alzheimer's disease in Han Chinese. *Neurobiol Aging* 42:217e1-3.

Jiang T, Wan Y, Zhang Y-D, Zhou J-S, Gao Q, Zhu X-C (2017). TREM2 Overexpression has No Improvement on Neuropathology and Cognitive Impairment in Aging APPswe/PS1dE9 Mice. *Molecular Neurobiology* 54:855-65.

Jin SC, Benitez BA, Karch CM, Cooper B, Skorupa T, Carrell D *et al.* (2014). Coding variants in TREM2 increase risk for Alzheimer's disease. *Hum Mol Genet* 23(21):5838-46.

Jin SC, Carrasquillo MM, Benitez BA, Skorupa T, Carrell D, Patel D *et al.* (2015). TREM2 is associated with increased risk for Alzheimer's disease in African Americans. *Mol Neurodegener* 10:19.

Johansen FE, Braathen R, Brandtzaeg P (2000). Role of J chain in secretory immunoglobulin formation. *Scand J Immunol* 52(3):240-8.

Jonsson T, Stefansson H, Steinberg S, Jonsdottir I, Jonsson PV, Snaedal J *et al.* (2013). Variant of TREM2 associated with the risk of Alzheimer's disease. *N Engl J Med* 368(2):107-16.

Jorm AF, Korten AE, Henderson AS (1987). The prevalence of dementia: a quantitative integration of the literature. *Acta Psychiatr Scand* 76(5):465-79.

Kang J, Lemaire HG, Unterbeck A, Salbaum JM, Masters CL, Grzeschik KH *et al.* (1987). The precursor of Alzheimer's disease amyloid A4 protein resembles a cell-surface receptor. *Nature* 325(6106):733-6.

Kang SS, Kurti A, Baker KE, Liu C-C, Colonna M, Ulrich JD *et al.* (2018). Behavioral and transcriptomic analysis of Trem2-null mice: not all knockout mice are created equal. *Hum Mol Genet* 27(2): 211–223.

Karch CM, Goate AM (2015). Alzheimer's disease risk genes and mechanisms of disease pathogenesis. *Biol Psychiatry* 77(1):43-51.

Karikari TK, Pascoal TA, Ashton NJ, Janelidze S, Benedet AL, Rodriguez JL *et al.* (2020). Blood phosphorylated tau 181 as a biomarker for Alzheimer's disease: a diagnostic performance and prediction modelling study using data from four prospective cohorts. *Lancet Neurol* 19(5):422-33.

Karsak M, Glebov K, Scheffold M, Bajaj T, Kawalia A, Karaca I *et al.* (2020). A rare heterozygous TREM2 coding variant identified in familial clustering of dementia affects an intrinsically disordered protein region and function of TREM2. *Hum Mutat* 41(1):169-81.

Kaufmann SH (2008). Immunology's foundation: the 100-year anniversary of the Nobel Prize to Paul Ehrlich and Elie Metchnikoff. *Nat Immunol* 9(7):705-12.

Keren-Shaul H, Spinrad A, Weiner A, Matcovitch-Natan O, Dvir-Szternfeld R, Ulland TK *et al.* (2017). A Unique Microglia Type Associated with Restricting Development of Alzheimer's Disease. *Cell* 169(7):1276-90.

Kettenmann H, Kirchhoff F, Verkhratsky A (2013). Microglia: new roles for the synaptic stripper. *Neuron* 77(1):10-8.

Kiialainen A, Hovanes K, Paloneva J, Kopra O, Peltonen L (2005). Dap12 and Trem2, molecules involved in innate immunity and neurodegeneration, are co-expressed in the CNS. *Neurobiol Dis* 18(2):314-22.

Kleinberger G, Yamanishi Y, Suárez-Calvet M, Czirr E, Lohmann E, Cuyvers E *et al.* (2014). TREM2 mutations implicated in neurodegeneration impair cell surface transport and phagocytosis. *Sci Transl Med* 6(243):243ra86.

Klesney-Tait J, Turnbull IR, Colonna M (2006). The TREM receptor family and signal integration. *Nat Immunol* 7(12):1266-73.

Knapskog AB, Henjum K, Idland A-V, Eldholm RS, Persson K, Saltvedt I *et al.* (2020). Cerebrospinal fluid sTREM2 in Alzheimer's disease: comparisons between clinical presentation and AT classification. *Sci Rep* 10:15886.

Kobayashi M, Konishi H, Sayo A, Takai T, Kiyama H (2016). TREM2/DAP12 Signal Elicits Proinflammatory Response in Microglia and Exacerbates Neuropathic Pain. *J Neurosci* 36(43):11138-11150.

Kober DL, Wanhainen KM, Johnson BM, Randolph DT, Holtzman MJ, Brett TJ (2014). Preparation, crystallization, and preliminary crystallographic analysis of wild-type and mutant human TREM-2 ectodomains linked to neurodegenerative and inflammatory diseases. *Protein Expr Purif* 96:32-8.

Kober DL, Alexander-Brett JM, Karch CM, Cruchaga C, Colonna M, Holtzman MJ *et al.* (2016). Neurodegenerative disease mutations in TREM2 reveal a functional surface and distinct loss-of-function mechanisms. *eLife* 5:e20391.

Köhler G and Milstein C (1975). Continuous cultures of fused cells secreting antibody of predefined specificity. *Nature* 256:495-7.

Koffie RM, Meyer-Luehmann M, Hashimoto T, Adams KW, Mielke ML, Garcia-Alloza M *et al.* (2009). Oligomeric amyloid beta associates with postsynaptic densities and correlates with excitatory synapse loss near senile plaques. *Proc Natl Acad Sci USA* 106:4012-7.

Konishi H, Kiyama H (2018). Microglial TREM2/DAP12 Signaling: A Double-Edged Sword in Neural Diseases. *Front Cell Neurosci* 12:206.

Krasemann S, Madore C, Cialic R, Baufeld C, Calcagno N, El Fatimy R *et al.* (2017). The TREM2-APOE Pathway Drives the Transcriptional Phenotype of Dysfunctional Microglia in Neurodegenerative Diseases. *Immunity* 47(3):566-81.

Kuang J, Yan X, Genders AJ, Granata C, Bishop DJ (2018). An overview of technical considerations when using quantitative real-time PCR analysis of gene expression in human exercise research. *PLoS One* 13(5):e0196438.

Kunkle BW, Grenier-Boley B, Sims R, Bis JC, Damotte V, Naj AC *et al.* (2019). Genetic meta-analysis of diagnosed Alzheimer's disease identifies new risk loci and implicates Aβ, tau, immunity and lipid processing. *Nat Genet* 51(3):414-30.

Kvartsberg H, Portelius E, Andreasson U, Brinkmalm G, Hellwig K, Lelental N *et al.* (2015). Characterization of the postsynaptic protein neurogranin in paired cerebrospinal fluid and plasma samples from Alzheimer's disease patients and healthy controls. *Alzheimers Res Ther* 7(1):40.

Lambert JC, Heath S, Even G, Campion D, Sleegers K, Hiltunen M *et al.* (2009). Genome-wide association study identifies variants at CLU and CR1 associated with Alzheimer's disease. *Nat Genet* 41(10):1094-9.

Lambert JC, Ibrahim-Verbaas CA, Harold D, Naj AC, Sims R, Bellenguez C *et al.* (2013). Meta-analysis of 74,046 individuals identifies 11 new susceptibility loci for Alzheimer's disease. *Nat Genet* 45(12):1452-8.

Lawson LJ, Perry VH, Dri P, Gordon S (1990). Heterogeneity in the distribution and morphology of microglia in the normal adult mouse brain. *Neuroscience* 39(1):151-70.

Lee H, Kirkby L, Brott BK, Adelson JD, Cheng S, Feller MB *et al.* (2014). Synapse elimination and learning rules coregulated by MHC Class I H2-Db. *Nature* 509(7499): 195-200.

Lehmann S, Delaby C, Boursier G, Catteau C, Ginestet N, Tiers L *et al.* (2018). Relevance of Aβ42/40 Ratio for Detection of Alzheimer Disease Pathology in Clinical Routine: The PLMR Scale. *Front Aging Neuroscience* 10:138.

Lessard CB, Malnik SL, Zhou Y, Ladd TB, Cruz PE, Ran Y *et al.* (2018). High-affinity interactions and signal transduction between Aβ oligomers and TREM2. *EMBO Mol Med* 10(11):e9027.

Levan-Petit I, Cardonna J, Garcia M, Migeon J, Corbi C, Preud'homme J-L, Lecron J-C (2000). Sensitive ELISA for Human Immunoglobulin D Measurement in Neonate, Infant, and Adult Sera. *Clinical Chemistry* 46(6 Pt1):876-8.

Levy-Lahad E, Wijsman EM, Nemens E, Anderson L, Goddard KA, Weber JL *et al.* (1995). A familial Alzheimer's disease locus on chromosome 1. *Science* 269(5226):970-3.

Lewczuk P, Ermann N, Andreasson U, Schultheis C, Podhorna J, Spitzer P *et al.* (2018). Plasma neurofilament light as a potential biomarker of neurodegeneration in Alzheimer's disease. *Alzheimers Res Ther* 10:71.

Leyns CEG, Ulrich JD, Finn MB, Stewart FR, Koscal LJ, Remolina Serrano J *et al.* (2017). TREM2 deficiency attenuates neuroinflammation and protects against neurodegeneration in a mouse model of tauopathy. *Proc Natl Acad Sci USA* 114(43):11524-11529.

Li Z, Woo CJ, Iglesias-Ussel MD, Ronai D, Scharff MD (2004). The generation of antibody diversity through somatic hypermutation and class switch recombination. *Genes Dev* 18:1–11.

Li J, Zhu Z (2010). Research and development of next generation of antibody-based therapeutics. *Acta Pharmacologica Sinica* 31:1198-1207.

Li L, Cheung T, Chen J, Herrup K (2011). A Comparative Study of Five Mouse Models of Alzheimer's Disease: Cell Cycle Events Reveal New Insights into Neurons at Risk for Death. *International Journal of Alzheimer's Disease* 2011:171464.

Li JT, Zhang Y (2018). TREM2 regulates innate immunity in Alzheimer's disease. *J Neuroinflammation* 15(1):107.

Li JW, Zong Y, Cao XP, Tan L, Tan L (2018). Microglial priming in Alzheimer's disease. *Ann Transl Med* 6(10):176.

Liddelow SA, Guttenplan KA, Clarke LE, Bennett FC, Bohlen CJ, Schirmer L *et al.* (2017). Neurotoxic reactive astrocytes are induced by activated microglia. *Nature* 541(7638):481-7.

Lill CM, Rengmark A, Pihlstrøm S, Fogh I, Shatunov A, Sleinman PM *et al.* (2015). The role of TREM2 R47H as a risk factor for Alzheimer's disease, frontotemporal lobar degeneration, amyotrophic lateral sclerosis, and Parkinson's disease. *Alzheimer's & Dementia* 11(12):1407-16.

Linnartz-Gerlach B, Bodea LG, Klaus C, Ginolhac A, Halder R, Sinkkonen L *et al.* (2019). TREM2 triggers microglial density and age-related neuronal loss. *Glia* 67(3):539-550.

Liu JKH (2014). The history of monoclonal antibody development – progress, remaining challenges and future innovations. *Annals of Medicine and Surgery* 3:113-16.

Liu D, Cao B, Zhao Y, Huang H, McIntyre RS, Rosenblat JD *et al.* (2018). Soluble TREM2 changes during the clinical course of Alzheimer's disease: A meta-analysis. *Neurosci Lett* 686:10-16.

Livesey FJ (2014). Human stem cell models of dementia. *Human Molecular Genetics* 23(1):R35-39.

Llewelyn MB, Hawkins RE, Russell SJ (1992). Discovery of antibodies. *BMJ* 305(6864):1269-72.

Lovestone S, Francis P, Kloszewska I, Mecocci P, Simmons A, Soininen H *et al.* (2009). AddNeuroMed--the European collaboration for the discovery of novel biomarkers for Alzheimer's disease. *Ann N Y Acad Sci* 1180:36-46.

Lue LF, Schmitz CT, Serrano G, Sue LI, Beach TG, Walker DG (2015). TREM2 Protein Expression Changes Correlate with Alzheimer's Disease Neurodegenerative Pathologies in Post-Mortem Temporal Cortices. *Brain Pathol* 25(4):469-80.

Ma L-Z, Tan L, Bi Y-L, Shen X-N, Xu W, Ma Y-H *et al.* (2020). Dynamic changes of CSF sTREM2 in preclinical Alzheimer's disease: the CABLE study. *Molecular Neurodegeneration* 15(1):25.

Mäkelä M, Kaivola K, Valori M, Paetau A, Polvikoski T, Singleton AB *et al.* (2018). Alzheimer risk loci and associated neuropathology in a population-based study (Vantaa 85+). *Neurol Genet* 4(1):e211.

Mandelkow EM, Mandelkow E (1998). Tau in Alzheimer's disease. *Trends Cell Biol* 8(11):425-7.

Mani JC, Marchi V, Cucurou C (1994). Effect of HIV-1 peptide presentation on the affinity constants of two monoclonal antibodies determined by BIAcore technology. *Mol Immunol* 31(6):439-44.

Marioni RE, Harris SE, Zhang Q, McRae AF, Hagenaars SP, Hill WD *et al.* (2018). GWAS on family history of Alzheimer's disease. *Transl Psychiatry* 8(1):99.

Martorana A, Di Lorenzo F, Belli L, Sancesario G, Toniolo S, Sallustio F *et al.* (2015). Cerebrospinal Fluid Aβ42 Levels: When Physiological Become Pathological State. *CNS Neurosci Ther* 21(12):921-5.

Matejuk A and Ransohoff RM (2020). Crosstalk between astrocytes and microglia: an overview. *Front Immunol* 11:1416.

Matsubara E, Soto C, Governale S, Frangione B, Ghiso J (1996). Apolipoprotein J and Alzheimer's amyloid beta solubility. *Biochem J* 316(Pt2):671-9.

Mattiace LA, Davies P, Yen SH, Dickson DW (1990). Microglia in cerebellar plaques in Alzheimer's disease. *Acta Neuropathol* 80(5):493-8.

Mattsson N, Insel PS, Palmqvist S, Portelius E, Zetterberg H, Weiner M *et al.* (2016). Cerebrospinal fluid tau, neurogranin, and neurofilament light in Alzheimer's disease. *EMBO Mol Med* 8:1184-96.

Mattsson N, Andreasson U, Zetterberg H, Blennow K, Alzheimer's Disease Neuroimaging Initiative (2017). Association of Plasma Neurofilament Light With Neurodegeneration in Patients With Alzheimer Disease. *JAMA Neurol* 74(5):557-66.

Mayeux R (2004). Biomarkers: potential uses and limitations. *NeuroRx* 1(2):182-8.

Mazaheri F, Snaidero N, Kleinberger G, Madore C, Daria A, Werner G *et al.* (2017). TREM2 deficiency impairs chemotaxis and microglial responses to neuronal injury. *EMBO Rep* 18(7):1186-98.

Meda L, Cassatella MA, Szendrei GI, Otvos Jr L, Baron P, Villalba M *et al.* (1995). Activation of microglial cells by β-amyloid protein and interferon-γ. *Nature* 374:647-50.

Meilandt WJ, Ngu H, Gogineni A, Lalehzadeh G, Lee S-H, Srinivasan K *et al.* (2020). Trem2 Deletion Reduces Late-Stage Amyloid Plaque Accumulation, Elevates the Aβ42:Aβ40 Ratio, and Exacerbates Axonal Dystrophy and Dendritic Spine Loss in the PS2APP Alzheimer's Mouse Model. *J Neurosci* 40(9): 1956–1974.

Menzies GE, Sims R, Williams J (2019 preprint). Molecular Dynamics simulations of Alzheimer's variants, R47H and R62H, in TREM2 provide evidence for structural alterations behind functional changes. *bioRxiv* doi: https://doi.org/10.1101/536540.

Meyer-Luehmann M, Spires-Jones TL, Prada C, Garcia-Alloza M, de Calignon A, Rozkalne A *et al.* (2008). Rapid appearance and local toxicity of amyloid-beta plaques in a mouse model of Alzheimer's disease. *Nature* 451(7179):720-4.

Mhatre M, Nguyen A, Kashani S, Pham T, Adesina A, Grammas P (2004). Thrombin, a mediator of neurotoxicity and memory impairment. *Neurobiol Aging* 25(6):783-93.

Mittelbronn M, Dietz K, Schluesener HJ, Meyermann R (2001). Local distribution of microglia in the normal adult human central nervous system differs by up to one order of magnitude. *Acta Neuropathol* 101(3):249-55.

Mócsai A, Ruland J, Tybulewicz VL (2010). The SYK tyrosine kinase: a crucial player in diverse biological functions. *Nat Rev Immunol* 10(6):387-402.

Molinuevo JL, Gispert JD, Dubois B, Heneka MT, Lleo A, Engelborghs S (2013). The AD-CSF-Index Discriminates Alzheimer's Disease Patients from Healthy Controls: A Validation Study. *Journal of Alzheimer's Disease* 36(1):67-77.

Morgan AR, Touchard S, Leckey A, O'Hagan C, Nevado-Holgado AJ, NIMA Consortium *et al.* (2019). Inflammatory biomarkers in Alzheimer's disease plasma *Alzheimers Dement* 15(6):776-87.

Morrison SL, Oi VT (1989). Genetically engineered antibody molecules. *Adv Immunol* 44:65-92.

Mucke L, Masliah E, Yu GQ, Mallory M, Rockenstein EM, Tatsuno G *et al.* (2000). High-level neuronal expression of abeta 1-42 in wild-type human amyloid protein precursor transgenic mice: synaptotoxicity without plaque formation. *J Neurosci* 20(11):4050-8.

Murphy K (2012). *Janeway's Immunobiology*. 8th edition. Garland Science, Taylor & Francis Group, LLC. USA.

Naj AC, Jun G, Beecham GW, Wang LS, Vardarajan BN, Buros J *et al.* (2011). Common variants at MS4A4/MS4A6E, CD2AP, CD33 and EPHA1 are associated with late-onset Alzheimer's disease. *Nat Genet* 43(5):436-41.

Nakamura A, Kaneko N, Villemagne VL, Kato T, Doecke J, Doré V *et al.* (2018). High performance plasma amyloid-β biomarkers for Alzheimer's disease. *Nature* 554:249-54.

National Center for Biotechnology Information (NCBI) [Internet]. Bethesda (MD): National Library of Medicine (US), National Center for Biotechnology Information; [1988] – [cited 24 Mar 2020]. Available from: https://www.ncbi.nlm.nih.gov.

Neuner SM, Heuer SE, Huentelman MJ, O'Connell KMS, Kaczorowski CC (2019). Harnessing Genetic Complexity to Enhance Translatability of Alzheimer's Disease Mouse Models: A Path toward Precision Medicine. *Neuron* 101(3):399-411.e5.

Newcombe EA, Camats-Perna J, Silva ML, Valmas N, Huat TJ, Medeiros R (2018). Inflammation: the link between comorbidities, genetics, and Alzheimer's disease. *J Neuroinflammation* 15(1):276.

Nimmerjahn A, Kirchhoff F, Helmchen F (2005). Resting microglial cells are highly dynamic surveillants of brain parenchyma in vivo. *Science* 308(5726):1314-8.

Nordengen K, Kirsebom BE, Henjum K, Selnes P, Gísladótti B, Wettergree M, Torsetnes SB, Grøntvedt GR, Waterloo KK, Aarsland D, Nilsson LNG, Fladby T (2019). Glial activation and inflammation along the Alzheimer's disease continuum. *J Neuroinflammation* 16(1):46.

Nossal GJ, Lederberg J (1958). Antibody production by single cells. *Nature* 181(4620):1419-20.

Oakley H, Cole SL, Logan S, Maus E, Shao P, Craft J *et al.* (2006). Intraneuronal beta-amyloid aggregates, neurodegeneration, and neuron loss in transgenic mice with five familial Alzheimer's disease mutations: potential factors in amyloid plaque formation. *J Neurosci* 26(40):10129-40.

O'Bryant SE, Xiao G, Barber R, Reisch J, Doody R, Fairchild T *et al.* (2010). A serum protein-based algorithm for the detection of Alzheimer disease. *Arch Neurol* 67(9):1077-81.

Ooi A, Wong A, Esau L, Lemtiri-Chlieh F, Gehring C (2016). A Guide to Transient Expression of Membrane Proteins in HEK-293 Cells for Functional Characterization. *Front Physiol* 7:300.

Osborn KE, Khan OA, Kresge HA, Bown CW, Liu D, Moore EE *et al.* (2019). Cerebrospinal fluid and plasma neurofilament light relate to abnormal cognition. *Alzheimers Dement (Amst)* 11:700-9.

Otto M, Wiltfang J, Tumani H, Zerr I, Lantsch M, Kornhuber J *et al.* (1997). Elevated levels of tau-protein in cerebrospinal fluid of patients with Creutzfeldt–Jakob disease. *Neuroscience Letters* 225(3):210-12.

Ozmen L, Albientz A, Czech C, Jacobsen H (2009). Expression of transgenic APP mRNA is the key determinant for beta-amyloid deposition in PS2APP transgenic mice. *Neurodegener Dis* 6(1-2):29-36.

Palmqvist S, Janelidze S, Quiroz YT, Zetterberg H, Lopera F, Stomrud E *et al.* (2020). Discriminative Accuracy of Plasma Phospho-tau217 for Alzheimer Disease vs Other Neurodegenerative Disorders. *JAMA* 324(8):772-81.
Paloneva J, Manninen T, Christman G, Hovanes K, Mandelin J, Adolfsson R *et al.* (2002). Mutations in two genes encoding different subunits of a receptor signaling complex result in an identical disease phenotype. *Am J Hum Genet* 71(3):656-62.

Paloneva J, Mandelin J, Kiialainen A, Böhling T, Prudlo J, Hakola P *et al.* (2003). DAP12/TREM2 Deficiency Results in Impaired Osteoclast Differentiation and Osteoporotic Features. *J Exp Med* 198(4):669-75.

Paolacci AR, Tanzarella OA, Porceddu E, Ciaffi M (2009). Identification and validation of reference genes for quantitative RT-PCR normalization in wheat. *BMC Mol Biol* 10:11.

Paolicelli RC, Bolasco G, Pagani F, Maggi L, Scianni M, Panzanelli P *et al.* (2011). Synaptic Pruning by Microglia Is Necessary for Normal Brain Development. *Science* 333(6048):1456-58.

Paresce DM, Ghosh RN, Maxfield FR (1996). Microglial cells internalize aggregates of the Alzheimer's disease amyloid beta-protein via a scavenger receptor. *Neuron* 17(3):553-65.

Parhizkar S, Arzberger T, Brendel M, Kleinberger G, Deussing M, Focke C *et al.* (2019). Loss of TREM2 function increases amyloid seeding but reduces plaque-associated ApoE. *Nat Neurosci* 22(2):191-204.

Park MT, Lee MS, Kim SH, Jo E-C, Lee GM (2004). Influence of culture passages on growth kinetics and adenovirus vector production for gene therapy in monolayer and suspension cultures of HEK 293 cells. *Appl Microbiol Biotechnol* 65(5):553-8.

Park J-S, Ji IJ, Kim D-H, An HJ, Yoon S-Y (2017). The Alzheimer's Disease-Associated R47H Variant of TREM2 Has an Altered Glycosylation Pattern and Protein Stability. *Front Neurosci.* 10: 618.

Parnetti L, Chiasserini D, Eusebi P, Giannandrea D, Bellomo G, De Carlo C *et al.* (2012). Performance of aβ1-40, aβ1-42, total tau, and phosphorylated tau as predictors of dementia in a cohort of patients with mild cognitive impairment. *J Alzheimers Dis* 29(1):229-38.

Pase MP, Beiser AS, Himali JJ, Satizabal CL, Aparicio HJ, DeCarli C *et al.* (2019). Assessment of Plasma Total Tau Level as a Predictive Biomarker for Dementia and Related Endophenotypes. *JAMA Neurol* 76(5):598-606.

Paternico D, Galluzzi S, Drago V, Bocchio-Chiavetto L, Zanardini R, Pedrini L *et al.* (2012). Cerebrospinal fluid markers for Alzheimer's disease in a cognitively healthy cohort of young and old adults. *Alzheimers Dement* 8:520–7.

Payne Jr WJ, Marshall DL, Shockley RK, Martin WJ (1988). Clinical laboratory applications of monoclonal antibodies. *Clin Microbiol Rev* 1(3): 313–329.

Pelvig DP, Pakkenberg H, Stark AK, Pakkenberg B (2008). Neocortical glial cell numbers in human brains. *Neurobiol Aging* 29(11):1754-62.

Pereira JB, Janelidze S, Ossenkoppele R, Kvartsberg H, Brinkmalm A, Mattsson-Carlgren N *et al.* (2021). Untangling the association of amyloid-β and tau with synaptic and axonal loss in Alzheimer's disease. *Brain* 144(1):310-24.

Petrovitch H, White LR, Izmirilian G, Ross GW, Havlik RJ, Markesbery W *et al.* (2000). Midlife blood pressure and neuritic plaques, neurofibrillary tangles, and brain weight at death: the HAAS. Honolulu-Asia aging Study. *Neurobiol Aging* 21(1):57-62.

Pfaffl MW (2001). A new mathematical model for relative quantification in real-time RT–PCR. *Nucleic Acids Res* 29(9):e45.

Pfrieger FW, Barres BA (1997). Synaptic efficacy enhanced by glial cells in vitro. *Science* 277:1684-7.

Piccio L, Buonsanti C, Cella M, Tassi I, Schmidt RE, Fenoglio C *et al.* (2008). Identification of soluble TREM-2 in the cerebrospinal fluid and its association with multiple sclerosis and CNS inflammation. *Brain* 131(Pt 11):3081-91.

Piccio L, Deming Y, Del-Águila JL, Ghezzi L, Holtzman DM, Fagan AM *et al.* (2016). Cerebrospinal fluid soluble TREM2 is higher in Alzheimer disease and associated with mutation status. *Acta Neuropathol* 131(6):925-33.

Portelius E, Zetterberg H, Skillbäck T, Törnqvist U, Andreasson U, Trojanowski JQ *et al.* (2015). Cerebrospinal fluid neurogranin: relation to cognition and neurodegeneration in Alzheimer's disease. *Brain* 138(Pt 11):3373-85.

Porter RR (1959). The hydrolysis of rabbit y-globulin and antibodies with crystalline papain. *Biochem J* 73:119-26.

Prada I, Ongania GN, Buonsanti C, Panina-Bordignon P, Meldolesi J (2006). Triggering receptor expressed in myeloid cells 2 (TREM2) trafficking in microglial

cells: continuous shuttling to and from the plasma membrane regulated by cell stimulation. *Neuroscience* 140(4):1139-48.

Prince, M, Knapp, M, Guerchet, M, McCrone, P, Prina, M, Comas-Herrera, A *et al. Dementia UK: Second Edition – Overview.* Alzheimer's Society, UK, 2014.

Protein [Internet]. Bethesda (MD): National Library of Medicine (US), National Center for Biotechnology Information; [1988] – Accession number NP_061838, Homo sapiens triggering receptor expressed on myeloid cells 2, isoform 1 precursor; [cited 24 Mar 2020]. Available from: https://www.ncbi.nlm.nih.gov/protein/NP_061838.1.

R&D Systems, Inc. [Internet]. A Biotechne brand [2020] – Human TREM2 Antibody; [cited 24 Mar 2020]. Available from: https://www.rndsystems.com/products/human-trem2-antibody_af1828.

Radde R, Bolmont T, Kaeser SA, Coomaraswamy J, Lindau D, Stoltze L *et al.* (2006). Abeta42-driven cerebral amyloidosis in transgenic mice reveals early and robust pathology. *EMBO Rep* 7(9):940-6.

Raha-Chowdhury R, Henderson JW, Raha AA, Stott SRW, Vuono R, Foscarin S *et al.* (2018). Erythromyeloid-Derived TREM2: A Major Determinant of Alzheimer's Disease Pathology in Down Syndrome. *J Alzheimers Dis* 61(3):1143–1162.

Raha-Chowdhury R, Henderson JW, Raha AA, Vuono R, Bickerton A, Jones E *et al.* (2019). Choroid plexus acts as gatekeeper for TREM2, abnormal accumulation of ApoE, and fibrillary tau in Alzheimer's disease and in Down syndrome Dementia. *J Alzheimers Dis* 69:91–109.

Ranaivo HR, Craft JM, Hu W, Guo L, Wing LK, Van Eldik LJ *et al.* (2006). Glia as a Therapeutic Target: Selective Suppression of Human Amyloid-β-Induced Upregulation of Brain Proinflammatory Cytokine Production Attenuates Neurodegeneration. *Journal of Neuroscience* 26(2):662-70.

Raschke WC, Baird S, Ralph P, Nakoinz I (1978). Functional Macrophage Cell Lines Transformed by Abelson Leukemia Virus. *Cell* 15:261-7.

Ray S, Britschgi M, Herbert C, Takeda-Uchimura Y, Boxer A, Blennow K *et al.* (2007). Classification and prediction of clinical Alzheimer's diagnosis based on plasma signaling proteins. *Nat Med* 13:1359-62.

Rayaprolu S, Mullen B, Baker M, Lynch T, Finger E, Seeley WW *et al.* (2013). TREM2 in neurodegeneration: evidence for association of the p.R47H variant with frontotemporal dementia and Parkinson's disease. *Molecular Neurodegeneration* 8:19.

Ritchie K, Kildea D (1995). Is senile dementia "age-related" or "ageing-related"? - evidence from meta-analysis of dementia prevalence in the oldest old. *Lancet* 346(8980):931-4.

Roblek M, Schüchner S, Huber V, Ollram K, Vlcek-Vesely S, Foisner R *et al.* (2010). Monoclonal Antibodies Specific for Disease-Associated Point-Mutants: Lamin A/C R453W and R482W. *PLoS One* 5(5):e10604.

Rocca WA, Hofman A, Brayne C, Breteler MM, Clarke M, Copeland JR *et al.* (1991). Frequency and distribution of Alzheimer's disease in Europe: a collaborative study of

1980-1990 prevalence findings. The EURODEM-Prevalence Research Group. *Ann Neurol* 30(3):381-90.

Roe K, Gibot S, Verma S (2014). Triggering receptor expressed on myeloid cells-1 (TREM-1): a new player in antiviral immunity? *Front Microbiol* 5:627.

Rogaev EI, Sherrington R, Rogaeva EA, Levesque G, Ikeda M, Liang Y *et al.* (1995). Familial Alzheimer's disease in kindreds with missense mutations in a gene on chromosome 1 related to the Alzheimer's disease type 3 gene. *Nature* 376:775-8.

Ruiz-Villalba A, van Pelt-Verkuil E, Gunst QD, Ruijter JM, van den Hoff MJB (2017). Amplification of nonspecific products in quantitative polymerase chain reactions (qPCR). *Biomol Detect Quantif* 14:7-18.

Satoh J-i, Kawana N, Yamamoto Y, Ishida T, Saito Y, Arima K (2013). A survey of TREM2 antibodies reveals neuronal but not microglial staining in formalin-fixed paraffin-embedded postmortem Alzheimer's brain tissues. *Alzheimers Res Ther* 5(4):30.

Schafer DP, Lehrman EK, Kautzman AG, Koyama R, Mardinly AR, Yamasaki R (2012). Microglia Sculpt Postnatal Neural Circuits in an Activity and Complement-Dependent Manner. *Neuron* 74(4): 691–705.

Scheff SW, Price DA, Schmitt FA, Mufson EJ (2006). Hippocampal synaptic loss in early Alzheimer's disease and mild cognitive impairment. *Neurobiology of Aging* 27(10):1372-84.

Scheuner D, Eckman C, Jensen M, Song X, Citron M, Suzuki N *et al.* (1996). Secreted amyloid beta-protein similar to that in the senile plaques of Alzheimer's disease is increased in vivo by the presenilin 1 and 2 and APP mutations linked to familial Alzheimer's disease. *Nat Med* 2(8):864-70.

Schlepckow K, Kleinberger G, Fukumori A, Feederle R, Lichtenthaler SF, Steiner H, *et al.* (2017). An Alzheimer-associated TREM2 variant occurs at the ADAM cleavage site and affects shedding and phagocytic function. *EMBO Mol Med* 9(10):1356-65.

Schlepckow K, Monroe KM, Kleinberger G, Cantuti-Castelvetri L, Parhizkar S, Xia D *et al.* (2020). Enhancing protective microglial activities with a dual function TREM2 antibody to the stalk region. *EMBO Mol Med* 12(4):e11227.

Schmid CD, Sautkulis LN, Danielson PE, Cooper J, Hasel KW, Hilbush BS *et al.* (2002). Heterogeneous expression of the triggering receptor expressed on myeloid cells-2 on adult murine microglia. *J Neurochem* 83(6): 1309-20.

Schroeder Jr HW, Cavacini L (2010). Structure and function of immunoglobulins. *J Allergy Clin Immunol* 125(2 Suppl 2):S41-52.

Sharif O, Gawish R, Warszawska JM, Martins R, Lakovits K, Hladik A (2014). The Triggering Receptor Expressed on Myeloid Cells 2 Inhibits Complement Component 1q Effector Mechanisms and Exerts Detrimental Effects during Pneumococcal Pneumonia. *PLoS Pathog* 10(6):e1004167.

Sheng JG, Zhou XQ, Mrak RE, Griffin WST (1998). Progressive Neuronal Injury Associated with Amyloid Plaque Formation in Alzheimer Disease. *Journal of Neuropathology & Experimental Neurology* 57(7): 714-17.

Sheng L, Chen M, Cai K, Song Y, Yu D, Zhang H *et al.* (2019). Microglial Trem2 induces synaptic impairment at early stage and prevents amyloidosis at late stage in APP/PS1 mice. *FASEB J* 33(9):10425-442.

Sherrington R, Rogaev EI, Liang Y, Rogaeva EA, Levesque G, Ikeda M *et al.* (1995). Cloning of a gene bearing missense mutations in early-onset familial Alzheimer's disease. *Nature* 375(6534):754-60.

Shlosberg D, Benifla M, Kaufer D, Friedman A (2010). Blood–brain barrier breakdown as a therapeutic target in traumatic brain injury. *Nat Rev Neurol* 6(7):393-403.

Silva MVF, Loures CMG, Alves LCV, de Souza LC, Borges KBG, Carvalho MDG (2019). Alzheimer's disease: risk factors and potentially protective measures. *J Biomed Sci* 26(1):33.

Sims R, van der Lee SJ, Naj AC, Bellenguez C, Badarinarayan N, Jakobsdottir J *et al.* (2017). Rare coding variants in PLCG2, ABI3, and TREM2 implicate microglial-mediated innate immunity in Alzheimer's disease. *Nat Genet* 49(9):1373-84.

Singh S, Tank NK, Dwiwedi P, Charan J, Kaur R, Sidhu P *et al.* (2018). Monoclonal antibodies: a review. *Current Clinical Pharmacology* 13(2):85-99.

Sjögren M, Davidsson P, Tullberg M, Minthon L, Wallin A, Wikkelsö C *et al.* (2001). Both total and hyperphosphorylated tau are increased in Alzeimer’s disease. *J Neurol Neurosurg Psychiatry* 70:624-30.

Sjögren M, Vanderstichele H, Agren H, Zachrisson O, Edsbagge M, Wikkelsø C *et al.* (2001). Tau and Abeta42 in cerebrospinal fluid from healthy adults 21-93 years of age: establishment of reference values. *Clin Chem* 47(10):1776-81.

Song WM, Joshita S, Zhou Y, Ulland TK, Gilfillan S, Colonna M (2018). Humanized TREM2 mice reveal microglia-intrinsic and -extrinsic effects of R47H polymorphism. *J Exp Med* 215(3):745-760.

Spires-Jones TL, Hyman BT (2014). The intersection of amyloid beta and tau at synapses in Alzheimer’s disease. *Neuron* 82:756-71.

Stanker LH, Branscomb E, Vanderlaan M, Jensen RH (1986). Monoclonal antibodies recognizing single amino acid substitutions in hemoglobin. *J Immunol* 136(11):4174-80.

Stavnezer J, Guikema JEJ, Schrader CE (2008). Mechanism and regulation of class switch recombination. *Annu Rev Immunol* 26:261-92.

Steele NZR, Carr JS, Bonham LW, Geier EG, Damotte V, Miller ZA *et al.* (2017). Fine-mapping of the human leukocyte antigen locus as a risk factor for Alzheimer disease: A case–control study. *PLoS Medicine* 14(3):e1002272.

Stelzmann RA, Schnitzlein HN, Murtagh FR (1995). An english translation of alzheimer's 1907 paper, “über eine eigenartige erkankung der hirnrinde”. *Clinical Anatomy* 8(6):429-31.

Stence N, Waite M, Dailey ME (2001). Dynamics of microglial activation: a confocal time-lapse analysis in hippocampal slices. *Glia* 33(3):256-66.

Stephens AS, Stephens SR, Morrison NA (2011). Internal control genes for quantitative RT-PCR expression analysis in mouse osteoblasts, osteoclasts and macrophages. *BMC Research Notes* 4:410.

Stevens B, Allen NJ, Vazquez LE, Howell GR, Christopherson KS, Nouri N *et al.* (2007). The classical complement cascade mediates CNS synapse elimination. *Cell* 131(6):1164-78.

Stokes Jr. J, Maris EP, Gellis SS (1944). Chemical, clinical, and immunological studies on the products of human plasma fractionation. XI. The use of concentrated normal human serum gamma globulin (human immune serum globulin) in the prophylaxis and treatment of measles. *J Clin Invest* 23(4):531-40.

Strittmatter WJ, Saunders AM, Schmechel D, Pericak-Vance M, Enghild J, Salvesen GS *et al.* (1993). Apolipoprotein E: high-avidity binding to beta-amyloid and increased frequency of type 4 allele in late-onset familial Alzheimer disease. *Proc Natl Acad Sci USA* 90(5):1977-81.

Suárez-Calvet M, Kleinberger G, Araque Caballero MÁ, Brendel M, Rominger A *et al.* (2016). sTREM2 cerebrospinal fluid levels are a potential biomarker for microglia activity in early-stage Alzheimer's disease and associate with neuronal injury markers. *EMBO Mol Med* 8(5):466-76.

Suárez-Calvet M, Morenas-Rodríguez E, Kleinberger G, Schlepckow K, Caballero MÁA, Franzmeier N *et al.* (2019). Early increase of CSF sTREM2 in Alzheimer's disease is associated with tau related-neurodegeneration but not with amyloid-β pathology. *Mol Neurodegeneration* 14:1.

Suh J, Choi SH, Romano DM, Gannon MA, Lesinski AN, Kim DY *et al.* (2013). ADAM10 missense mutations potentiate β-amyloid accumulation by impairing prodomain chaperone function. *Neuron* 80(2):385-401.

Sun X, Chen W-D, Wang Y-D (2015). β-Amyloid: the key peptide in the pathogenesis of Alzheimer's disease. *Front Pharmacol* 6:221.

Suzuki M, Kato C, Kato A (2015). Therapeutic antibodies: their mechanisms of action and the pathological findings they induce in toxicity studies. *J Toxicol Pathol* 28(3): 133–139.

Sweeney MD, Sagare AP, Zlokovic BV (2015). Cerebrospinal fluid biomarkers of neurovascular dysfunction in mild dementia and Alzheimer's disease. *J Cerec Blood Flow Metab* 35(7):1055-68.

Sweeney MD, Sagare AP, Zlokovic BV (2018). Blood-brain barrier breakdown in Alzheimer disease and other neurodegenerative disorders. *Nat Rev Neurol* 14(3):133-150.

Taciak B, Białasek M, Braniewska A, Sas Z, Sawicka P, Kiraga L *et al.* (2018). Evaluation of phenotypic and functional stability of RAW264.7 cell line through serial passages. *PLoS One* 13(6): e0198943.

Takahashi K, Rochford CD, Neumann H (2005). Clearance of apoptotic neurons without inflammation by microglial triggering receptor expressed on myeloid cells-2. *J Exp Med* 201(4):647-57.

Tarawneh R, D'Angelo G, Crimmins D, Herries E, Griest T, Fagan AM *et al.* (2016). Diagnostic and Prognostic Utility of the Synaptic Marker Neurogranin in Alzheimer Disease. *JAMA Neurol* 73(5):561-71.

Terry RD, Masliah E, Salmon DP, Butters N, DeTeresa R, Hill R *et al.* (1991). Physical basis of cognitive alterations in Alzheimer's disease: synapse loss is the major correlate of cognitive impairment. *Ann Neurol* 30(4):572-80.

Thomas P, Smart TG (2005). HEK293 cell line: A vehicle for the expression of recombinant proteins. *Journal of Pharmacological and Toxicological Methods* 51(3):187-200.

Thornton P, Sevalle J, Deery MJ, Fraser G, Zhou Y, Ståhl S *et al.* (2017). TREM2 shedding by cleavage at the H157-S158 bond is accelerated for the Alzheimer's disease-associated H157Y variant. *EMBO Mol Med* 9(10):1366-78.

Thul PJ, Åkesson L, Wiking M, Mahdessian D, Geladaki A, Blal HA *et al*. (2017). A subcellular map of the human proteome. *Science* 356(6340):eaal3321.

Tian X, Xie G, Xiao H, Ding F, Bao W, Zhang M (2019). CXCR4 knockdown prevents inflammatory cytokine expression in macrophages by suppressing activation of MAPK and NF-κB signaling pathways. *Cell & Bioscience* 9:55.

Toledo JB, Arnold SE, Raible K, Brettschneider J, Xie SX, Grossman M *et al.* (2013). Contribution of cerebrovascular disease in autopsy confirmed neurodegenerative disease cases in the National Alzheimer's Coordinating Centre. *Brain* 136(Pt 9):2697-706.

Tomkins O, Shelef I, Kaizerman I, Eliushin A, Afawi Z, Misk A *et al.* (2008). Blood-brain barrier disruption in post-traumatic epilepsy. *J Neurol Neurosurg Psychiatry* 79(7):774-7.

Tschopp J, Chonn A, Hertig S, French LE (1993). Clusterin, the human apolipoprotein and complement inhibitor, binds to complement C7, C8 beta, and the b domain of C9. *J Immunol* 151(4):2159-65.

Tsuchiya S, Yamabe M, Yamaguchi Y, Kobayashi Y, Konno T, Tada K (1980). Establishment and characterization of a human acute monocytic leukemia cell line (THP-1). *Int J Cancer* 26(2):171-6.

Turnbull IR, Gilfillan S, Cella M, Aoshi T, Miller M, Piccio L *et al.* (2006). Cutting edge: TREM-2 attenuates macrophage activation. *The Journal of Immunology* 177:3520-24.

Ueno M, Chiba Y, Murakami R, Matsumoto K, Kawauchi M, Fujihara R (2016). Blood-brain barrier and blood-cerebrospinal fluid barrier in normal and pathological conditions. *Brain Tumor Pathol* 33(2):89-96.

Uhlén M, Fagerberg L, Hallström BM, Lindskog C, Oksvold P, Mardinoglu A *et al.* (2015). Proteomics: Tissue-based map of the human proteome. *Science* 347(6620):1260419.

Ulland TK, Song WM, Huang SC, Ulrich JD, Sergushichev A, Beatty WL *et al.* (2017). TREM2 Maintains Microglial Metabolic Fitness in Alzheimer's Disease. *Cell* 170(4):649-63.e13.

Ulrich JD, Finn MB, Wang Y, Shen A, Mahan TE, Jiang H *et al.* (2014). Altered microglial response to Aβ plaques in APPPS1-21 mice heterozygous for TREM2. *Mol Neurodegener* 9:20.

Ulrich JD, Ulland TK, Mahan TE, Nyström S, Nilsson KP, Song WM *et al.* (2018). ApoE facilitates the microglial response to amyloid plaque pathology. *J Exp Med* 215(4):1047-58.

Vidarsson G, Dekkers G, Rispens T (2014). IgG subclasses and allotypes: from structure to effector functions. *Frontiers in Immunology* 5:520.

Viña J, Lloret A (2010). Why women have more Alzheimer's disease than men: gender and mitochondrial toxicity of amyloid-beta peptide. *J Alzheimers Dis* 20 Suppl 2:S527-33.

Vincent I, Zheng J-H, Dickson DW, Kress Y, Davies P (1998). Mitotic Phosphoepitopes Precede Paired HelicalFilaments in Alzheimer's Disease. *Neurobiology of Aging* 19(4):287-96.

Vitale M, Bottino C, Sivori S, Sanseverino L, Castriconi R, Marcenaro E *et al.* (1998). NKp44, a novel triggering surface molecule specifically expressed by activated natural killer cells, is involved in non-major histocompatibility complex-restricted tumor cell lysis. *J Exp Med* 187(12):2065-72.

Vladutiu AO (2000). Immunoglobulin D: properties, measurement, and clinical relevance. *Clinical and Diagnostic Laboratory Immunology* 7(2):131-40.

von Ahlfen S, Schlumpberger M (2010). Effects of low A260/A230 ratios in RNA preparations on downstream applications. *Qiagen Newsletter: Gene Expression and Function Studies* 15:7.

von Behring E, Kitasato S (1890). The mechanism of immunity in animals to diphtheria and tetanus. *Deutscbe Medizhiscbe Wocbenschift* (English translation) 6:1113-4.

Walker D, Lue L-F (2018). Defining Microglial Phenotypes in Alzheimer's Disease, in Dorszewska J and Kozubski W [eds], *Alzheimer's Disease - The 21st Century Challenge* electronic book. IntechOpen, London, UK.

Wang Y, Cella M, Mallinson K, Ulrich JD, Young KL, Robinette ML *et al.* (2015). TREM2 lipid sensing sustains the microglial response in an Alzheimer's disease model. *Cell* 160(6):1061-71.

Wang Y, Ulland TK, Ulrich JD, Song W, Tzaferis JA, Hole J (2016). TREM2-mediated early microglial response limits diffusion and toxicity of amyloid plaques. *J Exp Med* 213(5):667-75.

Wang S, Mustafa M, Yuede CM, Salazar SV, Kong P, Long H *et al.* (2020). Anti-human TREM2 induces microglia proliferation and reduces pathology in an Alzheimer's disease model. *J Exp Med* 217(9):e20200785.

Washington AV, Quigley L, McVicar DW (2000). Initial characterization of TREM-like transcript (TLT)-1: a putative inhibitory receptor within the TREM cluster. *Blood* 100(10):3822-4.

Watarai H, Sekine E, Inoue S, Nakagawa R, Kaisho T, Taniguchi M (2008). PDC-TREM, a plasmacytoid dendritic cell-specific receptor, is responsible for augmented production of type I interferon. *Proc Natl Acad Sci USA* 105(8): 2993–2998.

Wellington H, Paterson RW, Portelius E, Törnqvist U, Magdalinou N, Fox NC *et al.* (2016). Increased CSF neurogranin concentration is specific to Alzheimer disease. *Neurology* 86(9):829-35.

Wittenberg R, Hu B, Barraza-Araiza L, Rehill A (2019). *Projections of older people with dementia and costs of dementia care in the United Kingdom, 2019–2040*. Care Policy and Evaluation Centre, London School of Economics and Political Science, UK, 2019.

Wolfe MS (2014). Unlocking truths of γ-secretase in Alzheimer's disease: what is the translational potential? *Future Neurol* 9(4):419-29.

Woof JM, Kerr MA (2004). IgA function – variations on a theme. *Immunology* 113(2):175-7.

World Health Organisation [Internet]. *Dementia Fact Sheet December 2017*. World Health Organisation [2017] – [cited 2020 Mar 25]. Available from: https://www.who.int/news-room/fact-sheets/detail/dementia.

Wu T, Dejanovic B, Gandham VD, Gogineni A, Edmonds R, Schauer S *et al.* (2019). Complement C3 Is Activated in Human AD Brain and Is Required for Neurodegeneration in Mouse Models of Amyloidosis and Tauopathy. *Cell Rep* 28(8):2111-23.e6.

Wunderlich P, Glebov K, Kemmerling N, Tien NT, Neumann H, Walter J (2013). Sequential proteolytic processing of the triggering receptor expressed on myeloid cells-2 (TREM2) protein by ectodomain shedding and γ-secretase-dependent intramembranous cleavage. *J Biol Chem* 288(46):33027-36.

Wyss-Coray T, Loike JD, Brionne TC, Lu E, Anankov R, Yan F *et al.* (2003). Adult mouse astrocytes degrade amyloid-beta in vitro and in situ. *Nat Med* 9(4):453-7.

Xiang X, Piers TM, Wefers B, Zhu K, Mallach A, Brunner B *et al.* (2018). The Trem2 R47H Alzheimer's risk variant impairs splicing and reduces Trem2 mRNA and protein in mice but not in humans. *Mol Neurodegener* 13(1):49.

Xu Z, Zan H, Pone EJ, Mai T, Casali P (2012). Immunoglobulin class-switch DNA recombination: induction, targeting and beyond. *Nature Reviews Immunology* 12:517-31.

Yao H, Coppola K, Schweig JE, Crawford F, Mullan M, Paris D (2019). Distinct Signaling Pathways Regulate TREM2 Phagocytic and NFκB Antagonistic Activities. *Front Cell Neurosci* 13:457.

Ye J, Coulouris G, Zaretskaya I, Cutcutache I, Rozen S, & Madden TL (2012). Primer-BLAST: a tool to design target-specific primers for polymerase chain reaction. *BMC Bioinformatics* 13:134.

Yeh FL, Wang Y, Tom I, Gonzalez LC, Sheng M (2016). TREM2 Binds to Apolipoproteins, Including APOE and CLU/APOJ, and Thereby Facilitates Uptake of Amyloid-Beta by Microglia. *Neuron* 91(2):328-40.

Yoshiyama Y, Higuchi M, Zhang B, Huang SM, Iwata N, Saido TC *et al.* (2007). Synapse loss and microglial activation precede tangles in a P301S tauopathy mouse model. *Neuron* 53(3):337-51.

Yu J, Wiita P, Kawaguchi R, Honda J, Jorgensen A, Zhang K *et al.* (2007). Biochemical Analysis of a Common Human Polymorphism Associated with Age-Related Macular Degeneration *Biochemistry* 46(28):8451-61.

Yu JT, Jiang T, Wang YL, Wang HF, Zhang W, Hu N *et al.* (2014). Triggering receptor expressed on myeloid cells 2 variant is rare in late-onset Alzheimer's disease in Han Chinese individuals. *Neurobiol Aging* 35(4):937e1-3.

Yuan A, Rao MV, Veeranna, Nixon RA (2012). Neurofilaments at a glance. *Journal of Cell Science* 125:3257-63.

Yuan P, Condello C, Keene CD, Wang Y, Bird TD, Paul SM *et al.* (2016). TREM2 haplodeficiency in mice and humans impairs the microglia barrier function leading to decreased amyloid compaction and severe axonal dystrophy. *Neuron* 90(4):724-39.

Zempel H, Thies E, Mandelkow E, Mandelkow E-M (2010). Abeta oligomers cause localized Ca(2+) elevation, missorting of endogenous Tau into dendrites, Tau phosphorylation, and destruction of microtubules and spines. *J Neurosci* 30:11938-50.

Zetterberg H, Burnham SC (2019). Blood-based molecular biomarkers for Alzheimer's disease. *Molecular Brain* 12:26.

Zetterberg H, Bendlin BB (2021). Biomarkers for Alzheimer's disease—preparing for a new era of disease-modifying therapies. *Molecular Psychiatry* 26:296-308.

Zhao R, Hu W, Tsai J, Li W, Gan WB (2017). Microglia limit the expansion of β-amyloid plaques in a mouse model of Alzheimer's disease. *Mol Neurodegener* 12:47.

Zhao Y, Wu X, Li X, Jiang LL, Gui X, Liu Y *et al.* (2018). TREM2 Is a Receptor for β-Amyloid that Mediates Microglial Function. *Neuron* 97(5):1023-31.

Zhong L, Chen XF, Wang T, Wang Z, Liao C, Wang Z *et al.* (2017). Soluble TREM2 induces inflammatory responses and enhances microglial survival. *J Exp Med* 214(3):597-607.

Zhong L, Xu Y, Zhuo R, Wang T, Wang K, Huang R *et al.* (2019). Soluble TREM2 ameliorates pathological phenotypes by modulating microglial functions in an Alzheimer's disease model. *Nature Communications* 10:1365.

Zhou Y, Song WM, Andhey PS, Swain A, Levy T, Miller KR *et al.* (2020). Human and mouse single-nucleus transcriptomics reveal TREM2-dependent and TREM2-independent cellular responses in Alzheimer's disease. *Nat Med* 26(1):131-42.

Zlokovic BV, Martel CL, Matsubara E, McComb JG, Zheng G, McCluskey RT *et al.* (1996). Glycoprotein 330/megalin: probable role in receptor-mediated transport of

apolipoprotein J alone and in a complex with Alzheimer disease amyloid beta at the blood-brain and blood-cerebrospinal fluid barriers. *Proc Natl Acad Sci USA* 93(9):4229-34.

Zlokovic BV (2011). Neurovascular pathways to neurodegeneration in Alzheimer's disease and other disorders. *Nat Rev Neurosci* 12(12):723-38.

Appendix I – List of Chemicals

Cell Culture Reagents

Item	Product Code	Supplier
cOmplete™ protease inhibitor cocktail tablets	04693116001	Roche, Merck, UK
Dimethyl sulfoxide (DMSO)	D2650	Sigma-Aldrich, Merck, UK
Eagle's MEM (EMEM)	M2279	Sigma-Aldrich, Merck, UK
Fetal bovine serum (FBS), South American origin	10270106	Gibco, ThermoFisher Scientific UK
HAT supplement 50X	21060-017	Gibco, ThermoFisher Scientific UK
HT supplement 100X	11067-030	Gibco, ThermoFisher Scientific UK
L-glutamine	G7513	Sigma-Aldrich, Merck, UK
Lipofectamine™ 3000 reagent	15292465	ThermoFisher Scientific, UK
MEM non-essential amino acids 100X	11140-050	Gibco, ThermoFisher Scientific UK
Micro BCA™ protein assay kit	23235	ThermoFisher Scientific, UK
Opti-MEM™ reduced serum medium	31985062	ThermoFisher Scientific, UK
Penicillin-streptomycin	P4458	Sigma-Aldrich, Merck, UK
Phosphate Buffered Saline (PBS)	12037539	Gibco, ThermoFisher Scientific UK
Pierce™ RIPA Buffer	89900	ThermoFisher Scientific, UK
Polyethylene glycol 1500	10783641001	Sigma-Aldrich, Merck, UK
RPMI 1640, no glutamine	31870074	Gibco, ThermoFisher Scientific UK
Sodium pyruvate	S8636	Sigma-Aldrich, Merck, UK
Trypan blue solution 0.4%	SV30084.01	HyClone, Fisher Scientific, UK
Trypsin-EDTA (0.05%)	25-300-054	Gibco, ThermoFisher Scientific UK
Ultra-low IgG fetal bovine serum, US origin	16250078	Gibco, ThermoFisher Scientific UK

***Freezing media**: FBS + 10% DMSO*
***Growth media**: RPMI, 50 Units Penicillin-50µg/ml Streptomycin, 1mM sodium pyruvate, 2mM L-glutamine, 10% FBS (or 15% FBS for fusion/re-cloning media)*

Cloning Reagents

Item	Product Code	Supplier
Agar	BP2641-1	Fisher Scientific, UK
Ampicillin	A9518	Sigma-Aldrich, Merck, UK
Geneticin G-418 sulfate	11811023	ThermoFisher Scientific, UK
Glycerol	G6279	Sigma-Aldrich, Merck, UK
Luria Broth (LB) base	12795084	ThermoFisher Scientific, UK
SOC medium	15544034	ThermoFisher Scientific, UK
Sodium chloride	S/3120/65	Fisher Scientific, UK
DH5α™ competent cells	18265017	ThermoFisher Scientific, UK
Tryptone	1278-7099	Fisher Scientific, UK
Yeast extract	BP1422-2	Fisher Scientific, UK

***LB Agar**: 1% sodium chloride + 1% tryptone + 0.5% yeast extract + 1.5% agar*

Conjugation Reagents

Item	Product Code	Supplier
EZ-Link™ Sulfo NHS-LC-Biotin	21327	ThermoFisher Scientific, UK
Keyhole limpet hemocyanin	H-1757	Sigma-Aldrich, Merck, UK
Pierce™ immobilised TCEP disulfide reducing gel	77712	ThermoFisher Scientific, UK
Sodium chloride	S/3120/65	Fisher Scientific, UK
Sodium phosphate	S3139	Sigma-Aldrich, Merck, UK
Streptavidin-HRP	DY998	R&D Systems Inc., United States of America (USA)
Sulfo-SMCC	22322	ThermoFisher Scientific, UK

***Conjugation buffer**: 100mM sodium phosphate, 150mM sodium chloride, pH 7.9*

DNA Extraction and Amplification Reagents

Item	Product Code	Supplier
Agarose	BP1356	Fisher Scientific, UK
Boric acid	10553001	Fisher Scientific, UK
DNA Ladder (100bp)	G2101	Promega, UK
Ethylenediaminetetraacetic acid (EDTA)	17892	ThermoFisher Scientific, UK
GeneRuler 1kb DNA ladder	SM1331	ThermoFisher Scientific, UK
GoTaq® Green master mix	M7128	Promega, UK
High capacity RNA to cDNA kit	4387406	ThermoFisher Scientific, UK
Nuclease-free water	P119A	Promega, UK

PowerUp™ SYBR Green master mix	A25742	ThermoFisher Scientific, UK
Proteinase K Solution	25530-049	ThermoFisher Scientific, UK
Sodium dodecyl sulphate (SDS)	BP166-500	Fisher Scientific, UK
Sodium chloride	S/3120/65	Fisher Scientific, UK
SYBR™ Safe DNA gel stain	S33102	ThermoFisher Scientific, UK
Tris base	BP152-500	Fisher Scientific, UK

Mammalian Lysis Buffer: *0.1M Tris, 0.2M sodium chloride, 5mM EDTA, 0.2% SDS, pH8.5*
10X Tris-Borate-EDTA (TBE) Buffer: *0.9M Tris, 0.9M boric acid, 0.02M EDTA*

ELISA and SDS-PAGE Reagents

Item	Product Code	Supplier
Acetic acid glacial	A/0400/PB17	Fisher Scientific, UK
Acrylamide/Bisacrylamide, 40% solution	J60868	Alfa Aesar, ThermoFisher Scientific, UK
Amersham ECL detection reagents	RPN2106	GE Healthcare, UK
Amersham Protran 0.45µm nitrocellulose membrane	10600002	GE Healthcare, UK
Ammonium persulphate (APS)	A3678	Sigma-Aldrich, Merck, UK
Anti-mouse IgG1 antibody (RMG1-1)	406601	Biolegend UK Ltd.
Anti-mouse IgG3 antibody (RMG3-1)	406802	Biolegend UK Ltd.
Anti-mouse IgG (γ-chain specific) peroxidase antibody	A3673	Sigma-Aldrich, Merck, UK
Anti-mouse IgM (µ-chain specific) peroxidase antibody	SAB3701199	Sigma-Aldrich, Merck, UK
Bovine serum albumin (BSA)	A2153	Sigma-Aldrich, Merck, UK
Bromophenol blue	B5525	Sigma-Aldrich, Merck, UK
Coomassie Brilliant blue R-250	B0149	Sigma-Aldrich, Merck, UK
Gelatin	48722	Sigma-Aldrich, Merck, UK
Glycine	G/0800/60	Fisher Scientific, UK
Human TREM2 antibody, polyclonal goat	AF1828	R&D Systems Inc. USA
Mercaptoethanol (β)	M/P200/05	Fisher Scientific, UK
Methanol	M/4000/17	Fisher Scientific, UK
PageRuler™ Plus prestained protein ladder, 10-250kDa	26619	ThermoFisher Scientific, UK
Peroxidase AffiniPure donkey anti-mouse IgG	715-035-150	Jackson Immunoresearch, Stratech Scientific Ltd., UK

Peroxidase AffiniPure donkey anti-rabbit IgG	711-035-152	Jackson Immunoresearch, Stratech Scientific Ltd., UK
Peroxidase AffiniPure F(ab')$_2$ fragment donkey anti-goat IgG	705-036-147	Jackson Immunoresearch, Stratech Scientific Ltd., UK
Peroxidase AffiniPure goat anti-rat IgG	112-035-003	Jackson Immunoresearch, Stratech Scientific Ltd., UK
Potassium chloride	P/4280/53	Fisher Scientific, UK
Potassium phosphate	A12142	Alfa Aesar, ThermoFisher Scientific, UK
Recombinant human TREM2 protein	11084-H08H	Sino Biological Inc., Stratech Scientific Ltd., UK
Recombinant mouse TREM2 protein	50149-M08H	Sino Biological Inc., Stratech Scientific Ltd., UK
SIGMAFAST™ o-phenylenediamine dihydrochloride (OPD)	P9187	Sigma-Aldrich, Merck, UK
Skimmed milk powder	70166	Sigma-Aldrich, Merck, UK
Sodium carbonate	BP357-1	Fisher Scientific, UK
Sodium chloride	S/3120/65	Fisher Scientific, UK
Sodium dodecyl sulphate (SDS)	BP166-500	Fisher Scientific, UK
Sodium hydrogen carbonate	S/4200/60	Fisher Scientific, UK
Sodium phosphate	S3139	Sigma-Aldrich, Merck, UK
Sucrose	15503-022	ThermoFisher Scientific, UK
Tetramethylethylenediamine (TEMED)	BP150-20	Fisher Scientific, UK
Tris base	BP152-500	Fisher Scientific, UK
Tween-20	663684B	VWR, UK

***10X Phosphate buffered saline (PBS)**: 1.4M sodium chloride, 0.12M sodium phosphate, 0.03M potassium chloride, 0.02M potassium phosphate*
***Blocking buffer (ELISA)**: 2% BSA in 1X PBS-0.05% Tween-20*
***Blocking buffer (Western blot)**: 5% milk or 5% BSA in PBS-0.05% Tween-20*
***Coomassie (R-250) stain**: 0.25% Coomassie R-250, 10% acetic acid, 40% methanol*
***Coating buffer (ELISA)**: 15mM sodium carbonate, 35mM sodium hydrogen carbonate, pH9.6*
***Destain solution (Coomassie)**: 10% acetic acid, 40% methanol*
***Dilution buffer (ELISA)**: 0.1% BSA in 1X PBS-0.05% Tween-20*
***Resolving gel buffer**: 0.5M tris, 0.4% SDS (pH 6.8)*
***Running buffer (10X)**: 0.25M tris, 1.92M glycine, 1% SDS*
***SDS (Non-reducing) buffer (5X)**: 115mM tris, 584mM sucrose, 4% SDS, 0.015% bromophenol blue (pH 6.8)*
***SDS (Reducing) buffer (5X)**: Non-reducing loading buffer, 5% v/v β-mercaptoethanol*
***Stacking gel buffer**: 1.5M tris, 0.4% SDS (pH 8.8)*
***Transfer buffer (10X)**: 0.25M tris, 1.92M glycine (20% methanol added to 1X buffer)*
***Washing buffer**: 1X PBS-0.05% Tween-20 (pH 7.4)*

Flow Cytometry Reagents

Item	Product Code	Supplier
Alexa Fluor 647 anti-mouse IgM, RMM-1	406525	Biolegend UK Ltd.
Alexa Fluor 647 donkey anti-goat IgG	ab150131	Abcam
Alexa Fluor 647 donkey anti-rabbit IgG, Poly4064	406414	Biolegend UK Ltd.
Alexa Fluor 647 goat anti-mouse IgG, Poly4053	405322	Biolegend UK Ltd.
Anti-GFAP antibody	ab53554	Abcam
Human TruStain FcX™ antibody	422301	Biolegend UK Ltd.
Normal Goat Serum	S-1000	Vector Laboratories, UK
Normal Donkey Serum	D9663	Sigma-Aldrich, Merck, UK
Purified mouse IgG2a, κ Isotype Ctrl, MG2a53	401501	Biolegend UK Ltd.
TruStain FcX™ (anti-mouse CD16/32) antibody	101319	Biolegend UK Ltd.

***Blocking buffer**: 5% animal serum + 1:100 anti-mouse CD16/32 Fc antibody or 5µl/well anti-human Fc antibody*
***Dilution/washing buffer**: 2% FBS in PBS*

Immunisation Reagents

Item	Product Code	Supplier
Complete Freund's Adjuvant	F5881	Sigma-Aldrich, Merck, UK
Incomplete Freund's Adjuvant	F5506	Sigma-Aldrich, Merck, UK
Recombinant human TREM2 protein	11084-H08H	Sino Biological Inc., Stratech Scientific Ltd., UK
Recombinant mouse TREM2 protein	50149-M08H	Sino Biological Inc., Stratech Scientific Ltd., UK

Microglial Isolation and Immunostaining Reagents

Item	Product Code	Supplier
Anti-Iba1 rabbit polyclonal antibody	019-19741	Alpha Laboratories, UK
Avidin/Biotin Blocking Kit	SP-2001	Vector Laboratories, UK
CD11b Microbeads	130-093-634	Miltenyi Biotec, UK
DMEM/F-12	31331-028	Gibco, ThermoFisher Scientific UK
Goat anti-Mouse IgG (H+L) Cross-Adsorbed Antibody, Alexa Fluor 488	A-11001	ThermoFisher Scientific UK

Goat anti-Mouse IgG, Cross-Adsorbed Antibody, Alexa Fluor 568	A-11004	ThermoFisher Scientific UK
Goat anti-Rabbit IgG, Cross-Adsorbed Antibody, Alexa Fluor 488	A-11008	ThermoFisher Scientific UK
Hank's Balanced Salt Solution (HBSS), without Ca^{2+} and Mg^{2+}	14175-095	Gibco, ThermoFisher Scientific UK
Hoechst Trihydrochloride Trihydrate	H3570	ThermoFisher Scientific UK
MACS Separation Buffer	130-091-221	Miltenyi Biotec, UK
MCSF	416-ML/CF	R&D Systems Inc. USA
M.O.M. (Mouse-on-Mouse) Elite Immunodetection Kit, Peroxidase	PK-2200	Vector Laboratories, UK
Neural Tissue Dissociation Kit (P)	130-092-628	Miltenyi Biotec, UK
Normal Goat Serum	S-1000	Vector Laboratories, UK
Paraformaldehyde	158127	Sigma-Aldrich, Merck, UK
Percoll	17-0891-02	GE Healthcare, UK
Poly-L-Lysine Mw 70-150k	P6282	Sigma-Aldrich, Merck, UK
Streptavidin, Alexa Fluor 488	S-11223	ThermoFisher Scientific UK
TGFβ-1	130-095-067	Miltenyi Biotec, UK
Triton X-100	T9284	Sigma-Aldrich, Merck, UK

***Washing buffer**: 500ml 1X HBSS (without Ca2+ and Mg2+) MACS buffer: 1 x PBS, pH7.2, 0.5% BSA, 2mM EDTA*

Purification Reagents

Item	Product Code	Supplier
Glycine	G/0800/60	Fisher Scientific, UK
IsoStrip™ Mouse Monoclonal Antibody Isotyping Kit	11493027001	Roche, Merck, UK
Sodium azide	AC190381000	Acros Organics, Fisher Scientific, UK
Sodium chloride	S/3120/65	Fisher Scientific, UK
Tris base	BP152-500	Fisher Scientific, UK

***Binding buffer**: 10mM tris, 150mM sodium chloride, 0.1% sodium azide (pH 7.4)*
***Elution buffer**: 0.1M glycine (pH 2.5)*
***Neutralisation buffer**: 1M tris (pH 8)*